ME

MECHANICAL ENGINEERING
DEC 2 1959
LIBRARY

JOURNAL OF THE

AERO/SPACE SCIENCES

VOLUME 26 DECEMBER, 1959 NUMBER 12

PURDUE UNIVERSITY
DEC 7 1959
LIBRARY

CONTENTS

An Appreciation ..... THE EDITORS 769

Space Vehicle Environment ..... CARL GAZLEY, JR., W. W. KELLOGG, AND E. H. VESTINE 770

Photothermoelastic Investigation of Transient Thermal Stresses in a Multiweb Wing Structure ..... GEORGE GERARD AND HERBERT TRAMPOSCH 783

A Linear Perturbation Method for Stability and Flutter Calculations on Hypersonic Bodies ..... MAURICE HOLT 787

An Investigation of Optimal Zoom Climb Techniques ..... HENRY J. KELLEY 794

Thermal Buckling of Circular Cylindrical Shells Under Circumferential Temperature Gradients ..... DAVID ABIR AND S. V. NARDO 803

Heat Transfer to Separated and Reattached Subsonic Turbulent Flows Obtained Downstream of a Surface Step ..... R. A. SEBAN, A. EMERY, AND A. LEVY 809

Viscous Hypersonic Similitude ..... WALLACE D. HAYES AND RONALD F. PROBSTEIN 815

Buckling of a Cylindrical Shell Under a Circumferential Band Load ..... D. O. BRUSH AND F. A. FIELD 825

Readers' Forum 831

Index to Volume 26 853

Published by
INSTITUTE OF THE AERONAUTICAL SCIENCES, INC.

JOURNAL OF THE AERO/SPACE SCIENCES

Editor: W. R. SEARS
Director, Graduate School of Aeronautical Engineering, Cornell University

Associate Editor: ROBERT R. DEXTER *Managing Editor:* RITA J. TURINO

Editorial Assistant: CAROLINE TAYLOR

Editorial Committee

Aerodynamics and Fluid Mechanics

H. Julian Allen
Holt Ashley
Dean R. Chapman
Francis H. Clauser
Hugh L. Dryden
John C. Evvard
Antonio Ferri
Alexander Flax
Wallace D. Hayes
R. T. Jones
Carl Kaplan
H. W. Liepmann
C. C. Lin
H. F. Ludloff
Harold Luskin
Clark B. Millikan
Henry T. Nagamatsu
H. J. E. Reid
George S. Schairer
G. B. Schubauer
John Stack
Theodore Theodorsen
Arthur N. Tifford
Th. von Kármán

Flight Testing

R. R. Gilruth
Melvin N. Gough
W. L. Howland
W. F. Milliken, Jr.

Rotating Wing Aircraft

F. B. Gustafson
K. H. Hohenemser
Bartram Kelley
R. B. Maloy
Ralph McClarren
R. H. Miller
R. H. Prewitt
Igor I. Sikorsky

Structures

John E. Duberg
R. R. Heldenfels
N. J. Hoff
Samuel Levy
J. F. McBrearty
W. Ramberg
E. E. Sechler
F. R. Shanley
C. R. Strang
S. Timoshenko

Meteorology

C. F. Brooks
D. M. Little
F. W. Reichelderfer
K. C. Spengler

Vibration and Flutter

Lee Arnold
M. A. Biot
R. L. Bisplinghoff
Harold A. Cheilek
I. E. Garrick
Martin Goland

Aircraft Design

W. E. Beall
E. H. Heinemann
Hall L. Hibbard
Richard Hutton
C. L. Johnson
A. A. Kartveli
F. K. Teichmann

Electronics

K. C. Black
M. V. Kiebert, Jr.
David S. Little
Paul Rosenberg
Giles J. Strickroth

Physiologic Problems

H. G. Armstrong
Louis H. Bauer
Robert J. Benford
W. Randolph Lovelace, II
Ross A. MacFarland

Flight Propulsion

William Bollay
George W. Brady
R. P. Kroon
Frank E. Marble
Abe Silverstein
E. S. Taylor

Instruments

Alan G. Binnie
Charles H. Colvin
Frank R. Cook
C. S. Draper
S. G. Eskin
C. F. Savage
R. C. Sylvander

SUBSCRIPTION RATES

JOURNAL OF THE AERO/SPACE SCIENCES (formerly Journal of the Aeronautical Sciences), Published Monthly. United States and Possessions: 1 Year, $15.00; Single Copies, $1.50. Foreign Countries Including Canada (American Currency Rates): 1 Year, $16.00; Single Copies, $1.50.

AERO/SPACE ENGINEERING, Published Monthly. United States and Possessions: 1 Year, $5.00; Single Copies, $0.50. Foreign Countries Including Canada (American Currency Rates): 1 Year, $6.00; Single Copies, $0.50.

Notices of change of address should be sent to the Institute at least 30 days prior to actual change of address.

Manuscripts for publication, proofs, and all correspondence should be addressed to the Editorial Office of the JOURNAL.

Publication Office, 20th and Northampton Sts., Easton, Pa. Correspondence regarding subscriptions may be addressed to the Editorial Office of the JOURNAL OF THE AERO/SPACE SCIENCES, 2 East 64th Street, New York 21, N.Y.

© *Copyright, 1959, by the Institute of the Aeronautical Sciences, Inc.*

Second-Class Mail Privileges Authorized at Easton, Pa. Acceptance for mailing at a special rate of postage provided for in Section 1103, Act of October 3, 1917, authorized April 29, 1937.

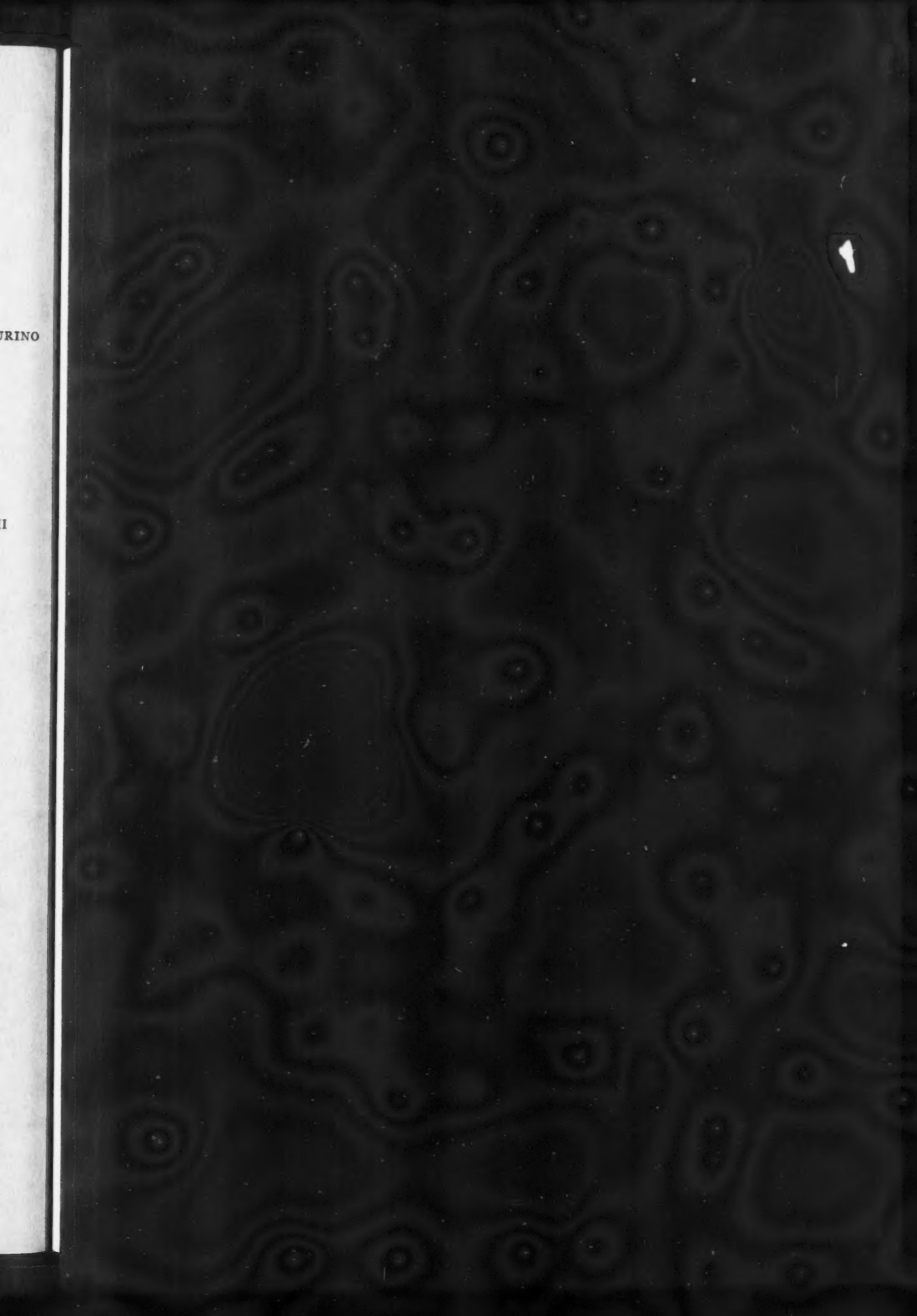

JOURNAL OF THE AERO/SPACE SCIENCES

VOLUME 26 DECEMBER, 1959 NUMBER 12

An Appreciation—

IT IS THE PRACTICE of the editors of the JOURNAL to enlist the assistance of a number of eminent aeronautical scientists and engineers to read and report to us on manuscripts submitted for publication. The advice of these experts is invaluable in helping the editors to select those papers suitable for the JOURNAL.

In the preparation of Volume 26, which closes with this issue, we have called on the persons listed below for these reports. We take this occasion to acknowledge their services and to extend our most sincere thanks. WILLIAM R. SEARS AND ROBERT R. DEXTER

H. N. ABRAMSON
MAC C. ADAMS
T. C. ADAMSON, JR.
FRED P. ADLER
H. JULIAN ALLEN
HOLT ASHLEY
JUDSON R. BARON
M. V. BARTON
SAMUEL BATDORF
RICHARD H. BATTIN
WELCOME W. BENDER
WILLIAM A. BENSER
GEORGE S. BENTON
J. G. BERRY
R. BETCHOV
P. P. BIJLAARD
M. A. BIOT
R. L. BISPLINGHOFF
A. C. BLASCHKE
W. BLEAKNEY
Z. O. BLEVISS
MARTIN H. BLOOM
S. M. BOGDONOFF
BRUNO A. BOLEY
KAREL J. BOSSART
RICHARD G. BOWMAN
JOHN M. BOZAJIAN
E. F. BRANAHL
WALTER BREUHAUS
BENJAMIN R. BRIGGS
JAMES E. BROADWELL
B. G. BROMBERG
A. E. BRYSON, JR.
ROBERT W. BUCHHEIM
ADOLF BUSEMANN
WILLIAM B. BUSH
W. F. CAMPBELL
C. C. CHANG
DEAN R. CHAPMAN
A. C. CHARTERS
ANDREW F. CHARWAT
JOSEPH V. CHARYK
H. K. CHENG
SIN-I CHENG
FRANCIS H. CLAUSER
MILTON U. CLAUSER
JOHN M. COAN
C. B. COHEN
JULIAN D. COLE
THOMAS L. COLEMAN
DONALD COLES
JAMES F. CONNORS
STANLEY CORRSIN
HUGH L. COX
JOHN L. CRIGLER
PAUL H. DENKE
F. W. DIEDERICH
L. H. DONNELL
ALLEN F. DONOVAN
NORRIS F. DOW
CHARLES S. DRAPER
D. C. DRUCKER
FRANKLIN P. DURHAM
E. R. G. ECKERT
A. J. EGGERS, JR.
F. E. EHLERS
FREDRIC F. EHRICH
J. M. ENGLISH
ALBERT EPSTEIN
A. C. ERINGEN
JOHN C. EVVARD
SAUL FELDMAN
ANTONIO FERRI
L. J. FILA
ALEXANDER H. FLAX
R. G. FLEDDERMANN
E. A. FLETCHER
L. E. FOGARTY
M. J. FORRAY
A. M. FREUDENTHAL
M. T. GANNON
WELKO E. GASICH
B. E. GATEWOOD
CARL GAZLEY
BARON T. GEORGE
GEORGE GERARD
R. E. GIBSON
ROBERT R. GILRUTH
MARTIN GOLAND
T. R. GOODMAN
SANFORD GORDON
DUNSTAN GRAHAM
ERNEST W. GRAHAM
K. G. GUDERLEY
R. L. GUSTAFSON
FRANK M. HAMAKER
H. A. HAMER
JEROME B. HAMMACK
ANDREW G. HAMMITT
LEONARD A. HARRIS
WILLIS HAWKINS
WALLACE D. HAYES
MAX A. HEASLET
JOHN M. HEDGEPETH
R. R. HELDENFELS
H. B. HELMBOLD
A. HERTZBERG
SEYMOUR C. HIMMEL
N. J. HOFF
GEORGE A. HOFFMAN
S. K. HOFFMAN
MARSHALL HOLT
JOHN C. HOUBOLT
WALTON L. HOWES
W. C. HUGLI
HERBERT G. HURRELL
KENNETH JARMOLOW
ROBERT E. JONES
ROBERT T. JONES
ABRAHAM KAHANE
BARTRAM KELLEY
NELSON H. KEMP
JOSEPH KEMPNER
BERTRAM KLEIN
J. J. KLEIN
F. D. KOCHENDORFER
H. H. KORST
L. S. G. KOVASZNAY
WILHELMINA D. KROLL
DONALD M. KUEHN
ARNOLD M. KUETHE
GERARD KUIPER
HERMANN H. KURZWEG
PACO A. LAGERSTROM
EDMUND V. LAITONE
S. H. LAM
FRANK LANE
H. L. LANGHAAR
JOHN LAUFER
H. R. LAWRENCE
JAMES P. LAYTON
B. J. LAZAN
LESTER LEES
EUGENE LEVIN
SAMUEL LEVY
TING Y. LI
PAUL LIBBY
R. L. LICHTEN
H. M. LIEBERSTEIN
SEYMOUR LIEBLEIN
H. W. LIEPMANN
C. C. LIN
H. E. LINDBERG
A. M. LIPPISCH
V. C. LIU
JOHN LIVINGOOD
R. KENNETH LOBB
JOSEPH G. LOGAN
EUGENE S. LOVE
G. M. LOW
Y. L. LUKE
BRUCE T. LUNDIN
HAROLD LUSKIN
H. J. MACKE
RICHARD MACNEAL
ARTUR MAGER
E. MANGANIELLO
G. N. MANGURIAN
CLIFFORD MANNAL
WALTER A. MARTIN
STEPHEN H. MASLEN
JOHN P. MAYER
BERNARD MAZELSKY
H. G. MCCOMB, JR.
S. E. MCCUNE
JOHN MEIRS
A. MENDELSON
R. X. MEYER
J. W. MILES
R. H. MILLER
CLARK B. MILLIKAN
HAROLD MIRELS
T. P. MITCHELL
F. K. MOORE
C. H. MURPHY, JR.
N. O. MYKLESTAD
W. J. MYKYTOW
H. T. NAGAMATSU
S. D. NARDO
J. A. O'MALLEY, JR.
E. T. ONAT
SHIH-I PAI
C. E. PAPPAS
JOHN B. PARKINSON
S. S. PENNER
C. D. PERKINS
T. H. H. PIAN
S. PINES
F. V. POHLE
E. C. POLHAMUS
WILLIAM PRAGER
HARRY PRESS
R. F. PROBSTEIN
W. DUNCAN RANNIE
AUGUST RASPET
HENRY J. E. REID
ERIC REISSNER
H. S. RIBNER
S. O. RICE
F. R. RIDDELL
T. R. RIEBEN
R. C. ROBERTS
R. E. ROBINSON
R. G. ROBINSON
WILLIAM P. RODDEN
PETER H. ROSE
R. M. ROSENBERG
IRA ROSS
V. J. ROSSOW
JOSEPH RUTKOWSKI
E. S. RUTOWSKI
B. SAELMAN
PAUL H. SAVET
S. A. SCHAAF
G. S. SCHAIRER
C. M. SCHMIDT
ARTHUR SCHNITT
G. B. SCHUBAUER
E. E. SECHLER
R. SEDNEY
PAUL SEIDE
H. SERBIN
S. F. SHEN
F. S. SHERMAN
MERVIN SIBULKIN
RONALD SMELT
A. M. O. SMITH
C. B. SMITH
E. H. SPAULDING
JOHN R. SPREITER
J. R. STALDER
E. V. STEARNS
HERBERT S. SUER
G. W. SUTTON
LAWRENCE TALBOT
WALTER P. TARGOFF
T. THEODORSEN
JOHN A. TIEDEMAN
LU TING
MURRAY TOBAK
H. B. TOLEFSON
MYRON TRIBUS
LEON TRILLING
JOHN T. TRUXAL
M. J. TURNER
R. J. VACCARO
E. R. VAN DRIEST
W. G. VINCENTI
GEORGE WALDMAN
PETER P. WEGENER
H. P. WHITAKER
M. L. WILLIAMS
R. J. WISNIEWSKI
D. S. WOOLSTON
HSUN-TIAO YANG
HIDEO YOSHIHARA
SHAO-WEN YUAN
A. T. ZAHORSKI
M. ZAID
R. W. ZIEMER

Space Vehicle Environment†

CARL GAZLEY, JR.,* W. W. KELLOGG,** AND E. H. VESTINE***
The RAND Corporation

Introduction and Summary

In space flight, as was the case during the ancient long and arduous terrestrial voyages over unknown oceans, there will be much more to look for than sea serpents and mermaids. Though the possibility of space serpents and celestial sirens might be intriguing, there will actually be required a long and continuous watch of the features of the physical environment, which will be needed for successful consummation of the flight. The future navigator and pilot will see and experience many new things in the universe about him. These will excite his wonder, and at least an indication of an explanation will be desired. Some of the answers afforded by past and present basic researches in astronomy, astrophysics, and geophysics will be provided in this paper, even though the information be imperfect.

It will be the purpose here to estimate and discuss various physical space attributes of the natural environment in the solar system. In particular, the discussion will be concerned with a cursory survey of the characteristics of solar radiations, the effects of solar and other thermal radiations on vehicle temperature, the characteristics of the Earth's magnetic fields and other magnetic fields in space, the Earth's exosphere and the solar corona, cosmic rays, and meteoroids. Estimates of the probability of vehicle skin penetration by meteoroids are also presented.

Solar Radiation

WHILE we know a good deal about the solar radiation in the visible and near-infrared part of the spectrum, and about the solar radiation in the radio wave spectrum, there is a great deal of short wavelength solar radiation which is absorbed in the upper atmosphere and cannot be observed from the surface. In fact, until high-altitude rockets and satellites were available, the radiation in the ultraviolet and X-ray region could only be guessed at.

This is unfortunate, since the short-wave radiation from the Sun has a very marked effect on our atmosphere, particularly the upper atmosphere. It was expected that this short-wave radiation changed markedly with activity on the Sun, since there were very pronounced changes in the conditions in our upper atmosphere which correlated with solar activity. For example, changes of solar activity were closely related to changes in the free electron density in the ionosphere, which could be observed by radio propagation methods, and with auroral and geomagnetic activity, which could also be observed in a number of ways from the surface of the Earth.

Received November 3, 1958. Revised and received July 2, 1959.

† Based on a paper presented at the Space Vehicles Session, IAS National Summer Meeting, Los Angeles, Calif., July 8–11, 1958.

* Engineer, Aeronautics Department, Engineering Division.
** Head, Planetary Sciences.
*** Member, Senior Staff.

Within the last three years, however, direct confirmation has been obtained of the changes in solar short-wave radiation by means of rocket observations. Since a rocket can only spend a short length of time above the atmosphere, it is difficult to observe time variations of solar X-ray or ultraviolet radiation. Observing the Sun from rockets is somewhat like a porpoise trying to get a reading on the cloud cover; he can poke his head out for a few seconds, and then he must fall back down into the gloom of his native realm. However, the Naval Research Laboratory scientists have been able to time their rocket ascents to coincide with disturbances on the Sun, and have been able to observe the enhanced radiation which comes from the Sun during these brief periods of time—periods which may last for but a few minutes.

Fig. 1 shows an overall view of the solar spectrum from about 0.2 to 3 microns. This was calculated by the Naval Research Laboratory[1] and relied on their rocket observations for the ultraviolet section and on observations by the Smithsonian Astrophysical Observatory[2] for the visible and infrared radiations. Fig. 2 shows the ultraviolet part of the spectrum in more detail. It should be noted that while the visible and infrared spectrum approaches a black body distribution with an equivalent temperature of about 5,700°K., the near ultraviolet departs from this black body distribution. As was noted in Fig. 1, it can also be seen that there is a good deal of small-scale variation from wavelength to wavelength, due to the fact that certain elements on the Sun's surface emit or absorb more strongly at certain wavelengths than others, and also due to absorption in the Sun's lower atmosphere. There is no easy explanation for the departures of the intensity in the ultraviolet from a black body at constant temperature. Generally, it is assumed that the gases which control the near ultraviolet emission from the Sun are in the lower part of the Sun's atmosphere and are some-

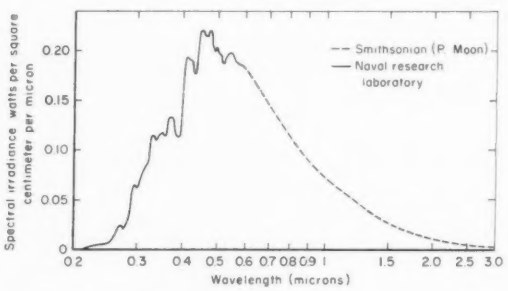

FIG. 1. The solar spectrum.

what cooler than the underlying gases in the photosphere, which is the source of the visible radiation.

In Fig. 3, which shows the extreme ultraviolet and X-ray spectrum as far as we know it,[3-5] it will be seen that the spectrum becomes even more complicated as one goes to shorter wavelengths. In particular, the ultraviolet emission lines which occur in the general neighborhood of 1,000 angstroms are very intense, and about 50 of these strong emission lines have already been identified in spectra obtained from rockets above the Earth's atmosphere by the Naval Research Laboratory. By far the most intense emission lines are those of hydrogen—lines which are given the names Lyman-alpha and Lyman-beta. It will be noted that there is some uncertainty in the exact value for the energy in the Lyman-alpha line, but that it is certainly very much more intense than the ultraviolet continuum. This line intensity therefore corresponds to a high equivalent black-body temperature, and may come from hydrogen in the chromosphere of the Sun, where the equivalent temperature can rise to the order of 100,000°K. Observations of Lyman-alpha during eclipses of the Sun, when the disc of the Sun (the photosphere) is blocked out, further bear out the chromospheric origin of this line.

These and even higher temperatures can also account for the strong X-ray radiation from the Sun's atmosphere, although this seems to be even less well understood. The values for the solar X-ray emission were taken from the NRL observations with rockets over a period of years. The reason for the large spread in the X-ray emission may be experimental error or it may be real changes with time in this part of the spectrum. There are many reasons for believing that the X-ray radiation below about 10 angstroms really does change with solar activity, since such changes in radiation would account for some of the phenomena which are observed in the atmosphere during solar activity, to which we have already referred. The most remarkable of these phenomena is perhaps that of radio blackout, in which, almost immediately following a solar flare, an increase in electron density in the lower part of the ionosphere, or D-region, causes an increased absorption of high frequency radio waves. A logical explanation of this increase in electron density in the upper atmosphere is that solar X-ray radiation in the vicinity of 2 to 5 angstroms has increased, causing this additional ionization to occur.

The gap from 100 to about 950 angstroms is a real gap. To our knowledge there have been no observations of solar radiation in this region, known as the "hard ultraviolet." It is a region of the spectrum in which detectors are difficult to come by, in which photographic film and normal optical techniques fail, and one which requires a very high altitude rocket to observe in order to be free of any residual absorption. It is hoped that in the next few years we will get some information in this important part of the spectrum.

Finally, it will be noted that the solar X-ray fluxes are of the order of 10^{-3} microwatts per square centimeter *per angstrom*, or less. The *integrated* energy in the X-ray region outside the Earth's atmosphere is thus of the order of 0.1 microwatt per square centimeter or less. This flux of energy is not to be confused with the radiation detected in the Van Allen radiation belt by recent satellites and space probes.[6] The radiation belt consists of charged particles which are trapped by the Earth's magnetic field. (See below, section on Cosmic Rays.) These charged particles are still not completely identified, but must be either electrons or protons, with energies ranging from 50 or 100 kev (if electrons) to over 50 Mev (if protons). It is possible that secondary X-rays (bremsstrahlen) are produced when the electrons impinge on the skin of a vehicle. In any case, the important fact to be considered is that the energy in the radiation belt, whether protons, electrons, or secondary X-rays, probably could penetrate into a vehicle with moderately thin walls, and could constitute a hazard to the occupants over a period of several hours. It is estimated by Van Allen that, in the heart of the radiation zones, the minimum exposure levels for an unshielded detector (or person) would be 5 to 10 roentgens per hour, assuming the flux is due to electrons or X-rays. It could be greater by a factor of ten, however, if the flux is due to protons with energies in the tens of Mev range. It is still not known just how penetrating this radiation is, but it is certainly much more penetrating than the direct solar X-rays, which could be stopped by a piece of metal foil or plastic material, and would therefore *not* be a hazard to an occupant of a space ship.

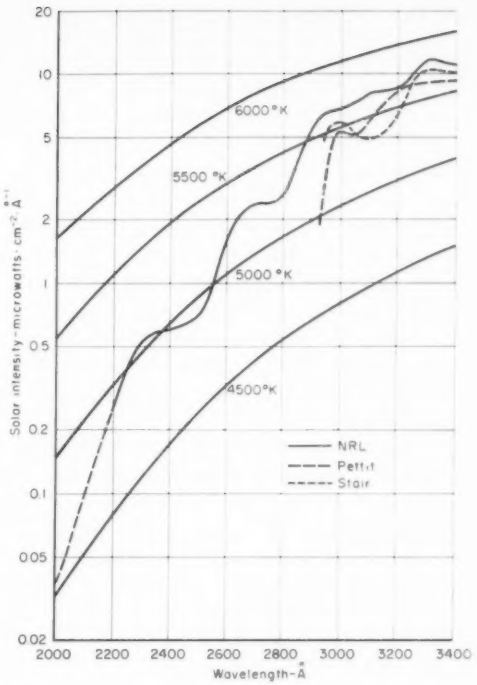

FIG. 2. The ultraviolet portion of the solar spectrum compared to black-body spectra.

Thermal Radiations

The primary mode of heat exchange between a space vehicle and its environment is radiation. These radiation exchanges and any internal heat generation thus determine the vehicle's internal temperature and its surface temperature. The surface receives thermal radiation from the Sun and, if close to a planet, reflected solar radiation as well as radiation from the atmosphere and the surface of the planet itself. In the thermal range, the Sun radiates approximately as a black body with a surface temperature of about 6,000°K. At the Earth's distance, this results in an energy flux of about 1.98 cal/(sq.cm.)(min.). The radiation from the planets depends on their temperatures and atmospheres. The amount of this radiation falling on the vehicle's surface which is actually absorbed depends on the spectral absorption characteristics of the surface material. Similarly, the amount of radiant energy emitted by the surface depends not only on the surface temperature but also the spectral emission characteristics of the surface.

To illustrate the effects of the spectral character of the surface, consider the equilibrium temperature of a body in the solar system. For simplicity, we shall consider, for the moment, a body far from any planet so that it receives heat only by solar radiation:

$$\text{Heat absorbed} = \alpha(E/r^2)A_c$$

where α is the surface absorptivity for solar radiation, E is solar radiation flux at the Earth's distance from the sun (r = one astronomical unit = 150,000,000 km.), r is the distance from the sun in astronomical units, and A_c is the projected area of the body normal to the radiant incidence. The heat emitted by the body is

$$\text{Heat emitted} = \epsilon\,\sigma_B T^4 A_s$$

where ϵ is the surface emissivity, $\sigma_B T^4$ is the emission of a black body at the same temperature, and A_s is the body's radiating surface area. For steady-state conditions with no internal heat generation, the radiant absorption and emission can be equated, giving

$$\alpha(E/r^2)A_c = \epsilon\,\sigma_B T^4 A_s$$

and the radiation equilibrium temperature is

$$T = [(\alpha/\epsilon)(E/\sigma_B r^2)(A_c/A_s)]^{1/4} \qquad (1)$$

The equilibrium temperature attained by a surface in space depends, then, on its distance from the Sun, the ratio of its projected area to radiating area, and the ratio of its absorptivity for solar radiation to its emissivity for its own radiation. This result is shown graphically in Fig. 4 for a spinning sphere ($A_c/A_s = 1/4$) with α/ϵ = 0.1, 1.0, and 10. The estimated average temperatures of the planets[7] are indicated. These are seen to be slightly below the line for a black body ($\alpha/\epsilon = 1.0$); this is due to the reflection of a portion of the solar radiation from the planetary atmosphere and surface (i.e.,

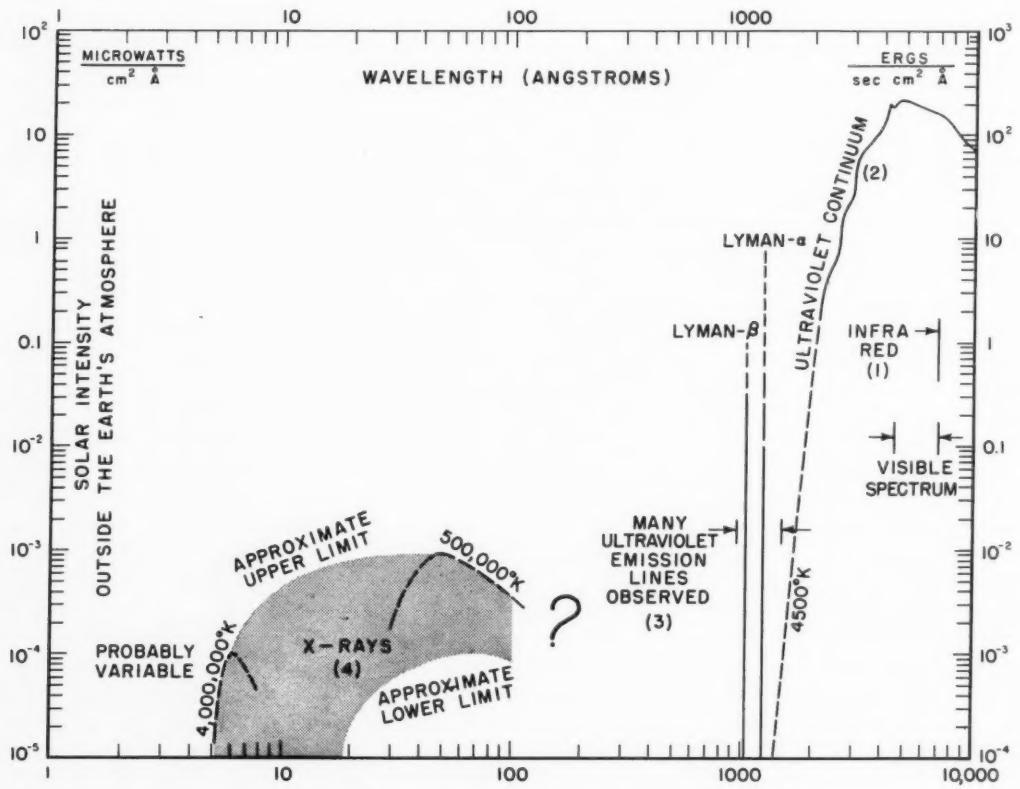

FIG. 3. Extreme ultraviolet and X-ray portion of the solar spectrum.

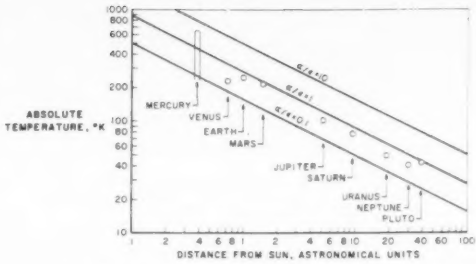

FIG. 4. Radiation equilibrium temperature of a spinning sphere as a function of its solar distance and surface radiation character.

$\alpha < 1.0$) and an effective emissivity close to unity (due to the multiple absorbing and emitting layers in the planetary atmosphere).

The absorptivity and emissivity of a material depends not only on the wavelength of the radiation—i.e., radiator temperature—but also on the chemical and mechanical character of the surface. Typical variations with radiator temperature are indicated in Fig. 5. The absorptivity and emissivity of most polished metal surfaces increase approximately linearly with temperature. The resulting ratio of absorptivity for solar radiation (radiator temperature $\sim$ 6,000°K.) to emissivity for its own radiation is appreciably greater than unity ($\alpha/\epsilon \approx 10$). This results in the familiar "greenhouse" effect, where a body absorbs solar radiation much more efficiently than it can emit its own radiation. On the other hand, a nonmetal may exhibit the opposite trend, the absorptivity and emissivity decreasing with radiator temperature. In this case, the surface is able to emit radiation more efficiently than it can absorb solar radiation; this results in a lower radiation equilibrium temperature. Rough or oxidized metal surfaces generally exhibit little effect of radiator temperature on absorptivity and emissivity. The effect of the absorptivity/emissivity ratio on the radiation equilibrium temperature is evident in Fig. 4. It is apparent that the surface spectral characteristics can result in appreciable effects on the radiation equilibrium temperature. For example, the radiation equilibrium temperatures of an oxidized metal and a shiny metal are greater by factors of approximately $10^{1/4} = 1.79$ and $\sqrt{10} = 3.16$ than the equilibrium temperature of a nonmetal. The surface material and surface condition are, therefore, of primary importance in determination of the radiation equilibrium temperature. If surface radiation is used to regulate a vehicle's temperature, the surface characteristics must be carefully chosen and maintained. This has been done successfully in the case of the Explorer satellite vehicles[8] where appropriate fractions of the surface were covered with Rokide ($\alpha/\epsilon = 0.437$) and two different steels ($\alpha/\epsilon = 1.92$ and 4.12). This resulted in average values of $\alpha/\epsilon = 1.37$ on the cylindrical section and $\alpha/\epsilon = 1.61$ on the nose cone.

If the space vehicle is near one of the planets, account must also be taken of reflected solar radiation from the planet, of radiation from the planet itself, and of the elimination of solar radiation if the vehicle is in the planet's shadow. In the neighborhood of the planet, the heat balance of Eq. (1) becomes

$$T/T_0 = \{2 - \alpha_p[1 - (1/4)(\epsilon/\alpha)]\}^{1/4} \qquad (2)$$

for the vehicle on the Sun side of the planet, and

$$T/T_0 = [\alpha_p\,(\epsilon/\alpha)(A_c/A_s)]^{1/4} \qquad (3)$$

for the vehicle on the dark side of the planet. In these equations T_0 is the radiation equilibrium of the vehicle far from any planet and at the same distance from the Sun and α_p is the absorptivity of the planet for solar radiation. The effects of the surface radiation characteristics on the radiation equilibrium temperature of a spinning sphere near a planet are shown in Fig. 6 for a planet having an absorptivity $\alpha_p = 0.5$. It is seen that the presence of the planet has an appreciable effect on the vehicle's radiation equilibrium temperature over a wide range of absorptivity/emissivity ratios. For a low value of α/ϵ (e.g., a nonmetal), the equilibrium temperature is relatively unchanged on the dark side of the planet but is about 30 per cent higher on the Sun side. For α/ϵ close to unity (e.g., rough metal), the equilibrium temperature is about 40 per cent lower on the dark side and about 13 per cent higher on the Sun side of the planet. For a high value of α/ϵ (e.g., a shiny metal), the surface equilibrium temperature is about 67 per cent lower on the dark side and only about 11 per

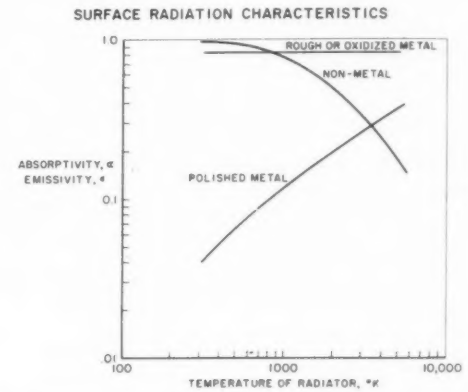

FIG. 5. Typical variation of surface absorptivity and emissivity with radiator temperature.

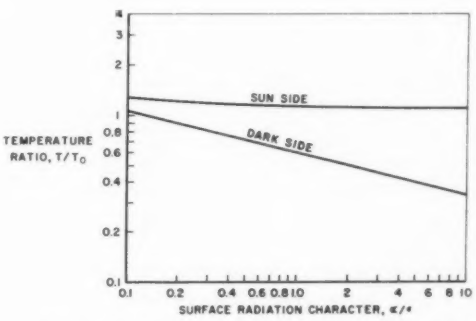

FIG. 6. Effect of near planet on surface radiation equilibrium temperature.

cent higher on the Sun side. It should be emphasized that these are equilibrium temperatures—attained only after a period of time sufficient for steady-state heat exchange to be achieved. Actually, flight near a planet is more apt to be a transitory nature, so that transient heat-transfer effects would become important. For example, the surface temperature of a satellite vehicle which passes from the dark side to the Sun side of a planet would tend to oscillate somewhere between the limits shown in Fig. 6. The amplitude of the oscillations would depend on the heat capacitance of the surface material and heat exchanges with internal equipment. A technique for the prediction of satellite temperature variation has been frequently described (e.g., see Buwalda and Hibbs[8]) and will not be discussed further here.

Any internal heat generation within the vehicle also affects the equilibrium surface temperature. In that case the heat balance of Eq. (1) is modified to

$$T/T_0 = [1 + (q_i/\epsilon \sigma_B T_0^4 A_s)]^{1/4} \qquad (4)$$

where q_i is the rate of internal heat generation and T_0 is the radiation equilibrium temperature the surface would attain with no internal heat generation.

For manned vehicles spending an appreciable time at distances from the Sun appreciably greater than the earth's distance, some form of internal heat generation would be necessary to keep the interior at tolerable temperature levels. The amount of this heat generation would depend on the Sun's distance and on the thermal insulation between the interior and the outer surface. As an extreme case, consider a vehicle at such a great distance from the Sun that solar radiation is negligible compared to the surface heat loss. In this case, an internal heat generation of about 100 watts/sq.m. would be required with about 1 in. of good insulation between the interior and the outer surface. This heat requirement could be reduced to lower values by the use of more insulation. For example, 1 ft. of insulation would reduce the required heat generation to about 20 watts/sq. m.

Magnetic Fields

The Geomagnetic Field in Space

The Earth's magnetic field in space is much like that due to a short magnet at the Earth's center, the magnet being so directed that its north pole will be nearest the general direction of the geographic south pole. The central axis of this magnet intersects the Earth's surface at the point 78.5° North and 291.0° East, called the geomagnetic north pole. The magnetic moment of this magnet, taken as a very short magnet, or dipole, was 8.06×10^{25} cgs units in 1922,[9] and has been decreasing slowly with time.

At points beyond the atmosphere at a distance r from the Earth's center, the magnetic field falls off rather nearly as the cube of the distance, or in terms of a surface value of about 0.5 gauss to 0.5 $(a/r)^3$ where a is the Earth's radius. The electric currents flowing in the atmosphere, believed mostly transients, will add to the main magnetic field. The main field includes also some higher order terms required in precise calculations of the field in space.

As mentioned below, magnetic fields may also arise from a ring current in the Earth's equatorial plane at a distance of a few Earth radii, and there are also other fields which may extend to considerable distances from the Earth.

Solar Magnetic Fields

The surface magnetic field of the Sun is not much larger than that of the earth, except within sunspots. The field may vary somewhat with time and, pending completion of measurements by astronomers, a magnetic moment of the Sun is difficult to assign. In the case of sunspots, there are usually local north and south magnetic poles in the sunspot groups. Magnetic moments may be as great as or greater than values 10^6 times that of the whole Earth when spot diameters reach 50,000–60,000 km., with magnetic fields of the order of 5,000 gauss.

Such sunspot fields could therefore be expected to extend well beyond Mercury and almost to the planet Venus with fairly readily measurable intensity, if it were not for the fact that the solar corona is likely to be a very good electrical conductor throughout a vast region; as a consequence, electromagnetic induction will nullify systematic features of the changing sunspot fields, except at points close to the Sun. However, it will be expected that portions of the actual magnetic fields of sunspots will be carried by material within moving prominences or the streaming corona, to the neighborhood of the Moon and Earth with measurable intensity of magnetic field. Hence the sunspot fields are expected to exist in fragmentary and badly organized form, within the solar system.

Magnetic Fields in Space

Simpson[10] and others have discussed the possibility that blobs of solar ionized gas carrying magnetic fields at times fill a good deal of the space—perhaps as far out as Jupiter.

The linear cross sections of such blobs is of course unknown, but they probably extend over a considerable range, from a few hundred kilometers across to many thousands of km. A satellite measuring magnetic fields on the way to the Moon might therefore expect to encounter the magnetic fields of such clouds. Since the clouds and the satellite may each be moving with velocities of the same order, magnetic pulses of duration somewhat less than a second to several seconds should result. The blobs may carry fields in excess of a galactic field of about 10^{-6} gauss, and probably needs to approach or exceed about 10^{-4} gauss to exist under the variegated environment of the solar and terrestrial fields. On a lunar flight, magnetic signals of order 10^{-4} gauss and duration of a second or so may therefore be encountered.

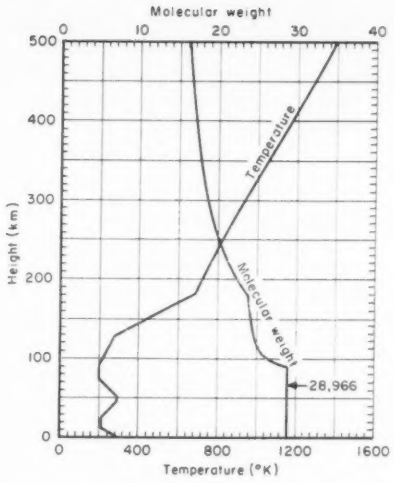

FIG. 7. Real kinetic temperature and molecular weight as functions of height, according to the ARDC Model Atmosphere (1956).

The Exosphere

The exosphere refers to the part of the atmosphere where molecules and atoms can move in ballistic orbits, traveling for many kilometers between collisions. This part of the atmosphere probably starts at around 300 km, or 200 miles, and extends on out for an indefinite distance. Prior to the Sputniks and satellites, the only direct information on the density in this part of the atmosphere came from a very limited number of rockets, the highest observation of density being at about 220 km. However, there were certain theoretical calculations which could be made for higher altitudes, and these indicated that the temperature in the exosphere must be very high, in the order of 1,500° to 2,000°K.

A recent, widely-publicized calculation of the density distribution in the upper atmosphere has been made by the Air Force Cambridge Research Center, based on the recommendations of The Working Group on Extensions to the Standard Atmosphere. The Air Force calculations required as inputs from this Working Group assumptions regarding the distribution of temperature and molecular weight as a function of height. These assumptions are shown in Fig. 7. It will be noted that the temperature increases throughout the upper part of the curve, from 200 km. on, and that the molecular weight decreases continuously. The reason for the *discontinuities* in the curve of molecular weight vs. height lies in the somewhat artificial assumptions made with regard to the way in which oxygen and nitrogen dissociate in the atmosphere. These discontinuities in the curve are obviously not real.

Given this temperature and molecular weight distribution, it is possible to calculate the pressure and density in the upper atmosphere as a function of height, and the results of this calculation are shown in Fig. 8. This is referred to as the ARDC Model Atmosphere 1956.[12]

As was mentioned, these estimates of temperature, molecular weight, pressure, density, etc., were necessarily based on theoretical deductions which were admittedly somewhat uncertain. With the advent of the Sputnik satellites it was possible to obtain a more direct estimate of the density in the region of between 200 and 300 km., since the rate at which the period of these satellites changed was directly proportional to the density at the altitude of perigee. It turns out that the ARDC Model Atmosphere gives densities which are *too low* in this altitude range. Various estimates of the discrepancy between the ARDC atmosphere and the densities based on Sputnik observations range from a factor of 3 to a factor of 10 at about 250 km. These estimates have been made independently by NRL, Smithsonian, RAND, and the Soviet scientists. At the present time, there does not seem to be any clear statement that can be made with regard to density, except to advise that it will probably turn out to be somewhat higher than previously thought. Except for calculations of drags on satellites, however, the ARDC Model Atmosphere will probably serve as a good enough approximation to the distribution of conditions in the exosphere, pending better information from future satellites.*

It may be of interest to note that a modification of the density distribution in the exosphere will also require a modification of the temperature distribution, since they are obviously interdependent. We are fairly certain about the temperatures up to about 150 km., since there are a number of good rocket observations which extend that far. In order for the density to increase at 250 to 300 km. by the large factor already noted, the in-

* Since submission of this article, the following detailed summaries of recent satellite observations have been made, and give improved upper air densities: Kallmann, H. K., *A Preliminary Model Atmosphere Based on Rocket and Satellite Data*, J. Geophys. Res., 1959 (in press); Schilling, G. F., and Sterne, T. E., *Densities and Temperatures of the Upper Atmosphere Inferred from Satellite Observations*, J. Geophys. Res., Vol. 64, pp. 1–4, 1959; and Harris, I., and Jastrow, R., *An Interim atmosphere derived from rocket and satellite data*, Planet. Space Sci., Vol. 1, pp. 20–26, 1959.

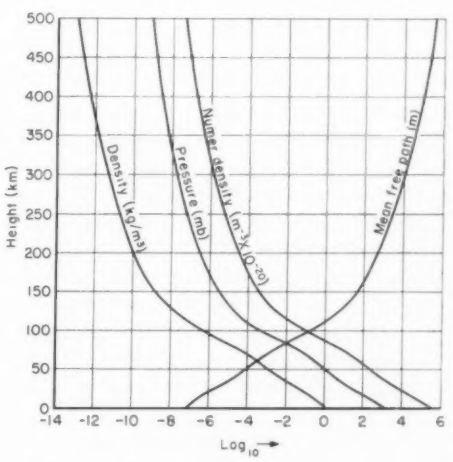

FIG. 8. Pressure, density, and mean free path as functions of height, according to the ARDC Model Atmosphere (1956).

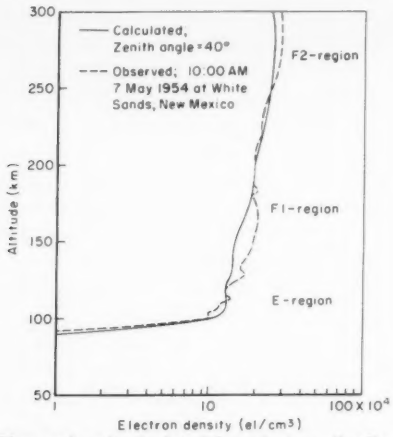

FIG. 9. Observed and calculated free electron distribution with height; zenith angle = 40°.

crease of temperature with height would have to be much more rapid than that shown in Fig. 7. Thus, temperatures at 300 km. may turn out to be 1,500° to 2,000°K. instead of about 900°K., as in the ARDC model, and will continue to increase with height.

In the course of the IGY satellite series it was proposed to put a very light inflatable sphere in orbit at a high altitude. The purpose of this inflatable sphere was specifically to obtain information on the density at very high altitudes, since it could be acted upon by drag more rapidly than will be a more dense vehicle such as a Vanguard, Explorer, or Sputnik satellite. From observations of the effects of drag on this inflatable sphere we could expect to have greatly improved values for the density and pressure.

When one looks at these curves of temperature, density, etc., for the upper atmosphere, it must be remembered that the situation is being greatly oversimplified. It is almost certain that there are very large variations in the conditions at these high altitudes from day to night and from place to place, probably variations by an order of magnitude or more. We do not know what these variations are, but we are quite sure they exist. For example, it is quite certain that during the day the temperature rises rapidly by many hundreds of degrees and then cools a corresponding amount during the night. This results in a bulging upward of the exosphere on the daylight side of the Earth, and a larger density during the day at any given altitude. It is known that these changes take place because one can occasionally observe the wind patterns at these altitudes, and one sees the violent surging back and forth of the atmosphere at around 300 km. Thus, one should never be too complacent about accepting a single curve of density or temperature versus height, since we know that the situation is very complex indeed. Furthermore, this irregularity in the exospheric conditions will make it difficult to interpret satellite drag data, since the location of perigee will change with time, thereby shifting the region where the density is to be determined. We are still in the early stages of trying to resolve this problem.

Another feature of the exosphere may be of importance to space flight—its ionization and conductivity. It is well known that the ionosphere contains free electrons, since these ionized layers have been observed for many years by radio techniques. Recently a combination of rocket and radio techniques in this country and in the Soviet Union have given more detailed information about the electron densities. One such determination, by NRL,[13] is shown in Fig. 9. On the same graph is shown a theoretical electron density curve computed by Hilde Kallmann of RAND.[14] It will be noted that at 300 km., under the conditions described, the electron density is 3×10^5 electrons per cm.^{3}. This is about the height of the F_2-layer, and above this the electron density presumably slowly decreases with height. A recent measurement of electron density above the F_2-layer (which is inaccessible by the usual radio techniques from the ground) has been made by the Soviet scientists,[15] who fired a rocket on February 21, 1958, to an altitude of 473 km., and determined that at that altitude the electron density was about 10^6 electrons per cm.^{3}, even more than in the F_2-region over White Sands. The implication is that the electron density distribution certainly does not fall off rapidly with altitude above the F_2-region, and this is further borne out by theory and by the interpretation, by Storey, of a radio phenomenon known as "whistlers," which give us an additional hint about the ionization in the exosphere.[16] The indications are that at about 500 km. and above from 10 to nearly 100 per cent of the particles are ionized.

These free electrons observed by radio and rocket-radio experiments are mostly "thermal electrons," that is, electrons which bounce about in a sort of equilibrium with the surrounding atmosphere. The exosphere is also populated by a relatively small number of very rapidly moving electrons, with many kilovolts of energy, which are trapped in the Earth's magnetic field and oscillate rapidly back and forth between the northern and southern hemispheres. It is these electrons, plus energetic protons, which are in large part the cause of the aurorae at high latitudes, and which are also the particles detected by the satellites and space probes, referred to earlier in this paper. However, it must be emphasized that these fast electrons account for but an infinitesimal part of the total free electron population in the exosphere (in the order of one fast electron in 10^{10} thermal electrons).

At higher levels of the exosphere, lighter gases, such as hydrogen and helium, provide an increasingly important contribution to the density and composition. Furthermore, the proportion of ionized particles to neutral atoms will progressively increase at greater distances from the Earth, because there will be few collisions between the positive ions and negative electrons; the probability for neutralization of the electric charges by recombination will be very small. At extremely high levels, or beyond the atmosphere in interplanetary space, protons and electrons will therefore dominate, together with some neutral hydrogen atoms.[17] Traces

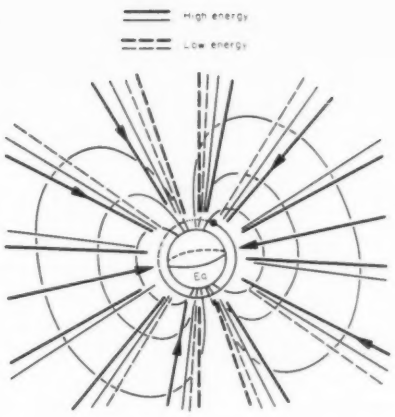

FIG. 10. Cosmic rays.

of other gases and atomic fragments will also exist here in the outer part of the solar corona. The particles within the solar corona will seldom hit one another, and on an average will travel half-way to the Sun before hitting anything. The particle density at the base of the exosphere can be taken as 3×10^7 cm.$^{-3}$(see reference 18). Indirect data on the solar corona and zodiacal light suggest that the region between the Earth and Moon has a particle density of the order of 10^3 cm.$^{-3}$.

The terrestrial exosphere may have a temperature of 1,000°C. to 2,500°C., say 2,000°C., and may be warmed in polar regions because hot coronal ionized gases can enter there more freely than across the equatorial magnetic field. This may provide greater polar drag on satellites than does the equatorial atmosphere. The temperature of the solar corona near the Sun will be about 1,000,000°C. It can be shown from theoretical calculations that this temperature should fall off as about the 2/7 power of the distance from the Sun expressed in terms of the solar radius R taken as unity. The temperature near the Earth and Moon is then about 220,000°C. This is so high that the energy of hydrogen atoms exceeds that needed to split the atoms into protons and electrons; consequently, scarcely any neutral hydrogen atoms will exist in the corona.

The relative heating effect of the hot solar corona on space vehicles will be negligible for a lunar flight. The heat flux from the solar corona per square cm. of area will be kinetic energy of motion, but the hot particles, though very energetic, are too few in number to heat up a metal surface very much. The number of protons and hydrogen atoms should be of the order of 10^3 to 10^4 per cc., so that the energy flux at 220,000° C. is only 10^{-7} the maximum solar radiation flux of about 1.98 cal/(sq. cm.)(min.).*

Hydromagnetic waves emitted by the solar atmosphere may occur as sound waves, traveling with very high velocities. The velocity of sound in the solar corona near the Earth and Moon is about 55 km./sec., which is that appropriate to the proton-electron gas, but no ordinary mechanism for transmitting sound will be operative. Since the mean orbital velocity of the Earth is only 30 km./sec., its motion and that of the Moon will be subsonic. In fact, even the planet Mercury, with an orbital velocity of 48 km./sec., will have a Mach ratio of about 0.6 and that for all other planets is less. There will also be no cap of compressed gas formed in front of the advancing planets. This is because each proton and electron in the coronal gas on an average travels farther than the diameter of a planet between collisions.[11] Thus the planets may be considered as bodies moving in rarefied gaseous medium—essentially in a free-molecule flow since the mean free path is of the same order as the body size.

Cosmic Rays

Cosmic rays[19] are noted in the upper atmosphere as atomic fragments traveling with a velocity very nearly that of light. They thus have great penetrating power, and may react to form numerous secondary particles on colliding with atoms in the lower ionosphere. They may be indistinguishable from the incoming primary particles at ground level.

Primary cosmic rays are very energetic. Those of about 18 billion electron volts (Bev) energy can penetrate the geomagnetic field to ground level at the Earth's equator, and about 3 Bev of energy are required to penetrate the atmosphere itself (see Fig. 10). The energies are greater therefore than those available from the man-made Brookhaven cosmotron. The geomagnetic field does not retard cosmic rays entering along the field near the geomagnetic pole, where enormous quantities of particles of moderate energies may enter, although these do not provide hazards to manned flight.

Information, at present incomplete, suggests that in addition to protons, about 15 per cent of the primary cosmic rays consist of α-particles, and that 1 or 2 per cent consist of heavier nuclei, but those of Li, Be, and B are not found for some reason. Less than 1 per cent are primary electrons and less than 1/10 per cent are gamma rays. The preliminary data for the satellites suggests a flux of order one particle per cm.^{2} per sec. per steradian at distances beyond the geomagnetic field.

The origin of cosmic rays has not yet been definitely determined. One simple mechanism that has been suggested is that sunspots or other fields in space may accelerate particles to high energies during a period of growth or decay of a magnetic field. For instance, at the edge of a sunspot a suitable formula derived by Swann[20] gives an electric field along the circular periphery to be $E = -R\Delta H/\Delta t$, where ΔH is the growth in field in time Δt, and R the radius of the spot. Clearly, if R is very large, as it might be in sunspots of large stars, or in areas within the gases of colliding galaxies, the driving force E might be so large that it could accelerate particles to high energies. Unfortunately, this mechanism does not seem adequate for the part of cosmic rays of solar origin, but there is some reason for believ-

* NOTE ADDED IN PROOF: It is understood that improved estimates by Chapman provide temperatures of order 100,000° C.

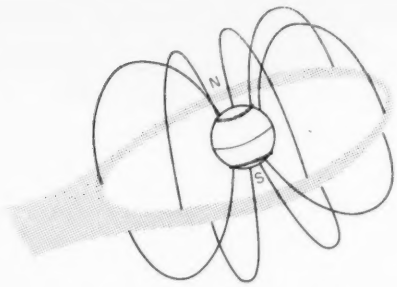

FIG. 11. Störmer current rings.

ing that some analogous mechanism may operate as a cause of cosmic rays originating in outer regions of space.

Solar particles moving with a velocity of about 1/3 that of light have been noted to leave the Sun in areas of solar flares. Methods of radio astronomy[21] have been used in these studies. During solar flares on about six occasions since the early 1940's, marked increases in cosmic rays have occurred over a period of hours to almost a day. On February 23, 1956, an increase at the ground of 90 per cent or so appeared in high latitudes of the Earth, and for the first time it was noted that the cosmic rays increased by a few per cent at the equator. This means the particles had an energy in excess of 18 billion electron volts (Bev). Effects persisted over a period of 16 hours or more in cosmic rays, and for several days high absorption of radio waves ensued. On the dark side of the Earth, unexposed to solar ultraviolet light or X-rays, vertical soundings of the ionosphere using radio waves revealed an excess of electrons, probably caused by particles of high energy, such as various secondaries, high-speed protons, and electrons. These probably ranged widely in energy. The orbits of such particles may be dominated by the geomagnetic field, so that they keep circling the Earth from west to east (or east to west), with some spiraling motion between the northern hemisphere and southern hemisphere. In this way they can possibly move in trapped orbits in the geomagnetic field, from which they would be able to escape only by collisions with other particles, or by entering localized field irregularities which can redirect their motion outward far beyond the atmosphere. The potential radiation hazard, like that of February 23, 1956, apparently does not occur very often, because this and some other large increases during flares have only appeared about once every three years.[22–24] But the flux at such times at the top of the atmosphere rises by several orders of magnitude above normal when energies somewhat less than 3 Bev are included.

Some ideas and results on corpuscular radiation as an aspect of solar radiation will next be discussed. The wave radiation is usually taken as that appropriate to a black body at 6,000°C., or in the case of X-rays to a temperature of 1,000,000°C., high in the solar atmosphere.

According to the Chapman-Ferraro theory of magnetic storms, corpuscular streams of electrons and protons are emitted from active regions on the Sun and proceed Earthward to cause magnetic storms and aurorae.[17] These particles, according to this theory and to several others related to it, travel to the Earth in about a day, so that the velocity may be about 10^8 cm./sec. The number density decreases rapidly with the distance from the Sun, but a few Earth-radii away from the Earth the ion density is supposed to be about 100 particles/cm.^{3}.

On entering the atmosphere the particles are supposed to be guided by the magnetic field so as to cause aurorae and polar magnetic storms, while a part remains as an equatorial ring current encircling the Earth at a distance of a few Earth-radii, the so-called Störmer current ring (see Fig. 11).

Due to thermal velocities, and divergence of solar streams, the number density of protons near the Earth will be much less than that initially developed in the solar atmosphere. Thus, as each solar particle moves radially outward from the Sun the initial area of cross section of the stream will be increased by about 216^2 or about 47,000 times, since the Earth's distance is about 216 solar diameters. Thus an initial density of 10^9 would be reduced to about 2×10^3/cc. If the stream were a blob of spherical section a similar reduction would be expected. But if the blob carried with it a magnetic field, and were composed of an almost completely ionized gas, as seems certain, the limited mobility of the protons and electrons across the field may greatly limit the expansion of the blob with distance from the sun. In a blob of sufficient cross section the time constant for decay may be many hours, so that the initial solar densities need not be reduced by many orders of magnitude on reaching the Earth. Such blobs can penetrate the geomagnetic field to a depth which might, very roughly, be that given by equating the kinetic energy of the blob per unit volume to that of the geomagnetic field. Thus if the velocity $v = 10^9$ cm./sec., which may ordinarily be a little high but not unreasonable, and the mass per unit volume is m, then $mv^2 = H^2/4\pi$ where H is the geomagnetic field. If the number density $N = 10^4$, and protons and electrons in equal numbers are the main constituent, and the interaction of the geomagnetic field with the field of the cloud be neglected, $mv^2 = 10^4 \times 1.67 \times 10^{-24} \times 10^{18} = 1.67 \times 10^{-2}$ ergs, or $H = 0.46$ gauss. The cloud of gas would then be stopped due to collisions with particles in the Earth's upper atmosphere. However, it is not certain that the blob's magnetic field will suffice to preserve the blob as an entity sufficiently long even for the very short time required. Also to be taken into account is the retarding influence on the blob due to electric currents induced within it as it progresses downward into the geomagnetic field. Some of the electrons will of course be trapped in Störmer orbits in the geomagnetic field, where they may have already been noted by Van Allen[6] in recent satellite measurements in Explorer I and III. Such particles stopped at suitable levels may of course move into the polar regions to produce aurorae and associated magnetic disturbances

noted there. A connection between particles noted by satellite and those causing aurorae has in fact been suggested by Van Allen. The radiation noted was of order 0.3 r in 5 hours or less as compared with the recommended permissible dose for human beings of 0.3 r/week, and later values rising to 10 r/hr. and more have been noted, as was mentioned previously above.

Meteoroids

The presence of meteoroids in interplanetary space are of interest to the designer of space vehicles because of the possibly disastrous effects of an encounter with such bodies. Meteoroids are solid bodies of various sizes moving in elliptical orbits about the Sun. Our previous experience with such bodies has been primarily confined to observing the effects occurring when they collide with the Earth and its atmosphere. Small bodies produce the familiar frequent luminous phenomena, known as meteors, observable in the night sky. Such small bodies suffer very appreciable mass loss by ablation during atmospheric interaction and drift down to the surface of the Earth as dust. Larger bodies, less frequent, produce spectacular "fireballs" and reach the surface of the Earth as meteorites. Very large bodies, very infrequent, reach the Earth with appreciable velocity and produce large craters—such as the one in Arizona which is about a mile in diameter and 600 ft. deep.

Our information about the size and number of meteoroids roaming in the solar system comes from visual, telescopic, and radio observation of the luminous and electrical phenomena produced by their interaction with the atmosphere (meteors) and by examination of the bodies reaching the ground (meteorites). Unfortunately, this does not tell us the original size, shape, frequency, structure, or velocity of the bodies before interaction with the atmosphere. These characteristics must be deduced by relatively indirect methods from the available observations. Consequently, various estimates of the size, mass, and frequency of meteoroids in space differ from each other by several orders of magnitude.

Meteoroids are essentially the debris of the solar system resulting from the breakup of comets and small planets. Their orbits are generally highly eccentric ellipses around the sun as shown schematically in Fig. 12. Most are on apparently random orbits and are known as sporadic. Others are distributed in well-defined orbits and produce the familiar meteor showers occurring annually when the Earth passes through their path. The relative velocity between the Earth and a meteoroid depends on the relative directions and velocities of the two bodies. The Earth moves in its orbit about the sun at a velocity of about 29.8 km./sec. while meteoroids on highly eccentric orbits can have velocities as high as 42.1 km./sec. Depending on whether there is a head-on collision or the meteor catches up with the Earth from the rear, the relative velocity can range between the sum of these numbers down to the Earth's escape velocity—i.e., from about 72 to 11 km./sec. This is illustrated qualitatively in Fig. 13 (which does not show the effects of the Earth's gravitational attraction).

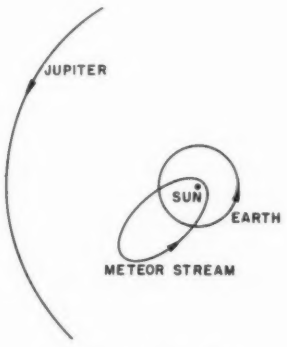

FIG. 12. Meteor orbit.

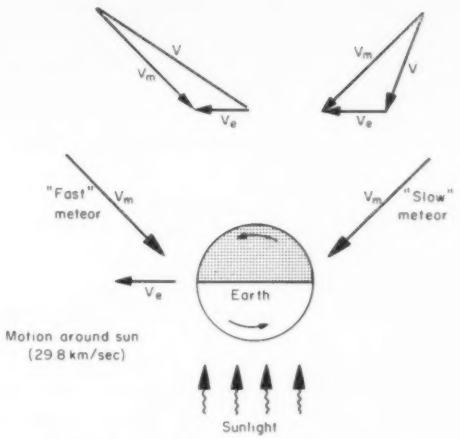

FIG. 13. Relative velocity between Earth and meteor.

It has been determined recently that meteors do not approach the Earth from a random direction, but rather that they, like other parts of the solar system, are concentrated in the ecliptic plane—i.e., the plane of the Earth's orbit. The distribution around the ecliptic plane, as determined by Prentice and reported by Lovell[25] is shown in Fig. 14. The concentration of still smaller particles in the ecliptic plane is known from zodiacal light observations. This concentration of meteoric material in the ecliptic plane implies that interplanetary trips should involve paths above or below that plane so as to minimize meteoroid encounters.

Because of the motion of the Earth, most meteoroid encounters occur on its front face. As is commonly known, more meteors may be observed after midnight than before midnight—i.e., when one is riding on the forward face of the Earth. The distribution of meteors in relative numbers is shown in Fig. 15, which is adapted from Lovell.[25] However, the direction of most meteors is found to be from behind the Earth—i.e., most of them are in direct, rather than retrograde, motion around the Sun. The distribution of direction, also adapted from Lovell,[25] is shown in Fig. 16. Since most

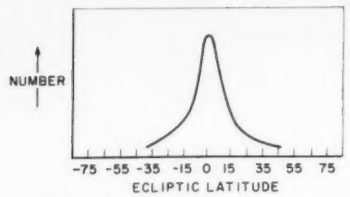

FIG. 14. Distribution of sporadic meteors around ecliptic.

FIG. 15. Distribution of meteoric encounters.

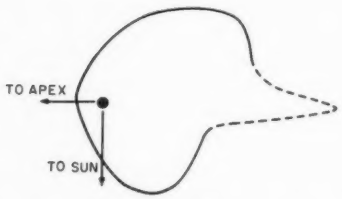

FIG. 16. Distribution of orbital directions.

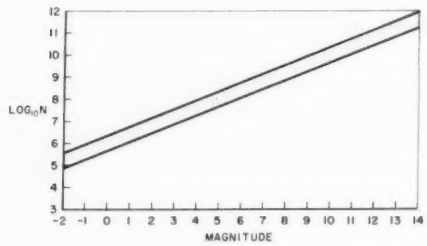

FIG. 17. Observed daily frequency of meteors in the Earth's atmosphere.

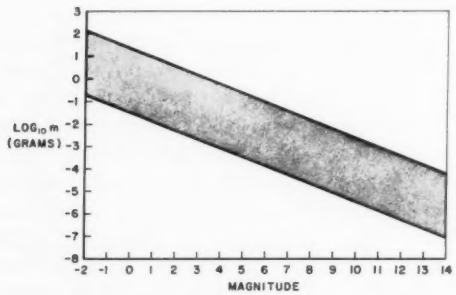

FIG. 18. Estimated meteoroid mass.

meteoroids thus apparently move around the Sun in the same direction as the Earth and other planets, to minimize high-velocity collisions, an interplanetary vehicle should also follow a direct, rather than a retrograde, orbit. This, of course, is desirable for reasons of fuel economy also.

The possibility of meteoroid collision with a space vehicle must currently be deduced from the observed frequency of meteor phenomena in the atmosphere. The daily frequency of sporadic meteors is shown in Fig. 17 as a function of the visual magnitude scale. This frequency may be as much as 10 times greater during a meteor shower. The magnitude scale is the customary astronomical scale in which each step in the magnitude scale denotes a change in luminous intensity by a factor of about 2.5. Brighter objects have negative magnitudes (Sun about -25, Moon about -12) and an increasing positive magnitude denotes decreasing intensity. Algebraically,

$$I \sim 10^{-0.43\mathfrak{M}} \tag{5}$$

A magnitude of about $+5$ is about the limit detectable with the naked eye. The upper line in Fig. 17 corresponds to the early estimate of Millman[26] based on visual observations and the recent estimate of Whipple[27] based on photographic observations. The lower line corresponds to the estimate of Watson[28] based on visual and telescopic observations and the estimate of McKinley[29] based on radio observations. These two lines represent, approximately, the limits of other recent estimates. It is interesting to note that, approximately, the number per unit magnitude vary as

$$N \sim 10^{0.43\mathfrak{M}} \tag{6}$$

With the definition of magnitude, Eq. (5), this gives

$$N \sim 1/I \tag{7}$$

That is, the number of meteors varies inversely with their luminous intensity.

While the frequency and magnitude are directly observable quantities, the deduction of the mass and size of the meteoroid from these and other observational data requires a knowledge of the physics involved in the meteoric interaction with the atmosphere. A number of investigators[30–33] have expressed the intensity in the form

$$I \sim m\, u^n \tag{8}$$

Now, while there is general agreement that the intensity varies directly with the initial meteoroid mass, the assumed velocity exponent, n, ranges from less than unity up to almost seven. The deduction of meteoroid mass is, therefore, very uncertain. The degree of uncertainty is illustrated in Fig 18 where the estimates of Whipple[27] and Watson[28] are shown. These lines encompass approximately the estimates of other investigators. Not shown in Fig. 18 is the uncertain effect of velocity; however, part of the discrepancy shown corresponds to the choice of velocity and velocity exponent. The effects of velocity and of the effects of in-

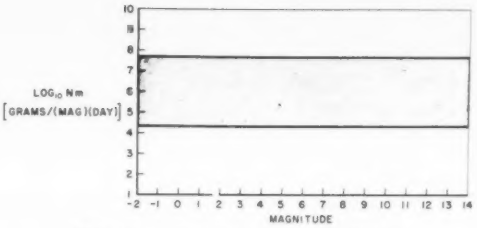

FIG. 19. Total mass per magnitude.

tensity-time variations have been discussed in detail by Kallmann.[34, 35] Watson[28] uses $n = 2.5$ and $u = 72$ km./sec. while Whipple[27] uses $n = 1$ and $u = 28$ km./sec. In any case, the direct proportionality between intensity and mass, Eq. (8), combined with Eq. (7) gives

$$N \sim 1/m \tag{9}$$

i.e., the frequency varies inversely with mass. This means that total mass in a magnitude (Nm) is constant. Fig. 19 shows the resulting range of estimates—varying from 2×10^4 to 5×10^7 g/(mag.)(day). This corresponds to a daily *total* mass of from 1 to 2,500 tons/day.

Of primary interest to the space vehicle designer is the frequency and mass of meteoroid particles. This may be obtained by combination of Figs. 17 and 18. The resulting range of estimates, shown in Fig. 20, is impressively wide; the upper limit is about 3,000 times greater than the lower limit! It is clear, therefore, that any estimate of meteoroid impact and penetration of the skin of a satellite or space vehicle can be only very crude.

From these estimates of the mass and frequency it is possible to estimate the concentration of meteoric material in the vicinity of the Earth's orbit. Considering the uncertainty in the estimates of both mass and frequency of meteoric encounters, a crude evaluation will suffice. This can be obtained by considering the effective volume of space swept out by the Earth in its daily motion. This amounts to about 6×10^{14} cu. km. Summation of the frequency and mass encountered over the range of magnitudes results in a mass density of 10^{-21} to 10^{-24} g/cc. This may be compared with the estimated density of matter in interstellar space, 10^{-24} to 10^{-26} g/cc.

The use of these estimates of mass and frequency of encounter with the Earth's atmosphere to predict encounters with space vehicles can be done crudely by simply scaling by the ratio of the surface areas of the Earth's atmosphere and the vehicle's surface. For example, a 1-meter diameter sphere would encounter fewer meteoroids by approximately a factor of 1.64×10^{14}, the ratio of the surface area of the Earth's atmosphere to the surface area of the sphere. A vehicle close to the Earth, such as a satellite, would be sheltered somewhat by the Earth from meteoroid collision. On the other hand, the gravitational attraction of the Earth would tend to increase the meteoroid concentration in its vicinity. However, the effects of these factors are probably small compared to other uncertainties.

The depth of penetration, or depth of surface mass loss by meteoroid impact, is a somewhat speculative calculation since the relative velocities are considerably above the laboratory level. A variety of theories for high-velocity impact and penetration, while agreeing with the available data up to about 10,000 ft/sec., deviate appreciably at meteor velocities.[26] Because of the present uncertainty in meteoroid number and mass, uncertainties in penetration dynamics are not presently serious. However, satellite data will presumably give better information in the near future on meteoroid hit probabilities; thus, a better understanding of penetration dynamics will soon be necessary.

At present it seems reasonable to adapt a relatively simple penetration model and to use the available experimental data for evaluation of proportionality constants. One of the more reasonable types of high-speed impact theory[36] visualizes the kinetic energy of the particle being used to melt, vaporize, or displace a certain volume of target material. This results in the proportionality

$$\text{Crater Volume} \sim \text{Particle Kinetic Energy}$$

or

$$\text{Crater Depth} \sim (\text{Particle Kinetic Energy})^{1/3}$$

The experimental high-speed impact data of Van Valkenburg[37] and of Huth, et al.,[38] as well as the shell-crater data collected by Baldwin,[39] yield a proportionality constant

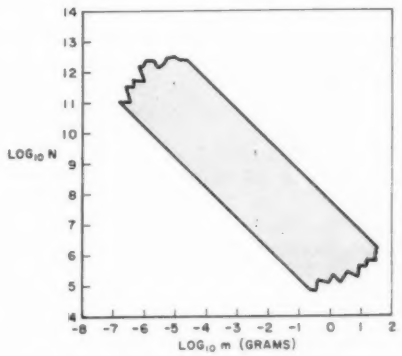

FIG. 20. Estimated mass and frequency.

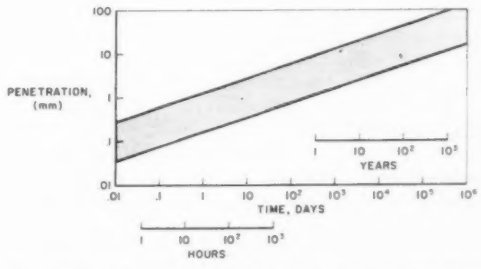

FIG. 21. Time for penetration of skin of a one-meter diameter sphere.

$$\text{Penetration, mm.} \simeq 2\,(\text{Particle Kinetic Energy, joules})^{1/3} \quad (10)$$

This relation, together with the mass and frequency estimates, allows one to calculate the penetration frequency for a vehicle's skin. The result is shown in Fig. 21 for a sphere of 1 meter diameter.* Here again the relative uncertainty of mass and frequency estimates is evident. These results indicate that a 1 mm. skin will be punctured sometime between 10 hours and 220 days, and that a 1 cm. skin would suffer puncture sometime between 1 year and 550 years. Grimminger's 1948 estimates[40] lie somewhat below the band shown in Fig. 21. Whipple's recent estimate[27] lies about in the middle of the band. Recent results from the Explorer I satellite[41] are relatively meager and generally confirm qualitatively the estimates presented here. However, interpretation of the experimental results are subject to the same uncertainties in mass and penetration as are the estimates described above.

The encounter with smaller particles—i.e., too small to penetrate—would be more frequent, of course. Thus one might expect a "sandblasting" of the surface before penetration occurs. Whipple[27] has estimated that this surface erosion by small meteoroid particles would be comparable to that produced by solar corpuscular radiation and by interaction with the gases of the solar corona. He estimates that the erosion due to these three effects would destroy the optical properties of a surface after about 1 year.

References

[1] Boyd, R. L. F., and Seaton, M. J., (Eds.), *Rocket Exploration of the Upper Atmosphere*, Johnson, F. S., Purcell, J. D., Tousey, R., and Wilson, N., "The Ultraviolet Spectrum of the Sun," pp. 279–288; Pergamon Press, London, 1954.

[2] Moon, P., *Proposed Standard Solar-Radiation Curves for Engineering Use*, J. Franklin Inst., Vol. 230, pp. 583–617, 1940.

[3] Johnson, F. S., Malitson, H. H., Purcell, J. D., and Tousey, R., *Emission Lines in the Extreme Ultraviolet Spectrum of the Sun*, Astrophys. Jour., Vol. 127, pp. 80–95, 1958.

[4] Friedman, H., *Photoelectric Measurements of Solar X-Rays and Ultraviolet Radiation*, Neuvième Rapport de la Commission pour l'Etude des Relations entre les Phénomènes Solaries et Terrestres, pp. 41–51, ICSU, J. and R. Sennac, Paris, 1957.

[5] Chubb, T. A., Friedman, H., Kreplin, R. W., and Kupperian, J. E., Jr., *Lyman Alpha and X-Ray Emissions During a Small Solar Flare*, J. Geophys. Res., Vol. 62, No. 3, pp 389–398, 1957.

[6] Van Allen, J. A., Ludwig, G. H., Ray, E. C., and McIlwain, C. E., *The Observation of High-Intensity Radiation by Satellites 1958-Alpha and Gamma*, Paper No. 5, IGY Satellite Report Series No. 3, May 1, 1958. (See also article by Van Allen and Frank, to be published in Nature.)

[7] Kuiper, G. P., *The Atmospheres of the Earth and Planets*, 2nd Ed., The University of Chicago Press, 1952.

[8] Buwalda, E. P., and Hibbs, A. R., *Satellite Temperature Measurements for 1958 Alpha—Explorer I*, Paper No. 4, IGY Satellite Report Series No. 3, May 1, 1958.

[9] Vestine, E. H., et al., *The Geomagnetic Field, Its Description and Analysis*, Carnegie Institution of Washington Publication 580, Washington, 1947.

[10] Simpson, J., *Symposium on Cosmic Terrestrial Relationships*, Spring Meeting, American Geophysical Union, May 1958.

[11] Chapman, S., *Notes on the Solar Corona and the Terrestrial Ionosphere*, Smithsonian Contributions to Astrophysics, Vol. 2, pp. 1–14, 1957.

[12] Minzer, R. A., and Ripley, W. S., *The ARDC Model Atmosphere, 1956*, Air Force Surveys in Geophysics, No. 86, Air Force Cambridge Research Center, December, 1956. See also, Minzer, R. A., Ripley, W. S., and Condron, T. P., *U.S. Extension to the ICAO Standard Atmosphere*, U.S. Government Printing Office, 1958.

[13] Seddon, J. C., Pickar, A. D., and Jackson, J. E., *Continuous Electron Density Measurements up to 200 km.*, J. Geophys. Res., Vol. 59, No. 4, pp. 513–524, 1954.

[14] Kallmann, H. K., *Properties of the Atmosphere Between 90 and 300 km.*, Vistas in Astronautics, Pergamon Press, pp. 130–134, 1958.

[15] *Soviet Rocket Exploration of the Upper Layers of the Atmosphere*, Pravda, March 27, 1958.

[16] Storey, L. R. O., *An Investigation of Whistling Atmospherics*, Phil. Trans. Roy. Soc. London, Vol. 246A, pp. 113–142, 1953–54.

[17] Chapman, S., and Bartels, *Geomagnetism*, Vols. 1 and 2, Oxford, 1940.

[18] Hynek, J. A. (Ed.), *Astrophysics, A Topical Symposium*, McGraw-Hill Book Company, Inc., New York, 1951.

[19] Bates, D. R. (Ed.), *The Planet Earth*, Wilson, J. G., "Cosmic Rays," Chap. XVI, Pergamon Press, London, 1957.

[20] Swann, W. F. G., Phys. Res., Vol. 43, pp. 217–220, 1933.

[21] Bowen, E. G., *Washington Conference on Radio Astronomy—1954*, J. Geophys. Res., Vol. 59, p. 163, 1954.

[22] Forbush, S. E., *Large Increase of Cosmic-ray Intensity Following Solar Flare on February 23, 1956*, J. Geophys. Res., Vol. 61, pp. 155–156, 1956; *idem*, *World-wide Cosmic-ray Variations, 1937–1952*, J. Geophys. Res., Vol. 59, pp. 525–542, 1954.

[23] Firor, T. J., *Cosmic Radiation Intensity-Time Variations and Their Origin; IV. Increases Associated with Solar Flares*, Phys. Rev., Vol. 94, pp. 1017–1028, 1954.

[24] Bailey, D. K., *Disturbances in the Lower Ionosphere Observed at VHF Following the Solar Flare of 23 February, 1956, with Particular Reference to Auroral-Zone Absorption*, J. Geophys. Res., Vol. 62, pp. 431–463, 1957.

[25] Lovell, A. C. B., *Meteor Astronomy*, Oxford University Press, 1954.

[26] Millman, P. M., quoted by McKinley (see reference 29).

[27] Whipple, F. L., *The Meteoric Risk to Space Vehicles*, Proceedings of the Eighth Congress of the International Astronautical Federation, Barcelona, 1957, Springer-Verlag, Vienna, 1958.

[28] Watson, F. S., *Between the Planets*, The Blakiston Co., Philadelphia, 1941.

[29] McKinley, D. W. R., *Variation of Meteor Echo Rates with Radar System Parameters*, Canadian J. of Phys., Vol. 29, p. 403, 1951.

[30] Opik, E. J., *Meteors and the Upper Atmosphere*, The Irish Astronomical Journal, Vol. 3, pp. 165–181, 1955.

[31] Herlofsen, N., *The Theory of Meteor Ionization*, Reports on Progress of Physics, Vol. 11, pp. 444–454, 1948.

[32] Gazley, C., Jr., *Meteoric Interaction with the Atmosphere—Theory and Observations of Drag and Heating*, Paper presented at Conference on High Speed Aerodynamics and Structures, Buffalo, January, 1956.

[33] Hansen, C. F., *The Erosion of Meteors and High-Speed Vehicles in the Upper Atmosphere*, NACA TN 3962, March, 1957.

[34] Kallman (-Bijl), H. K., *Relationship Between Masses and Visual Magnitudes of Meteors*, Meteors (A Symposium on Meteor Physics), Special Supplement (Vol. 2) to J. Atm. Terr. Phys., Pergamon Press, 1955.

(*Continued on page 814*)

* Since this paper was written, a more recent estimate has been made based on more extensive penetration calculations: Bjork, R.L., and Gazley, C., Jr., *Estimated Damage to Space Vehicles by Meteoroids*, The RAND Corporation, Research Memorandum RM-2332, February, 1959. This shifts the band of Fig. 21 downward by approximately an order of magnitude.

Photothermoelastic Investigation of Transient Thermal Stresses in a Multiweb Wing Structure†

GEORGE GERARD* AND HERBERT TRAMPOSCH**
New York University

Summary

Photothermoelastic experiments were performed on a long multiweb wing model for which a theoretical analysis is available in the literature. The experimental procedures utilized to simulate the conditions prescribed in the theory are fully described.

Correlation of theory and experiment in terms of dimensionless temperature, stress, time, and Biot Number revealed that the theory predicted values higher than the experimentally observed maximum thermal stresses at the center of the web. Detailed temperature measurements in the flange suggested that the major source of this discrepancy can be traced to the one-dimensional heat conduction analysis of the flange employed in the theory.

Symbols

(See Fig. 1 for geometric parameters of multiweb beam.)

B = Biot Number, $B = ht_s/k$
c = specific heat, B.t.u./lb.-°F.
D = diffusivity, $D = k/\rho c$, in.²/hr.
E = modulus of elasticity, psi
f = material fringe constant, psi-in./fringe
h = heat-transfer coefficient, B.t.u./hr.-ft.²-°F.
k = thermal conductivity, B.t.u./hr.-ft.²-°F./in.
n = fringe order
t_w = web thickness, in.
t_s = cover flange thickness, in.
T = temperature, °F.
$\bar{T}$ = dimensionless temperature, $\bar{T} = (T - T_i)/(T_{aw} - T_i)$
T_{aw} = adiabatic wall temperature, °F.
T_i = initial temperature, °F.
α = thermal expansion coefficient, micro. in./in.-°F.
θ = Fourier Number, $\theta = D\tau/t_s^2$
ρ = density, pci
σ = stress, psi
$\bar{\sigma}$ = dimensionless stress, $\bar{\sigma} = \sigma/\alpha E(T_{aw} - T_i)$
τ = time, hr.

Introduction

IT IS WELL RECOGNIZED that the thermal environment associated with advanced aircraft may result in significant thermal stresses of a transient or steady-state nature. Although it is frequently possible to employ structural configurations which minimize thermal stresses, a basic understanding of thermal stress processes is of importance for many cases in which design approaches cannot be fully utilized.

In general, the more complex part of any thermal stress problem is concerned with the heat-transfer aspects. Due to the difficulties involved in treating radiation, conduction, and convection simultaneously, radiation and convection are often neglected in the available thermal stress literature. In addition, the conduction aspects are frequently treated as a one-dimensional problem.

Because of the simplifying assumptions introduced in the theory, it is of importance to verify the results of the analysis by suitable experiments. Since electrical resistance strain gages under variable temperature conditions often lose the simplicity characteristic of their room temperature operation, other methods for quantitative measurements of thermal stresses are of considerable interest.

The photothermoelastic technique has been developed as a new experimental approach to thermal stress problems. This technique extends the conventional photoelastic method of experimental stress analysis to the measurement and visualization of complete thermal stress fields arising from transient or steady-state temperature gradients. Since photoelastically sensitive plastics generally creep when exposed to elevated temperatures, temperature gradients are established by refrigeration.

Considerable progress has been achieved in applying the photothermoelastic technique to structures of relatively complex configuration since the exploratory study of reference 1 and the photothermoelastic material property investigation of reference 2. The early investigations were concerned with establishing the quantitative value of photothermoelasticity by tests on simple geometrical models proceeding from measured temperature distributions. These results established that, with relatively simple techniques, accuracies well within ±10 per cent are readily attainable. It is estimated that with precise techniques, accuracies within ±2 per cent can be achieved.

In reference 3, experiments on cemented I-beams and idealized multicell box structures indicated that transient thermal stress theories can be completely evaluated by photothermoelasticity, if certain dimensionless parameters can be reproduced experimentally. Successful simulation of initial conditions, Biot Numbers, and Fourier Numbers were achieved, and it

Received November 20, 1958. Revised and received March 23, 1959.

† Sponsored by USAF through the Office of Scientific Research, Air Research and Development Command. Contract No. AF-18(600)-1471.

* Associate Director of Research, College of Engineering.

** Engineering Scientist, Research Division, College of Engineering.

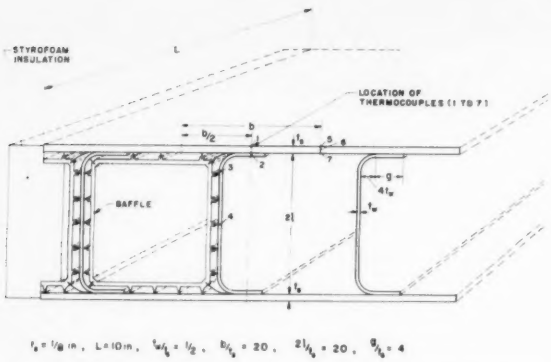

FIG. 1. Cross section of the scale model of a wing structure. Part of the convective baffles are shown.

was found that thermal stresses predicted by the available theories were always higher than experimental results. The source of discrepancy was traced to simplifying assumptions in the theories which treated the flange as a one-dimensional conduction medium.

The investigation reported herein is concerned with the correlation between theory and photothermoelastic tests on a representative multiweb wing structure. The model was constructed according to the configuration analyzed by Griffith and Miltonberger.[4]

This theory considers the transient thermal stresses produced in a wing structure by aerodynamic heating as a result of a sudden velocity change. The analysis included the effect of the joint conductivity between skin and web, and was performed with the aid of an electronic differential analyzer. The results were plotted in dimensionless form as functions of three parameters involving the geometry, the heat-transfer coefficient on the two outside surfaces, and the joint conductivity.

The correlation between theory and photothermoelastic results presented herein is important in two respects. It provides a test of the validity of the theory, and, at the same time, marks the emergence of photothermoelasticity as a quantitative tool for engineering use.

Experimental Procedure

Model Configuration

The configuration and dimensions of the model tested in this study are shown in Fig. 1. The details of the model conform to those analyzed in reference 4. The length of the model was chosen to insure that there was no influence of end effects at the vertical center region, and thus the model could be considered to be infinitely long in a theoretical sense.

The model was cemented together from epoxy resin material machined to the proper shapes from 1/4 in. thick plates and 1 in. diameter rods. Details of the cementing technique are presented in reference 3. Photographs of the model in several assembly stages are shown in Fig. 2.

Temperature Measurements

Temperatures in the model were sensed by seven thermocouples installed in the locations shown in Fig. 1. Thermocouples 1–4 were arranged to measure the temperature distribution in the flange-web conductive path while thermocouples 5–7 measured the distribution through the flange. The seven thermocouples were located in one half of the center cell only since past experience indicated symmetrical temperature distributions in the model when thermally loaded on both top and bottom surfaces.

The thermocouples were constructed from 0.005 in. diameter copper and constantan duplex wire by carbon arc welding. They were installed in the model using the same epoxy cement used to fabricate the model itself.

Temperature recording at a selected time was achieved by use of a high-speed switching unit connected to the vertical deflection circuit of a high gain cathode-ray oscilloscope. In the horizontal direction, the electron beam was moved by means of a conventional voltage divider network. The two circuits were synchronized resulting in a series of points on the oscilloscope screen which was photographed. A complete description of the temperature recording scheme is presented in reference 5.

By following well-established compensation and calibration techniques, the overall accuracy of the temperature measurements was estimated to be within $\pm 3°$F. of the true value.

Fringe Order Observations

In photothermoelasticity, thermal stresses are obtained directly from the observed fringe orders using an optical calibration constant for the material. The thermal strains are automatically corrected for since an isotropic field does not produce any fringes.

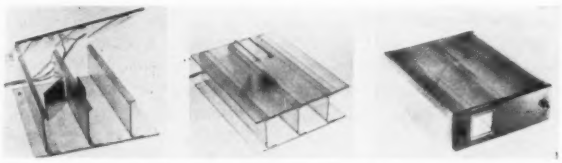

FIG. 2. Model in several assembly stages.

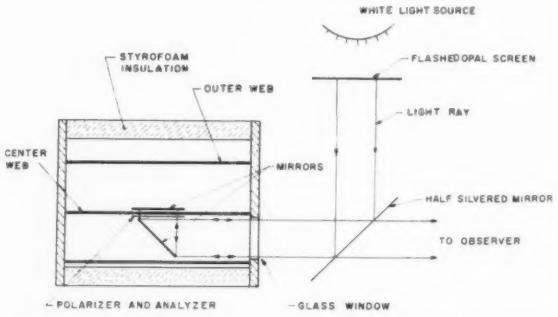

FIG. 3. Fringe pattern observation arrangement—schematic.

In this investigation, only the maximum thermal stresses which occur at the center of the web are of interest. Consequently, this was the only area observed. In cases where the stress distribution in the web is of interest, techniques discussed in reference 3 may be employed.

Because of the small thickness of the web, a doubling polariscope arrangement was utilized, as shown in Fig. 3. Furthermore, a white light source was used to improve the accuracy since the relatively small temperature gradient in the web resulted in a very wide fringe at the center. The fringe order was observed simultaneously with the temperature recording. The accuracy of the fringe order observation was estimated to be within ±3.5 per cent.

Thermal Loading

The theory of reference 4 is based upon a step function thermal input. This initial condition was simulated experimentally by applying simultaneously large, flat, dry-ice slabs to the top and bottom model surfaces. The thermal conditions associated with the use of dry-ice produce the required step function change in temperature and at the same time result in a constant adiabatic wall temperature of −110°F.

The heat-transfer coefficient, however, decreases somewhat with time, as discussed in reference 3. By focusing attention on the time range during which the web thermal stress reaches a maximum, the variable heat-transfer coefficient can be represented by an average value without introducing a significant error. The heat-transfer coefficient is used only in determining Biot Numbers, which influences the correlation between theory and experiment in a very minor way.

The theory of reference 4 neglects convective heat transfer within the wing structure. In using a plastic model, the time scale for the conductive heat-transfer process is greatly expanded, as compared to a geometrically similar metallic model, because of the low relative diffusivity of plastics. Consequently, whereas convective heat transfer may be relatively unimportant for a metal model, its influence may become significant during the much longer times involved in the conductive heat-transfer process for the plastic model.

In order to simulate the conditions of the theory, convective baffles were used in the model which effectively reduced the convective heat transfer to zero. The design of the baffles, shown in Fig. 1, prevented convective currents from circulating from the flange to the web. Low thermal capacity and high thermal resistance were achieved by using cotton filled hollow baffles which subdivided the cell cross section into a series of small cells.

Correlation of Theoretical and Experimental Data

Experimental Results

By utilizing the procedures discussed, two experiments were conducted. The first utilized the convective baffle to simulate the conditions of the theory of reference 4 as closely as possible. In the second test, the convective baffles were removed in order to provide some insight into the reduction in thermal stresses afforded by convective heat transfer.

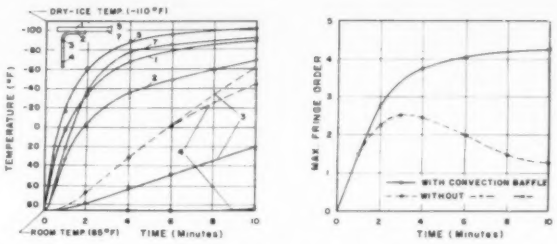

FIG. 4. Observed maximum fringe orders and recorded temperature distribution of the multiweb model.

The results of these tests are shown in Fig. 4 in terms of the measured temperature distributions and the observed fringe orders. It is apparent that the convective currents within the model were quite effective in reducing fringe orders, and the necessity of baffling was obvious in order to satisfy the conditions of the theory. Its effect on the temperature distributions was included in Fig. 4 only for points 3 and 4 where it was most pronounced, and was omitted elsewhere to avoid crowding the temperature curves.

In order to reduce these data for comparison with theory, the pertinent thermal conditions of the tests are given in Table 1. Also shown are the physical properties of the epoxy model material. The material used to construct the model was from the same batch on which the values given in reference 2 were obtained.

The thermal stresses in the web can be computed directly from the fringe orders, n, by use of the relation

$$\sigma = nf/t_w \tag{1}$$

The values of E and f used correspond to T average and are listed in Table 1. For reduction of σ to the nondimensional form, values of E obtained from the bending tests described in reference 2 and listed in Table 1 were used. In any case, however, the variation in E and f over the temperature range shown in Table 1 is relatively small.

TABLE 1
Test Conditions and Physical Property Data

t_s = 0.125 in.
t_w = 0.063 in.
T_i = 85°F.
T_{ac} = −110°F.
$h_{average}$ = 8 B.t.u./hr.-ft.²-°F.

τ	h
1 min.	8.5
3	8.0
5	7.5

c = 0.30 B.t.u./lb.-°F.
k = 1.36 B.t.u./hr.-ft.²-°F./in.
ρ = 0.0437 pci
α = 30.1 microin./in.-°F.

T (°F.)	E (ksi)	f (psi-in./fringe)
85	480	58
20	500	62
−60	540	64

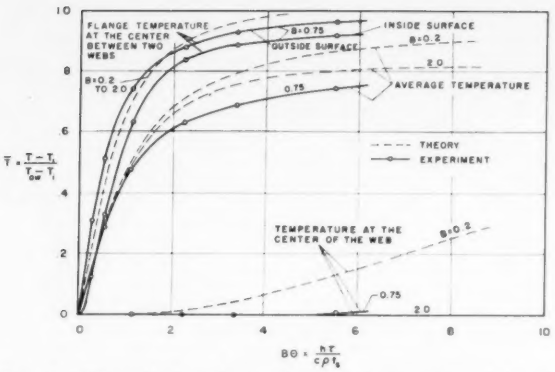

FIG. 5. Theoretical and experimental temperature data at several locations within the model.

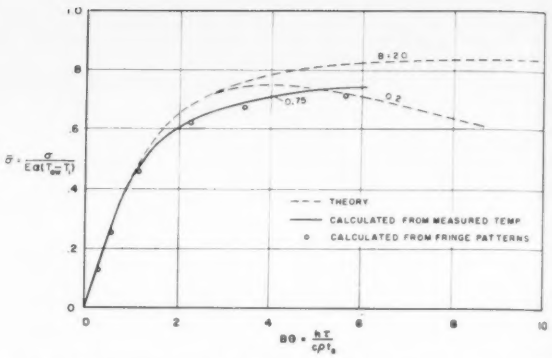

FIG. 6. Maximum thermal stress data at the center of the web correlating theory and experiment.

Correlation of Results

The evaluation of the theory was relatively straightforward. The theoretically predicted temperature and stress distributions, and the test values of Fig. 4 were plotted as functions of time in nondimensional form using the data of Table 1. Fig. 5 shows the correlation of the average temperature integrated over the model cross section in addition to the local temperatures at the center of the web and at the flange along a line centered between two webs. Fig. 6 shows the correlation of the maximum thermal stresses at the center of the web.

Agreement between theory and experiment for $\bar{T}$ and $\bar{\sigma}$ was observed only for values of $B\Theta$ less than 1. Then, with the exception of the temperature at the center of the web, the two results gradually departed from each other. It is to be noted in Fig. 6 that as a check on the interpretation of thermal stresses from fringe patterns, the thermal stresses computed from the measured temperatures agreed within the experimental error with the stresses calculated from the observed fringe orders.

The experiments representing a Biot Number of $B = 0.75$, an infinite joint conductivity, and the particular model geometry, indicated that the theoretical results were approximately 10 per cent higher than the maximum thermal stresses observed experimentally. Based on results of reference 3, it can be expected that the theory will diverge further from experiment if the Biot Number is increased. For lower Biot Numbers, the difference will be less pronounced, and agreement between theory and experiment can be expected.

The major source of discrepancy between theory and experiment can be traced directly to the temperature conditions in the flange. In Fig. 5, a definite temperature gradient through the thicknesses of the flange can be observed. This suggests that at the Biot Number of the experiments, and especially at higher Biot Numbers, two-dimensional conduction analysis of the flange is required in place of the one-dimensional analysis currently used.

Conclusions

The experiments demonstrated the applicability of the photothermoelastic method in evaluating transient thermal stress theories of aircraft wing structures. The observed discrepancy between theory and experiment of 10 per cent led to the following conclusions as far as the theory is concerned:

(a) The results of reference 4 can be applied as long as the Biot Number is low.

(b) When the Biot Number is in the range of 0.75 and greater, the temperature gradient through the flange thickness should be considered for accurate results. Under these conditions, a theory incorporating a two-dimensional conduction analysis of the flange can be expected to lead to a substantial reduction in the observed discrepancy between theory and experiment.

From an experimental standpoint, the following conclusions are significant in the development of photothermoelasticity as an engineering tool:

(c) A theory can be completely evaluated by the photothermoelastic technique if certain dimensionless parameters are reproduced experimentally.

(d) In the absence of theory, the photothermoelastic technique can be used to determine dimensionless $\bar{\sigma}$ values for application to metallic structures of the same configuration.

(e) Experiments conducted without convective baffles indicated that the thermal stresses in a structure of low thermal diffusivity will be considerably reduced by the convective heat transfer within the structure. With the development of proper scaling techniques, convection effects may be evaluated experimentally in conjunction with conduction effects.

References

[1] Gerard, G., and Gilbert, A. C., *Photothermoelasticity: An Exploratory Study*, J. Appl. Mech. Vol. 24, No. 3, pp. 355–360, September, 1957.

[2] Tramposch, H., and Gerard, G., *The Physical Properties of Several Materials for Use in Photothermoelastic Investigations*, J. Appl. Mech., Vol. 25, No. 4, pp. 525–528, December, 1958.

[3] Tramposch, H., and Gerard, G., *Correlation of Theoretical and Photothermoelastic Results on Thermal Stresses in Idealized Wing Structures*, ASME Preprint No. 59—A-36, 1959.

[4] Griffith, G. E., and Miltonberger, G. H., *Some Effects of Joint Conductivity on the Temperatures and Thermal Stresses in Aerodynamically Heated Skin-Stiffener Combinations*, NACA TN 3699, June, 1956.

[5] Tramposch, H., Papirno, R., and Gerard, G., *A Rapid Scanning System for Recording Thermocouple Outputs*, ASTM Bulletin No. 238, pp. 41–43, May, 1959.

A Linear Perturbation Method for Stability and Flutter Calculations on Hypersonic Bodies†

MAURICE HOLT*
Brown University

Summary

The equations governing linear perturbations in three space variables and time of steady supersonic potential flow past bodies of revolution are derived. The equations are referred to a characteristic coordinate system, and a general numerical process of solution is described. The assumption of potential flow simplifies the theory considerably and is justified in most flutter calculations and in estimating the contribution to stability derivatives from the rear part of a body. However, there is no obstacle in principle to generalizing the technique to apply to nonisentropic flow fields.

As an example, to represent the contribution of a typical hypersonic afterbody, the static stability derivatives associated with the exterior surface of a converging conical duct are calculated.

Dynamic stability derivatives can be found by a simple extension of this calculation.

Symbols

x^i	= position vector
g_{ij}	= metric tensor
i, j	= suffixes, each with values 1, 2, 3
U^i	= velocity vector in basic flow
P	= pressure in basic flow
R	= density in basic flow
S	= entropy in basic flow
u, p, ρ, s	= increments in velocity, pressure, density, and entropy in perturbed flow
t	= time
α, β	= characteristic coordinates
h_α, h_β	= length parameters along α and β lines, respectively
ψ	= angle between meridian plane and fixed meridian plane
r	= distance from axis of symmetry
C	= speed of sound in basic flow
c	= speed of sound in perturbed flow
Q	= fluid speed in basic flow
μ	= Mach angle in basic flow
θ	= angle between flow direction and axis in basic flow
u, v, w	= velocity components in characteristic coordinate system
φ	= velocity potential

Received June 11, 1959. Based on the paper presented at the Aeroelasticity—II Session, IAS 26th Annual Meeting, N.Y., Jan. 26–29, 1958.

† The work was carried out in the Aerodynamics Section of the Division stated below and supported under Contract AF 04(647)-305 by the Air Research and Development Command of the USAF.

* Associate Professor of Applied Mathematics. Also, Consultant, Research and Advanced Development Division, AVCO Manufacturing Corporation.

(1) Introduction

THE STEADY HYPERSONIC FLOW past a body of revolution with a blunt nose and conical afterbody can be considered in two stages. On the forward part of the body, the shock is very close to the surface, and the complex mixed-flow pattern can be described with fair accuracy by a shock-layer theory. At a certain distance beyond the sonic point, where the shock layer becomes too thick for this simplified treatment, a change must be made to the method of characteristics for supersonic flow.

Corresponding divisions have to be made in the treatment of an oscillating hypersonic body, required for an estimate of the various stability and flutter derivatives. Unsteady forces on the forward part of the nose can be found by extending shock-layer theories to take account of time-dependent effects. On the rear portion of the body, which is our concern now, the unsteady motion can frequently be represented by a potential. The assumption of potential disturbances is justified in panel flutter calculations and is also consistent with the current treatment of the steady flow problem on the rear part of a hypersonic body.

In the present report, the equation governing unsteady first-order disturbances of steady isentropic flow with axial symmetry is derived. First, the author's linearized method of characteristics is extended to take account of unsteady disturbances. The equation satisfied by the disturbance potential is then derived in terms of characteristic variables defined by the basic flow, the time, and the angle contained by a meridian plane and a plane of symmetry. The equation is linear, hyperbolic, and of the second order. The third angular variable only appears in one term and can be separated out.

In calculating stability or flutter calculations, we need to consider steady motion or periodic motion. In all these cases, the equation can be reduced to a linear hyperbolic equation in the characteristic variables with known coefficients (which are complex in the case of periodic motion). In special cases, this may be solvable by Riemann's method, but in most practical cases of aerodynamic interest the complicated form of the boundary conditions rules out an analytical approach and a numerical step-by-step process must be used. The process described here is simpler than the method of characteristics for nonlinear applications since integration is over the known network of char-

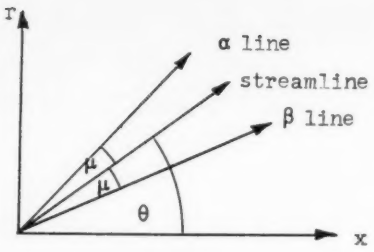

FIG. 1.

acteristic lines associated with the basic steady flow field.

The application of the process, to the calculation of stability derivatives on a converging conical afterbody, illustrates the perturbation of a nonuniform basic flow field. In contrast to the situation in linearized theory, the coefficients in the equation governing the perturbed flow here are variable and have to be evaluated in a preliminary calculation of the basic flow field by a method of characteristics. In calculating the perturbed field, we can eliminate the time as an independent variable, either by combining suitable, steady, perturbed flow fields in the manner described by Tobak and Wehrend[1] and Ribner and Malvestuto,[2] or by considering harmonic body motions of small amplitude.

(2) Time-Dependent, Linear Perturbations of Steady Flow

In reference 3, the author derives a linearized method of characteristics for calculating perturbations of a given three-dimensional field of flow. This only takes account of steady perturbations, and we begin by extending the theory to deal with unsteady disturbances.

Using the notation of reference 3, let x^i be the position vector with metric tensor g_{ij} $(i, j = 1, 2, 3)$. The velocity vector, pressure, density, and entropy in the basic field are denoted by U^i, P, R, and S, respectively. These variables depend only on the position vector x^i. Corresponding variables in the perturbed field are $U^i + u^i$, $P + p$, $R + \rho$, $S + s$; these depend on x^i and also on the time t.

The disturbance to the basic flow field is assumed to result from unsteady motion of the body of small amplitude. Further, the basic flow is in the normal supersonic range, so that the hypersonic similarity parameter is small. It follows that the additional field —namely, the difference between the basic and perturbed fields—can be defined by linearized equations, in which only first-order terms in u^i, p, ρ, and s are retained.

The equations governing the perturbed flow are

Momentum

$$(\partial u_i/\partial t) + (U^j + u^j)(U_{i,j} + u_{i,j}) + [1/(R + \rho)](P + p)_{,i} = 0 \quad (2.1)$$

Continuity

$$[1/(R + \rho)(C + c)^2](\partial p/\partial t) + g^{jk}(U_{j,k} + u_{j,k}) + [(U^k + u^k)/(R + \rho)(C + c)^2](P + p)_{,k} = 0 \quad (2.2)$$

Conservation of Entropy

$$(\partial s/\partial t) + (U^j + u^j)(S_{,j} + s_{,j}) = 0 \quad (2.3)$$

State

$$P + p = f(R + \rho, S + s) \quad (2.4)$$

The basic flow variables alone satisfy these equations also, with the time dependent terms omitted. If we subtract the basic flow equations from the corresponding Eqs. (2.1) to (2.4) and retain only terms linear in u^i, p, ρ, s we obtain the equations governing the additional flow field. These equations differ from corresponding equations derived in reference 3 only in terms $\dot{u}_i$ in Eq. (2.1), $\dot{p}/RC^2$ in Eq. (2.2) and $\dot{s}$ in Eq. (2.3). We can, therefore, follow the procedure used in reference 3 and refer Eqs. (2.1)–(2.4) to the system of characteristic coordinates defined by the basic flow.

At present, we are only interested in the case of basic axially symmetrical flow. The coordinate system then consists of characteristic surfaces of revolution

$$\alpha = \text{constant}, \quad \beta = \text{constant}$$

and meridian planes ψ = constant. The characteristic surfaces are determined by the basic flow, of course. In any meridian plane, the α curves are inclined at the angle $\theta + \mu$ and β curves at the angle $\theta - \mu$ to the axis of symmetry. Length parameters h_α, h_β are introduced, so that $h_\alpha d\alpha$ and $h_\beta d\beta$ are elements of length along α lines and β lines, respectively. Let x, r, ψ be cylindrical polar coordinates referred to the body axis, and u, v, w, corresponding velocity components of the additional field. The characteristic equations are then

$$-Q \sin\theta(\partial u/h_\beta\partial\beta) + Q\cos\theta(\partial v/h_\beta\partial\beta) - C(\partial w/r\partial\psi) - C(v/r) - (\cot\mu/R)(\partial p/h_\beta\partial\beta) - \sin(\theta - \mu)\dot{u} + \cos(\theta - \mu)\dot{v} - (1/RC)\dot{p} + K + L = 0 \quad (2.5)$$

$$Q\sin\theta(\partial u/h_\alpha\partial\alpha) - Q\cos\theta(\partial v/h_\alpha\partial\alpha) - C(\partial w/r\partial\psi) - C(v/r) - (\cot\mu/R)(\partial p/h_\alpha\partial\alpha) + \sin(\theta + \mu)\dot{u} - \cos(\theta + \mu)\dot{v} - (1/RC)\dot{p} + K + M = 0 \quad (2.6)$$

$$(1/2)Q\sec\mu\{(1/r)\{[\partial(rw)/h_\alpha\partial\alpha] + [\partial(rw)/h_\beta\partial\beta]\}\} + (1/R)(\partial p/r\partial\psi) + \dot{w} = 0 \quad (2.7)$$

where K, L, M are linear functions of u, v, w, p, and ρ defined in reference 3. They will be evaluated below. In general, these equations are combined with the entropy equation, the equation of state, and the continuity equation.

In many applications, both the basic flow and its unsteady perturbation can be treated as potential flows. This is justified when disturbances propagated downstream from the body are far more significant than disturbances propagated toward the body after reflection at the shock, as is the case in most panel flutter problems and some stability calculations.

Accordingly, we may write

$$u_i = \varphi_{,i} = (\partial\varphi/\partial x^i)$$

where $\varphi = \varphi(x^i, t)$

Eqs. (2.5), (2.6), and (2.7) then reduce to a single second-order equation for φ.

(3) The Equation for the Disturbance Potential

First, we record certain relations connecting the characteristic coordinate system and the physical variables of the basic flow.

From Fig. 1, showing the directions of α line (a "minus" Mach line), β line (a "plus" Mach line), and streamline, we find

$$\left.\begin{aligned} \partial r/h_\alpha \partial\alpha &= \sin(\theta+\mu), \quad \partial x/h_\alpha\partial\alpha = \cos(\theta+\mu), \\ \partial r/h_\beta\partial\beta &= \sin(\theta-\mu), \quad \partial x/h_\beta\partial\beta = \cos(\theta-\mu) \end{aligned}\right\} \tag{3.1}$$

The characteristic equations governing the basic flow may be written (see, for example, reference 4)

$$(\partial\theta/\partial\alpha) + (\sin\mu\cos\mu/C^2R)(\partial P/\partial\alpha) + (j/r)h_\alpha \sin\theta\sin\mu = 0 \tag{3.2}$$

$$(\partial\theta/\partial\beta) - (\sin\mu\cos\mu/C^2R)(\partial P/\partial\beta) - (j/r)h_\beta \sin\theta\sin\mu = 0 \tag{3.3}$$

where $j = 0$ in plane flow, $j = 1$ in flow with axial symmetry.

Cross differentiation of Eqs. (3.1) with use of Eqs. (3.2) and (3.3) leads to the relations

$$\partial h_\alpha/\partial\beta = \operatorname{cosec} 2\mu\{h_\beta[-\mu_\alpha - (\sin\mu\cos\mu/C^2R)P_\alpha - (j/r)h_\alpha\sin\theta\sin\mu] - h_\alpha\cos 2\mu[\mu_\beta + (\sin\mu\cos\mu/C^2R)P_\beta + (j/r)h_\beta\sin\theta\sin\mu]\} \tag{3.4}$$

$$\partial h_\beta/\partial\alpha = \operatorname{cosec} 2\mu\{h_\beta\cos 2\mu[-\mu_\alpha - (\sin\mu\cos\mu/C^2R)P_\alpha - (j/r)h_\alpha\sin\theta\sin\mu] - h_\alpha[\mu_\beta + (\sin\mu\cos\mu/C^2R)P_\beta + (j/r)h_\beta\sin\theta\sin\mu]\} \tag{3.5}$$

where we have written

$$\mu_\alpha = \partial\mu/\partial\alpha, \quad P_\alpha = \partial P/\partial\alpha, \text{ etc.}$$

The additional pressure is defined by Eq. (2.7), which may be written

$$(1/R)(\partial p/r\partial\psi) = -(\partial^2\varphi/r\partial\psi\partial t) - [(1/2)Q\sec\mu/r][(\partial^2\varphi/h_\alpha\partial\alpha\partial\psi) + (\partial^2\varphi/h_\beta\partial\beta\partial\psi)] \tag{3.6}$$

Since R, Q, μ depend only on α and β, Eq. (3.6) may be integrated to give

$$(p/R) = -\dot\varphi - (1/2)Q\sec\mu[(\varphi_\alpha/h_\alpha) + (\varphi_\beta/h_\beta)] \tag{3.7}$$

Hence,

$$(p_\beta/R) = -[(\varphi_\alpha/h_\alpha) + (\varphi_\beta/h_\beta)]\{(\cos^2\mu P_\beta/RC\sin 2\mu) + (Q\sin\mu\,\mu_\beta/2\cos^2\mu)\} - (P_\beta/RC^2)\dot\varphi - \dot\varphi_\beta + (1/2)Q\sec\mu[(\varphi_\alpha/h_\alpha^2)(\partial h_\alpha/\partial\beta) + (\varphi_\beta/h_\beta^2)(\partial h_\beta/\partial\beta)] \tag{3.8}$$

We now introduce the potential φ into Eq. (2.5). From the relations

$$\varphi_\alpha = \varphi_x x_\alpha + \varphi_y y_\alpha, \quad \varphi_\beta = \varphi_x x_\beta + \varphi_y y_\beta$$

and Eqs. (3.1), we obtain

$$u = \varphi_x = \operatorname{cosec} 2\mu\{(\varphi_\beta/h_\beta)\sin(\theta+\mu) - (\varphi_\alpha/h_\alpha)\sin(\theta-\mu)\} \tag{3.9}$$

$$v = \varphi_y = \operatorname{cosec} 2\mu\{(\varphi_\alpha/h_\alpha)\cos(\theta-\mu) - (\varphi_\beta/h_\beta)\cos(\theta+\mu)\} \tag{3.10}$$

Hence,

$$Q\{-\sin\theta(u_\beta/h_\beta) + \cos\theta(v_\beta/h_\beta)\} = -(Q\cos\mu/\sin 2\mu)(\varphi_{\beta\beta}/h_\beta^2) + (Q\cos\mu/\sin 2\mu)(\varphi_{\alpha\beta}/h_\alpha h_\beta) + (Q\varphi_\alpha/h_\alpha h_\beta\sin^2 2\mu)\{-(\cos\mu\sin 2\mu/h_\alpha)(\partial h_\alpha/\partial\beta) - 2\cos\mu\cos 2\mu\,\mu_\beta + (\theta_\beta - \mu_\beta)\sin\mu\sin 2\mu\} + (Q\varphi_\beta/h_\beta^2\sin^2 2\mu)\{(\cos\mu\sin 2\mu/h_\beta)(\partial h_\beta/\partial\beta) + 2\cos\mu\cos 2\mu\,\mu_\beta + (\theta_\beta + \mu_\beta)\sin\mu\sin 2\mu\} \tag{3.11}$$

$$-(C/r)(\partial w/\partial\psi) = -(C/r^2)(\partial^2\varphi/\partial\psi^2) \tag{3.12}$$

$$-C(v/r) = -(C/r\sin 2\mu)\{(\varphi_\alpha/h_\alpha)\cos(\theta-\mu) - (\varphi_\beta/h_\beta)\cos(\theta+\mu)\} \tag{3.13}$$

From reference 3 we find, after some reduction, that

$$K + L = (\rho/R^2)\cot\mu(P_\beta/h_\beta) + (c/QR\sin^2\mu\cos\mu)[(P_\beta/h_\beta) + (P_\alpha/h_\alpha)] + (1/h_\beta\sin^2 2\mu)\{[(\varphi_\beta/h_\beta) - (\varphi_\alpha/h_\alpha)\cos 2\mu][-(P_\beta/RC) + Q_\beta\sin\mu + Q\theta_\beta\cos\mu]\} + (1/h_\alpha\sin^2 2\mu)\{[(\varphi_\alpha/h_\alpha) - (\varphi_\beta/h_\beta)\cos 2\mu][-(P_\alpha/RC) + Q_\alpha\sin\mu + Q\theta_\alpha\cos\mu]\} \tag{3.14}$$

We may write

$$(\rho/R^2)\cot\mu(P_\beta/h_\beta) + (c/QR\sin^2\mu\cos\mu)[(P_\beta/h_\beta) + (P_\alpha/h_\alpha)] = -\{(\cot\mu/RC^2)(P_\beta/h_\beta) + (1/C^4\sin 2\mu)[(P_\beta/h_\beta) + (P_\alpha/h_\alpha)](d^2P/dR^2)\}\{(1/2)Q\sec\mu[(\varphi_\alpha/h_\alpha) + (\varphi_\beta/h_\beta)] + \dot\varphi\}$$

and so reduce Eq. (3.14) to the form

$$K + L = -(1/RC \sin^2 2\mu)[(\varphi_\alpha/h_\alpha) + (\varphi_\beta/h_\beta) + (2\dot{\varphi} \cos \mu/Q)] \{2 \cos^2 \mu(P_\beta/h_\beta) + (R/C^2)[(P_\beta/h_\beta) + (P_\alpha/h_\alpha)](d^2P/dR^2)\} + (\varphi_\beta/h_\beta \sin^2 2\mu) \{(1/h_\beta)[-(P_\beta/RC) + Q_\beta \sin \mu + Q\theta_\beta \cos \mu] - (\cos 2\mu/h_\alpha)[-(P_\alpha/RC) + Q_\alpha \sin \mu + Q\theta_\alpha \cos \mu]\} + (\varphi_\alpha/h_\alpha \sin^2 2\mu) \{(1/h_\alpha)[-(P_\alpha/RC) + Q_\alpha \sin \mu + Q\theta_\alpha \cos \mu] - (\cos 2\mu/h_\beta)[-(P_\beta/RC) + Q_\beta \sin \mu + Q\theta_\beta \cos \mu]\} \quad (3.15)$$

Finally,

$$-\sin(\theta - \mu)\dot{u} + \cos(\theta - \mu)\dot{v} - (1/RC)\dot{p} = (\ddot{\varphi}/C) + (1/\sin 2\mu)[(\dot{u}_\beta/h_\beta)(1 - \cos 2\mu) + (2\dot{u}_\alpha/h_\alpha)] \quad (3.16)$$

Using Eqs. (3.8), (3.11), (3.13), and (3.15), we can now evaluate the coefficients of φ_α, φ_β, etc., in Eq. (2.5).

We shall reduce each term separately.

Coefficient of φ_β:

This is

$$(Q/h_\beta^2 \sin^2 2\mu)\{2 \cos \mu \cos 2\mu(\mu_\beta) + (\theta_\beta + \mu_\beta) \sin \mu \sin 2\mu\} + (1/h_\beta^2)\{(\cot \mu \cos^2 \mu/RC \sin 2\mu)P_\beta + (Q\mu_\beta/2 \cos \mu)\} - (1/RCh_\beta \sin^2 2\mu)\{2 \cos^2 \mu(P_\beta/h_\beta) + (R/C^2)[(P_\beta/h_\beta) + (P_\alpha/h_\alpha)](d^2P/dR^2)\} + (C/rh_\beta \sin 2\mu) \cos(\theta + \mu) + (1/h_\beta \sin^2 2\mu)\{(1/h_\beta)[-(P_\beta/RC) + Q_\beta \sin \mu + Q\theta_\beta \cos \mu] - (\cos 2\mu/h_\alpha)[-(P_\alpha/RC) + Q \sin \mu + Q\theta_\alpha \cos \mu]\} = (P_\beta/RCh_\beta^2 \sin^2 2\mu) \times \{-1 - \sin^2 \mu - 2 \sin^2 \mu \cos^2 \mu - (R/C^2)(d^2P/dR^2)\} + (Q\theta_\beta \cos \mu/h_\beta^2 \sin^2 2\mu)(1 + 2 \sin^2 \mu) + (P_\alpha/RCh_\alpha h_\beta \sin^2 2\mu)\{\cos 2\mu(1 + \sin^2 \mu) - (R/C^2)(d^2P/dR^2)\} + (2\mu_\beta \cos \mu/h_\beta^2 \sin 2\mu) - (Q \cos \mu \cos 2\mu/h_\alpha h_\beta \sin^2 2\mu)\theta_\alpha + (C/rh_\beta \sin 2\mu) \cos(\theta + \mu)$$

which, with the aid of Eqs. (3.2) and (3.3) reduces to

$$(1/h_\beta^2 \sin^2 2\mu)\{[\cos 2\mu - 1 - (d^2P/dR^2)](P_\beta/RC) + 2Q\mu_\beta \cos \mu\} + [jQ \cos \mu \sin(\theta + \mu)/rh_\beta \sin 2\mu] + (P_\alpha/RCh_\alpha h_\beta \sin^2 2\mu)[2 \cos 2\mu - (R/C^2)(d^2P/dR^2)]$$

The first term vanishes since we may write

$$Q^2 \sin^2 \mu = dP/dR$$

whence, using the relation

$$dP/R = -QdQ$$

$$-(2dP/RQ^2) + 2 \cot \mu \, d\mu = (1/C^4)(d^2P/dR^2)DP$$

or

$$(dP/RC)[2 \sin^2 \mu + (R/C^2)(d^2P/dR^2)] = 2 \cos \mu \, Q \, d\mu \quad (3.16a)$$

Hence, the coefficient of φ_β is

$$(P_\alpha/RCh_\alpha h_\beta \sin^2 2\mu)[2 \cos 2\mu - (R/C^2)(d^2P/dR^2)] + (jQ \cos \mu/rh_\beta \sin 2\mu) \sin(\theta + \mu)$$

Coefficient of φ_α:

After reduction similar to that applied to the coefficient of φ_β, this becomes

$$(P_\beta/RCh_\alpha h_\beta \sin^2 2\mu)[2 \cos 2\mu - (R/C^2)(d^2P/dR^2)] + [jQ \cos \mu \sin(\theta - \mu)/rh_\alpha \sin 2\mu]$$

Coefficient of $\varphi_{\beta\beta}$: This is evidently zero.

Coefficient of $\varphi_{\alpha\beta}$: $2Q \cos \mu/h_\alpha h_\beta \sin 2\mu$

Coefficient of φ_t: $-(1/C^4 \sin 2\mu)[(P_\beta/h_\beta) + (P_\alpha/h_\alpha)](d^2P/dR^2)$

Coefficient of $\varphi_{\beta t}$: $[(1 - \cos 2\mu)/h_\beta \sin 2\mu] + (\cot \mu/h_\beta) = (2/h_\beta \sin 2\mu)$

Coefficient of $\varphi_{\alpha t}$: $2/h_\alpha \sin 2\mu$

Complete Potential Equation:

This is

$$(Q \operatorname{cosec} \mu/h_\alpha h_\beta)\varphi_{\alpha\beta} - (Q \sin \mu/r^2)\varphi_{\psi\psi} + (\varphi_{tt}/C) + (2/\sin 2\mu)[(\varphi_{\alpha t}/h_\alpha) + (\varphi_{\beta t}/h_\beta)] - (1/C^4 \sin 2\mu) \times [(P_\alpha/h_\alpha) + (P_\beta/h_\beta)](d^2P/dR^2)\varphi_t + (1/h_\alpha \sin^2 2\mu)\{(P_\beta/RCh_\beta)[2 \cos 2\mu - (R/C^2)(d^2P/dR^2)] + (jQ/r) \cos \mu \sin 2\mu \sin(\theta - \mu)\}\varphi_\alpha + (1/h_\beta \sin^2 2\mu)\{(P_\alpha/RCh_\alpha)[2 \cos 2\mu - (R/C^2)(d^2P/dR^2)] + (jQ/r) \cos \mu \sin 2\mu \sin(\theta + \mu)\}\varphi_\beta = 0 \quad (3.17)$$

Since the variable ψ only appears explicitly in the second term of Eq. (3.17), we may write

$$\varphi = \sum_1^n \Phi_n(\alpha, \beta, t) \cos n\psi \quad (3.18)$$

Further, when the motion of the body is assumed to be periodic of small amplitude, we may superpose solutions of the type

$$\varphi = \sum_1^n a_n F^n(\alpha, \beta) e^{i\omega t} \cos n\psi \tag{3.19}$$

The reduced potential then satisfies the equation

$$F_{\alpha\beta}{}^n + (h_\beta \sin\mu/Q \sin^2 2\mu)\{2i\omega \sin 2\mu + (P_\beta/RCh_\beta)[2\cos 2\mu - (R/C^2)(d^2P/dR^2)] + jQ/r \cos\mu \sin 2\mu \sin(\theta-\mu)\}F_\alpha{}^n + (h_\alpha \sin\mu/Q \sin^2 2\mu)\{2i\omega \sin 2\mu + (P_\alpha/RCh_\alpha)[2\cos 2\mu - (R/C^2)(d^2P/dR^2)] + (jQ/r)\cos\mu \sin 2\mu \sin(\theta+\mu)\}F_\beta{}^n + (h_\alpha h_\beta \sin\mu/Q) \times \{(n^2Q \sin\mu/r^2) - (\omega^2/C) - (i\omega/C^4 \sin 2\mu)[(P_\alpha/h_\alpha) + (P_\beta/h_\beta)](d^2P/dR^2)\} F^n = 0 \tag{3.20}$$

Eq. (3.20) may be written

$$F_{\alpha\beta}{}^n + aF_\alpha{}^n + bF_\beta{}^n + c_n F^n = 0 \tag{3.21}$$

where, in general, a, b, and c_n are functions of α and β defined by the basic flow. Eq. (3.21) is a linear, homogeneous, hyperbolic equation in two independent variables α and β. In principle, given correctly formulated boundary conditions, it can be solved by Riemann's method.[5] In the general case, the coefficients are complex and may only be known in tabular form so that it is usually necessary to solve the equation numerically.

(4) Boundary Conditions

The form of the boundary conditions will depend on the nature of the problem. In all problems, we shall have a surface boundary condition stating that there is no relative motion normal to the body. In addition, we shall be given values of φ or its derivatives along some leading minus characteristic surface which marks the beginning of the supersonic flow region where the perturbation technique can be applied. In stability calculations, these initial data are obtained from the solution to the perturbed flow problem on the forward part of the body. In flutter calculations, the disturbance is assumed to result from local oscillations of a panel. On the leading characteristic surface through the front edge of this panel, φ must be constant.

The direction cosines of the normal to the surface are

$$(-\sin\theta, \quad \cos\theta \cos\psi, \quad \cos\theta \sin\psi)$$

and the velocity components are

$$[\varphi_x, \ \varphi_y \cos\psi - (1/y)\varphi_\psi \sin\psi, \ \varphi_y \sin\psi + (1/y)\varphi_\psi \cos\psi]$$

Substituting from Eq. (3.19), we find that the surface boundary condition is

$$-\sum_0^n a_n F_x{}^n \sin\theta + \sum_0^n a_n F_y{}^n \cos\theta = u_r \tag{4.1}$$

where $u_r e^{i\omega t}$ is the component of body velocity along the outward normal.

Depending on the type of motion executed by the body, which may include distortions of a periodic character, we shall get sets of relations between the coefficients in Eq. (4.1). In flutter problems, u_r may involve a large number of harmonics in ψ, and we have to derive a large number of conditions on $a_n F^n$ from Eq. (4.1). However, the flutter modes will generally have symmetry properties which simplify these conditions. In stability calculations, we need only consider small steady deviations from the steady symmetrical state, and it is usually only necessary to consider zero and first-order harmonics in ψ.

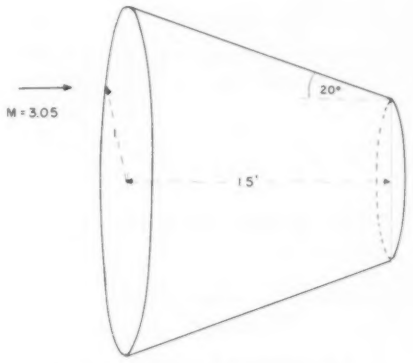

FIG. 2. Geometry of conical duct.

To illustrate our approach, we derive the boundary conditions corresponding to a periodic vertical plunging motion of the body of small amplitude such that the downward velocity at time t is $u_1 e^{i\omega t}$. Eq. (4.1) then becomes

$$-\sum_0^n a_n F_x{}^n \sin\theta + \sum_0^n a_n F_y{}^n \cos\theta = -u_1 \cos\theta \tag{4.2}$$

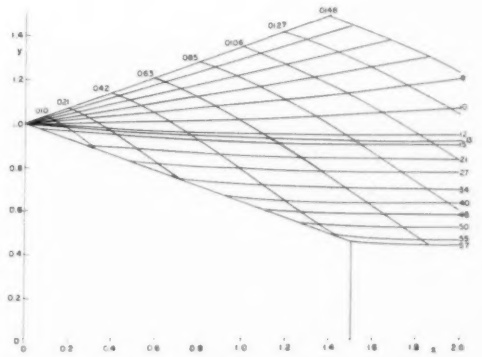

FIG. 3. Basic flow pattern around duct.

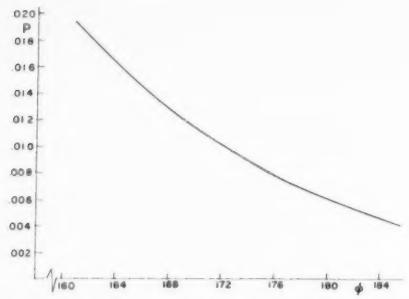

FIG. 4. Basic pressure variation in fan.

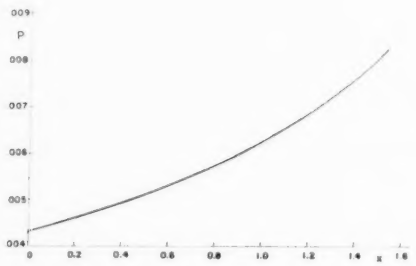

FIG. 5. Basic pressure variation on body.

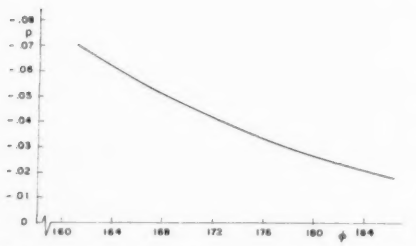

FIG. 6. Disturbance pressure variation in fan.

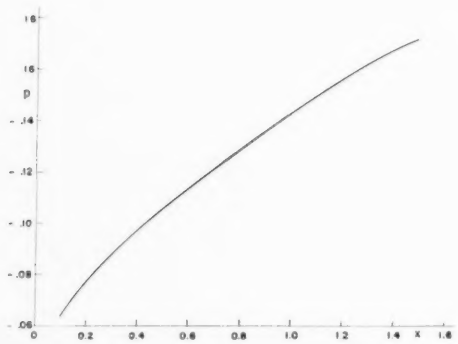

FIG. 7. Disturbance pressure variation on body.

Following Ferri[6] and earlier writers, we may assume that small disturbances to the steady supersonic motion of a body of revolution at zero incidence only involve zero and first-order harmonics in ψ.

Then

$$a_n = 0 \quad \text{for} \quad n > 1$$

and we obtain the following relation for a_1 from Eq. (4.2):

$$a_1 F_x^1 \sin\theta - a_1 F_y^1 \cos\theta = u_1 \cos\theta \qquad (4.3)$$

The function F^1 and its derivatives in Eq. (4.3) are evaluated at the surface, and derivatives with respect to x and y can be replaced by derivatives with respect to α and β according to Eqs. (3.9) and (3.10).

(5) Application

To represent the effect of an afterbody on a blunt-nosed projectile in hypersonic flight, the above technique is applied to calculate stability derivatives on an open-ended converging conical duct. Only the external flow field is considered since this is independent of the internal flow. The main-stream flow conditions are chosen to simulate the local conditions applying on an afterbody of a hypersonic projectile. We therefore consider the flow field near the duct in a uniform stream of Mach Number 3.05. The dimensions of the duct are shown in Fig. 2. The radius of the upstream section is 1 ft., its length is 1.5 ft. and the semiangle of the cone is 20°.

We first calculate the undisturbed flow field. This is illustrated in Fig. 3. At the forward rim of the duct the flow turns through a centered expansion which, in the limit, at the rim itself, tends to a Prandtl-Meyer expansion. Starting from uniform conditions on the forward characteristic of the fan 1.0–0148, the equations of steady isentropic flow for a perfect gas with $\gamma = 1.2$ are integrated by the method of characteristics up to the final ray of the fan 1.0–13. The method of characteristics is then applied to calculate the flow field near the surface of the duct satisfying initial conditions just found along the line 1.0–13 and boundary conditions on the surface.

This preliminary calculation determines the geometry of the characteristic network of lines α = constant, β = constant and data relating to the undisturbed flow at network points. We now know the independent variables and coefficients in the potential equation governing perturbations of this basic flow field. To calculate a stability derivative, C_{M_α}, for example, we consider the change in the basic flow pattern introduced by setting the duct at a small angle of incidence ϵ. The disturbance potential can be represented by a single term

$$F_1(\alpha, \beta) \cos\psi$$

where F_1 satisfies Eq. (3.20) with $n = 1$. This simplifies to the form

$$\frac{F_{\alpha\beta}}{h_\alpha h_\beta} + \left[\frac{\{2\cos 2\mu - (\gamma-1)\}}{\sin^2\mu\{(\gamma-1)+2\sin^2\mu\}}\frac{\partial\mu}{h_\beta\partial\beta} + \frac{\sin(\theta-\mu)}{2y}\right]\frac{F_\alpha}{h_\alpha} + \left[\frac{\{2\cos 2\mu - (\gamma-1)\}}{\sin^2\mu\{(\gamma-1)+2\sin^2\mu\}}\frac{\partial\mu}{h_\alpha\partial\alpha} + \frac{\sin(\theta+\mu)}{2y}\right]\frac{F_\beta}{h_\beta} + \frac{\sin^2\mu}{y^2}F = 0 \quad (5.1)$$

where the suffix 1 has been dropped. Eq. (5.1) is integrated by a method of characteristics over the basic flow field. The boundary conditions are (1) on the leading characteristic, the disturbance is uniform so that F_α and F_β are constant, (2) at the corner, the perturbed flow tends to a Prandtl-Meyer flow, and (3) on the afterbody surface the normal velocity component is zero.

The integration of Eq. (5.1) by a method of characteristics over a known network is much easier than the process required to determine the basic flow field. It leads to values of F_α and F_β on the afterbody surface from which we can calculate the changes in surface pressure and, hence, the value of $C_{M\alpha}$.

The results of calculating the steady perturbations are shown in Figs. 4–7. Figs. 4 and 5 show the basic pressure variation in the fan and on the body surface. The pressure decreases through the expansion fan and increases along the body, primarily due to the increased effect of the radial term. Figs. 6 and 7 show the corresponding disturbance pressures, expressed as coefficients of $\cos\psi$ for unit angle of incidence.

When the surface pressure distributions are integrated, it is found that

$$C_{N\alpha} = 1.157, \quad C_{M\alpha} = -0.1127 \quad (5.2)$$

In a definition of these coefficients, the maximum diameter of the duct (2 ft.) is used as the reference length, and the maximum cross-sectional area (π sq. ft.) is used as the reference area. Moments are taken about the horizontal diameter in the forward face and counted as positive when tending to depress the base.

To determine dynamic stability derivatives, for example, $C_{M\dot\alpha}$ and $C_{N\dot\alpha}$, we consider the perturbation due to vertical plunging motion of the body of small amplitude and low frequency. The equation for disturbance potential is then, in dimensionless form,

$$\frac{F_{\alpha\beta}}{h_\alpha h_\beta} + \left[\frac{2i\nu\sin\mu}{Q\sin 2\mu} + \left\{\frac{[2\cos 2\mu - (\gamma-1)]}{\sin^2\mu[(\gamma-1)+2\sin^2\mu]}\frac{\partial u}{h_\beta\partial\beta} + \frac{\sin(\theta-\mu)}{2y}\right\}\right]\frac{F_\alpha}{h_\alpha} + \left[\frac{2i\nu\sin\mu}{Q\sin 2\mu} + \left\{\frac{[2\cos 2\mu - (\gamma-1)]}{\sin^2\mu[(\gamma-1)+2\sin^2\mu]}\frac{\partial\mu}{h_\alpha\partial\alpha} + \frac{\sin(\theta+\mu)}{2y}\right\}\right]\frac{F_\beta}{h_\beta} + \left[\frac{\sin^2\mu}{y^2} - \frac{\nu^2\sin\mu}{QC} - \frac{i\nu Q}{\sin\mu}\left(\frac{\partial\mu}{h_\alpha\partial\alpha} + \frac{\partial\mu}{h_\beta\partial\beta}\right)\right]F = 0 \quad (5.3)$$

where $F = f + ivg$, and ν is the reduced frequency. We equate real and imaginary parts in Eq. (5.3), neglecting terms of order ν^2. We find that the equation for f is the same as the equation for F in steady flow—namely,

$$L(f) \equiv (f_{\alpha\beta}/h_\alpha h_\beta) + a(f_\alpha/h_\alpha) + b(f_\beta/h_\beta) + (\sin\mu/y^2)f = 0 \quad (5.4)$$

where a, b are the appropriate coefficients in Eq. (5.1). The equation for g is

$$(g_{\alpha\beta}/h_\alpha h_\beta) + (1/Q\cos\mu)(f_\alpha/h_\alpha) + (ag_\alpha/h_\alpha) + (1/Q\cos\mu)(f_\beta/h_\beta) + (bg_\beta/h_\beta) - (Q/\sin\mu)[(\partial\mu/h_\alpha\partial\alpha) + (\partial\mu/h_\beta\partial_\beta)]f + (\sin^2\mu/y^2)g = 0 \quad (5.5)$$

or

$$L(g) = -(1/Q\cos\mu)[(f_\alpha/h_\alpha) + (f_\beta/h_\beta)] + (Q/\sin\mu)[(\mu_\alpha/h_\alpha) + (\mu_\beta/h_\beta)]f \quad (5.6)$$

The boundary conditions for the function f are the same as those for F in steady flow. We have

$$f_\alpha/h_\alpha = -\sin\mu, \quad f_\beta/h_\beta = \sin\mu \quad (5.7)$$

on the leading characteristic, and

$$(f_\alpha/h_\beta) - (f_\beta/h_\beta) = -2\sin\mu\cos\theta$$

at the corner or on the surface of the duct.

The corresponding boundary conditions for g are

$$g_\alpha/h_\alpha = g_\beta/h_\beta = 0 \quad (5.8)$$

on the leading characteristic, and

$$(g_\alpha/h_\alpha) - (g_\beta/h_\beta) = 0 \quad (5.9)$$

at the corner or on the surface of the duct.

This analysis shows that the calculation of dynamic stability derivatives can be achieved by a simple extension of the program for finding static derivatives. The numerical work was carried out by Mr. J. Morriello.

References

[1] Tobak, Murray, and Wehrend, William R., *Stability Derivatives of Cones at Supersonic Speeds*, NACA TN 3788, 1956.

[2] Ribner, Herbert S., and Malvestuto, Frank S., Jr., *Stability Derivatives of Triangular Wings at Supersonic Speeds*, NACA TR 908, 1948.

[3] Holt, Maurice, *The Method of Characteristics for Steady Supersonic Rotational Flow in Three Dimensions*, J. Fluid Mech., Vol. 1, Part 4, p. 409, 1956.

[4] Howarth, L., *Modern Developments in Fluid Dynamics, High Speed Flow*, Vol. 1, Chapter III, pp. 73–104, Oxford at the Clarendon Press, 1953.

[5] Courant, R., and Hilbert, D., *Methoden der Mathematischen Physik, Band II*, Berlin, 1937.

[6] Ferri, Antonio, *The Method of Characteristics for the Determination of Supersonic Flow over Bodies of Revolution at Small Angles of Attack*, NACA TR 1044, 1951.

An Investigation of Optimal Zoom Climb Techniques†

HENRY J. KELLEY*

Grumman Aircraft Engineering Corporation

Summary

The problem of optimal zoom climb maneuvering of a turbojet aircraft has been investigated using the Mayer formulation of the calculus of variations. The Euler-Lagrange equations governing optimum symmetric flight have been integrated numerically by digital computation.

Discontinuities in thrust arising from turbojet afterburner blowout have been treated, and conditions which must be satisfied across the interface generated by the discontinuity have been derived.

Arbitrary control techniques have been compared with the optimum, and it has been found that performance is relatively insensitive to piloting technique unless a time limitation is imposed which requires high maneuvering load factors.

Symbols

J	=	functional to be minimized
F	=	integrand of functional
t	=	time
$G_{1,2,3}$	=	subsidiary differential expressions
$\bar{F}$	=	modified integrand defined by Eq. (6)
$\lambda_{1,2,3}$	=	multiplier variables
P	=	function of final values of variables
H	=	constant defined by Eq. (19)
V	=	true air speed
γ	=	flight path angle (see Fig. 1)
h	=	altitude
W	=	weight
α	=	angle of attack (see Fig. 1)
T	=	thrust
D	=	drag
L	=	lift
g	=	acceleration of gravity
$u(x)$	=	Heaviside step function
$\delta(x)$	=	Dirac delta function
ϕ	=	function defined by Eq. (33)
h_e	=	energy height, defined by Eq. (41)

Introduction

ALTHOUGH the problems of optimizing climb and range performance have been studied on a steady-state basis since the beginnings of flight, it is only in relatively recent years that the more general problem, in which forward and normal accelerations are taken into account, has received attention in applications to high-performance aircraft and missiles. It was, in fact, near the end of World War II, when the German jet interceptor Me262 came into flight test status, that it was recognized that the amounts of time and fuel expended in accelerating to combat air speed during climb had become appreciable in relation to those required for the climb to altitude itself, and that a departure from the aerodynamicist's "maximum rate-of-climb" concept was in order.

This was first noted by Lippisch[2] in a study of performance calculation methods for jet-propelled aircraft. He pointed out that the optimum climb scheduling problem is essentially one of the calculus of variations, but it was for his colleague Kaiser[3] at Messerschmitt A.G. to derive and propose the technique which has since become widely referred to as the "energy climb" schedule.

This was accomplished outside the framework of the calculus of variations by virtue of an assumption that drag can be represented as a function of air speed and altitude only, on the basis of lift = weight. Under this simplifying assumption the optimization problem proved to be tractable by relatively simple methods. The $L = W$ approach has been examined by many investigators subsequently—e.g., Lush,[4] Garbell,[5] Rutowski,[6] and Miele[7]—and the resulting solutions in most cases exhibit sufficiently small path curvature and slope over a central portion of the path as to be reasonably compatible with the basic assumption. Certain portions of the solutions comprising vertical climbing and diving flight, however, must be excluded from consideration on the basis of conflict with the $L = W$ assumption, and this leaves the simplified approach incapable of handling cases in which initial or final points off the central path are specified.

The popularity of the simplified approach as exemplified by the "energy climb" concept still persists, and, notwithstanding the fact that results so obtained are of considerable practical interest from an engineering viewpoint, the real reason for this is undoubtedly that when the "refinement" of realistic drag representation is brought in, the resulting equations arising from variational treatment present a task of solution which is more complex by an order of magnitude.

The first serious efforts at attacking the optimum flight path problem by means of the calculus of variations were made at the RAND Corporation in the late 1940's, starting with the work of E. M. Liebhold.[1]

Presented at the Aerodynamics—III Session, IAS 27th Annual Meeting, N. Y., Jan. 26–29, 1959.

† This paper is based on a section of a New York University doctoral thesis,[1] the numerical portions of which were sponsored by Grumman Aircraft Engineering Corp. The writer is indebted to Dr. Frank Lane, faculty adviser, for much helpful advice and encouragement. The assistance of Gerald Taylor and Mrs. Lilly Baach of Grumman's Research Department in computer programing and preparation of results in figure form is gratefully acknowledged.

* Section Leader—Systems Research, Research Department.

A short time later, a very general and rigorous formulation of the problem for paths of least time was given by a consultant to RAND, Dr. Magnus R. Hestenes, a mathematician of first rank in the field of calculus of variations.[9]

An analog computer exploration of solutions of the Euler equations governing optimum paths was then made at RAND by Mengel,[10] revealing serious difficulties associated with the fact that solutions are extremely sensitive to variations in initial conditions imposed on the Euler multiplier variables. This means that multivariable problems attacked by analog or numerical integration procedures offer extreme difficulty in satisfaction of boundary conditions imposed on final values of the variables, a fact which seems to have discouraged efforts along this line, judging from the scarcity of published results.*

At about this time (1951), B. Garfinkel of the Aberdeen Ballistics Laboratory published his formulation of the optimum path problem in terms of the Mayer problem in the calculus of variations, a decisive step toward a unified theory in which problems of minimum time, maximum range or altitude, minimum fuel, etc., may all be treated with a single set of equations. Although this treatment[12] is sophisticated in many ways—e.g., handling of constraints and data discontinuities—it is interesting to note that the acceleration effects which had originally been the spur for departure from the old steady-state methods were omitted.

In more recent years, the prolific investigators Cicala and Miele, often in collaboration, have dominated the field with their contributions. Although these are too numerous to catalog in these introductory remarks, special attention should be drawn to Miele's powerful analytical Green's theorem approach which he has exploited in cases reducible to two variable problems,[7, 13] and to the fundamental work of Cicala on the Mayer formulation[14] and on phenomena of discontinuous solutions.[15]

Theoretical Analysis

In the present paper we are concerned with an application of the theory in which maneuvering drag plays so dominant a role as to preclude simplified analysis of the $L = W$ type. The case of interest is the zoom climb maneuver of a turbojet powered aircraft, a tactic of practical interest in interception of high flying targets where efficient conversion of kinetic to potential energy is sought.

In the study of zoom climb paths we must deal with a discontinuity in thrust arising from afterburner blowout, the well-known characteristic of a turbojet afterburner to cease functioning above a certain altitude. The thrust is then a discontinuous function of air speed and altitude known a priori; it does not possess partial derivatives with respect to these variables along the blowout boundary in the V-h plane. Since the partial derivatives of thrust enter the Euler-Lagrange equations governing optimal flight, a special treatment of conditions prevailing across this boundary is required. This situation is to be carefully distinguished from the more commonly occurring case of discontinuities arising in the unknown functions which are to be found in the course of solution.

The work of reference 1, upon which this paper is based, contains a fairly detailed derivation of the Euler-Lagrange equations featuring a parametric formulation of the problem as one of Mayer type. For the sake of brevity in the present paper it seemed advisable to simplify as far as possible. To this end we have omitted the range and fuel consumption variables appearing in more general cases and abandoned the use of a parameter in the role of independent variable as unessential to the application at hand. We will no more than sketch out the derivation of the Euler-Lagrange equations for optimal flight, since this matter has been amply covered in the literature.[9, 14, 16, 17] On the question of natural boundary and transversality conditions, we will simply state the well-known results for completeness; the reader is referred to the work of Cicala[14] and Miele[13] for discussion of this and of the advantages of the Mayer formulation.

Equations of Motion

The following system of equations for flight in the vertical plane has been "tailored" to minimum complexity in our turbojet zoom climb application by means of a number of assumptions which hold reasonably well for this case: (1) weight sensibly constant over the short zoom interval, (2) thrust component normal to the flight path negligible, and (3) effects of Earth's curvature, rotation, and gravity variation with altitude negligible.

Acceleration tangential to the path:

$$G_1 = -\dot{V} + (g/W)(T - D) - g \sin \gamma = 0 \quad (1)$$

Acceleration normal to the path:

$$G_2 = -\dot{\gamma} + (gL/WV) - (g/V) \cos \gamma = 0 \quad (2)$$

Altitude:

$$G_3 = -\dot{h} + V \sin \gamma = 0 \quad (3)$$

The coordinates and axis system employed are illustrated in Fig. 1.

Formulation of the Optimum Path Problem

A general statement of the optimum flight path problem may be given in terms of an integral

$$J = \int_{t_0}^{t_f} F \, dt \quad (4)$$

* It is understood that Prof. D. O. Dommasch has undertaken numerical work under sponsorship of USAF Wright Air Development Center; circulation seems to be restricted by safeguards on proprietary rights on contractor's data as well as by security classification. Professor Dommasch's earlier published analysis[11] appears not to have taken advantage of the previous RAND work.

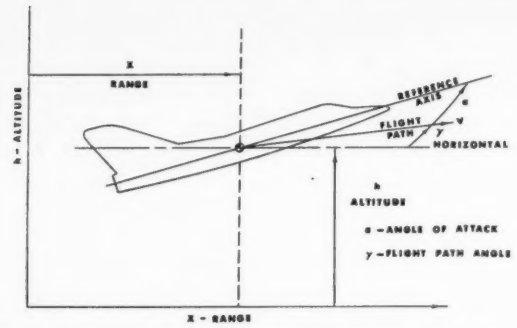

FIG. 1. Coordinates and axis system for symmetric flight.

representing some quantity whose maximum or minimum or, in general, stationary value (extremum) is sought along with the argument functions upon which the integrand F depends. The integral J is termed a functional, since it clearly depends on the entire course of the argument functions rather than on a number of discrete variables.

By a suitable choice of sign for the integrand F, we can, if we wish, always state our problem in terms of a minimum problem—i.e., by simply changing the sign of F if we are actually seeking a maximum. This is no more than an arbitrary sign convention; once a set of functions have been found which render J stationary, we must look further to ascertain whether the stationary value is indeed a minimum, just as in minimum problems of elementary calculus.

The functions upon which F depends are, in the present case, the variables V, γ, h, and the control variable α, angle of attack. These are, of course, not free of choice but subject to the subsidiary conditions represented by the three equations of motion (1), (2), and (3).

Further restrictions on the problem variables may be imposed in terms of prescribed boundary values. These may be statements of fixed values, or they may be expressed by equations relating initial or final values of the variables. There is obviously a limit to the number of boundary conditions which may be imposed in a reasonable problem, and this matter will be discussed subsequently. Where fewer boundary conditions than this limiting number are actually imposed, the problem is said to have partially "free" boundary values. An unspecified or "open" boundary condition on a particular variable requires that the most favorable boundary value of that variable be determined as part of the extremum problem.

A number of additional requirements must be met as necessary that the problem as stated actually possess a solution, and these range from the obvious one that the subsidiary and boundary conditions be noncontradictory to more subtle considerations on continuity and differentiability of the integrand and the variables of the problem. Even rather stringent conditions of this latter type do not provide insurance against degeneracy and nonexistence of a true extremum. In spite of continuing mathematical effort over the years, it is no simple matter to determine a priori whether or not a problem is reasonable—i.e., whether a solution actually exists. Even after a set of functions which make J stationary have been found, the investigation of the extremal character of this solution is often far from straightforward.

This is particularly true when the matter of boundary conditions is under question, for it is not difficult to demonstrate cases in which moderate changes in boundary values transform a legitimate problem into one for which no solution exists. Examples of apparently reasonable variational problems which do not have solutions are to be found in the lecture notes of Courant.[18]

Since the main interest of the following brief treatment lies in the formalism of the Mayer approach, it will be assumed in this section that the integrand and problem variables possess as many differentiability properties as may be necessary to avoid difficulty. In so doing, it is not intended to imply that troubles of continuity are unlikely to occur in cases of interest, for rather the reverse is true in many practical applications of the theory. We will later examine the situation arising in the case of discontinuous thrust.

The Multiplier Rule

With a formal similarity to the Lagrange multiplier technique of differential calculus, we may now restate the minimum problem in terms of a single integral without subsidiary conditions:

$$J = \int_{t_0}^{t_f} \bar{F}\, dt \tag{5}$$

in which

$$\bar{F} = F + \lambda_1 G_1 + \lambda_2 G_2 + \lambda_3 G_3 \tag{6}$$

The functional J is now to be made stationary with respect to the same functions V, γ, h, and α plus the additional functions λ_1, λ_2, and λ_3. For background information on the multiplier rule we refer the reader to the texts of Courant[19] and Bliss.[20]

The Euler-Lagrange Equations

We will omit the derivation of necessary conditions by the vanishing of the first variation of the integral J, referring the reader to reference 1 or the literature previously cited. A principal result may be stated briefly as follows: the *variational derivative* of $\bar{F}$ with respect to each variable must vanish.

$$[\bar{F}]_V = (\partial\bar{F}/\partial V) - (d/dt)(\partial\bar{F}/\partial\dot{V}) = 0 \tag{7}$$

$$[\bar{F}]_\gamma = (\partial\bar{F}/\partial\gamma) - (d/dt)(\partial\bar{F}/\partial\dot{\gamma}) = 0 \tag{8}$$

$$[\bar{F}]_h = (\partial\bar{F}/\partial h) - (d/dt)(\partial\bar{F}/\partial\dot{h}) = 0 \tag{9}$$

$$[\bar{F}]_\alpha = (\partial\bar{F}/\partial\alpha) - (d/dt)(\partial\bar{F}/\partial\dot{\alpha}) = 0 \tag{10}$$

Since the derivatives of the λ multiplier variables do not appear in $\bar{F}$, the variational derivatives of $\bar{F}$ with respect to the λ's are merely the ordinary derivatives;

the vanishing of these quantities reproduces the original subsidiary equations (1), (2), and (3).

The preceding Euler-Lagrange equations apply for a general integrand $\bar{F}$ which is free of derivatives higher than the first. That part of $\bar{F}$ associated with the subsidiary conditions need not contain such higher derivatives, for these conditions can always be written in first-order form, if necessary by the introduction of additional variables.

We shall consider only cases in which the quantity to be minimized depends entirely on final values of the problem variables:

$$J = P(V_f, \gamma_f, h_f, \alpha_f, t_f) \tag{11}$$

The integrand F in such cases may be expressed as

$$F = (d/dt)P(V, \gamma, h, \alpha, t) \tag{12}$$

(Assuming that initial values are fixed, it is clear that minimizing $P_f - P_0$ is the same as minimizing P_f.) The form of F is then

$$F = (\partial P/\partial V)\dot{V} + (\partial P/\partial \gamma)\dot{\gamma} + (\partial P/\partial h)\dot{h} + (\partial P/\partial \alpha)\dot{\alpha} + (\partial P/\partial t) \tag{13}$$

Thus, the integrand will in the cases considered be free of higher derivatives of the problem variables, and the Euler-Lagrange equations as written above will apply.

It is significant that the variational derivative of Eq. (13) with respect to each problem variable *vanishes identically*, as may be verified directly. This is a simple consequence of the fact that an integral representation is unnecessary in these cases where J depends only on final values, except as a matter of convenience in treatment of the subsidiary differential conditions.

This special case in which the quantity to be minimized depends on final (or initial) values only is known as the Mayer problem. It is characterized by the fact that the Euler equations are the same regardless of the function to be minimized. Such a formulation has obvious merit in development of a unified theory allowing treatment of a variety of problems in that a single set of equations may be employed.

The Mayer formulation, moreover, is considerably more general than might at first appear (see Bliss,[20] Part II, Section 69). In fact, in cases where the integrand F is of a more general form than was assumed in Eq. (12), we may introduce an additional variable x defined by

$$-(dx/dt) + F = 0 \tag{14}$$

and then regard the problem as one of minimizing x_f subject to Eq. (14) as a subsidiary condition, thus converting the problem to one of Mayer type. The only complication arising from such a procedure is that F may not be linear in the derivatives of the variables, or that it may contain higher derivatives; these, however, do not constitute essential difficulties.

The Euler-Lagrange equations corresponding to Eqs. (7), (8), (9), and (10) in the present example are the following:

Airspeed V:

$$\dot{\lambda}_1 + \lambda_1(g/W)(\partial/\partial V)(T - D) + \lambda_2[(g/W)(\partial/\partial V)(L/V) + (g/V^2)\cos\gamma] + \lambda_3 \sin\gamma = 0 \tag{15}$$

Flight Path Angle γ:

$$\dot{\lambda}_2 - \lambda_1 g\cos\gamma + \lambda_2(g/V)\sin\gamma + \lambda_3 V\cos\gamma = 0 \tag{16}$$

Altitude h:

$$\dot{\lambda}_3 + \lambda_1(g/W)(\partial/\partial h)(T - D) + \lambda_2(g/WV)(\partial L/\partial h) = 0 \tag{17}$$

Angle of Attack α:

$$-\lambda_1(g/W)(\partial D/\partial\alpha) + \lambda_2(g/WV)(\partial L/\partial\alpha) = 0 \tag{18}$$

A first integral of this system exists in the case where the known functions appearing in the equations of motion do not depend explicitly on the independent variable t (see reference 1):

$$H = \lambda_1\dot{V} + \lambda_2\dot{\gamma} + \lambda_3\dot{h} = \text{constant} \tag{19}$$

This often proves convenient in computations either as a check or as a replacement for one of the other Euler equations.

Boundary Conditions

The system of Euler equations including the equations of motion is of sixth order in the aggregate and, according to the usual rules, this permits specification of six initial and final conditions. In a case where initial and final values of the independent variable t are fixed, for example, this suggests the possibility of specifying both initial and final values of the variables V, γ, and h. Were this permissible, it would imply that the value of a functional J depending in a particular case, say, on final values of V, γ, and/or h could be chosen beforehand.

A closer inspection of the Euler equations, however, shows that this is not the case because of their linearity and homogeneity in the λ variables. This means that imposition of three boundary variables on the λ's is not equivalent mathematically to specifying the same number on the other problem variables, since only ratios of the λ variables are of importance. It can be seen that multiplying the boundary values of the λ variables by a constant factor, for example, would have no effect on the solution for the problem variables.

The gist of this matter is that the effective order of the set of equations in the λ's is one less than the apparent order. This is demonstrated by means of a transformation of variables in reference 1. This phenomenon associated with the homogeneity of the Euler equations in the λ variables arises whenever the Mayer formulation is employed.

Thus, it appears that a maximum of five boundary conditions can be imposed on the problem variables according to the physical situation of interest. For a discussion of the effects of leaving certain variables unspecified—i.e., imposing less than the maximum permissible number of boundary conditions—the reader

is referred to reference 1 and the papers mentioned earlier. In the simple cases where the functional to be minimized is identified with the final value of a problem variable or that of the independent variable t, the requirements are simply the following:

(1) If the final value of the problem variable is left open, the corresponding λ has the final value zero. If the final value is to be a minimum, the corresponding λ has the final value unity.

(2) If the final value of the independent variable (time in the present example) is left open, the quantity H has the value zero. If time is to be minimized, then $H = -1$.

It should be noted that seeking a minimum final value for any expression depending explicitly on the control variable (α in the present case), such as the variable itself, for example, does not constitute a "reasonable" problem, owing to the fact that the control variable is capable of discontinuous behavior.

In connection with these remarks on boundary values, we take the opportunity to observe the following important fact: *every solution of the system of equations represents the solution of several problems*, depending on which boundary values are regarded as having been specified. Thus, as long as the final value of the λ corresponding to a particular variable is nonzero (or $H \neq 0$ in the case of t), the time history can be regarded as representing a case in which the final value of the variable has been made stationary. This is a result of the fact previously mentioned that the λ variables can be multiplied by any desired constant without affecting the solution for the problem variables. This is another interesting attribute of the Mayer formulation in which the same set of equations applies regardless of which variable's final value is to be extremized.

Treatment of Thrust Discontinuity: Afterburner Blowout

The following treatment of thrust as a discontinuous function of air speed and altitude employs the method of the Dirac delta function. This powerful technique has only in recent years been placed on a firm mathematical basis.[21, 22]

Its use in the present application necessitates interpretation of the infinite discontinuities arising from the partial derivatives of thrust in the Euler equations in terms of symbolic functions. In order to make our operations legitimate, we should return to the integral form, the first variation, from which the Euler equations were derived. This approach has been adopted in reference 1; for present purposes we shall apply a less rigorous but more direct treatment to the Euler equations themselves.

We first define the Heaviside unit step function

$$u(x) = 0, \qquad x < 0 \tag{20}$$

$$u(x) = 1, \qquad x > 0 \tag{21}$$

The derivative of u does not exist at the point of discontinuity. If a function $\delta(x)$ is imagined as having $u(x)$ as its first integral,

$$u(x) = \int_{-\infty}^{x} \delta(\xi)d\xi \tag{22}$$

this function would necessarily be zero for all $\xi \neq 0$, and would be required to be infinite at $\xi = 0$ in such a way as to produce a unit integral for $x > 0$. Such a definition is not satisfactory mathematically. The usefulness of the delta function, however, has been such as to stimulate mathematical endeavor justifying the employment of this symbol. Schwartz's theory allows its use as a *symbolic function*,[21] with the interpretation that when multiplied by a continuous function and integrated from $-\infty$ to $+\infty$,

$$\int_{-\infty}^{\infty} \phi(\xi)\ \delta(\xi)d\xi = \phi(0) \tag{23}$$

the delta function picks out the value of the function at the origin. (See Friedman[22] for a detailed treatment of symbolic functions.) Thus, the "values" of $\delta(x)$ are never in themselves considered, but only the values of integrals involving the function.

In the case of a turbojet afterburner (or ramjet) subject to blowout beyond some boundary of altitude and air speed, the thrust may be thought of as being represented by two functions, $T_1(h, V)$ and $T_2(h, V)$, the second replacing the first as the boundary $h = h^*(V)$ is crossed, as in Sketch 1.

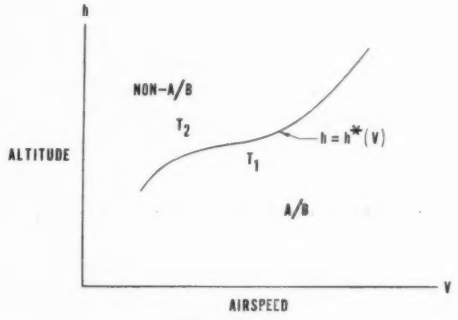

SKETCH 1.

The discontinuity at $h = h^*$ may be represented as in Sketch 1 by means of the Heaviside unit step function:

$$\left.\begin{aligned} T &= T_1(h, V)[1 - u(h - h^*)] + \\ &\qquad T_2(h, V)[u(h - h^*)] \\ &= T_1(h, V) + \Delta T u(h - h^*) \end{aligned}\right\} \tag{24}$$

Partial derivatives of thrust may then be represented symbolically in terms of delta functions:

$$\begin{aligned} \partial T/\partial h = {} & (\partial T_1/\partial h)[1 - u(h - h^*)] + \\ & T_1[-\delta(h - h^*)] + (\partial T_2/\partial h)[u(h - h^*)] + \\ & T_2[\delta(h - h^*)] \end{aligned} \tag{25}$$

$$\begin{aligned} \partial T/\partial V = {} & (\partial T_1/\partial V)[1 - u(h - h^*)] + \\ & T_1[(dh^*/dV)\delta(h - h^*)] + (\partial T_2/\partial V)u(h - h^*) + \\ & T_2[-(dh^*/dV)\delta(h - h^*)] \end{aligned} \tag{26}$$

These partials appear in two Euler equations as follows:

$$\dot{\lambda}_1 + \lambda_1(g/W)(\partial T/\partial V) + \ldots = 0 \tag{27}$$

$$\dot{\lambda}_3 + \lambda_1(g/W)(\partial T/\partial h) + \ldots = 0 \tag{28}$$

Special care in handling the terms containing the partials must be exercised in this case because the factor λ_1 has a finite discontinuity which would prevent evaluation of an integral containing it in product with a delta function.

With the first equation this difficulty may be avoided by dividing through by λ_1 before integrating.

$$\int_{h^{*-}}^{h^{*+}} (\dot{\lambda}_1/\lambda_1)dh + \int_{h^{*-}}^{h^{*+}} (g/W)(\partial T/\partial V)dh + \ldots = 0 \tag{29}$$

$$[\dot{h}^* \ln \lambda_1]_{h^{*-}}^{h^{*+}} + [(g/W)(T_1 - T_2) \times (dh^*/dV)u(h - h^*)]_{h^{*-}}^{h^{*+}} = 0 \tag{30}$$

$$\dot{h}^* \ln (\lambda_1^{*+}/\lambda_1^{*-}) + (g/W)(T_1 - T_2)(dh^*/dV) = 0 \tag{31}$$

The behavior of λ_1 through the thrust discontinuity may then be expressed as

$$\lambda_1^{*+} = \lambda_1^{*-}e^{\phi} \tag{32}$$

where

$$\phi = g(T_2 - T_1)(dh^*/dV)/W^*\dot{h}^* \tag{33}$$

Treatment of the Euler equation for λ_3 cannot be similarly implemented. However, consideration of the combination

$$\dot{\lambda}_1 + (dh^*/dV)\dot{\lambda}_3 + (g/W)[(\partial T/\partial V) + (dh^*/dV)(\partial T/\partial h)]\lambda_1 + \ldots = 0 \tag{34}$$

recommends itself as an alternative because of this expression's freedom from delta function terms. The bracketed quantity is proportional to the derivative of thrust in a direction tangential to the blowout curve $h = h^*(V)$, and, hence, exhibits no worse misbehavior than a jump discontinuity:

$$(\partial T/\partial V) + (dh^*/dV)(\partial T/\partial h) = [(\partial T_1/\partial V) + (dh^*/dV)(\partial T_1/\partial h)]\,[1 - u(h - h^*)] + [(\partial T_2/\partial V) + (dh^*/dV)(\partial T_2/\partial h)][u(h - h^*)] \tag{35}$$

Since the combined equation (34) is free of delta functions, it follows that the λ combination

$$\lambda_1 + (dh^*/dV)\lambda_3 \tag{36}$$

is continuous, and, therefore,

$$\lambda_1^{*+} + (dh^*/dV)\lambda_3^{*+} = \lambda_1^{*-} + (dh^*/dV)\lambda_3^{*-} \tag{37}$$

and

$$\lambda_3^{*+} = \lambda_3^{*-} - [1/(dh^*/dV)]\lambda_1^{*-}(e^{\phi} - 1) \tag{38}$$

which is the desired relation for behavior of λ_3 at blowout.

It may be of interest to examine this for small slope of the blowout boundary dh^*/dV. Expanding the exponential in powers of its argument,

$$\Delta\lambda_3 = \lambda_3^{*+} - \lambda_3^{*-} = -[\lambda_1^{*-}/(dh^*/dV)] \times [1 + \phi + (\phi^2/2) + \ldots - 1] = -\lambda_1^{*-}\{[\phi/(dh^*/dV)] + [\phi^2/2(dh^*/dV)] + \ldots\} \tag{39}$$

For $dh^*/dV = 0$, corresponding to blowout with altitude only at $h = h^*$, λ_1 is continuous, since $\phi = 0$, and

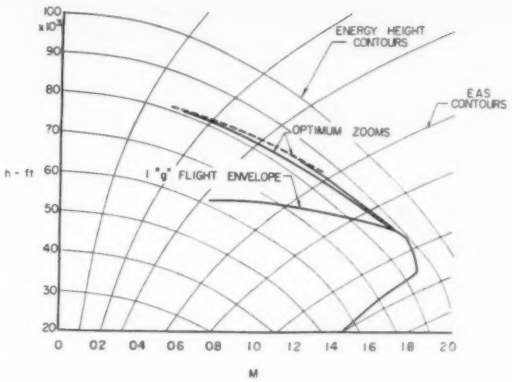

FIG. 2. Optimum zoom climb trajectories.

$$\Delta\lambda_3 = -\lambda_1^*[g(T_2 - T_1)/W^*\dot{h}^*] \tag{40}$$

Interception Tactics

The advent of bomber aircraft having supersonic performance capability has greatly intensified the difficulties of interceptor operations. The turbojet interceptor of the generation presently in development will usually attain its best speed performance at a lower altitude than its target, and will characteristically accelerate rather sluggishly once past the transonic drag rise owing to the small margin of thrust over drag typical of the supersonic region.

During the climb and acceleration, the interceptor will ordinarily have available only coarse and intermittent vectoring information provided by a ground control intercept (GCI) center. Only when the fighter's airborne intercept (AI) radar has acquired the target will sufficiently accurate information on target range, speed, direction, and altitude be forthcoming to permit initiation of an attack. Experience has shown that range limitations of the AI radar represent the greatest impediment to a successful intercept, and this is particularly true in nearly head-on situations where a high closing speed reduces the time available for maneuvering before firing of weapons.

Consequently, the interceptor pilot must attempt during the vectoring phase to situate himself as favorably as possible with regard to altitude and air speed so as to provide for last-minute contingencies. This will most often consist of approaching, and if possible attaining, the point of highest total energy (potential plus kinetic) on the interceptor's altitude - air-speed envelope. Thus, following detection and lock-on to the target, the pilot can decide how best to make use of this stored energy, whether it be in a final corrective turn, or in a zoom to bring a high-altitude target well within the effective range of the weapons.

Optimal Zoom Climbs

In Fig. 2 is shown the air-speed - altitude performance envelope of our example airplane. Points on the envelope are determined by equivalence of level flight drag and afterburning thrust. The rather well-defined

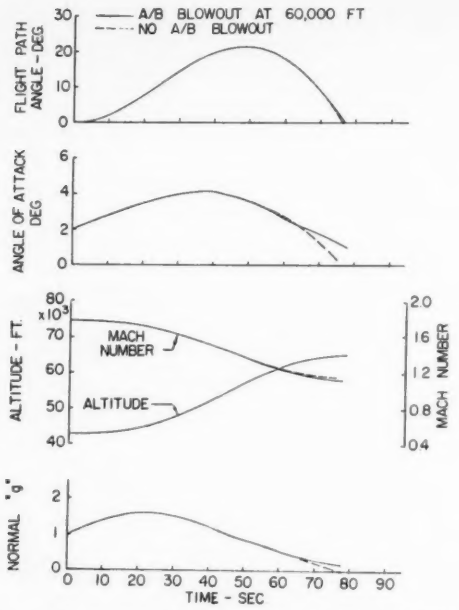

FIG. 3. Optimum zoom climb trajectory (air speed 177 knots equivalent air speed at maximum altitude).

maximum Mach Number point in the vicinity of 35,000 ft. is typical of turbojet aircraft as affected by change in the atmospheric characteristic to isothermal above the tropopause. The subsonic high-altitude portion of the envelope is representative of minimum air-speed flight at high angles of attack approaching buffet, and its usefulness is accordingly rather limited.

A family of curves representing various levels of the "energy height" quantity,

$$h_e = h + (V^2/2g) \tag{41}$$

are also shown, and the point of tangency of such a curve with the level flight performance envelope is the point of maximum total energy.

The technique of attack to be used following radar acquisition of the target will, in general, not lend itself to scheduling for optimum performance, owing to the pilot's necessary preoccupation with the radar display and the aiming and firing of weapons. It seems desirable, however, to investigate the character of optimum maneuvers for the purpose of determining whether or not departures from the optimum technique are accompanied by significant performance losses.

The rapid conversion of kinetic into potential energy in a zoom climb maneuver is a matter which has been the subject of much calculation, speculation, and flight-test activity in regard to the relative merits of various techniques. We will present in this section some results of optimum zoom calculations for our example airplane and compare the performance so attained with that for certain arbitrary schedules. The effect of loss of thrust augmentation through afterburner blowout will also be examined.

The set of Euler equations (15)–(18) in conjunction with the equations of motion have been solved numerically by a finite difference procedure on an IBM Model 650 calculator. The method employed is of the predictor-corrector type, a modification of Adams' method due to R. McGill of Grumman Aircraft.[23] This technique has proved itself versatile and accurate in a wide variety of applications.

With initial conditions on air speed, path angle, and altitude fixed at the values for level flight at the maximum energy point of the envelope, the set of equations has been integrated numerically for various initial values of the λ multiplier variables. As has been mentioned earlier, the solutions are dependent only upon ratios of these variables, and, accordingly, a two-parameter family of optimum flight paths depending upon initial λ_2/λ_1 and λ_3/λ_1 is obtained.

Zoom Climb Solutions With Time Open

The variety of optimum maneuvers included in this family is awesome—e.g., whip stalls, dives, partial loops. We therefore seek some means of confining the calculations to maneuvers of interest—namely, those terminating in level flight at a higher altitude than the initial one.

We note that the quantity H defined by Eq. (19) is constant in the present example since none of the functions of the problem depend on time explicitly. By tenporarily restricting our attention to the case $H = 0$, corresponding to no limitation on final time, we have the advantage of reducing our problem to exploration of a one-parameter family of solutions. In this particular case, since $\gamma(0) = 0$, this can be accomplished by fixing initial λ_2/λ_1 at the value appropriate to an angle of attack for level flight, as may be seen from an inspection of the equations.

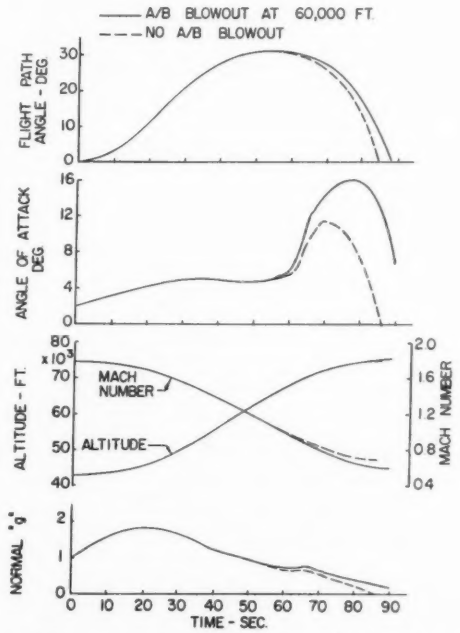

FIG. 4. Optimum zoom climb trajectory (air speed 74 knots equivalent air speed at maximum altitude).

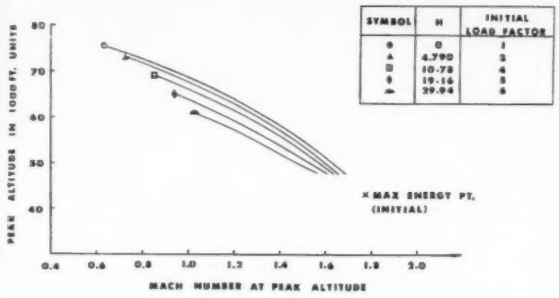

FIG. 5. Peak altitudes of optimum zoom programs.

The maneuvers of this family which are of practical interest happen to fall within a fairly narrow band of initial values of the remaining parameter, $0.01 < \lambda_{3_0}/\lambda_{1_0} < 0.02$. Loci of two of these zoom climb maneuvers in the h-V plane are shown in Fig. 2.

Although only two zoom paths have been shown in Fig. 2 for clarity, a considerable number of additional paths have been calculated. The points of apogee have been used to define the curve labeled as the absolute zoom climb ceiling.

The two representative maneuvers are shown in time history form in Figs. 3 and 4. These may be regarded as maximum altitude maneuvers for a given air-speed loss, or, alternately, as minimum speed loss zooms to particular final altitudes. The open condition on final time, $H = 0$, implies that imposition of any elapsed time restrictions different from those shown would result in less favorable conditions at apogee.

These maneuvers are evidently mild ones as far as steepness and acceleration are concerned. They do not appear to lend themselves to statements of simple rules for pilot instruction purposes. The considerable increase in angle of attack near the end of the higher altitude zoom (Fig. 4) is associated with transonic variations in aerodynamic characteristics. This occurs at a much reduced level of dynamic pressure (note curves of q and equivalent air speed of Fig. 2) and cannot be expected to exert an important result on apogee height.

Effect of Afterburner Blowout

In the calculations presented it has been assumed that the turbojet thrust characteristic switches from afterburning to nonafterburning at 60,000 ft. altitude, independent of air speed. The time history calculation has been stopped at this point, the thrust data changed, and an increment in λ_3 introduced according to the formula developed previously. In more realistic calculations, afterburner blowout as a function of both altitude and air speed would be introduced, and in this case both λ_1 and λ_3 would be treated as discontinuous at the blowout point as discussed earlier.

The effect of A/B blowout is indicated in Figs. 3 and 4 where the dashed curves shown for comparison have been calculated assuming sustained afterburning thrust. The difference is seen to be small even for the higher altitude zoom, the increment in apogee height being of the order of hundreds of feet rather than thousands. It seems evident that loss of afterburning would have greater effect on maneuvers intended to maintain altitude above the level flight envelope than it does on the short-term transient maneuvers presently under consideration.

Effect of Time Restrictions

Having thus located the λ_3 range of interest in the time open case, it has been found relatively easy to proceed in steps to cases for $H \neq 0$. Zoom climb ceilings for various values of H are presented in Fig. 5. A typical history of a restricted time zoom is shown in Fig. 6. This particular maneuver involves relatively high maneuvering load factor, about $4g$ initially.

Fig. 7 presents plots of kinetic energy at apogee for zooms to various altitudes as a function of total elapsed time. The reduction in final kinetic energy as the allotted time is reduced is seen to be gradual in the vicinity of the flat peaks at $H = 0$. This indicates that the matter of timing is not a particularly sensitive one as far as performance penalty is concerned, unless the variation from the optimum allotted time is large.

For purposes of presentation and discussion we have characterized the maneuvers as optimal in the sense of maximum speed or kinetic energy at the final point (apogee) with final altitude and time specified. We again call attention to the possibility of equivalent interpretations for the maneuvers as maximum altitude zooms for fixed final speed and time, or, for that matter, as minimum time zooms (if $H \neq 0$) to fixed final speed and altitude.

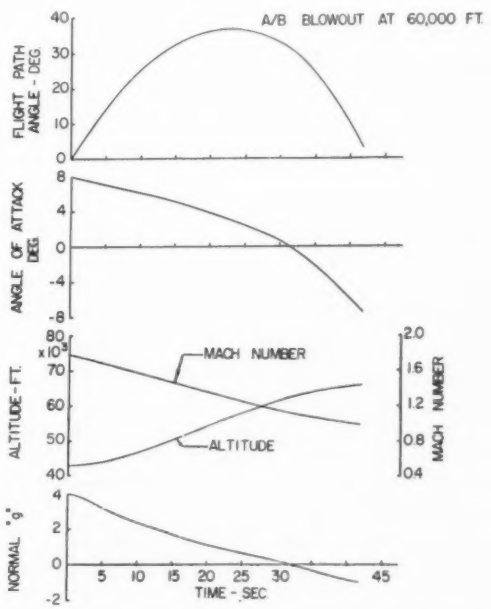

FIG. 6. Optimum zoom climb trajectory (air speed 153 knots equivalent air speed at maximum altitude).

Comparison of Optimum and Arbitrary Zoom Techniques

We have calculated for comparison a family of zoom maneuvers performed with load factor programs as sketched in the lower portion of Fig. 7. These have been called, for want of better terminology, piecewise constant load factor zooms. The programs consist of load factor constant at two different levels with a step function type of behavior in transition.

The results of these calculations are displayed in Fig. 5 by the coded points. The relatively mild $2g$ to $0g$ program compares favorably with optimum program results. This is an indication that details of piloting technique are not of great importance where the elapsed time is in the vicinity of the optimum.

The comparison is less favorable where time restriction requires larger maneuvering load factors, as shown by the $3g$ to $-1g$ points. These entail appreciably greater losses in kinetic energy than do optimum programs for the same elapsed time.

Fig. 8 presents a comparison of the optimum zoom ceiling with the vertical ascent solution of the simplified $L = W$ theory. Also shown is the envelope of the $2g$–$0g$ family of zooms. It is apparent that the simplified theory overestimates the performance attainable by an appreciable margin.

It may be concluded that performance losses in zoom climb maneuvers are not particularly sensitive to piloting technique unless fairly severe restrictions on elapsed time are imposed. A corresponding study for a rocket-augmented interceptor would be of interest in regard to future work of this kind.

References

[1] Kelley, H. J., *An Investigation by Variational Methods of Flight Paths for Optimum Performance*, Sc.D. Thesis, Guggenheim School of Aeronautics, New York University, May, 1958.

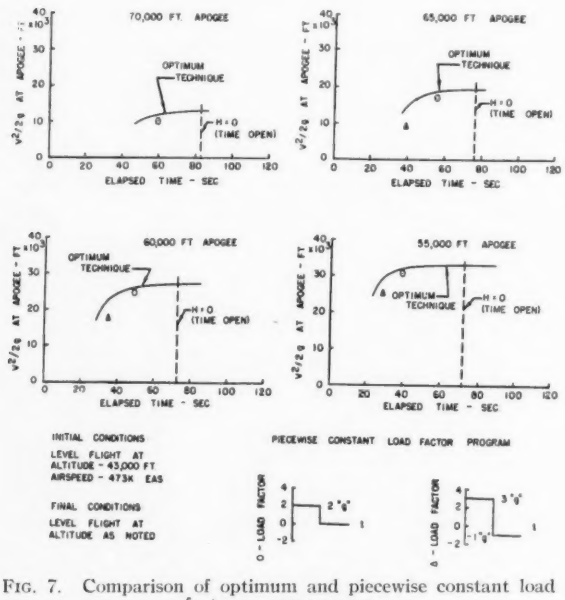
70,000 FT APOGEE
65,000 FT APOGEE
60,000 FT APOGEE
55,000 FT APOGEE
OPTIMUM TECHNIQUE
H = 0 (TIME OPEN)
ELAPSED TIME - SEC
INITIAL CONDITIONS
LEVEL FLIGHT AT ALTITUDE - 45,000 FT AIRSPEED - 473K EAS
FINAL CONDITIONS
LEVEL FLIGHT AT ALTITUDE AS NOTED
PIECEWISE CONSTANT LOAD FACTOR PROGRAM
O - LOAD FACTOR
Δ - LOAD FACTOR

FIG. 7. Comparison of optimum and piecewise constant load factor zoom programs.

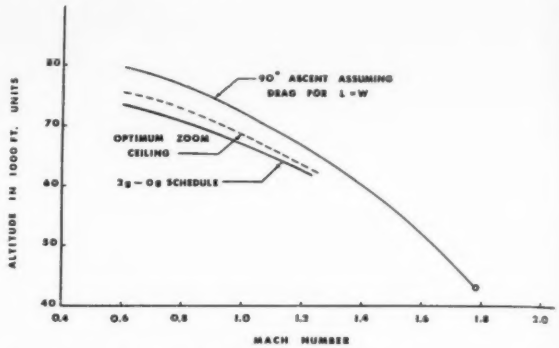

FIG. 8. Comparison of optimum zoom ceiling and vertical ascent solution of the simplified $L = W$ theory.

[2] Lippisch, A., *Flugmechanische Beziehungen der Flugzeuge mit Strahlantrieb*, AMC Translation Report No. F-TS-685-RE, October, 1946.

[3] Kaiser, F., *Der Steigflug mit Strahlflugzeugen—Teil 1, Bahngeschwindigkeit besten Steigens*, Versuchsbericht 262-02-L44, Messerschmitt A.G., Augsburg, April, 1944 (translated as Ministry of Supply RTP/TIB Translation GDC/15/148T).

[4] Lush, K. J., *A Review of the Problem of Choosing a Climb Technique with Proposals for a New Climb Technique for High Performance Aircraft*, Aeronautical Research Council Report Memo. No. 2557, 1951.

[5] Garbell, M. A., *Optimum Climbing Techniques for High-Performance Aircraft*, Garbell Aeronautical Series, No. 8, San Francisco, 1953.

[6] Rutowski, E. S., *Energy Approach to the General Aircraft Performance Problem*, Journal of the Aeronautical Sciences, Vol. 21, No. 3, pp. 187–195, March, 1954.

[7] Miele, A., *Optimum Climbing Technique for a Rocket-Powered Aircraft*, Jet Propulsion, Vol. 25, No. 8, August, 1955.

[8] Liebhold, E. M., *Application of the Calculus of Variations to Guided Missile Flight Paths for Obtaining Maximum Range*, RAND R-138, February, 1949.

[9] Hestenes, M. R., *A General Problem in the Calculus of Variations with Applications to Paths of Least Time*, RAND RM-100, March, 1950.

[10] Mengel, A. S., *Optimum Trajectories*, Proceedings of Project Cyclone Symposium 1 on REAC Techniques, March, 1951.

[11] Dommasch, D. O., *Methods of Dynamic Performance as Applied to the Minimum Time to Climb Problem*, Princeton University Aeronautical Engineering Report 331, March, 1955.

[12] Garfinkel, B., *Minimal Problems in Airplane Performance*, Quart. of Appl. Math., Vol. IX, No. 2, 1951.

[13] Miele, A., *An Extension of the Theory of the Optimum Burning Program for the Level Flight of a Rocket-Powered Aircraft*, Purdue University, School of Aeronautical Engineering, Report No. A-56-1, Technical Note No. AFOSR-TN-56-302, June, 1956.

[14] Cicala, P., *Le Evoluzioni Ottime di un Aereo*, Atti della Accademia delle Scienze di Torino, Classe di Scienze Matematiche, Fisiche e Naturali, Vol. 89, 1954–1955.

[15] Cicala, P., *Soluzioni Discontinue nei Problemi di Volo Ottimo*, Atti della Accademia delle Scienze di Torino, Classe di Scienze Matematiche, Fisiche e Naturali, Vol. 90, 1955–1956.

[16] Lush, K. J., *Optimum Climb Theory and Techniques of Determining Climb Schedules from Flight Test*, Part 1 of Chapter 7, NATO AGARD Flight Test Manual, Vol. 1, 1954.

[17] Cicala, P., and Miele, A., *Brachistocronic Maneuvers of a Variable Mass Aircraft in a Vertical Plane*, Readers' Forum, Journal of the Aeronautical Sciences, Vol. 22, No. 8, pp. 577, 588, August, 1955.

[18] Courant, R., *Calculus of Variations and Supplementary Notes and Exercises*, 1945–1946, revised and amended by J. Moser,

(*Continued on page 824*)

Thermal Buckling of Circular Cylindrical Shells Under Circumferential Temperature Gradients†

DAVID ABIR* AND S. V. NARDO**

Polytechnic Institute of Brooklyn

Summary

The thermal buckling of thin-walled circular cylindrical shells due to axial stresses caused by variations in temperature around the circumference is analyzed. This problem is of considerable importance in the structural design of high-speed airplanes and missiles, since they are subjected to high rates of aerodynamic heating.

The analysis is performed with the aid of Donnell's equations, which can be shown to be satisfactory for the problem under consideration. The variation of the thermal stress with the circumferential coordinate is represented by Fourier series; the stresses are assumed constant through the thickness and in the axial direction.

The conclusion reached is that the axial buckling stress under variable thermal stress conditions is close to the critical stress of the cylinder when it is subjected to uniform axial compression, if the variation of the intensity of the thermal stress is not large within a half-wavelength of the buckling pattern.

Symbols

A_n = radial deflection coefficient
a = radius of median surface
B_n = axial deflection coefficient
C = buckling stress coefficient
C_n = circumferential deflection coefficient
E = Young's modulus of elasticity
h = thickness of wall
K = a constant defined by Eq. (5)
L = length of shell
M_x = axial bending moment per unit of axial length
m = number of half-waves along generator
n = number of full waves around circumference
R = a number (eigenvalue)
r = $1/R$
s = a stress coefficient
U = a ratio defined by Eq. (21)
u^* = axial displacement
u = $(=u^*/a)$ dimensionless axial displacement
v^* = circumferential displacement
v = $(=v^*/a)$ dimensionless circumferential displacement
w^* = radial displacement
w = $(=w^*/a)$ dimensionless radial displacement
x^* = axial coordinate
x = $(=x^*/a)$ dimensionless axial distance
i, p, q = dummy symbols, subscripts, numbers
α = a ratio defined by Eq. (27)
μ = $(=L/a)$ dimensionless length of shell
ν = Poisson's ratio
σ_x = axial stress
σ_{cr} = critical stress
φ = circumferential coordinate
∇^2 = Laplace's operator

Received August 14, 1958. Revised and received August 14, 1959.

† This paper is based on a dissertation submitted to the Polytechnic Institute of Brooklyn in partial fulfillment of the requirements for the degree of Doctor of Philosophy in Applied Mechanics. This research was supported by the United States Air Force under Contract No. AF 33(616)-3885, monitored by the Aeronautical Research Laboratory, WADC.

The authors gratefully acknowledge the help of Prof. N. J. Hoff, who first suggested the problem and who provided helpful suggestions, guidance, and advice during the course of the work.

* Formerly, Research Fellow. Now, Senior Lecturer, Technion, Haifa, Israel.

** Professor of Aeronautical Engineering.

Introduction and Conclusions

As the bodies of hypersonic airplanes and missiles are often thin circular or almost circular cylindrical shells, and because they are subjected to high rates of aerodynamic heating, the calculation of the structural stability of thin circular cylindrical shells under thermal stresses has attained considerable importance in aeronautical engineering. Earlier investigations have shown that buckling is unlikely to occur when the temperature varies only in the radial direction or only in the axial direction. On the other hand, it was expected that circumferential variations of the temperature would give rise to conditions similar to those existing in the flat or almost flat coverplates of wings which are known to buckle under thermal stresses. The purpose of the present investigation is to show that this expectation is correct.

The analysis is carried out with the aid of Donnell's equations which are accurate enough for engineering purposes when the wavelength of the buckled shape is smaller than the radius of the cylinder. This condition is usually satisfied in cylindrical shells of interest to the aircraft designer. The thermal stress is assumed to be constant through the wall thickness of the shell and in the axial direction. Its variation with the circumferential coordinate is represented by Fourier series.

The interesting conclusion reached in the analysis is that the critical value of the axial compressive stress under variable thermal stress conditions does not differ much from the critical stress of the cylinder when it is subjected to uniform axial compression, provided the variation of the intensity of the thermal stress within one-half wavelength is not large. This conclusion is plausible on physical grounds, but it is significant be-

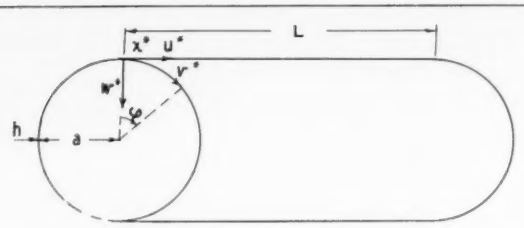

FIG. 1. Coordinates, displacements, and dimensions of shell.

cause it permits the approximate evaluation of the critical condition without any lengthy calculation.

Statement of the Problem

The equilibrium conditions of the thin-walled circular cylindrical shell can be expressed by Donnell's equations[1] with sufficient accuracy for the present purpose. They are used here in the form given by Hoff:[2]

$$\nabla^8 w + 4K^4(\partial^4 w/\partial x^4) + 4K^4\nabla^4[(\sigma_x/E)(\partial^2 w/\partial x^2)] = 0 \quad (1)$$

$$\nabla^4 u = \nu(\partial^3 w/\partial x^3) - (\partial^3 w/\partial x\,\partial\varphi^2) \quad (2)$$

$$\nabla^4 v = (2 + \nu)(\partial^3 w/\partial x^2\,\partial\varphi) + (\partial^3 w/\partial\varphi^3) \quad (3)$$

where σ_x is the axial stress; E, Young's modulus of elasticity; ν, Poisson's ratio; a, radius of the median surface of the shell; h, thickness of the wall; L, length of the shell; x^* and φ, coordinates shown in Fig. 1; u^*, v^*, w^*, displacements shown in Fig. 1; x, u, v, w, dimensionless distance and displacements, respectively, defined by

$$x = x^*/a; \quad u = u^*/a; \quad v = v^*/a; \quad w = w^*/a \quad (4)$$

K, a constant for a given shell, defined by

$$4K^4 = 12(1 - \nu^2)(a/h)^2 \quad (5)$$

and ∇^2, Laplace's operator, defined by

$$\nabla^2 = (\partial^2/\partial x^2) + (\partial^2/\partial\varphi^2)$$

The shell is assumed to be very long compared to the half-wavelength in the x direction. Variation of the axial stress around the circumference is assumed to be represented by the infinite series

$$\sigma_x = ER\sum_{p=0}^{\infty} s_p \cos p\varphi \quad (6)$$

where R is a number (an eigenvalue) to be evaluated for each loading case defined by specific values of the coefficients s_p. Compressive stress is designated by a positive sign.

The homogeneous boundary conditions that are to be satisfied by the solution are those corresponding to simple supports—namely,

$$\left.\begin{aligned} v &= 0 \\ w &= 0 \\ \sigma_x &= [E/(1 - \nu^2)]\{(\partial u/\partial x) + \nu[(\partial v/\partial\varphi) - w]\} = 0 \\ M_x &= \{Eh^3/[12(1 - \nu^2)a]\}[\partial^2 w/\partial x^2 + \nu(\partial^2 w/\partial\varphi^2)] = 0 \end{aligned}\right\} \text{ at } x^* = 0 \text{ and } L \quad (7)$$

Solution of the Differential Equations

The deflection functions describing the buckling deformations and satisfying the boundary conditions (7) are represented by Fourier series:

$$w = \sin(m\pi x/\mu)\sum_{n=0}^{\infty} A_n \cos n\varphi \quad (8)$$

$$u = \cos(m\pi x/\mu)\sum_{n=0}^{\infty} B_n \cos n\varphi \quad (9)$$

$$v = \sin(m\pi x/\mu)\sum_{n=0}^{\infty} C_n \sin n\varphi \quad (10)$$

where the coefficients A_n, B_n, C_n are to be determined so as to satisfy the differential equations (1), (2), (3). μ is the dimensionless ratio

$$\mu = L/a \quad (11)$$

m is the number of half-waves along the generator of the shell, and n is the number of full waves around the circumference.

In order to satisfy Eq. (2), w and u are substituted from Eqs. (8) and (9) into Eq. (2). Solution for B_n yields, in terms of A_n,

$$B_n = \frac{[n^2 - \nu(m\pi/\mu)^2](m\pi/\mu)}{[(m\pi/\mu)^2 + n^2]^2} A_n \quad (12)$$

Similar manipulations carried out in connection with Eq. (3) give

$$C_n = \frac{[n^2 + (2 + \nu)(m\pi/\mu)^2]n}{[(m\pi/\mu)^2 + n^2]^2} A_n \quad (13)$$

Somewhat lengthier manipulations are needed in order to satisfy Eq. (1). Two differentiations of the right-hand member of Eq. (8) with respect to x, followed by a multiplication by (σ_x/E) from Eq. (6), lead to

$$(\sigma_x/E)(\partial^2 w/\partial x^2) = -R(m\pi/\mu)^2(\sin m\pi x/\mu) \times \sum_{n=0}^{\infty}\sum_{p=0}^{\infty} A_n s_p \cos n\varphi \cos p\varphi$$

Through a simple trigonometric substitution this equation becomes

$$(\sigma_x/E)(\partial^2 w/\partial x^2) = -(R/2)(m\pi/\mu)^2(\sin m\pi x/\mu) \times \sum_{n=0}^{\infty}\sum_{p=0}^{\infty} A_n s_p[\cos(n + p)\varphi + \cos(n - p)\varphi] \quad (14)$$

The double infinite series of Eq. (14) can be put into the following more convenient form:

$$(\sigma_x/E)(\partial^2 w/\partial x^2) = -(R/2)(m\pi/\mu)^2 (\sin m\pi x/\mu) \times \left\{\left(A_0 s_0 + \sum_{i=0}^{\infty} A_i s_i\right) + \sum_{q=1}^{\infty}\left[\sum_{i=0}^{q} A_i s_{q-i} + \sum_{i=q}^{\infty} A_i s_{i-q} + \sum_{i=0}^{\infty} A_i s_{i+q}\right]\cos q\varphi\right\} \quad (15)$$

It is by no means obvious that Eq. (15) follows from Eq. (14), inasmuch as quite a bit of mathematical manipulation is involved. The leading terms of Eqs. (14) and (15) can be written out and systematically arranged to show that Eq. (15) is indeed equivalent to Eq. (14). The intermediate steps, however, may be found in reference 3.

Operation on this equation by ∇^4, and multiplication by $4K^4$, give

$$4K^4\nabla^4[(\sigma_x/E)(\partial^2 w/\partial x^2)] = -2K^4R(m\pi/\mu)^2(\sin m\pi x/\mu) \times \left\{(m\pi/\mu)^4\left(A_0 s_0 + \sum_{i=0}^{\infty} A_i s_i\right) + \sum_{q=1}^{\infty}[(m\pi/\mu)^2 + q^2]^2 \times \left[\sum_{i=0}^{q} A_i s_{q-i} + \sum_{i=q}^{\infty} A_i s_{i-q} + \sum_{i=0}^{\infty} A_i s_{i+q}\right]\cos q\varphi\right\}$$

The dummy symbol "q" may be changed into "n" in this expression. Hence,

$$4K^4\nabla^4[(\sigma_x/E)(\partial^2 w/\partial x^2)] = -2K^4R(m\pi/\mu)^2 \times (\sin m\pi x/\mu)\left\{(m\pi/\mu)^4\left(A_0 s_0 + \sum_{i=0}^{\infty} A_i s_i\right) + \sum_{n=1}^{\infty}[(m\pi/\mu)^2 + n^2]^2\left[\sum_{i=0}^{n} A_i s_{n-i} + \sum_{i=n}^{\infty} A_i s_{i-n} + \sum_{i=0}^{\infty} A_i s_{i+n}\right]\cos n\varphi\right\} \quad (16)$$

Differentiation of w in Eq. (8) yields

$$4K^4(\partial^4 w/\partial x^4) = 4K^4(m\pi/\mu)(\sin m\pi x/\mu)\sum_{n=0}^{\infty} A_n \cos n\varphi \quad (17)$$

and operation on Eq. (8) by ∇^8 gives

$$\nabla^8 w = (\sin m\pi x/\mu)\sum_{n=0}^{\infty}[(m\pi/\mu)^2 + n^2]^4 A_n \cos n\varphi \quad (18)$$

Eq. (1) is satisfied by substitution of the last three expressions, which leads to

$$(\sin m\pi x/\mu)\sum_{n=0}^{\infty}[(m\pi/\mu)^2 + n^2]^4 A_n \cos n\varphi + 4K^4(m\pi/\mu)^4 (\sin m\pi x/\mu)\sum_{n=0}^{\infty} A_n \cos n\varphi - 2K^4R(m\pi/\mu)^2 (\sin m\pi x/\mu)\left\{(m\pi/\mu)^4\left(A_0 s_0 + \sum_{i=0}^{\infty} A_i s_i\right) + \sum_{n=1}^{\infty}[(m\pi/\mu)^2 + n^2]^2\left[\sum_{i=0}^{n} A_i s_{n-i} + \sum_{i=n}^{\infty} A_i s_{i-n} + \sum_{i=0}^{\infty} A_i S_{i+n}\right]\cos n\varphi\right\} = 0$$

This equation holds for every value of n. Thus, for $n = 0$,

$$(\sin m\pi x/\mu)(m\pi/\mu)^8 A_0 + 4K^4(m\pi/\mu)^4 (\sin m\pi x/\mu)A_0 - 2K^4R(m\pi/\mu)^6 (\sin m\pi x/\mu)\left(A_0 s_0 + \sum_{i=0}^{\infty} A_i s_i\right) = 0 \quad (19a)$$

and for $n = 1, 2, 3, \ldots, \infty$,

$$(\sin m\pi x/\mu)\sum_{n=1}^{\infty}[(m\pi/\mu)^2 + n^2]^4 A_n \cos n\varphi + 4K^4(m\pi/\mu)^4 (\sin m\pi x/\mu)\sum_{n=1}^{\infty} A_n \cos n\varphi - 2K^4R(m\pi/\mu)^2 (\sin m\pi x/\mu)\sum_{i=1}^{\infty}[(m\pi/\mu)^2 + n^2]^2 \times \left[\sum_{i=0}^{n} A_i s_{n-i} + \sum_{i=n}^{\infty} A_i s_{i-n} + \sum_{i=0}^{\infty} A_i s_{i+n}\right]\cos n\varphi = 0 \quad (19b)$$

Eqs. (19) are identities. Consequently, the sums of the multipliers of like trigonometric terms must vanish—i.e.,

$$(m\pi/\mu)^4 A_0 + 4K^4 A_0 - 2K^4R(m\pi/\mu)^2 \times \left(A_0 s_0 + \sum_{i=0}^{\infty} A_i s_i\right) = 0, \quad (n = 0)$$

and

$$[(m\pi/\mu)^2 + n^2]^4 A_n + 4K^4(m\pi/\mu)^4 A_n - 2K^4R(m\pi/\mu)^2[(m\pi/\mu)^2 + n^2]^2\left[\sum_{i=0}^{n} A_i s_{n-i} + \sum_{i=0}^{\infty} A_i s_{i-n} + \sum_{i=0}^{\infty} A_i s_{i+n}\right] = 0, \quad (n = 1, 2, \ldots, \infty)$$

These two equations can be rearranged as follows:

$$A_0 s_0 + \sum_{i=0}^{\infty} A_i s_i = \{[(m\pi/\mu)^2/2K^4] + [2/(m\pi/\mu)^2]\}(A_0/R), \quad (n = 0) \quad (20a)$$

$$\sum_{i=0}^{n} A_i s_{n-i} + \sum_{i=n}^{\infty} A_i s_{i-n} + \sum_{i=0}^{\infty} A_i s_{i+n} = \left(\{[(m\pi/\mu) + n^2]^2/2K^2(m\pi/\mu)^2\} + \{2(m\pi/\mu)^2/[(m\pi/\mu)^2 + n^2]^2\}\right)(A_n/R), \quad (n = 1, 2, \ldots, \infty) \quad (20b)$$

By introducing the notations

$$U_n = \{[(m\pi/\mu)^2 + n^2]^2/2K^4(m\pi/\mu)^2\} + \{2(m\pi/\mu)^2/[(m\pi/\mu)^2 + n^2]^2\} \quad (21)$$

and

$$r = 1/R \quad (22)$$

the conditions of equilibrium, Eqs. (20), become

$$(U_0 r - s_0)A_0 - \sum_{i=0}^{\infty} A_i s_i = 0, \quad (n = 0) \quad (23a)$$

$$U_n r A_n - \sum_{i=0}^{n} A_i s_{n-i} - \sum_{i=n}^{\infty} A_i s_{i-n} - \sum_{i=0}^{\infty} A_i s_{i+n} = 0, \quad (n = 1, 2, \ldots, \infty) \quad (23b)$$

Eqs. (23) must hold for every value of n. Their expansion over the range $i = 0, 1, 2, \ldots, \infty$, for each

value of n, results in the following infinite set of linear homogeneous equations in the unknown deflection-coefficients A_i:

$$\left.\begin{array}{lllllll}
n=0: & 2(U_0r-2s_0)A_0-2s_1A_1 & -2s_2A_2 & -2s_3A_3 & -2s_4A_4- & \cdots=0\\
n=1: & -2s_1A_0+(U_1r-2s_0-s_2)A_1 & -(s_1+s_3)A_2 & -(s_2+s_4)A_3 & -(s_3+s_5)A_4- & \cdots=0\\
n=2: & -2s_2A_0-(s_1+s_3)A_1 & +(U_2r-2s_0-s_4)A_2 & -(s_1+s_5)A_3 & -(s_2+s_6)A_4- & \cdots=0\\
n=3: & -2s_3A_0-(s_2+s_4)A_1 & -(s_1+s_5)A_2 & +(U_3r-2s_0-s_6)A_3 & -(s_1+s_7)A_4- & \cdots=0\\
n=4: & -2s_4A_0-(s_3+s_5)A_1 & -(s_2+s_6)A_2 & -(s_1+s_7)A_3 & +(U_4r-2s_0-s_8)A_4- & \cdots=0\\
\cdots & \cdots & \cdots & \cdots & \cdots & \cdots
\end{array}\right\} \quad (24)$$

The coefficients of $A_i (i = 0, 1, 2, \ldots, \infty)$ in this infinite set of equations form the following infinite, symmetric, matrix:

$$\begin{vmatrix}
2(U_0r-2s_0) & -2s_1 & -2s_2 & -2s_3 & -2s_4 & \cdots\\
-2s_1 & U_1r-2s_0-s_2 & -s_1-s_3 & -s_2-s_4 & -s_3-s_5 & \cdots\\
-2s_2 & -s_1-s_3 & U_2r-2s_0-s_4 & -s_1-s_5 & -s_2-s_6 & \cdots\\
-2s_3 & -s_2-s_4 & -s_1-s_5 & U_3r-2s_0-s_6 & -s_1-s_7 & \cdots\\
-2s_4 & -s_3-s_5 & -s_2-s_6 & -s_1-s_7 & U_4r-2s_0-s_8 & \cdots\\
\cdots & \cdots & \cdots & \cdots & \cdots & \cdots
\end{vmatrix} \quad (25)$$

For the infinite set of Eqs. (24) to have nontrivial solutions—i.e., in order for the unknown deflection-coefficients A_i $(i = 0, 1, 2, \ldots, \infty)$ to have values other than zero—the infinite determinant of the coefficients of A_i must vanish. These coefficients are arranged in the matrix (25). Division by 2 of the first row and the first column yields

$$\begin{vmatrix}
(1/2)(U_0r-2s_0) & -s_1 & -s_2 & -s_3 & -s_4 & \cdots\\
-s_1 & U_1r-2s_0-s_2 & -s_1-s_3 & -s_2-s_4 & -s_3-s_5 & \cdots\\
-s_2 & -s_1-s_3 & U_2r-2s_0-s_4 & -s_1-s_5 & -s_2-s_6 & \cdots\\
-s_3 & -s_2-s_4 & -s_1-s_5 & U_3r-2s_0-s_6 & -s_1-s_7 & \cdots\\
-s_4 & -s_3-s_5 & -s_2-s_6 & -s_1-s_7 & U_4r-2s_0-s_8 & \cdots\\
\cdots & \cdots & \cdots & \cdots & \cdots & \cdots
\end{vmatrix} = 0 \quad (26)$$

To use the above criterion in a given problem, the coefficients characterizing the load, s_p, are first inserted into Eq. (26). A specific integral value of m is chosen and the U_n quantities are calculated. The determinant is truncated and evaluated, leading to an algebraic equation in r. The degree of the equation depends, of course, on how the determinant is truncated. Solution of the equation yields r as a function of n. Of interest is the root r which is a maximum inasmuch as $r = 1/R$ and R is to be a minimum. This procedure must be repeated for other integral values of m until the maximum of all the maximum r's is obtained.

This procedure, while straightforward in principle, can be long and laborious. A considerable simplification would be effected if the U_n's could be assumed constant and equal, say, to U. Under these conditions, evaluation of the determinant would lead to an algebraic equation in (Ur) and it is clear that maximum r would correspond to the minimum value of U for the largest root Ur.

If the cylinder is long, then m will be large compared to n. Thus, in Eq. (21), $(m\pi/\mu)^2$ is large compared to n^2. If this is the case, the U_n's will be very nearly equal and advantage can be taken of the simplification possible under these conditions. Hence, in the evaluation of the critical load in any practical application, the maximum root Ur is obtained corresponding to specific s_p's, and the minimum U substituted into the value of the root to obtain maximum r.

U_n can most easily be minimized by treating a function of m and n as a single parameter which is assumed to be continuous. By denoting

$$\alpha = [(m\pi/\mu)^2 + n^2]^2/2(m\pi/\mu)^2 \quad (27)$$

Eq. (21) can be written

$$\partial U_n = (\alpha/K^4) + (1/\alpha)$$

$$\partial U_n/\partial\alpha = (1/K^4) - (1/\alpha^2) = 0$$

$$\alpha = K^2 \quad (28)$$

Substitution of Eq. (28) into Eq. (21) yields the minimum value of U_n:

$$U_{min} = 2/K^2 \quad (29)$$

It is to be noted that minimum U is a constant for a given shell geometry and material. It may also be of interest to note that if Eq. (28) is inserted into Eq. (27), the result,

$$[(m\pi/\mu)^2 + n^2]^2/(m\pi/\mu)^2 = 2K^2 = (2a/h)[3(1 - \nu^2)]^{1/2} \quad (30)$$

is in agreement with the result from the classical treatment of the theory of shell instability (see reference 4, p. 457).

In the following sections the critical axial compressive stress is computed for a number of simple loading cases. The procedure loses its validity if the variation of the prescribed thermal stress and the geometry of the cylinder are such that U_n values must be taken into consideration for which $n > m\pi/\mu$.

Uniform Axial Compression

Under the conditions of uniform axial compressive stresses,

$$s_0 = 1$$

$$s_p = 0 \quad \text{when } p \neq 0 \quad (31)$$

and from Eq. (6),

$$\sigma_x = ER \quad (32)$$

Upon the substitution of Eq. (31) into the determinant (26), the following is obtained:

$$\begin{vmatrix} (1/2)(U_0r - 2) & 0 & 0 & 0 & 0 & . \\ 0 & (U_1r - 2) & 0 & 0 & 0 & . \\ 0 & 0 & (U_2r - 2) & 0 & 0 & . \\ 0 & 0 & 0 & (U_3r - 2) & 0 & . \\ 0 & 0 & 0 & 0 & . & \\ . & . & . & . & . & \\ . & . & . & . & . & \\ . & . & . & . & . & \end{vmatrix} = 0$$

In this particular loading case, any one of the quantities on the principal diagonal may be set equal to zero. Thus, with the approximation that for large m,

$$U_0 = U_1 = U_2 = \ldots = U$$

$$r = 1/R = 2/U$$

or

$$R_{min} = U_{min}/2$$

From Eq. (29)

$$R_{min} = (2/K^2)/2 = (1/K^2) \quad (33)$$

Substituting the above value of R_{min} into Eq. (32), and recalling the definition of K [Eq. (5)],

$$\sigma_{x_{cr}} = [E/3(1 - \nu^2)](h/a) \quad (34)$$

This result is the well-known solution for the critical stress of a uniformly compressed circular cylinder from the classical treatment of shells (see reference 4, p. 457). The values of m and n are undetermined, but for the case of axisymmetric buckling, $n = 0$, the half-wavelength and the number of half-waves m can easily be obtained from Eq. (30).

Pure Bending

The load coefficients in this case are

$$s_1 = 1, \quad s_p = 0 \quad \text{when } p \neq 1 \quad (35)$$

Eq. (6) becomes

$$\sigma_x = ER \cos \varphi \quad (36)$$

and the stability determinant reduces to

$$\begin{vmatrix} (1/2)U_0r & -1 & 0 & 0 & 0 & \ldots. \\ -1 & U_1r & -1 & 0 & 0 & \ldots. \\ 0 & -1 & U_2r & -1 & 0 & \ldots. \\ 0 & 0 & -1 & U_3r & -1 & \ldots. \\ 0 & 0 & 0 & -1 & U_4r & \\ . & . & . & . & . & \\ . & . & . & . & . & \\ . & . & . & . & . & \end{vmatrix} = 0 \quad (37)$$

If the determinant is truncated so as to obtain a 2 by 2 determinant, the resultant quadratic equation is

$$(1/2)U^2r^2 - 1 = 0$$

for

$$U_0 = U_1 = \ldots = U$$

and

$$R = 1/r = U/\sqrt{2}$$

Thus,

$$R_{min} = U_{min}/\sqrt{2} \quad (38)$$

When $R_{min} = U_{min}/2$, the maximum compressive stress in Eq. (36) will correspond to the critical stress for uniform axial compression. Hence, the above value for R_{min} [Eq. (38)] corresponds to a maximum compressive stress which is approximately 40 per cent higher than that corresponding to the uniform axial compression critical stress.

TABLE 1

Order of determinant	R_{min}	Per cent above uniform compression case
2	$U_{min}/1.414$	41
3	$U_{min}/1.732$	15
4	$U_{min}/1.848$	8
5	$U_{min}/1.902$	5

Taking a 3 by 3 determinant yields the result $R_{min} = U/\sqrt{3}$. Calculations for fourth and fifth order determinants give values for R_{min} of $U_{min}/1.848$ and $U_{min}/1.902$, respectively. These results are summarized in Table 1.

It appears reasonable to conclude that as determinants of higher order are taken, the critical value of the maximum compressive stress in the case of pure bending will approach approximately the critical stress for uniform axial compression.

Other Cases of Loading

In addition to the cases of loading corresponding to uniform axial compression and pure bending, a number of other cases of loading were also worked out, using the procedure outlined in the preceding section for pure bending. The additional cases of loading were the following:

(a) $s_2 = 1, \quad s_p = 0 \quad$ when $p \neq 2$
(b) $s_3 = 1, \quad s_p = 0 \quad$ when $p \neq 3$
(c) $s_0 = s_1 = s_2 = s_3 = 1/4; \quad s_p = 0 \quad$ when $p > 3$

The peripheral variation of axial stresses in cases (a) and (b) are self-equilibrating, while case (c) corresponds to a superposition of the uniform axial compression, pure bending, and cases (a) and (b). The values of the load coefficients in (c) were intentionally chosen to give a sum total of 1.0 in order that the results could be compared with the case of uniform axial compression.

TABLE 2
Values of C for Various Cases of Loading*

Order of determinant	Pure bending	Case (a) $s_2 = 1$	Case (b) $s_3 = 1$	Case (c) combined loading $s_0 = s_1 = s_2 = s_3 = 1/4$
2	0.707	1.00		1.00
3	0.577	0.707	1.00	0.707
4	0.541	0.610	0.707	0.620
5	0.525	0.561	0.707	0.575

*$C = 0.5$ for uniform axial compression.

In Table 2, the results of all the loading cases worked out in this paper are summarized. The results are presented in a manner that allows an easy comparison with the case of uniform axial compression. In the table, the values of a critical stress coefficient, C, are given for the various loading cases and for orders of determinants ranging from 2 to 5. The coefficient C is defined as

$$R_{min} = CU_{min} \tag{39}$$

It will be recalled that for the case of uniform axial compression a value of R_{min} equal to $U_{min}/2$ led to the classical result for the buckling of a circular thin-walled cylinder [Eq. (34)]. Thus, the coefficient C in this case is 0.5.

For the cases of loading shown in Table 2, it is seen that as the approximation to the stability determinant is improved—i.e., as determinants of higher order are taken—the critical value of the maximum compressive stress gets closer to the critical value for the case of uniform axial compression. It appears plausible, therefore, to conclude for practical applications that the critical value of a thermal and/or applied axial stress distribution around the periphery of a long thin-walled circular cylinder can be assumed to be reached when the maximum compressive stress is equal to the critical stress in uniform axial compression, provided that the intensity of the stress variation over one-half wavelength is not large.

References

[1] Donnell, L. H., *Stability of Thin-Walled Tubes under Torsion*, NACA Report 479, Washington, D.C., 1933.

[2] Hoff, N. J., *Buckling of Thin Cylindrical Shell under Hoop Stresses Varying in Axial Direction*, Journal of Applied Mechanics, Vol. 24, No. 3, September, 1957.

[3] Abir, D., Nardo, S. V., and Hoff, N. J., *Thermal Buckling of Circular Cylindrical Shells Under Circumferential Temperature Gradients, Section 2 of Thermal Buckling of Circular Cylindrical and Conical Thin-Walled Shells*, WADC Technical Report 58-104, ASTIA Document No. AD 151068, WADC, April, 1958.

[4] Timoshenko, S., *Theory of Elastic Stability*, 1st Ed., McGraw-Hill Book Co., Inc., New York, 1936.

Microcards for Volumes 1–5 Available

Microcards for Volumes 3–5 of the JOURNAL are now available (Vols. 1 and 2 were republished in this form earlier). All five volumes are priced at $5.50 each, and are obtainable through:

J. S. Canner & Company, Inc.
Boston, Roxbury 20, Mass.

Heat Transfer to Separated and Reattached Subsonic Turbulent Flows Obtained Downstream of a Surface Step†

R. A. SEBAN,* A. EMERY,** AND A. LEVY**

University of California at Berkeley

Summary

Local heat-transfer coefficients and recovery factors are presented for separated and reattached turbulent flows as obtained by a downward step in an otherwise flat surface in a two-dimensional, subsonic, air flow. The region downstream of the step, the focus of this investigation, contained a region of separated flow with reattachment at about five step heights downstream, followed by a section of reattached flow. The salient feature of the results is the maximum in the local heat-transfer coefficient at the reattachment point, with values thereof diminishing in the separated region and also in the reattached region, where they tend toward values characteristic of turbulent boundary-layer flow. It is found that for most of the region the heat-transfer coefficient depends on the velocity to about the 0.8 power, though a decreased dependence may exist in the separated region. Recovery factors have the characteristically low values associated with separated flows, and do not attain values typical of turbulent boundary-layer flows within the downstream lengths available.

Symbols

c_p = specific heat at constant pressure
d = step height
h = local heat-transfer coefficient
k = thermal conductivity
L = length dimension, used here as unit length
q = heat flux
s = distance between separation and reattachment
T = temperature
T_0 = wall temperature
T_a = adiabatic wall temperature
T_1 = free-stream temperature
T_s = stagnation temperature
u = velocity
u_1 = free-stream velocity
u_a = reference velocity
u_{1s} = free-stream velocity just upstream of step
u_{1e} = free-stream velocity downstream of reattachment
x = distance downstream from leading edge
x' = distance downstream from step
x'' = distance downstream from reattachment point
ν = kinematic viscosity

Received October 21, 1958. Revised and received March 23, 1959.

† A large part of this research was accomplished with the support of the United States Air Force under Contract AF33(616)-348, directed toward the investigation of heat transfer in regions of separated flow.

* Professor of Mechanical Engineering.

** Research Assistant, Institute of Engineering Research.

Introduction

THE PURPOSE of this paper is to exhibit certain experimental results for the local heat-transfer coefficient and the recovery factor for separated and reattached boundary-layer flows which are two-dimensional, subsonic, and primarily turbulent. For a flow so complicated and so marginally amenable to theoretical consideration, these results are insufficient for a comprehensive specification of the heat transfer in such regions, but rather they are intended to give an initial exposition of the heat-transfer performance, which does in fact lead to some preliminary generalizations which agree with what is known about the flow.

Attainment of the flows for which the heat-transfer results are here reported was made through the use of a downward step in the surface upon which a boundary layer had been formed, with a sufficient continuation of the surface in the downstream direction to enable a reattachment of the flow. The "separation" thus achieved is not that connoted by the usual boundary-layer theory, but, when the length of the separated flow is large compared to the initial boundary-layer thickness, the distinction is likely not to be of critical importance in so far as the characteristics of the separated region are concerned. Greater influence is expected from the form of the closed streamline region, delineated by the solid surface and a zero streamline within the viscid layer, so that some geometrical similarity appears to be prerequisite to any extrapolation of these results. For this reason some additional results that were obtained by securing separation by means of a rod spanning a plate are presented separately in the Appendix.

The region interior to separated and reattached flows of this type has often received the appelation of a "dead water" region to indicate the more or less quiescent conditions from which there is a minimal tractive effect on the external separated flow. It is known experimentally, however, from results of mean speed surveys, such as those of Arie and Rouse[1] and Hsu,[2] that this inner region contains a circulatory flow which appears to be steady and which near the surface provides an upstream velocity of the order of 1/5 the free-stream velocity. Similar findings were obtained from the systems for which the heat-transfer results

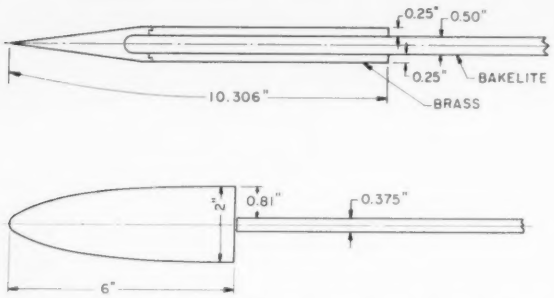

FIG. 1. Elevation of the models with the large and small steps.

are reported here. Upon reattachment, caused by the interactive influences of the broadening of the separated flow and the potential motion, the boundary-layer flow begins a redevelopment which leads ultimately to distributions of the mean speed and turbulent energy which are characteristic of an undistorted turbulent boundary-layer flow. A length of many boundary-layer thicknesses is required for this redevelopment, and it was not attained in the downstream distances available in the experimental arrangements from which the results presented here were derived.

Experimental Technique

The models from which the results were obtained were each mounted centrally in and spanning the 6 in. width of the 6 in. by 9 in. closed test section of a wind tunnel. They were made of bakelite, being heated by means of electric current passing through nichrome ribbons, 0.002 in. thick and 1 in. wide, affixed to the model surface with lengthwise dimension parallel to that of the flow. Small spaces between the ribbons were provided for the location of pressure taps, and thermocouples mounted immediately below the ribbons were used for the indication of ribbon temperature. Ribbons were placed on both sides of the model to provide symmetrical thermal as well as hydrodynamic conditions.

One model provided a 0.25-in. downward step in its surface, and this was achieved by the modification of a flat plate model that has been described previously in the report of other results.[5] 1/4-in. thick brass plates were placed on the surfaces, with a modified nose section to accommodate the greater thickness, and this provided the configuration shown on Fig. 1. In this revision the pressure taps were continued through the plates to the surface and the plates were electrically insulated from the ribbons. The addition of the plates, of course, provided a path of longitudinal conduction for the heat generated in the ribbons and consequently this generation could no longer be specifically associated with a flux to the boundary-layer flow.

A larger step, 0.81 in. in height, was provided with the other model shown on Fig. 1. This combined two parts, a half elliptical cylinder and a flat plate, with the latter mounted downstream to provide the step in the surface. The plate, 0.375 in. thick and 12 in. long, was completely instrumented with surface ribbons, thermocouples, and pressure taps. The cylindrical section was unheated and contained only pressure taps.

Observations were made at various air speeds from 150 to 500 ft./sec., with stagnation pressures near atmospheric and stagnation temperatures of the order of 90°F. Without heating, adiabatic wall temperatures were observed. With heating, to give temperature differences of the order of 20°F. between surface and stagnation, the observed heat generation and surface temperature enabled the ultimate evaluation of the local heat-transfer coefficient.

As presented here the recovery factors are defined in terms of the local free-stream velocity as deduced from the pressure tap indications,

$$r = 1 - [(T_s - T_a)/(u_1^2/2c_p)]$$

The local heat-transfer coefficient is

$$h = q/(T_0 - T_a)$$

As presented here these quantities were evaluated directly from observation. Recovery factors are given only for air speeds greater than 350 ft./sec.; for which the error in that quantity is estimated to be less than 2 per cent. The error in the heat-transfer coefficient depends more critically on location and air speed; for the results presented the error does not exceed 5 per cent.

In addition to these observations, mean speed surveys were made in the boundary layer at various points along the model. These are portrayed elsewhere[3, 4] and they constitute the basis for the various

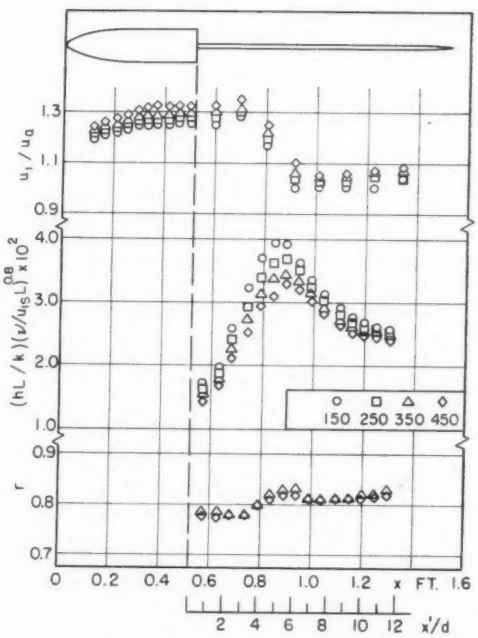

FIG. 2. Results obtained with the 0.81-in. step. The reference velocity, u_a, here is the upstream velocity, and the values in ft./sec., are shown on the Figure to identify the points.

remarks concerning the flow in this presentation, which is devoted primarily to the heat-transfer characteristics of this type of flow system.

Results for the 0.81-In. Step

With this model, heat-transfer coefficients and recovery factors were obtained only in the region downstream of the step, while surface pressure determinations to free-stream velocity values were obtained in both the upstream and downstream regions. These results are shown on Fig. 2, as a function of the distance downstream from the stagnation point on the cylinder which is a convenient specification of distance rather than one of primary importance. Passing the step, it measures downstream distance and the height of the step is not included in it. Shown also on the Figure is the distance, x', downstream of the step, and this is made nondimensional in terms of the step height. As reference velocity for the free-stream velocity distribution the velocity upstream of the model is used, while in the representation of the heat-transfer coefficient the reference velocity is taken as that just upstream of the step.

The values of the local free-stream velocity are indicated by Fig. 2 to be almost constant just upstream of the step. Passing the step, there is a slight acceleration, followed by a decrease of the velocity to the minimum value which is attained near the reattachment point. Thereafter there exists an almost constant free-stream velocity.

Heat-transfer coefficients are shown in terms of the group which correlates such coefficients for turbulent boundary-layer flow, and the 0.8 power dependence on the velocity does exist, particularly in the downstream region. A maximum in the coefficient occurs at about five step heights downstream, and this is the region in which the separated flow is reattached to the surface. There and in the separated region an improved correlation would be obtained by using a power of less than 0.8 on the velocity but the result as exhibited is not inferior in view of the range of velocities involved.

Recovery factors have a magnitude of the order of 0.80, substantially below the value of 0.89 that is typical of a turbulent boundary-layer flow of air. There is no marked change as the reattachment point is passed, and the results that follow indicate that on this model the downstream distance was insufficient for the realization of a significant increase in the recovery factor.

Results for the 0.25-In. Step

Fig. 3 shows the results obtained from the model with the 0.25-in. step, the form of the representation being the same as that of Fig. 2, but with the reference velocity taken at the station at $x = 0.67$ ft., this being used both for the representation of the free-stream velocity and the heat-transfer coefficient.

With this small step, as realized by the attachment of brass plates to the flat plate model, temperature

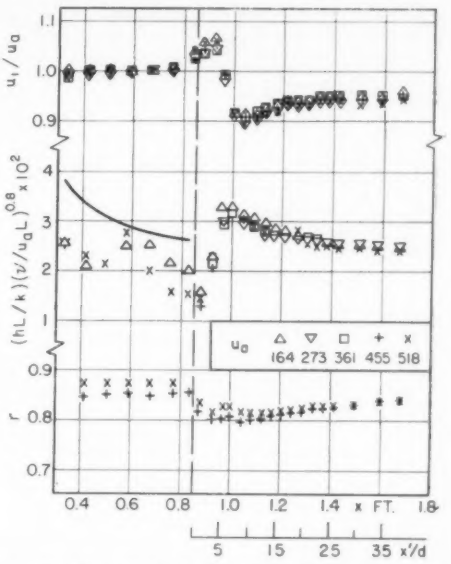

FIG. 3. Results obtained with the 0.25-in. step. The reference velocity, u_a, here is the local velocity of the plate at a distance of $x = 0.67$ ft. from the leading edge, and the values, in ft./sec., are given on the Figure to identify the points. The heavy vertical line indicates the position of the step.

measurements were made below the ribbons in the upstream section. From those indications and from the heat dissipation in the ribbon heat-transfer coefficients were evaluated as though the heat generated had passed out normally to the boundary layer. Because of longitudinal conduction in the brass this was not true, and, hence, the indicated coefficients are erroneous. Consequently only two sets of such apparent heat-transfer coefficients are shown in that region. These may be explained by accounting for the conductivity of the brass and, in addition, assuming a fixed transition point near $x = 0.30$ ft. This assumption is admittedly somewhat unrealistic and may provide a correction for effects actually of different origin, as might be produced by a variable contact resistance between the brass, the paper insulation, and the ribbon at the contact surface. There was also an apparently greater heat conduction to the tunnel side walls in the forward region, accounting for the variable behavior of the recovery factor there.

The important results are those obtained for the region downstream of the step, and these are, in general, similar to those obtained with the larger step. Reattachment appears to occur at about six step heights according to the evidence of the heat-transfer performance shown on Fig. 3 and the indication of mean speed surveys. Within the separated region the correlation of heat-transfer coefficients again applies fairly well, though on first inspection the reduction in the coefficients does not appear to be as great as existed with the larger step. Later examination shows, however, that the two sets of results do correspond. Downstream of reattachment the correlation of coefficients improves continually as the flow becomes more like that of an undisturbed turbulent boundary layer.

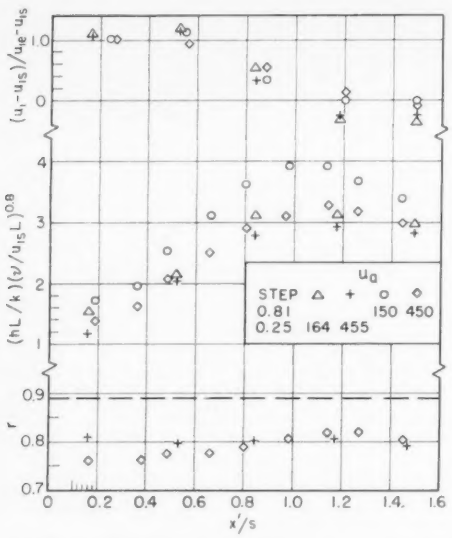

FIG. 4. Heat transfer in the separated region. The unit of the abscissa is the distance, s, from the step to the estimated point of reattachment, being five and six step heights for the large and small steps, respectively. Here the reference velocity for the heat-transfer coefficient is the velocity just upstream of the step. Free-stream velocities have been normalized in terms of this velocity and the velocity further downstream.

This approach is closer with the smaller step because of the relatively greater downstream distance in number of step heights that existed with this model. This effect is also apparent in the results for the recovery factor, which in this case shows an increase after flow reattachment, though the increase is gradual and the value of 0.89 typical of turbulent boundary-layer flow is never attained.

The Region of Separated Flow

Even a cursory examination of the results of Figs. 2 and 3 reveals similarities in the regions of separated flow, and the immediate quest is for a representation in which the similarity will be emphasized. Theoretical considerations are not yet well founded enough for such an indication, and the guides must be empirical. A dimensionless distance, in measures of step height, suggests itself, and it will, in fact, serve to show some similarity, but a representation of that kind indicates also that a measure in proportion to the distance to the reattachment point is even more appropriate. Despite the partial uncertainty in the location of that point, this has been made the basis of Fig. 4, with the distance to reattachment taken as five step heights for the larger step and six heights for the smaller. On this Figure the distributions of free-stream velocity have been altered to a form providing coincidence at the step and at large distances downstream, and the velocity in the heat-transfer correlation is taken as that at the step. For clarity, the number of the results presented has been reduced to those for the highest and lowest speeds for the large and the small step, respectively.

Fig. 4 emphasizes the similarity in the free-stream velocity distribution, which differs for the two situations only near the reattachment point, where for the small step the velocities were slightly lower than those ultimately attained downstream. It is significant that the major part of the separated region is at almost constant pressure, as indicated both by the results that are shown and those obtained by static tube surveys made normal to the surface.

The results for the local heat-transfer coefficient, shown here with a reference velocity corresponding to that just upstream of the step, again show the relative inferiority of the 0.8 power correlation. For the larger step, it is clear that no single power law will suffice for the entire separated region, though a lower power would improve the correlation somewhat. Average values of the coefficient, for the entire separated region, depend on the velocity to about the 0.60 power. For the present, however, the 0.8 power may be considered to provide a degree of correspondence adequate with respect to the novelty of the results. New in this sense is the similarity of the local coefficients in the representation of the Figure, and their consistent trend from the maximum value near reattachment to reduced values as the step is approached, the reduction being twofold in the short distance involved.

While no theory for the prediction of local coefficients of heat transfer in the separated region exists, Chapman[6] indicated how average values might be obtained by using his theory for separated laminar flows. He extended this to turbulent flows to indicate that the average heat-transfer coefficient might be much greater than that for a turbulent boundary-layer flow of the same longitudinal extent as that of the separated region. Conversely, the experimental results reveal that the heat transfer in the separated region is much less.

In the region of separated flow there is scarcely any discriminatory behavior of the recovery factor within the possible errors of measurement in the quantity, though with the larger step there is a slow rise toward the reattachment point. A magnitude of about 0.78 to 0.80 is typical, and this is characteristic of what has been found for other separated and reattached flows, as in the case of the rod on the plate, for which the results are presented in the Appendix; at the back of a cylinder equipped with a downstream splitter plate;[7] and for very much smaller separation by Seban[8] behind wires, and by Brinich[9] behind small roughness elements in supersonic flow.

The Reattached Region

After reattachment, the mean speed distribution in the boundary layer gradually returns to a profile typical of turbulent boundary-layer flow. In a relatively short distance it takes the form of a power law, of exponent greater than 1/7, and with increasing distance downstream this exponent diminishes slowly toward the value appropriate to the Reynolds Number involved. Klebanoff and Diehl[10] have shown that this requires a long downstream distance and have shown also that the small changes in mean speed distribution that

occur make this profile a poor index of the completeness of flow redevelopment. In the present experimental models the distances downstream from reattachment were short, about six step heights for the larger step and 35 for the small step, and these were far too short for redevelopment, although after about 20 step heights power law profiles were attained.

The recovery factor itself indicates the unbalanced energy distribution in the flow. As shown particularly on Fig. 3, the recovery factor varies little within about six or seven step heights downstream of reattachment and thereafter begins a gradual increase, but even in the 35 step heights available with the model having the small step a value of only 0.845 was attained. This indicates that a substantially greater downstream distance is needed for the realization of the value of 0.89 typical of a fully developed turbulent boundary layer.

Examination of the heat-transfer coefficient indicates a reduced sensitivity to the degree of flow development, and, to indicate this, the values of the coefficient are shown on Fig. 5 in terms of the distance downstream of the estimated point of reattachment. In this case, the reference velocity is taken as that in the downstream region, rather than that at the step which was used in the conditions in the separated region as given in Fig. 4. For comparison with the results for the large step, two predicted values for a turbulent boundary layer are shown, one for heating beginning at the reattachment point and the other for heating beginning at the step, as it actually did. Near reattachment the points are nearer the former curve, but near the end of the test section, at six step heights downstream of reattachment, they are also only 5 per cent above the latter

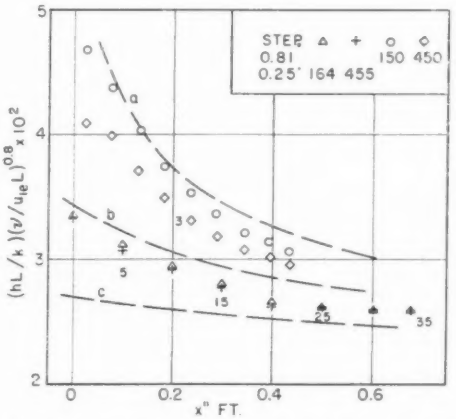

FIG. 5. Heat transfer in the reattached region. The abscissa is the distance downstream from the estimated reattachment point, and the reference velocity is that of the downstream region. The curves are the Colburn equation

$$hx/k = 0.030\,(u_1 x/\nu)^{0.8}\,(\nu/\alpha)^{1/3}$$

based on various origins for x.

(a) For the large step with origin at reattachment.

(b) For the large step with origin at the step, where heating did begin.

(c) For the small step with origin at the point where heating did begin.

The numbers near the points for the results are the number of step heights downstream of the reattachment point.

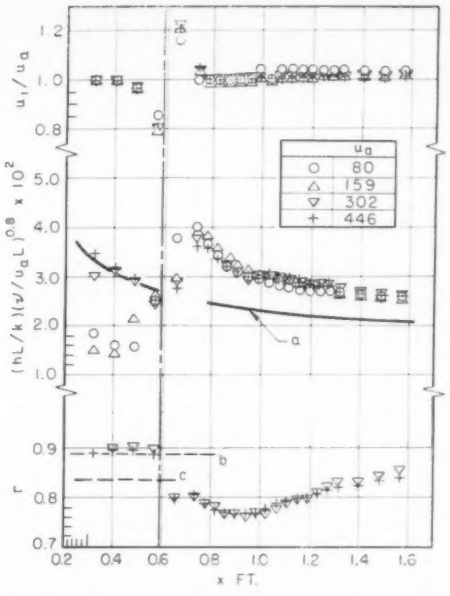

FIG. 6. Results obtained with a 0.125-in. rod on a flat plate. The reference velocity, u_a, in ft./sec., is that at $x = 0.40$ ft. Curve a indicates the heat-transfer performance obtained without the rod. Line b indicates the magnitude of the cube root of the Prandtl Number. The position of the rod at $x = 0.59$ ft. is indicated by the heavy vertical line on the Figure.

prediction, and the trend is toward it. For the small step, only the prediction made for the actual heated length is shown and the relation of the experimental values to it is the same, but the approach is less rapid than with the small step, being within 5 per cent at about 17 step heights downstream. This is rather the reverse of expectation, in that the heat-transfer coefficient would approach the value for a turbulent boundary layer either more rapidly for the small step or, possibly, in the same way in both cases. The salient feature is, however, not so much the degree of approach but the closeness thereof, as indicative of the reduced sensitivity of the heat-transfer coefficient to the exact nature of the attached flow.

Conclusion

As indicated at first, it is the intent of this paper to demonstrate the character of the local heat transfer in regions of turbulent separated and reattached boundary-layer flow. This has been done by the use of experimental results from two models having backward facing steps and, while they certainly do pertain only to systems of this general kind of geometry, certain general features are apparent.

The 0.8 power dependence of the heat-transfer coefficient on the velocity is maintained to some degree in the entire downstream region. A maximum in the heat-transfer coefficient at the reattachment point is a characteristic feature of all the results, as is the decrease in the heat-transfer coefficient as the separation point is approached from downstream.

The local recovery factor is of the order of 0.80 in the

entire separated region, a value that seems to some extent to be characteristic of separated flows. After reattachment there is a slow increase and it appears that a very long downstream distance is required for the return to equilibrium conditions that result in the value of about 0.89, typical of a turbulent boundary-layer flow.

Appendix

In connection with showing the experimental results attained with the steps it is relevant to consider certain additional results obtained with the plate before its modification for the realization of the small step. By placing a bakelite rod 0.125 in. in diameter upon the surface of the plate at a distance of 0.59 ft. from the leading edge, a separated and reattached flow was obtained, with separation occurring at a very short distance upstream of the cylinder. In this location the interval between instrument locations was greater so that less detail was obtained in the separated region, but the downstream distance available was almost 100 rod diameters.

Fig. 6 shows the results in the form used for the results for the steps. General similarity is indicated, though there are some differing features. If the maximum in the heat-transfer coefficient is taken to indicate the reattachment point, then this was at 0.75 ft., or about 15 rod diameters, and at that point the coefficient is about 50 per cent above the value predicted for a turbulent boundary layer with the same heated length. Also, the return to the prediction is slower, with a final difference of 20 per cent at the end of the plate, exceeding substantially what was found with the step. This may be an inference of proportionately greater flow disturbance with the rod, though the mean speed profiles in the boundary layer showed nothing definitive in this regard.

The recovery factor magnitudes show also a reduced rate of return toward the "fully developed value," reaching only 0.85 at 100 diameters downstream, and showing also a minimum downstream of the reattachment point. With the rod, the immediate downstream values are like those of the step but after reattachment there is a further decrease to a minimum of 0.76.

References

[1] Arie, M., and Rouse, H., *Experiments on Two-Dimensional Flow Over a Normal Wall*, J. Fluid Mech., Vol. 1, July, 1956.

[2] Hsu, H., *Characteristics of Mean Flow and Turbulence at an Abrupt Two-Dimensional Expansion*, Ph.D. dissertation, State University of Iowa, 1950.

[3] Seban, R. A., *Heat Transfer and Flow With Separated and Reattached Boundary Layers as Produced by Surface Irregularities*, WADC Report TR-56-217, 1956.

[4] Emery, A., *Heat Transfer Downstream of a Step in a Plate*, M.S. thesis, University of California at Berkeley, January, 1958.

[5] Seban, R. A., and Doughty, D. L., *Heat Transfer to Turbulent Boundary Layers With Variable Free-Stream Velocity*, Trans. ASME, Vol. 78, No. 1, 1956.

[6] Chapman, D., *A Theoretical Analysis of Heat Transfer in Regions of Separated Flow*, NACA TN 3792, 1956.

[7] Seban, R. A., and Levy, A., *The Effect of a Downstream Splitter Plate on the Heat Transfer From a Circular Cylinder Normal to an Air Stream*, WADC Report TR-57-479, 1957.

[8] Seban, R. A., Levy, S., Doughty, D., and Drake, R. M., *Effect of Single Roughness Elements on the Heat Transfer From a 1:3 Elliptical Cylinder*. Trans. ASME, Vol. 76, No. 4, 1954.

[9] Brinich, P., *Recovery Temperatures and Heat Transfer Near Two-Dimensional Roughness Elements at Mach 3.1*, NACA TN 4213, 1958.

[10] Klebanoff, P., and Diehl, R., *Some Features of Artificially Thickened Fully Developed Turbulent Boundary Layers With Zero Pressure Gradient*, NACA TN 2475, 1951.

Space Vehicle Environment

(*Continued from page 782*)

[35] Kallmann (-Bijl), H. K., *Quantitative Estimate of Frequency and Mass Distribution of Dust Particles Causing the Zodiacal Light Effect*, Memores de la Societe Royale des Sciences de Liege, Series 4, Vol. 15, Universite de Liege, Liege, 1955.

[36] Bjork, R. L., The RAND Corporation, Personal communication, June 1958.

[37] Van Valkenburg, M. E., *Modeling of High-Speed Impacts Through the Use of Plastics*, Paper presented at The RAND Symposium on High-Speed Impact, February, 1955.

[38] Huth, J. H., Thompson, J. S., and Van Valkenburg, M. E., *Some New Data on High-Speed Impact Phenomena*, J. Appl. Mech., March, 1957.

[39] Baldwin, R. B., *The Face of the Moon*, The University of Chicago Press, 1949.

[40] Grimminger, G., *Probability that a Meteorite Will Hit or Penetrate a Body Situated in the Vicinity of the Earth*, J. Appl. Phys., October, 1948.

[41] Manring, E., and Dubin, M., *Satellite Micrometeorite Measurements*, Paper No. 3, IGY Satellite Report Series No. 3, May 1, 1958.

Viscous Hypersonic Similitude†

WALLACE D. HAYES* AND RONALD F. PROBSTEIN**

Princeton University and Brown University

Summary

An extension of classical hypersonic similitude is developed which takes into account the interaction effect of the displacement thickness of the boundary layer. A basic result of this viscous similitude is that the total drag including frictional drag obeys the classical similarity law for the pressure drag. Additional similarity conditions governing viscous effects must be imposed in this similitude.

Underlying the similitude is a new hypersonic boundary-layer independence principle. According to this principle, the principal part of a hypersonic boundary layer with given pressure and wall temperature distributions and free-stream total enthalpy is independent of the (high) external Mach Number distribution outside the boundary layer.

Various features of viscous hypersonic similitudes are discussed. It is found, for example, that it applies to three-dimensional boundary-layer interaction effects on flat bodies, provided the concepts of strip theory may be applied, and provided the aspect ratio is an invariant.

Symbols

a	= speed of sound
c	= chord of body
c_p	= specific heat at constant pressure
C	= $\mu_b T_\infty / \mu_\infty T_b$
C_f	= skin-friction coefficient
C_D	= drag coefficient
C_p	= pressure coefficient
C_q, C_Q	= heat-transfer coefficients
C_L	= lift coefficient
f	= dimensionless stream function
g	= total enthalpy ratio
h	= enthalpy
H	= $h + (1/2)u^2$, total enthalpy
k	= heat-conduction coefficient
K	= $M_\infty \tau$, basic similitude parameter
p	= pressure
q	= local heat-transfer rate
Q	= total heat-transfer rate
r_b	= radius of body of revolution
$\mathfrak{R}$	= gas constant
s	= viscosity dependence exponent
T	= absolute temperature
T_0	= stagnation temperature
u, v, w	= velocity components
U	= free-stream velocity
x, y, z	= coordinates
α	= angle of attack
γ	= isentropic exponent for perfect gas
δ	= boundary-layer total thickness
δ^*	= boundary-layer displacement thickness
Δ	= shock layer thickness
η	= dimensionless Howarth-Dorodnitsyn variable
λ	= mean free path
μ	= viscosity coefficient
ρ	= density
σ	= shear stress
τ	= thickness ratio
ξ	= dimensionless distance along boundary layer
$\bar{\chi}$	= $M_\infty{}^3\sqrt{C}/\sqrt{Re_\infty}$, interaction parameter
Pr	= $c_p\mu/k$, Prandtl Number
Re	= $\rho u c/\mu$, Reynolds Number
St	= $q/\rho u(h_r - h_b)$, Stanton Number
AR	= aspect ratio

Subscripts

∞	= free stream
b	= body or wall
s	= shock
δ	= outside the boundary layer

(1) Introduction

CLASSICAL hypersonic similitude, the first theory of which was given by Tsien,[1] is exclusively concerned with the flow of an inviscid fluid. It has long been appreciated that viscous interaction effects are very important in hypersonic flows on slender bodies, and that their neglect imposes a severe limitation on the application of the classical similitude. The purpose of this paper is to present appropriate similitude laws for steady hypersonic flow on slender bodies with viscous interaction effects taken into account.

The present work stems from a joint undertaking of the authors[2] in preparing a book on hypersonic flow theory. The book includes treatments of the hypersonic boundary layer and of interaction effects (besides the classical similitude), and, to a large extent, the present results are constructed directly from results given in the book.

An immediate consequence of the equivalence principle given by Hayes[3] is that hypersonic similitude has a great generality and is applicable to fluids obeying general equations of state and to general three-dimensional bodies. In viscous hypersonic similitude, most of this generality is lost. Additional assumptions must be made—e.g., that the fluid is a perfect gas—including assumptions on the dependence of the viscosity on the temperature. And a three-dimensional form of the similitude is only available in case the concept of strip theory in the inviscid flow is applicable. Laminar boundary-layer theory is assumed to apply; this assumption is a realistic one under flight condi-

Presented at the Aerodynamics—IV Session, IAS 27th Annual Meeting, N.Y., Jan. 26–29, 1959. Revised and received June 10, 1959.

† This investigation was supported by the USAF, in part under Contract No. AF49(638)-465 monitored by the Office of Scientific Research, and in part under Contract No. AF 33(616)-5442 monitored by the Aeronautical Research Laboratory, Wright Air Development Center.

* Professor of Aeronautical Engineering, Princeton University.

** Professor of Engineering, Brown University.

tions for which hypersonic interaction effects are important.

The basic requirement that we impose on this viscous similitude is that the ratio of displacement thickness of the boundary layer to body thickness be fixed in the similitude. Thus, the emphasis here is on interaction effects in which the existence of the boundary layer has an appreciable influence on the pressure distribution. Another quantity which must be fixed in the similitude is the ratio of body temperature to stagnation temperature. The body temperature is a fundamental parameter in all hypersonic flows in which real-fluid effects are involved.

(2) Mach Number Independence Principle

A basic principle in hypersonic flow theory, given as a similitude by Oswatitsch[4] in the case of a perfect gas, is the principle that a limiting solution is obtained in a suitable limiting process in which the free-stream Mach Number M_∞ is made to approach infinity. For a general fluid, the free-stream density ρ_∞ and the velocity U of the undisturbed flow must be fixed, and the quantities a_∞, p_∞, T_∞, and h_∞ approach zero in the limiting process. If M_∞ is sufficiently large, the solution behind the bow shock wave becomes independent of M_∞, and hence of p_∞ or T_∞.

The authors' point of view is that this principle should not be considered as a similitude, and is, in fact, more than a similitude. The flow field in front of the bow shock is not a part of the flow field of interest, and two flows with different sufficiently high values of M_∞ are not merely similar but are essentially identical.

The pertinent point here is that this Mach Number independence principle applied with ρ_∞ and U fixed in a given fluid applies to all real fluid effects, including not only viscosity and heat conduction but also relaxation, diffusion, and rarefied gas effects. Of course, if the principle were to be interpreted as a similitude, a viscous hypersonic similitude would be obtained.

With a perfect gas of constant isentropic exponent γ, the self-similar properties of the fluid permit us to relax the requirement that ρ_∞ and U be fixed, provided the gas is inviscid. The similarity thereby obtained is essentially the dimensional similarity always obtainable with an inviscid perfect gas of constant γ.

(3) Hypersonic Similitude

Following the equivalence principle for hypersonic similitude on a family of affinely related slender bodies of characteristic thickness ratio τ in a general fluid, it is necessary that the quantities ρ_∞, $U\tau$, and p_∞ be fixed and that both τ and M_∞^{-1} be small. For the Mach Number independence principle to hold $M_\infty\tau$ must be very large, and the dependence on p_∞ may be dropped. With a flat or quasi-cylindrical body $\tau/\mathcal{R}$ must be fixed, where $\mathcal{R}$ is the aspect ratio of the body; and any quantity such as α/τ, where α is the angle of attack, must be fixed.

If, with a flat or quasi-cylindrical body, the quantity $\tau/\mathcal{R}$ is small, so that $\tau^2/\mathcal{R}^2$ may be neglected in comparison with one, the flow field may be calculated stripwise, and the concept of strip theory applies. In this case, the dependence on the parameter $\tau/\mathcal{R}$ in the similitude may be dropped. We shall be considering primarily two-dimensional and axisymmetric bodies, for which this parameter does not enter.

For a perfect gas of constant isentropic exponent γ, the results of the similitude may be expressed in dimensionless form. For a family of affinely related bodies of thickness ratio τ in two-dimensional flow, the pressure coefficient C_p may be expressed

$$C_p = (p - p_\infty)/(1/2)\rho_\infty U^2 = \tau^2 \Pi(x/c,\ y/c;\ K,\ \gamma) \tag{3-1}$$

where K is the basic similitude parameter defined as

$$K = M_\infty \tau \tag{3-2}$$

The essential feature of the similitude is the reduction of the dependence of C_p on M_∞ and τ separately to a dependence of C_p/τ^2 on the single parameter K.

An important feature of inviscid hypersonic flows on slender bodies is that they are locally hypersonic. The local Mach Number may be much smaller than M_∞ but it is always of the order of M_∞ or τ^{-1}, whichever is smaller. Since we require that τ be small, the local Mach Number must everywhere be large. The importance of this fact here is that the Mach Number M_δ just outside the boundary layer must be large.

(4) The Hypersonic Boundary Layer

When the flow in the inviscid flow field just outside a boundary layer is hypersonic, the boundary layer has certain special properties which characterize it. The material within the boundary layer is very much hotter and, consequently, at a much lower density than the material outside the boundary layer. While the displacement thickness of the boundary layer is of the same order of magnitude as the overall thickness, the difference between the two, the momentum thickness, and the enthalpy defect thickness, are all much thinner. In addition, the viscosity variation with temperature at the relatively much lower temperatures in and near external flow conditions is unimportant. Typical velocity, density, and mass-flow profiles are sketched for an insulated body in Fig. 1, and for a highly cooled body in Fig. 2.

The boundary-layer equations in two-dimensional or axisymmetric steady flow may be written as

$$(\partial \rho u r_b^j/\partial x) + (\partial \rho v r_b^j/\partial y) = 0 \tag{4-1a}$$

$$\rho u(\partial u/\partial x) + \rho v(\partial u/\partial y) = \rho_\delta u_\delta (du_\delta/dx) + (\partial/\partial y)[\mu(\partial u/\partial y)] \tag{4-1b}$$

$$\rho u(\partial H/\partial x) + \rho v(\partial H/\partial y) = (\partial/\partial y)\{(\mu/Pr)(\partial H/\partial y) + \mu[1 - (1/Pr)][\partial(1/2)u^2/\partial y]\} \tag{4-1c}$$

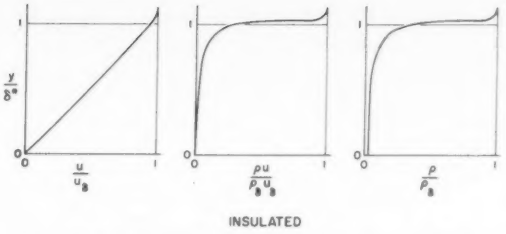

FIG. 1. Typical hypersonic boundary-layer profiles for an insulated body.

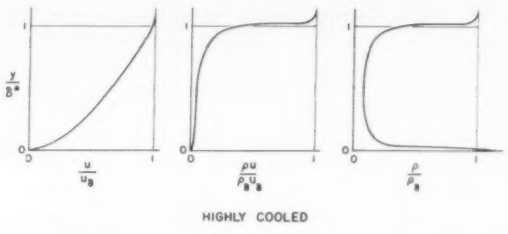

FIG. 2. Typical hypersonic boundary-layer profiles for a highly cooled body.

Here $j = 0$ in two-dimensional flow, $j = 1$ in axisymmetric flow, $r_b(x)$ is the cylindrical radius from the axis of symmetry in the latter case, and H is the total enthalpy equal to $h + (1/2)u^2$. The transformation

$$\xi(x) = \int_0 \rho_b \mu_b u_\delta r_b^{2j} dx \tag{4-2a}$$

$$\eta = (u_\delta r_b^j/\sqrt{2\xi}) \int_0 \rho dy \tag{4-2b}$$

$$f = \int_0 (u/u_\delta) d\eta \tag{4-2c}$$

$$g = H/H_\delta \tag{4-2d}$$

$$N = \rho\mu/\rho_b\mu_b \tag{4-2e}$$

changes the boundary-layer equations into the form

$$(Nf_{\eta\eta})_\eta + ff_{\eta\eta} + 2(d \ln u_\delta/d \ln \xi)[(\rho_\delta/\rho) - f_\eta^2] = 2\xi(f_\eta f_{\eta\xi} - f_\xi f_{\eta\eta}) \tag{4-3}$$

$$[(N/Pr)g_\eta]_\eta + fg_\eta + (u_\delta^2/H_\delta)\{N[1 - (1/Pr)]f_\eta f_{\eta\eta}\}_\eta = 2\xi(f_\eta g_\xi - f_\xi g_\eta) \tag{4-4}$$

with subscripts indicating partial differentiation. This transformation combines the Mangler and Howarth-Dorodnitsyn transformations.

At this point, we make the assumption that the fluid is a perfect gas of constant γ so that we may replace ρ_δ/ρ by h/h_δ in Eq. (4-3). The easily proved identity

$$(h/h_\delta) - f_\eta^2 = (H_\delta/h_\delta)(g - f_\eta^2) \tag{4-5}$$

permits us to write Eq. (4-3) in the form

$$(Nf_{\eta\eta})_\eta + ff_{\eta\eta} + \beta(g - f_\eta^2) = 2\xi(f_\eta f_{\eta\xi} - f_\xi f_{\eta\eta}) \tag{4-6}$$

with

$$\beta(x) = \beta(\xi) = 2(H_\delta/h_\delta)(d \ln u_\delta/d \ln \xi) \tag{4-7}$$

The substitution of Eq. (4-5) has the same effect as does the Stewartson-Illingworth transformation.

For a boundary layer in which the external flow is hypersonic, $h_\delta \ll H_\delta$, and $(1/2)u_\delta^2 \doteq H_\delta$. With this approximation, we may write in place of Eq. (4-4)

$$[(N/Pr)g_\eta]_\eta + fg_\eta + 2\{N[1 - (1/Pr)]f_\eta f_{\eta\eta}\}_\eta = 2\xi(f_\eta g_\xi - f_\xi g_\eta) \tag{4-8}$$

The usual boundary conditions for Eq. (4-3) or (4-6) and Eq. (4-4) or (4-8) are

$$f(0, \xi) = 0, \quad f_\eta(0, \xi) = 0, \quad g(0, \xi) = g_b(\xi) \tag{4-9a}$$

$$f_\eta \to 1, \quad g \to 1, \quad \text{as } \eta \to \infty \tag{4-9b}$$

These are expressed for a given temperature distribution on the body. If the heat transfer is specified, the condition on $g(0, \xi)$ is replaced by one on $g_\eta(0, \xi)$.

Application of the perfect gas laws and the hypersonic approximations to Eq. (4-7) gives us the hypersonic formula for β

$$\beta = -[(\gamma - 1)/\gamma] \times \left(\int_0 \mu_b T_b^{-1} p r_b^{2j} dx \Big/ \mu_b T_b^{-1} p^2 r_b^{2j}\right)(dp/dx) \tag{4-10}$$

It should be noted that β, as given by Eq. (4-10), is homogeneous of degree zero in the quantities p, r_b, and $\mu_b T_b^{-1}$, and also in the independent variable x. These facts will be needed in establishing a viscous similitude. We may also note that the differential quantity $d \ln \xi$ has the same properties.

It is assumed that the viscosity is a function of temperature alone. The ratio of temperature to external stagnation temperature T/T_0 is equal to h/H_δ in a perfect gas. We may express the latter quantity as

$$h/H_\delta = g - f_\eta^2 + (h_\delta/H_\delta)f_\eta^2 \doteq g - f_\eta^2 \tag{4-11}$$

The third term in this expression, the one in h_δ/H_δ, is negligible for a hypersonic boundary layer, except very near the outer edge of it. With this exception, we may write N as

$$N = \mu T_b/\mu_b T = n(T)/n(T_b) \doteq n[T_0(g - f_\eta^2)]/n[T_0 g_b] \tag{4-12}$$

If $\mu \propto T^s$, then $n \propto T^{s-1}$, and

$$N \doteq [(g - f_\eta^2)/g_b]^{s-1} \tag{4-13}$$

The importance of the fact that the approximations of Eqs. (4-12) and (4-13) are not valid very near the outer edge of the boundary layer will be discussed in the next section.

We next examine the displacement thickness δ^* defined by

$$\delta^* = (1/\rho_\delta)\int_0^\infty [(\rho_\delta/\rho) - (u/u_\delta)]\rho dy = (\rho dy/\rho_\delta d\eta)\int_0^\infty [(\rho_\delta/\rho) - f_\eta] d\eta \tag{4-14}$$

With the aid of Eq. (4-5) we may re-express δ^* as

$$\delta^* = (H_\delta/h_\delta)(\sqrt{2\xi}/r_b{}'\rho_\delta u_\delta)[\Delta^* + \Theta - (h_\delta/H_\delta)\Theta] \tag{4-15}$$

where

$$\Delta^* = \int_0^\infty (g - f_\eta)d\eta \tag{4-16a}$$

$$\Theta = \int_0^\infty (1 - f_\eta)f_\eta d\eta \tag{4-16b}$$

Neglecting the third term in the parenthesis of Eq. (4-15), we may write

$$\delta^*/C = (H_\delta/h_\delta)\sqrt{\rho_\delta\mu_b/\rho_\delta{}^2u_\delta c} \times \sqrt{2\xi[d(x/c)/d\xi]}(\Delta^* + \Theta) \tag{4-17}$$

where c is some reference chord length.

The shear stress on the body surface is denoted σ (to differentiate it from the thickness ratio) and equals $\mu\ \partial u/\partial y$ evaluated at the wall. We may express σ in terms analogous to those used in Eq. (4-17) as

$$\sigma = \rho_\delta u_\delta{}^2\sqrt{\rho_\delta\mu_b/\rho_\delta{}^2u_\delta c}\ \sqrt{d\xi/2\xi d(x/c)}(f_{\eta\eta_b}) \tag{4-18}$$

The heat flux to the body q equals $(\mu/Pr)\ \partial H/\partial y$ evaluated at the wall. We obtain

$$q = \rho_\delta u_\delta H_\delta\sqrt{\rho_b\mu_b/\rho_\delta{}^2u_\delta c}\ \sqrt{d\xi/2\xi d(x/c)} \times (g_{\eta_b}/Pr_b) \tag{4-19}$$

We may apply the concept of the scale transformation to any boundary layer. Under such a scale transformation we specify p, T_b, u_δ, etc., as functions of x/c and make a change in c. The boundary-layer equations are essentially invariant under this transformation, and $cd\xi/\xi dx$ is a function of x/c alone. The lateral scale varies as $c^{1/2}$, and the shear stress and heat flux vary as $c^{-1/2}$. With three-dimensional boundary layers on surfaces of small curvature, there is a functional dependence on $z/\mathcal{A}\mathrm{R}c$, where $\mathcal{A}\mathrm{R}$ is an aspect ratio which is invariant in the transformation.

A special case of interest is that in which the fluid is a perfect gas of constant γ within the principal part of the hypersonic boundary layer, but for which the perfect gas law and value of γ do not fit the state of the fluid and value of γ just outside the boundary layer. The principal part of the hypersonic boundary layer here may be defined as that part within which the approximation of Eq. (4-11) is valid.

In this case, we set

$$\rho_\delta/\rho = (\rho_\delta/\rho_b)(h/h_b) \tag{4-20}$$

and, within the region of validity of Eq. (4-11), we set

$$(\rho_\delta/\rho) - f_\eta{}^2 \doteq (\rho_\delta/\rho_b)(H_\delta/h_b)(g - f_\eta{}^2) \tag{4-21}$$

The term h_δ in Eqs. (4-7), (4-15), and (4-17) is replaced by $\rho_b h_b/\rho_\delta$, and the factor $(\gamma - 1)/\gamma$ in Eq. (4.10) is interpreted in terms of the value of γ within the boundary layer. The homogeneity properties of β according to Eq. (4-10) are unchanged.

(5) The Hypersonic Boundary Layer Independence Principle

We now point out the existence of an independence principle for hypersonic boundary layers. In order to introduce this principle, we first examine, as a simple example, the case of the self-similar boundary layer with zero pressure gradient. The momentum equation, Eq. (4-6) in this case, with f a function $f(\eta)$ of η alone, becomes

$$(Nf_{\eta\eta})_\eta + ff_{\eta\eta} = 0 \tag{5-1}$$

The transformation of Crocco[5] is

$$\phi = f_\eta \tag{5-2a}$$

$$\Phi(\phi) = Nf_{\eta\eta} \tag{5-2b}$$

and changes Eq. (5-1) into the form

$$\Phi\Phi'' + N\phi = 0 \tag{5-3}$$

The boundary conditions here are

$$\Phi'(0) = 0 \tag{5-4a}$$

$$\Phi(1) = 0 \tag{5-4b}$$

We further assume that $Pr = 1$ and the body is insulated, in which case the solution for the energy equation is simply $g = 1$. The main question now is whether a limiting solution exists in the limit $M_\delta \to \infty$, with $h_\delta/H_\delta \to 0$. We employ the approximation of Eq. (4-11), which is valid in this limit, and assume Eq. (4-13). We then must have

$$N \propto (1 - \phi)^{s-1} \tag{5-5}$$

near $\phi = 1$. Examination of Eq. (5-3) shows that

$$\Phi \propto (1 - \phi)^{(1/2)(1+s)}/(1 - s^2)^{1/2} \tag{5-6}$$

near $\phi = 1$, and that a solution of Eq. (5-3) satisfying the boundary condition $\Phi(1) = 0$ is obtained as long as $s > -1$. If $s = 1$, the solution is logarithmic. Since in practice s is of the order of $1/2$ or 1, a suitable solution in the limiting case is always obtainable. We may expect that the convergence to this limiting solution is uniform in an appropriate sense.

From a physical point of view, this result is readily generalized. The pertinent feature is that with the fluid composition, the pressure distribution, the temperature distribution of the body surface, and the (approximately constant) velocity of the exterior flow given, the solution within the principal part of the boundary layer does not depend upon the value of the exterior Mach Number M_δ or, hence, upon the related exterior density ρ_δ, provided M_δ is very large. An appreciable dependence upon M_δ or ρ_δ appears only within a thin transitional layer at the outer edge of the boundary layer. In the example above, the thickness of this layer is of the order of $M_\delta{}^{-s-1}$ times the displacement thickness.

It is also clear that this independence of the external Mach Number applies also to three-dimensional boundary layers of the mean-surface type, with the

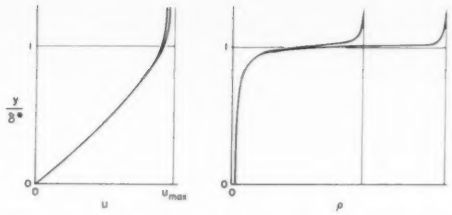

FIG. 3. Profiles for two hypersonic boundary layers illustrating independence principle.

condition $\partial p/\partial n = 0$ applicable. In addition, it must apply to a large number of real-fluid effects within the boundary layer not considered here in detail. These include diffusion of different species, chemical reaction in the layer or with the surface material, evaporation or ablation of the surface material, and even radiation, provided the cool material outside the boundary layer is not itself radiating and is either extremely opaque or extremely transparent.

We do not consider this independence principle as a similitude because two boundary layers differing only in their M_δ or ρ_δ distributions are essentially identical rather than only similar. From the boundary-layer point of view and with the boundary-layer assumptions, the flow field of interest lies within the principal part of the boundary layer covered by the independence principle. The thin transitional layer acts as a surface discontinuity, for which there is a finite but small thickness and a structure, which separates the principal part of the boundary layer from the external flow field. This external flow field is not a flow field of interest from the boundary-layer point of view.

Note that no question has been raised as to the factors controlling the pressure distribution. Consistent with the classical point of view in boundary-layer theory, we consider the pressure distribution as one of the parts of the problem which can be arbitrarily specified. There is, of course, an interaction between the displacement thickness distribution of the boundary layer and the external flow field; it is precisely this phenomenon which we undertake to consider in developing a viscous hypersonic similitude.

The hypersonic boundary-layer independence principle is illustrated in Fig. 3, with typical velocity and density profiles for two boundary layers with essentially identical principal parts.

(6) General Features of a Viscous Similitude

The flow field outside the boundary layer on a body is the same as the flow field with an inviscid flow on the same body increased in its dimensions by the displacement thickness of the boundary layer. If we are to have hypersonic similitude for this external flow field on a family of bodies, the total thickness distributions of the bodies including the displacement thickness must be affinely related. We require that the bodies themselves be affinely related, and conclude that the distribution of displacement thickness follow the same affine law as does the total thickness (see Fig. 4). Thus, we must have

$$\delta^*/\tau c = \text{funct. } (x/c) \tag{6-1}$$

in two-dimensional or axisymmetric flow. The pressure distributions on related bodies following the hypersonic similarity laws are themselves affinely related. We require that the distribution of the quantity $\mu_b T_b^{-1}$ be also affinely related, with

$$\mu_b T_b^{-1} = M \cdot \text{funct. } (x/c) \tag{6-2}$$

where M is a function of the parameters of the problem, primarily of U and of the fluid. We require that $h_b/H_\delta = g_b$ be a function of x/c alone, that

$$g_b = g_b(x/c) \tag{6-3}$$

And we require that $N\ (\eta, \xi)$ be a function of x/c and η alone, that

$$N = N(\eta, x/c) \tag{6-4}$$

A similar assumption is needed for the Prandtl Number. And, of course, we have the basic requirement that K defined in Eq. (4-2) and γ be invariant.

With the hypersonic assumptions in a perfect gas of constant γ, the requirements above ensure us that β is a function of x/c alone, that ξ is proportional to a function of x/c alone, and that two boundary layers satisfying the requirements are similar. With the boundary layers similar, Δ^* and Θ of Eqs. (4-16) are functions of x/c alone, and from Eq. (4-17) we may replace requirement (6-1) by the requirement that

$$(H_\delta/\tau h_b)\sqrt{\rho_b\mu_b/\rho_\delta^2 u_\delta c} = \text{funct. } (x/c) \tag{6-5}$$

Note that the condition Eq. (6-2) is not independent of Eq. (6-5). With the hypersonic assumptions, the perfect gas properties, and requirement Eq. (6-3), we may change Eq. (6-5) to

$$1/\tau\sqrt{Re_b} = \text{funct. } (x/c) \tag{6-6}$$

where

$$Re_b = \rho_b U c/\mu_b \tag{6-7}$$

and we have replaced u_δ by U.

In view of the requirements of Eqs. (6-2) and (6-3), we need apply Eq. (6-6) only at some single reference

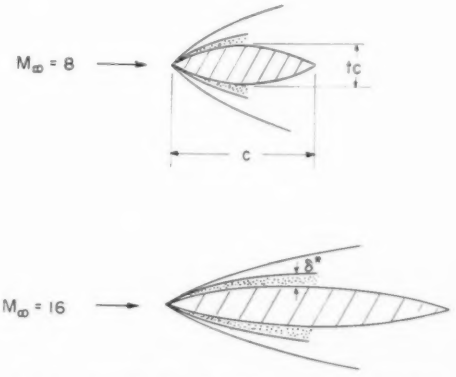

FIG. 4. Related bodies in viscous hypersonic flow.

point; the quantity $\tau\sqrt{Re_b}$ defined in terms of ρ_b and μ_b at that reference point must be an invariant. Since K is an invariant (unless it is infinite), we may multiply the quantity of Eq. (6-6) by K^2 to obtain an alternative invariant. With some analysis, noting that ρ_δ/ρ_∞ is invariant, we conclude that

$$\tilde{\chi} = M_\infty{}^3\sqrt{C}/\sqrt{Re_\infty} \tag{6-8}$$

must be invariant, where

$$C = \mu_b T_\infty/\mu_\infty T_b \tag{6-9}$$

evaluated at the reference point, and

$$Re_\infty = \rho_\infty U c/\mu_\infty \tag{6-10}$$

The quantity $\tilde{\chi}$ is the basic interaction parameter of Probstein and Lees (see reference 2), evaluated in terms of the total chord length.

It is impossible to find a viscous similitude for a fluid obeying a general equation of state. After imposing the principal requirements above, we must conclude that such a general solution is similar only to itself. A similitude can be obtained for a fluid which obeys a general equation of state in the exterior inviscid flow field but which obeys the perfect gas laws and the viscosity law Eq. (4-13) within the boundary layer. This case is rather artificial and will not be explored here. We shall consistently assume that the inviscid part of the flow follows the perfect gas laws (with γ constant). This assumption is realistic for atmospheric air in flows at moderate values of the similarity parameter K.

The results of viscous hypersonic similitude in terms of quantities evaluated on the body surface may now be expressed. We presume the affine relationship of those functions which need to be specified, such as $y_b(x/c)$ and $h_b(x/c)$. A parameter equivalent to $\delta^*/\tau c$ must be made invariant, and also a parameter h_b/H_δ with h_b evaluated at a given reference point. For the pressure on the body, we obtain the classical result expressed with viscous effects as

$$C_p = \tau^2\Pi(x/c;\ K,\ \tilde{\chi},\ h_b/H_\delta;\ \gamma,\ Pr) \tag{6-11}$$

The presence of γ as a parameter is the remnant in a perfect gas of the requirement in the general inviscid similitude that the gas must be specified. The presence of Pr serves as a reminder that suitable behavior of various viscous parameters is required within the boundary layer.

The expression of Eq. (4-18) for the shear stress may be changed, using the hypersonic approximations and dividing by the parameter appearing in Eq. (6-6). The result is

$$C_f = \sigma/(1/2)\rho_\infty U^2 = \tau^3\Phi(x/c;\ K,\ \tilde{\chi},\ h_b/H_\delta;\ \gamma,\ Pr) \tag{6-12}$$

For the heat transfer, we may define a heat-transfer coefficient

$$C_q = q/\rho_\infty U H_\delta = \tau^3\Psi(x/c;\ K,\ \tilde{\chi},\ h_b/H_\delta;\ \gamma,\ Pr) \tag{6-13}$$

The Stanton Number St is particularly useful if heat-transfer rates are very small (with $g_b'(\xi) \ll 1$), and follows the same law as does C_q. According to the Reynolds analogy concept, the Stanton Number should be proportional to C_f, and this is consistent with our result that St and C_f obey the same similarity law.

In the limit $K \to \infty$, we may drop the dependence on K in the functional equations above because of the applicability of the Mach Number independence principle. In this case, we must replace the parameter $\tilde{\chi}$ by $1/\tau\sqrt{Re_b}$.

For the total-force coefficients, functional expressions are obtained similar to those of the classical similitude. We may note that the τ^3 dependence of C_f in Eq. (6-12) is the same as the classical one for the drag coefficient C_D. We may define a total heat-transfer coefficient C_Q in the same manner as C_q, dividing the total heat-transfer rate by the reference surface area. The results are

$$C_L = \tau^2\Lambda(K,\ \tilde{\chi},\ h_b/H_\delta;\ \gamma,\ Pr) \tag{6-14a}$$

$$C_D = \tau^3\Delta(K,\ \tilde{\chi},\ h_b/H_\delta;\ \gamma,\ Pr) \tag{6-14b}$$

$$C_Q = \tau^3\,\Xi(K,\ \tilde{\chi},\ h_b/H_\delta;\ \gamma,\ Pr) \tag{6-14c}$$

The pitching moment coefficient obeys the same law as does the lift coefficient. These formulas hold also for a body of revolution at zero incidence (for which $C_L = 0$, of course), defined in terms of a lateral projected area.

It must be kept in mind that suitable specifications must be made with respect to the variations of viscosity and Prandtl Number with the state of the material. The expressions above are applicable to any valid similitude, but we have yet to inquire into more specific requirements guaranteeing a similitude. This is done in the next section.

Since the quantity M_δ is almost never an invariant, the hypersonic boundary-layer independence principle must almost always be employed in viscous hypersonic similitude. The only exceptions are the case in which τ is held fixed and the case in which both the Prandtl Number Pr and the quantity μ/T are constants through the boundary layer. Note that in the viscous similitude the case in which τ is held fixed is not completely trivial as it is in classical hypersonic similitude.

(7) Viscous Hypersonic Similitudes

We now list the main forms obtainable for hypersonic similitude with boundary-layer interaction effects included.

(A) *General Equation of State in Boundary Layer*

The gas considered behaves as a perfect gas of constant γ outside the boundary layer, but obeys a general equation of state within the boundary layer. The viscosity and Prandtl Numbers are specified functions of state. We require now that the state of the fluid be the same within the boundary layer at corresponding points of two similar flows. From the fact that the temperature must be the same in the two flows, we

conclude that U must be an invariant. And from the same fact with regard to the pressure, we conclude that $\tau^2\rho_\infty U^2$ (and also p_∞) must be an invariant. From the invariance of the parameter $1/\tau\sqrt{Re_b}$ we conclude that $\tau^2 c$ is an invariant. We obtain in place of Eq. (6-11) the law for C_p

$$C_p = \tau^2\Pi(x/c;\ K,\ U,\ \tau^2\rho_\infty,\ \tau^2 c,\ h_b/H_\delta;\ \text{gas}) \quad (7\text{-}1)$$

with corresponding expressions for the other quantities. Since H_δ is essentially the same as $1/2\ U^2$, we may replace h_b/H_δ by T_b.

In this version of the similitude, the analysis of Section (4) above is not applicable. What is used is the scale transformation discussed near the end of Section (4), for which there is no restriction that the fluid be a perfect gas.

(B) *Viscosity a General Function of Temperature*

The fluid behaves as a perfect gas of constant γ within the boundary layer as well as outside the boundary layer. The values of γ inside and outside the boundary layer are not necessarily the same, but, if not, both values of γ must be invariant in the similitude. It can be shown that the restriction that γ be constant within the boundary layer may be replaced by the restriction that it be a specified function of the temperature there. For simplicity, we require that the gas constant $\mathcal{R}$ be invariant. The viscosity is a given function $\mu(T)$ of the temperature alone, as is also the Prandtl Number $Pr(T)$.

We require that the temperature of the gas be the same within the boundary layer at corresponding points of similar flows, and conclude that U must be an invariant. In place of Eq. (6-11), we obtain

$$C_p = \tau^2\Pi(x/c;\ K,\ U,\ \tau^4\rho_\infty c,\ h_b/H_\delta;\ \gamma,\ \mathcal{R},\ \mu) \quad (7\text{-}2)$$

in which the specification on μ includes one on its functional dependence on temperature. The analogous specification on $Pr(T)$ is understood in Eq. (7-2). As in similitude (A), we may replace h_b/H_δ by T_b.

It should be noted that the specifications as to γ and viscous properties are automatically taken care of if the gas itself is fixed, provided only the constant value of γ in the inviscid flow is invariant.

(C) *Viscosity Proportional to T^s*

Again, the fluid must be a perfect gas of constant γ within and outside the boundary layer. Temperatures are not required to be the same at corresponding points in similar flows, and we may, in general, not relax the requirement that γ be constant within the boundary layer. The viscosity is proportional to T^s, as in Eq. (4-13), and the Prandtl Number is constant.

Here we obtain Eq. (6-11) with only the additional specification that the parameter s be an invariant. We may note that the quantity C defined in Eq. (6-9) is proportional to $M_\infty{}^{-2(1-s)}$, so that $\tilde{\chi}$ may be replaced by $M_\infty{}^{2+s}/\sqrt{Re_\infty}$.

Can we check these similitudes with the results of other work? Unfortunately, the available experimental results are far too meager to permit any comparison. However, there is a body of theoretical investigations on the effects of the interaction of the displacement thickness with the external hypersonic flow. An account of these may be found in Chapter 9 of reference 2. These theoretical results are all consistent with our viscous hypersonic similitude and indicate that the similitude should not be considered completely unfamiliar or unexpected.

(8) Similitude in an Isothermal Atmosphere

To exemplify the special similitude rules which may appear in particular circumstances, we consider next the case of an isothermal atmosphere of given composition. Since the composition of the gas is specified, the values of γ and $\mathcal{R}$ are fixed; since the atmosphere is isothermal, the free-stream velocity of sound a_∞ is fixed. Since $K = M_\infty\tau$ is an invariant, so also must be the quantity $U\tau$. The quantity $\tilde{\chi}$ or $1/\tau\sqrt{Re_b}$ must be invariant, of course, as well as h_b/H_δ. Similitude (A) of Section (7) provides no similitude at all in this case and is not considered.

With similitude (B), the quantity U is an invariant, hence, τ is also. We conclude that the quantity Re_b and, thus, also $\rho_\infty c$ must be invariants in this case. In place of Eq. (7-2), we have

$$C_p = \tau^2\Pi(x/c;\ \tau,\ U,\ \rho_\infty c,\ h_b/H_\delta;\ a_\infty,\ \text{gas}) \quad (8\text{-}1)$$

with h_b/H_δ replaceable by T_b. We may note that M_δ is the same at corresponding points in similar flows and, thus, that the hypersonic boundary-layer independence principle is not needed in this case. As will be pointed out below, similarity of rarefied gas effects is also included here. With τ an invariant, the proportionality of C_p to τ^2 in Eq. (8-1) is meaningless and is only included for consistency with the other formulas.

With similitude (C), the parameter $\tilde{\chi}$ may be replaced by $M_\infty{}^{2+s}/\sqrt{Re_\infty}$, and we conclude that $\tau^{3+2s}\rho_\infty c$ must be an invariant. Thus, in place of Eq. (6-11), we obtain

$$C_p = \tau^2\Pi(x/c;\ U\tau,\ \tau^{3+2s}\rho_\infty c,\ h_b/H_\delta;\ a_\infty,\ \text{gas}) \quad (8\text{-}2)$$

In this case, we may replace the parameter h_b/H_δ by $\tau^2 T_b$.

(9) Momentum Integral Balance

It is instructive to check the drag result of Eq. (6-14b) with the use of a momentum integral about a suitable contour. We use the contour given in Fig. 5, and express the drag for a two-dimensional body in terms of integrals across the flow field with x constant and equal to its value at the trailing edge. We obtain

$$(1/2)\rho_\infty U^2 c C_D = p_\infty y_s - \int_{y_b}^{y_s} p\,dy + \int_{y_b}^{y_s} (U-u)\rho u\,dy \quad (9\text{-}1)$$

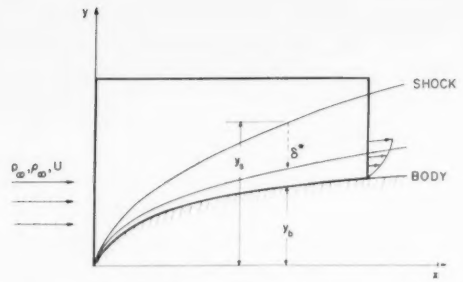

FIG. 5. Contour for momentum integral balance.

from a direct application of the concepts of Euler's momentum integral. We recall the basic definition of δ^* through the relation

$$\int_{y_b}^{y_s} \rho u dy = \int_{y_b+\delta^*}^{y_s} \rho_{\text{inv.}} u_{\text{inv.}}\, dy \qquad (9\text{-}2)$$

in which the subscript inv. refers to the inviscid flow giving the same flow external to the boundary layer. Noting that $u_{\text{inv.}} = u_\delta$ near the body, we may write for the integral in $(U - u)$ of Eq. (9-1)

$$\int_{y_b}^{y_s} (U - u)\rho u dy = \int_{y_b+\delta^*}^{y_s} (U - u_{\text{inv.}})\rho_{\text{inv.}} u_{\text{inv.}} dy + \int_{y_b}^{y_s} (u_\delta - u)\rho u dy \qquad (9\text{-}3)$$

We recognize the first integral on the right of Eq. (9-3) as being a term which would appear in the definition for the inviscid pressure drag on the equivalent body, the body increased in thickness by the displacement thickness. We may express this drag as

$$(1/2)\rho_\infty U^2 c C_{D y_b+\delta^*} = p_\infty y_s - \int_{y_b+\delta^*}^{y_s} p dy + \int_{y_b+\delta^*}^{y_s} (U - u_{\text{inv.}})\rho_{\text{inv.}} u_{\text{inv.}} dy \qquad (9\text{-}4)$$

The remaining drag we may express in terms of the momentum thickness

$$\theta = \rho_\delta^{-1} u_\delta^{-2} \int_{y_b}^{y_s} (u_\delta - u)\rho u dy = (\sqrt{2\xi}/r_b^j \rho_\delta u_\delta)\Theta \qquad (9\text{-}5)$$

expressed in the same terms as δ^* in Eq. (4-15). This remaining drag is a momentum defect drag, defined in terms of a drag coefficient as

$$(1/2)C_{D\text{mom.}} = (\Theta/c) - (1/2)C_{p_b}(\delta^*/c) \qquad (9\text{-}6)$$

We may decompose the drag on a slender body into pressure drag and skin friction drag, thus

$$C_D = C_{D y_b} + C_{D_f} \qquad (9\text{-}7)$$

each part of which obeys the same τ^3 law as does the total drag. The results of our momentum integral analysis permit us an alternative decomposition of the drag into pressure drag on the equivalent body plus momentum defect drag, as

$$C_D = C_{D y_b+\delta^*} + C_{D\text{mom.}} \qquad (9\text{-}8)$$

Since the momentum thickness θ is proportional to $\tau^2\delta^*$ in the similitude and since C_p is proportional to τ^2, we may again say that both parts of the drag in Eq. (9-8) obey the τ^3 law of the total drag.

The thickness of the transitional layer may be shown to be of the order of τ^{1+s} times δ^* if $\mu \propto T^s$, while $u_\delta - u$ is of the order of $\tau^2 u_\delta$ there. Thus, the drag contribution of either pressure or momentum integrals taken across the transitional layer has a τ^{4+s} dependence and is negligible if τ is small.

We have said nothing so far about base pressure. From the drag given in Eq. (9-1) should be subtracted a term $p_{\text{base}} y_b$ corresponding to a base pressure thrust. Alternatively, if we wish to use the ambient pressure as a reference pressure, the pressure integral in Eq. (9-1) is $\int (p - p_\infty) dy$ between $y = y_b$ and $y = y_s$, and the $p_\infty y_s$ term is removed. We must now add a term $(p_\infty - p_{\text{base}})y_b$ to the drag, corresponding to the more conventional base-pressure drag. In any case, it is necessary that the base pressure follow the similarity law if the base-pressure thrust or the base-pressure drag is to follow the similarity law given for the drag.

(10) Three-Dimensional Boundary-Layer Effects

Three-dimensional boundary layers are of two main types, which may be denoted as mean-surface three-dimensional boundary layers and as proper three-dimensional boundary layers. In the former category are boundary layers which are thin sheaths on relatively flat surfaces, for which the boundary layer thickness is much less than the radii of curvature of the surface. A characteristic direction for a mean-surface boundary layer is the direction normal to the surface. In the latter category are boundary layers whose thickness may be of the same order of magnitude or larger than a characteristic minimum transverse body radius of curvature. In this latter category is included the boundary layer on a needle or along a corner. A proper boundary layer generally has the free-stream flow direction as a characteristic direction, with no essential distinction between the two lateral directions. Of course, a proper boundary layer may appear locally on a body for which the boundary layer is mostly of the mean-surface type. An important subcategory of mean-surface boundary layers comprises boundary layers with an almost unidirectional external flow and with small cross flow. In this case, the external free-stream direction and the perpendicular to it tangent to the body surface are to be distinguished. Boundary layers on slender bodies in a hypersonic flow have an almost unidirectional external flow.

We shall concern ourselves primarily with mean-surface boundary layers with small cross flow. The body itself must be quasi-cylindrical in the sense associated with the mean-surface approximation in linearized flow theory. The ratio $\delta^*/\tau c$ is not negligible if interaction effects are important, and the requirement that δ^* is small with respect to a transverse radius of curvature means that τc is also. For a flat or quasi-planar body, this means that τ^2/AR^2 is small, while for a

quasi-cylindrical body $\tau/\mathcal{A}$ must be small. Here, $\mathcal{A}$ is a suitably defined aspect ratio of the body. These requirements on $\tau^2/\mathcal{A}^2$ or $\tau/\mathcal{A}$ are sufficient to ensure the validity of strip theory,[2] with possible exceptions in local regions.

On a slender body in an inviscid hypersonic flow for which strip theory is applicable, the solution is independent of the otherwise important parameter $\tau/\mathcal{A}$. The pressure on the body and the shape function for the body are functions not only of x/c but also of $z/\mathcal{A}c$, where z is the lateral coordinate on the mean surface. But, the solution in terms of x/c for each value of $z/\mathcal{A}c$ is essentially a two-dimensional solution, so that the variable $z/\mathcal{A}c$ has more the nature of a parameter than of an independent variable.

We shall not go into a detailed analysis of the three-dimensional boundary layer, but only into a proportionality argument sufficient to show the appropriate similarity law. The lateral pressure gradient from a pressure gradient following the similitude is proportional to $\rho_\infty U^2\tau^2/\mathcal{A}c$. The lateral curvature of a streamline within the boundary layer is proportional to $\rho_b^{-1}U^{-2}$ times this, or to $1/\mathcal{A}c$. The lateral slope is then proportional to $1/\mathcal{A}$. The change in boundary-layer thickness due to three-dimensional effects from a simple continuity argument is δ^* times the change in a streamtube width divided by the streamtube width. Thus, we obtain

$$(1/\delta^*)(d\delta^*/dx)_{3\text{-dim.}} \propto [(1/\mathcal{A})/\mathcal{A}c] = 1/\mathcal{A}^2c \quad (10\text{-}1)$$

We then conclude that

$$(1/\tau)(d\delta^*/dx)_{3\text{-dim.}} \propto (\delta^*/\tau C)(1/\mathcal{A}^2) \quad (10\text{-}2)$$

For similarity, the relative displacement thickness appearing from three-dimensional effects must be proportional to the displacement thickness itself, and we conclude that the aspect ratio $\mathcal{A}$ must be an invariant. The aspect ratio is, thus, the basic similarity parameter governing three-dimensional boundary-layer interaction effects, subject to the restriction that $\tau^2/\mathcal{A}^2$ or $\tau/\mathcal{A}$ is sufficiently small. Note that, if the concept of strip theory were not applicable, the parameter $\tau/\mathcal{A}$ would also be a similarity parameter for the basic similitude.

Eq. (10-2) also tells us that three-dimensional effects are negligible with respect to the basic boundary-layer interaction only if the aspect ratio is large enough that $1/\mathcal{A}^2$ may be neglected in comparison with one. If $\mathcal{A}$ is of the order of one or larger, these three-dimensional effects may not be neglected.

We turn now to the more restrictive similitude in which both τ and $\mathcal{A}$ are held fixed. In this case, strip theory is not needed, and similarity is obtained for general hypersonic three-dimensional boundary layers on general slender bodies. Included herein are proper three-dimensional boundary layers as well as mean-surface three-dimensional boundary layers with small cross flow. The hypersonic boundary-layer independence principle is not needed and, as we shall note in the next section, similarity is also obtained with respect to rarefied gas effects.

(11) Rarefied Gas Effects

So far, we have considered only cases for which the usual continuum gasdynamical equations hold, with laminar boundary layers without slip or vorticity interaction taken into account. Rarefied gas effects are characterized by the Knudsen Number, or ratio of mean-free path λ to a characteristic dimension. This Knudsen Number is, apart from a multiplicative constant, equal to M/Re, where Re is based on the characteristic dimension. If the characteristic dimension is a boundary-layer thickness and Re is based on the chord, the Knudsen Number may be taken as $M/\sqrt{Re}$. In the interior of a hypersonic boundary layer, the Mach Number is of the order of one, and the Knudsen Number for the boundary-layer thickness is proportional to $1/\sqrt{Re_b}$.

If similarity is to be obtained with respect to rarefied gas effects, the Knudsen Number must be an invariant. With the invariance of $\bar{\chi}$ or of $1/\tau\sqrt{Re_b}$ already established, the thickness ratio τ and the free-stream Mach Number M_∞ (except with $K \to \infty$) must both be invariants. With τ invariant, M_δ is the same at corresponding points in similar flows, and the hypersonic boundary-layer independence principle is not needed. In addition, as shown in the last section, similarity is automatically obtained for all three-dimensional viscous effects.

The requirement that τ be an invariant, although very restrictive, does give a true similitude. This similitude applies primarily to the viscous or rarefied gas effects; in an inviscid flow the only similitude is that obtained by the scale transformation or by dimensional analysis and is trivial in the sense of hypersonic similitude.

Similitude (A) of Section (7) does not apply here, and rarefied gas effects cannot be included. With similitude (B) applied to a given gas, we obtain the requirement that $\rho_\infty c$ is an invariant. This result was also obtained in the case of a constant temperature atmosphere, and we note that the quantities T_∞ and a_∞ must be invariant in this case. With similitude (C) of Section (7), we may conclude that $\rho_\infty c U^{1-2s}$ is an invariant. With a hard sphere atomic model, we would have $s = 1/2$ and $\rho_\infty\lambda$ constant and again have $\rho_\infty c$ an invariant

(12) The Weak Interaction Case

We have consistently taken the position that the displacement thickness of the boundary layer must be taken into account, that $\delta^*/\tau c$ is not negligibly small. We now look briefly at the case in which $\delta^*/\tau c$ is very small, so that the pressure distribution on the body is essentially what it would be in an inviscid flow. In this case, $\bar{\chi}$ or $1/\tau\sqrt{Re_b}$ is not an invariant in a similitude.

In place of the τ^3 dependence of C_f obtained in Eq. (6-12), we find that C_f is proportional to $\tau^2/\sqrt{Re_b}$ or to $\sqrt{C/Re_\infty}$; the same result holds for the heat-transfer coefficient C_q. The contribution of skin friction to the drag coefficient has the same dependence as does C_f

and is very small compared with the pressure drag coefficient. The pressure drag is a functional of $dy_b/dx + d\delta^*/dx$, and a functional analysis shows that the increase in pressure coefficient due to small displacement thickness is proportional to $\delta^*/\tau c$ times the inviscid pressure coefficient. This leads to an increase in the pressure drag coefficient, which is of the same order of magnitude as the frictional drag coefficient. The total increment in drag coefficient is, thus, proportional to $\tau^2/\sqrt{Re_b}$.

Since the increment in the drag coefficient is relatively very small, the similitude is no different from the classical inviscid similitude as far as forces on the body are concerned; and the parameters describing viscous effects may be dropped in Eqs. (6-11), (6-14a), and (6-14b). However, the heat transfer is zero in the inviscid theory, and Eq. (6-13) and (6-14c) do apply, with $\tau^2/\sqrt{Re_b}$ in place of τ^3 and with only $\bar{\chi}$ dropped in the expression of functional dependence.

In similitude (A) for a perfect gas of Section (7), only K need be specified for the force coefficients, while the parameters given in Eq. (7-1) with $\tau^2 c$ dropped must be specified for the heat transfer. In similitude (B), the parameter $\tau^1\rho_\infty c$ is dropped in functionally expressing the heat transfer. Analogously, the parameters $\rho_\infty c$ and $\tau^{4+s}\rho_\infty c$ are dropped in similitudes (A) and (B) in a constant density atmosphere. Rarefied gas effects are always weak if the interaction is weak and need not be considered. With respect to their influence on the pressure distribution, three-dimensional boundary-layer effects may be expected to possibly be important locally, but certainly not in the large. For similarity of the heat-transfer distribution on a body for which strip theory is applicable, we would again require the aspect ratio AR to be an invariant.

(13) Similitude with Blunted Noses

An interesting extension of the classical inviscid similitude to take the effect of slight blunting into account has been found by Cheng.[6] His result is that, with a slightly blunted nose, the quantity $M_\infty(d/c)^{(1+j)/(3+j)}$ is a basic similitude parameter which must be invariant in hypersonic similitude. Here d is the effective width or diameter of the blunt nose.

Our conclusion is that this similitude may *not* be extended to the viscous case, or only under conditions so restrictive as to make the result uninteresting. The reason for this conclusion lies in a basic assumption underlying Cheng's extension This assumption is that the equivalence principle holds for the flow with a blunted nose. The assumption necessarily fails locally in the vicinity of the nose itself, and the layer of fluid of increased entropy nearest the body cannot follow the similitude. But, it is precisely in this entropy layer that the boundary layer grows, so that with a blunted nose the boundary layer cannot follow the similitude.

Addendum

Attention is called to a note of Lunev,[7] in which are stated conclusions similar to those of ours given as similitude (C).

References

[1] Tsien, H. S., *Similarity Laws of Hypersonic Flows*, J. Math. Phys., Vol. 25, pp. 247–251, 1946.

[2] Hayes, W. D., and Probstein, R. F., *Hypersonic Flow Theory*; Academic, New York, 1959.

[3] Hayes, W. D., *On Hypersonic Similitude*, Quart. Appl. Math., Vol. 5, pp. 1′5–1′6, 1947.

[4] Cswatitsch, K., *Ähnlichkeitsgesetze für Hyperschallströmung*, ZAMP, Vol. 2, pp. 249–264, 1951.

[5] Crocco, L., *Lo strato limite laminare nei gas*, Monografe Scientifche di Aeronautica 3, Rome, 1946 (translated as North American Aviation Aerophysics Lab. Report AL-684, Los Angeles, Calif., 1948).

[6] Cheng, H. K., *Similitude of Hypersonic Real-Gas Flows Over Slender Bodies With Blunted Noses*, Journal of the Aero/Space Sciences, Vol. 26, No. 9, pp. 575–585, September, 1959.

[7] Lunev, V. V., *On the Similarity of Hypersonic Viscous Flow on Streamlined Slender Bodies* (in Russian), Prikl. Mat. Mekh., Vol. 23, pp. 193–197, 1959. See Appl. Mech. Rev., Vol. 12, No. 3994, 1959.

Optimal Zoom Climb Techniques

(*Continued from page 802*)

1956–1957, New York University, Institute of Mathematical Sciences (mimeographed lecture notes).

[19] Courant, R., and Hilbert, D., *Methoden der Mathematischen Physik*, Julius Springer, Berlin; Vol. 1, 1924, 1931; Vol. 11, 1937 (translated and revised edition of Vol. I, Interscience Publishers, 1953; Vol. II forthcoming).

[20] Bliss, G. A., *Lectures on the Calculus of Variations*, University of Chicago Press, Chicago, 1946.

[21] Schwartz, L., *Théorie des Distributions*, Tome I et II, Actualitiés Scientifiques et Industrielles 1091 and 1122, Hermann et Cie, Paris, 1950, 1951.

[22] Friedman, B., *Principles and Techniques of Applied Mathematics*, John Wiley and Sons, Inc., New York, 1956.

[23] Leavenworth, B. M., *A Routine for the Solution of Ordinary Differential Equations on the IBM 650*, IBM 650 Seminar, Endicott, N.Y., June 18–22, 1956.

Buckling of a Cylindrical Shell Under a Circumferential Band Load

D. O. BRUSH* AND F. A. FIELD**

Lockheed Aircraft Corporation

Summary

A method is presented for calculating the buckling pressure for a long, circular cylindrical shell subjected to external pressure over a circumferential band of arbitrary width. The "Euler" buckling pressure is determined. Stability is based on the principle of minimum potential energy, and the Ritz procedure is used to reduce the system to a finite number of degrees of freedom.

Results are compared for two methods of loading: (1) a fluid pressure which remains evenly distributed during buckling, and (2) a physical-body pressure which becomes concentrated at the high points of the deformed shell. It is found that, where shell radius/thickness ratios are greater than 200 and pressure band width/radius ratios are less than 1.0, the greatest difference between average buckling pressures for the two methods of loading is not more than about 30 per cent. In this range, the buckling pressures are approximately in inverse proportion to band width for both kinds of loading.

Numerical results are presented in the form of graphs showing the buckling pressure parameter as a function of the radius/thickness ratio and the pressure band width/radius ratio.

Symbols

a	=	mean radius of the undeformed shell
b	=	ratio of pressure band width to shell diameter (Fig. 2)
E	=	compression modulus of elasticity
h	=	shell thickness
K_{ij}	=	stability determinant coefficients, Eqs. (25)
m	=	axial wave length parameter
n	=	circumferential wave length parameter
p	=	uniform or average external pressure, psig
P	=	pa/Eh
U_b	=	bending strain energy of the shell
U_m	=	membrane strain energy of the shell
V	=	total potential energy of the system
u, v, w	=	dimensionless axial, tangential, and radial displacement components of a point on the shell's middle surface. w is positive inward
x, ϕ	=	dimensionless cylindrical coordinates (Fig. 3)
$X_1, \ldots, X_5$	=	dimensionless displacement parameters
$\alpha_1, \alpha_2, \alpha_3$	=	coefficients from the potential energy of the external pressure Eqs. (17) and (20).
$\epsilon_x, \epsilon_\phi, \gamma_{x\phi}$	=	strains at a point in the shell's middle surface
$\kappa_x, \kappa_\phi, \kappa_{x\phi}$	=	curvature changes at a point in the shell's middle surface
ν	=	Poisson's ratio
Ω	=	potential energy of the external pressure

The subscripts F and R refer to the loading cases, fluid pressure and ring pressure, respectively.

Presented at the Structures Session, IAS 27th Annual Meeting, N.Y., Jan. 26–29, 1959.

* Head, Applied Mechanics-Statics, Structures Department, Lockheed Missiles and Space Division.

** Senior Scientist, Aerodynamics Department, Lockheed Missiles and Space Division.

Introduction

IN THE NORMAL HANDLING and storage of missiles, the cylindrical structure frequently is subjected to circumferentially distributed radial loads. For example, such loads are present when a missile is at rest in ground-handling support-frames. If the shell is thin and not stiffened in the region of load application, the load may cause the structure to buckle. A method is presented here for determining the buckling pressure for a long, circular cylindrical shell subjected to external pressure over a circumferential band of arbitrary width (see Fig. 1).

The corresponding problem of pre-buckling stresses and deflections is treated by Timoshenko in reference 1. The buckling of a cylinder subjected to uniform external pressure over its entire lateral surface has been analyzed by Flügge,[2] Langhaar and Boresi,[3] and others, while buckling due to a radial circumferential line load has been treated by Hahne.[4]

Calculation of the buckling pressure in the present problem is complicated by the fact that the pre-buckling stresses are not constant throughout the shell, but are functions of the shell's axial coordinate. Hoff recently published an analysis of buckling under hoop stresses which vary in the axial direction.[5] His equations may be used for the calculation of circumferential buckling stresses caused by a band of pressure, but his series solution is not well suited for bands which are narrow compared with the total length of the cylinder. The present solution is devised for narrow bands such as the one shown in Fig. 1.

The general method of analysis is as follows. An approximate energy method is used to determine the infinitesimal or "Euler" buckling pressure. Stability is based on the principle of minimum potential energy. The nonlinear terms necessary for buckling are included

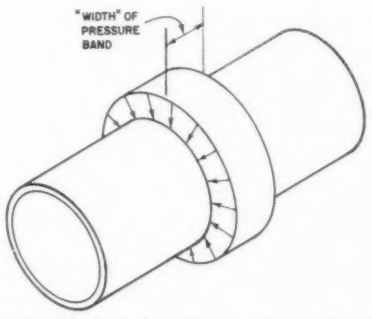

FIG. 1. Method of loading—undeformed shell.

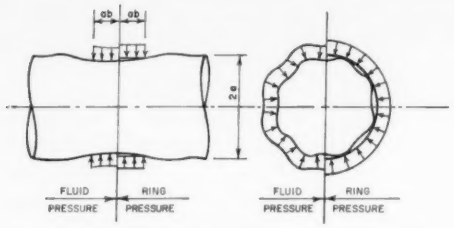

FIG. 2. Method of loading—deformed shell.

from the outset in the strain-displacement relations. The Ritz procedure is used to reduce the system to a finite number of degrees of freedom, and the second variation with respect to the displacement parameters is calculated to determine the minimum potential energy. This method of analysis follows the general infinitesimal buckling theory used by Langhaar and Boresi in reference 3. Similar analyses are discussed by Marguerre in reference 6.

In an investigation of buckling under radial loads, the question arises as to whether, for the same average pressure, the response of the shell to a fluid pressure loading is different from its response to a pressure applied by a physical body. In particular, as the shell begins to buckle, pressure exerted by a physical body becomes concentrated at the high points of the shell, but fluid pressure remains evenly distributed. Therefore, physical-body pressure inhibits the formation of a buckle pattern, and the average pressure at buckling may be higher than for fluid pressure loading. The question is of special interest, for example, in the analysis of a missile shell subjected to a dead-weight load during ground-handling.

In order to gain some insight into this effect, the two methods of loading shown in Fig. 2 are investigated in the present analysis. The elastic interaction, during buckling, between the shell and a particular physical ring encircling the shell is not considered; the pressure is assumed to remain constant during buckling in both cases. In this way, any difference in average buckling pressures depends only on whether the applied pressure remains evenly distributed or becomes concentrated at the high points of the shell.

The shell is assumed to be very thin-walled, and the stresses are assumed to be elastic.

Potential Energy of the System

In the coordinate systems and displacement components shown in Fig. 3, x, u, v, and w have been made dimensionless by dividing the corresponding distances by the radius a. For example, component w is the ratio of the radial displacement to the radius of the shell.

The total potential energy is given by the equation

$$V = U_m + U_b + \Omega \tag{1}$$

where U_m and U_b are the membrane and bending strain energies of the shell, and Ω is the potential energy of the external pressure.

Strain Energy of the Shell

The strain energy expressions for the shell are given in reference 7 in terms of the strains and curvature changes of the shell's middle surface [Eqs. (255) and (256), reference 7]. In the notation of the present analysis they may be written

$$U_m = [Ea^2h/2(1-\nu^2)] \times \int_0^{\infty}\int_0^{2\pi} \{\epsilon_x^2 + \epsilon_\phi^2 + 2\nu\epsilon_x\epsilon_\phi + [(1-\nu)/2]\gamma_{x\phi}^2\} d\phi\, dx \tag{2}$$

$$U_b = [Eh^3/24(1-\nu^2)] \times \int_0^{\infty}\int_0^{2\pi} [\kappa_x^2 + \kappa_\phi^2 + 2\nu\kappa_x\kappa_\phi + 2(1-\nu)\kappa_{x\phi}^2] d\phi\, dx \tag{3}$$

Appropriate nonlinear strain-displacement relations for Eq. (2) may be found in reference 8 (Eq. I.125) for shells of any shape. Specialization of the equations for cylindrical coordinates results in the equations

$$\left.\begin{aligned} \epsilon_x &= (\partial u/\partial x) + (1/2)[(\partial u/\partial x)^2 + (\partial v/\partial x)^2 + (\partial w/\partial x)^2] \\ \epsilon_\phi &= (\partial v/\partial\phi) - w + (1/2)\{(\partial u/\partial\phi)^2 + [(\partial v/\partial\phi) - w]^2 + [v + (\partial w/\partial\phi)]^2\} \\ \gamma_{x\phi} &= (\partial u/\partial\phi) + (\partial v/\partial x) + (\partial u/\partial x)(\partial u/\partial\phi) + (\partial v/\partial x)[(\partial v/\partial\phi) - w] + (\partial w/\partial x) \times [v + (\partial w/\partial\phi)] \end{aligned}\right\} \tag{4}$$

Novozhilov has shown that, for deformations in which the strain components and rotations are small compared with unity, the four terms $\partial u/\partial x$, $[(\partial v/\partial\phi) - w]$, $\partial u/\partial\phi$, and $\partial v/\partial x$ in Eq. (4) are of the order of magnitude of the strain components (reference 8, paragraphs 46 and 48). For such deformations, then, nonlinear terms containing these four quantities may be neglected in Eq. (4). The resulting approximate strain-displacement relations are

$$\left.\begin{aligned} \epsilon_x &= (\partial u/\partial x) + (1/2)(\partial w/\partial x)^2 \\ \epsilon\phi &= (\partial v/\partial\phi) - w + (1/2)[v + (\partial w/\partial\phi)]^2 \\ \gamma_x\phi &= (\partial u/\partial\phi) + (\partial v/\partial x) + (\partial w/\partial x)[v + (\partial w/\partial\phi)] \end{aligned}\right\} \tag{5}$$

Novozhilov's argument, as presented in reference 8, applies to shells of any shape. Its application to flat plates leads to the well-known von Kármán equations for moderately large deflections of flat plates.

For the very thin shells under consideration, the bending strain-energy is in general much less influential

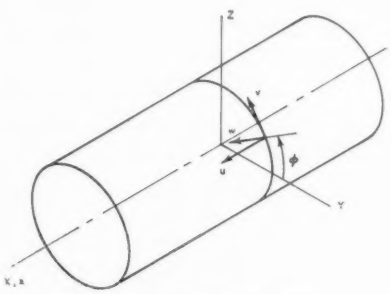

FIG. 3. Coordinate systems.

than the membrane strain-energy. Therefore, only linear terms in w are included in the curvature change - displacement relations for Eq. (3). They are

$$\kappa_x = \partial^2 w/\partial x^2, \quad \kappa_\phi = (\partial^2 w/\partial \phi^2) + w, \quad \kappa_{x\phi} = \partial^2 w/\partial x \partial \phi \tag{6}$$

Eqs. (5) and (6) are somewhat more general than the corresponding relations underlying the popular Donnell buckling equations. [In the latter, the number of circumferential waves in the buckle pattern is assumed to be large. Then v may be neglected compared with $\partial w/\partial \phi$ in Eq. (5), and w may be neglected compared with $\partial^2 w/\partial \phi^2$ in Eq. (6).]

Potential Energy of the External Pressure for the Fluid Pressure Loading

The potential energy of the external fluid pressure may be written

$$\Omega_F = -pa \int_0^b (\pi a^2 - A_F^*) dx \tag{7}$$

where A_F^* is the area of the deformed cross section. A_F^* may be obtained from the relation

$$\int\int dY^* \, dZ^* = \int Y^* (dZ^*/d\phi) d\phi \tag{8}$$

where, from Fig. 3,

$$\left.\begin{aligned} Y^* &= a[(1 - w)\cos\phi - v \sin\phi] \\ Z^* &= a[(1 - w)\sin\phi + v\cos\phi] \end{aligned}\right\} \tag{9}$$

Then substitution into Eq. (7) yields, for the potential energy of the external fluid pressure,

$$\begin{aligned} \Omega_F = -\pi p a^3 b + pa^3 \int_0^b \int_0^{2\pi} \{ &(1 - w)[(1 - w) + (dv/d\phi)] \cos^2\phi + v[v + (dw/d\phi)] \sin^2\phi - \\ &(1/2)(1 - w)[v + (dw/d\phi)] \sin 2\phi - \\ &(1/2)v[(1 - w) + (dv/d\phi)] \sin 2\phi \} \, d\phi dx \end{aligned} \tag{10}$$

Potential Energy of the External Pressure for the Ring Pressure Loading

For the ring pressure loading, the potential energy of the external pressure is simply

$$\Omega_R = -pa(\pi a^2 - A_R^*) b \tag{11}$$

where A_R^* is the circular area enclosed by the ring after the shell deforms.

Expansion in Terms of Displacement Functions

Eq. (1), together with (2), (3), and either (10) or (11), represents the total potential energy of the system. Following the Ritz procedure, the potential energy is integrated by expressing the displacement components u, v, and w in terms of appropriate functions of ϕ and x.

The displacement components are assumed to have the following forms in the circumferential coordinate:

$$\left.\begin{aligned} u &= u_0 + u_1 \cos n\phi \\ v &= v_1 \sin n\phi \\ w &= w_0 + w_1 \cos n\phi \end{aligned}\right\} \tag{12}$$

where u_0, u_1, v_1, w_0, and w_1 are functions of x, and n is an integer greater than one.

In the axial coordinate, the functions are assumed to have these forms:

$$\left.\begin{aligned} u_0 &= X_1 e^{-mx} \sin mx \\ u_1 &= X_2 e^{-mx} \sin mx \\ v_1 &= X_3 e^{-mx}(\cos mx + \sin mx) \\ w_0 &= X_4 e^{-mx}(\cos mx + \sin mx) \\ w_1 &= X_5 e^{-mx}(\cos mx + \sin mx) \end{aligned}\right\} \tag{13}$$

where $X_1, \ldots, X_5$ are dimensionless constants, and m is positive. The functions satisfy the boundary conditions $u = \partial w/\partial x = 0$ at $x = 0$.

The membrane strain energy is obtained in terms of the displacement functions by introducing Eqs. (12), (13), and (5) into Eq. (2). In this substitution, and in the remainder of the analysis, certain terms are neglected. The stability criterion is based on a virtual deformation from a loaded, but unbuckled, equilibrium configuration. In the unbuckled form, $X_2 = X_3 = X_5 = 0$. Consequently, cubic terms in the displacement parameters which do not contain X_1 or X_4 make no contribution to the second variation. Furthermore, all terms in the potential energy expression which are quartic in the displacement parameters are small compared with the cubic or quadratic terms. In the remainder of the analysis, therefore, we neglect all quartic terms and those cubic terms which do not contain X_1 or X_4.

Accordingly, the membrane strain energy in terms of the parameters $X_1, \ldots, X_5$ becomes

$$\begin{aligned} U_m = [\pi E a^2 h/2(1 - \nu^2)m]\big(&[(1/2)m^2] X_1^2 + \{(1/4)m^2 + [(1 - \nu)/16]n^2\} X_2^2 + \\ &\{[(1 - \nu)/4]m^2 + (3/4)n^2\} X_3^2 + [3/2]X_4^2 + [3/4]X_5^2 + [-\nu m] X_1 X_4 + \{[(1 + \nu)/4]mn\} X_2 X_3 + \\ &[-(\nu/2)\, m] X_2 X_5 + [-(3/2)n] X_3 X_5 + [(4\nu/15)m] X_1 X_3^2 + [-(8\nu/15)mn] X_1 X_3 X_5 + \\ &[(4\nu/15)mn^2] X_1 X_5^2 + \{[2(1 - \nu)/15]\, mn\} X_2 X_3 X_4 + \{-[2(1 - \nu)/15]\, mn^2\} X_2 X_4 X_5 + \\ &\{-(3/5) + [4(1 - \nu)/15]m^2\} X_3^2 X_4 + \{(6/5)n + [-(4/15) + (4/5)\nu]m^2 n\} X_3 X_4 X_5 + \\ &[-(8\nu/15)m^2] X_4^3 + [-(4\nu/5)m^2 - (3/5)n^2] X_4 X_5^2 \big) \end{aligned} \tag{14}$$

Similar substitution of Eqs. (12), (13), and (6) into Eq. (3) yields, for the bending strain energy,

$$\begin{aligned} U_b = [\pi E a^2 h/2(1 - \nu^2)m][(1/12)(h/a)^2] \times \\ \{[2m^4 - 2\nu m^2 + (3/2)] X_4^2 + \\ [m^4 + m^2 n^2 + (3/4)(1 - n^2)^2 - \nu m^2] X_5^2 \} \end{aligned} \tag{15}$$

The potential energy of the external fluid pressure is obtained by introducing Eqs. (12) and (13) into Eq. (10). It becomes

$$\Omega_F = [\pi Ea^2h/2(1-\nu^2)m][-4(1-\nu^2)P_F] \times \{[\alpha_1]X_4 + [(1/2)\alpha_2]X_3^2 + [\alpha_2]X_4^2 + [(1/2)\alpha_2]X_5^2 + [-n\,\alpha_2]X_3X_5\} \quad (16)$$

where

$$\left.\begin{aligned} P_F &= (p/E)(a/h), \quad \alpha_1 = 1 - e^{-mb}\cos mb, \\ \alpha_2 &= -(1/8) \times \\ &\quad [3 - e^{-2mb}(2 + \cos 2mb + \sin 2mb)] \end{aligned}\right\} \quad (17)$$

From Fig. 2 and Eq. (12) the area $A_R{}^*$ can be seen to be

$$A_R{}^* = \pi a^2(1 - w_0 + w_1)^2 \quad (18)$$

Consequently, substitution of Eqs. (12), (13), and (18) into Eq. (11) yields, for the potential energy of the external ring pressure,

$$\Omega_R = [\pi Ea^2h/2(1-\nu^2)m][-4(1-\nu^2)mbP_R] \times \{[\alpha_3]X_4 + [-\alpha_3]X_5 + [-(1/2)\alpha_3^2]X_4^2 + [-(1/2)\alpha_3^2]X_5^2 + [\alpha_3^2]X_4X_5\} \quad (19)$$

where

$$\left.\begin{aligned} P_R &= (p/E)(a/h) \\ \alpha_3 &= e^{-mb}(\cos mb + \sin mb) \end{aligned}\right\} \quad (20)$$

For simplicity, the terms for both cases will be included in one set of equations in the remainder of the analysis. *It will be understood that $\Omega_R = P_R = 0$ for the fluid pressure loading, and $\Omega_F = P_F = 0$ for the ring pressure loading.* Accordingly, the total potential energy of the system may be written

$$V = U_m + U_b + \Omega_F + \Omega_R \quad (21)$$

where the four terms on the right are given by Eqs. (14), (15), (16), and (19), respectively.

Determination of the Buckling Pressure

The stability of the system can be determined by considering a virtual deformation from a loaded, but unbuckled, equilibrium configuration and examining the corresponding second variation of the potential energy. For this purpose it is necessary to determine the relationship between load and deformation before buckling.

The Unbuckled Form

The relationships between the external pressure and displacement parameters X_1 and X_4 may be obtained by use of the principle of stationary potential energy. In Eq. (21), only those terms corresponding to a linear analysis of axially symmetrical deformations need be retained. Then, from the relations

$$\partial V/\partial X_1 = \partial V/\partial X_4 = 0 \quad (22)$$

we obtain

$$\left.\begin{aligned} X_4 &= \frac{4(1-\nu^2)[\alpha_1 P_F + mb\alpha_3 P_R]}{3 + (1/3)(h/a)^2[m^4 - \nu m^2 + (3/4)] - \nu^2} \\ X_1 &= (\nu/m)X_4 \end{aligned}\right\} \quad (23)$$

Second Variation of the Potential Energy

To determine the second variation of the total potential energy, the displacement parameters $X_1, \ldots, X_5$ are given the virtual increments $\xi_1, \ldots, \xi_5$, respectively. Then the corresponding second variation of the potential energy is represented by the relation

$$\delta^2 V = \sum_1^5 \sum_1^5 K_{ij}\xi_i\xi_j \quad (24)$$

Omitting the unessential factor $\pi Ea^2h/[2(1-\nu^2)m]$, the coefficients K_{ij} are found from Eq. (21) to be

$$\begin{aligned} K_{11} &= (1/2)m^2 \\ K_{22} &= (1/4)m^2 + [(1-\nu)/16]n^2 \\ K_{33} &= (3/4)n^2 + [(1-\nu)/4]m^2 + [(4\nu/15)m]X_1 + \{[4(1-\nu)/15]m^2 - (3/5)\}X_4 - 2(1-\nu^2)\alpha_2 P_F \\ K_{44} &= (3/2) - [(8\nu/5)m^2]X_4 + (1/12)(h/a)^2[2m^4 + (3/2) - 2\nu m^2] - 2(1-\nu^2)[2\alpha_2 P_F - m\,b\,\alpha_3^2 P_R] \\ K_{55} &= (3/4) + (1/12)(h/a)^2[m^4 + m^2n^2 + (3/4)(1-n^2)^2 - \nu m^2] + [(4\nu/15)mn^2]X_1 - \\ &\qquad [(4\nu/5)m^2 + (3/5)n^2]X_4 - 2(1-\nu^2)[\alpha_2 P_F - m\,b\,\alpha_3^2 P_R] \\ K_{14} &= -(\nu/2)m \\ K_{23} &= [(1+\nu)/8]m\,n + \{[(1-\nu)/15]m\,n\}X_4 \\ K_{25} &= -(\nu/4)m - \{[(1-\nu)/15]m\,n^2\}X_4 \\ K_{35} &= -(3/4)n - [(4\nu/15)m\,n]X_1 + \{(3/5)n + [-(2/15) + (2\nu/5)]m^2 n\}X_4 + 2(1-\nu^2)n\,\alpha_2 P_F \\ K_{45} &= -2(1-\nu^2)m\,b\,\alpha_3^2 P_R \end{aligned} \quad (25)$$

where X_1 and X_4 are given by Eq. (23).

The Stability Criterion

The system is in stable equilibrium provided that the potential energy is a minimum. Therefore, stability depends on the sign of the second variation. Eq. (24) is a quadratic form in the virtual displacements ξ_i. The appropriate condition for the limit of positive definiteness of the quadratic form, and of stability of the system, is that the determinant of the coefficients K_{ij} be equal to 0:

$$\begin{vmatrix} K_{11} & 0 & 0 & K_{14} & 0 \\ 0 & K_{22} & K_{23} & 0 & K_{25} \\ 0 & K_{23} & K_{33} & 0 & K_{35} \\ K_{14} & 0 & 0 & K_{44} & K_{45} \\ 0 & K_{25} & K_{35} & K_{45} & K_{55} \end{vmatrix} = 0 \tag{26}$$

Eq. (26) can be written

$$(K_{11}K_{44} - K_{14}^2)\begin{vmatrix} K_{22} & K_{23} & K_{25} \\ K_{23} & K_{33} & K_{35} \\ K_{25} & K_{35} & K_{55} \end{vmatrix} - K_{11}K_{45}^2\begin{vmatrix} K_{22}K_{23} \\ K_{23}K_{33} \end{vmatrix} = 0 \tag{27}$$

For fluid pressure loading, the second term in Eq. (27) is equal to zero. Calculations show that for ring pressure loading, the influence of that term is negligible. Consequently it was omitted from Eq. (27) in most of the numerical calculations. For the remaining determinantal equation, the solution $(K_{11}K_{44} - K_{14}^2) = 0$ represents axially symmetrical buckling. (For that mode $\xi_2 = \xi_3 = \xi_5 = 0$.) Unsymmetrical modes may be shown to be less stable. Consequently, the equation for the buckling pressure may be written

$$\begin{vmatrix} K_{22} & K_{23} & K_{25} \\ K_{23} & K_{33} & K_{35} \\ K_{25} & K_{35} & K_{55} \end{vmatrix} = 0 \tag{28}$$

The characteristic equation of the determinant in Eq. (28) is of the form

$$a + bP + cP^2 + dP^3 = 0 \tag{29}$$

where P is the buckling pressure parameter. The coefficients a, b, c, and d are functions of the five quantities ν, a/h, b, m, and n. Poisson's ratio was assumed to be 0.3 in all the calculations. For a given shell (i.e., a given a/h and b), each set of values of m and n defines a particular buckled shape. The shell may be assumed to buckle along the lines of least resistance. Therefore the correct buckled shape is the one corresponding to minimum buckling pressure. For each shell then, m and n are selected by trial to give the minimum pressure. Numerical calculations indicated that the same minimum buckling pressure is obtained for a wide range of pairs of values of m and n.

For shell thicknesses in the practical range, Eq. (29) may be conveniently solved by use of the iterative scheme

$$P_{n+1} = -(a/b) - (c/b)P_n^2 - (d/b)P_n^3 \tag{30}$$

where $P_0 = 0$. Only one or two iterations are necessary. A digital computer was used for the numerical work.

Results

Results of the analysis for the external fluid pressure are compared in Fig. 4 with Flügge's analysis[2] for cylinders subjected to uniform external pressure over their entire lateral surface and simply supported by rigid rings at the ends. The curve representing Flügge's results was obtained by interpolation from reference 2, Fig. 112. The comparison indicates close agreement between the wide pressure band range of the present analysis and the long-cylinder range of Flügge's solution. For intermediate band widths, the comparison indicates that the unloaded portions of the shell outside the pressurized band furnish about 30 per cent less stabilizing elastic restraint than would be furnished by rigid, simple-support rings located at the edges of the pressurized band.

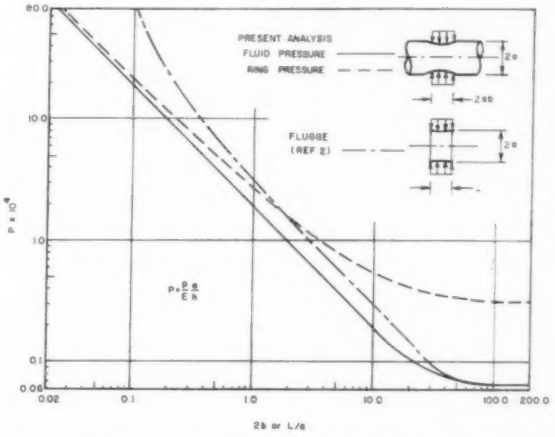

FIG. 4. Comparison of results for $a/h = 200$.

The change in the slope of the curve in the short-cylinder range of Flügge's analysis represents an increased stability stemming from the increased proximity of the rigid end rings. The present analysis indicates that the buckling pressure is inversely proportional to the width of the pressure band for narrow as well as intermediate width bands.

Another comparison with an existing solution is available in Hahne's analysis[4] of a cylinder subjected to a radial circumferential line load. In that paper, numerical examples are calculated for an a/h ratio of 100 and cylinder-length/radius ratios of 4 and 6. For both, the calculated buckling load was 4.6×10^{-4} (in terms of pounds per inch of circumference, divided by $h \times E$). As a consequence of the inverse relationship between buckling pressure and band width, the analogous quantity is readily calculated for the present analysis. For $a/h = 100$, it is found to be $P(2b) = 5.8 \times 10^{-4}$. The agreement with Hahne's solution is fair.

The buckling pressures calculated for the ring pres-

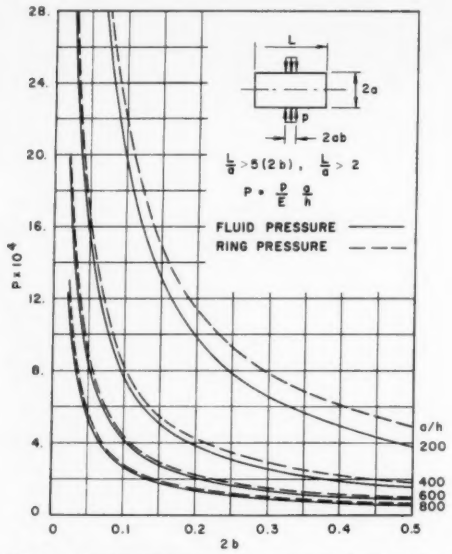

FIG. 5. Buckling pressure vs. pressure band width.

sure loading of the present analysis are always higher than those determined for the fluid pressure loading. The difference reflects the fact that pressure applied to only the high points of the deformed shell inhibits the formation of bulges.

The number of circumferential waves in the buckle pattern decreases for wider pressure bands, and a decrease in number of waves is accompanied by an increase in wave depth. Therefore, the difference in buckling pressures between the fluid and ring pressure loadings increases for wider bands. The deflection functions, Eqs. (12) and (13), however, are poorly suited for ring pressure loading in the extremely wide-band range, and the ring pressure solution in this range is probably too high to be of practical significance.

In Fig. 5 the results of the analysis are shown for several values of the radius/thickness ratio for the band-width range of greatest interest. In applying these results to shells of finite length, it is probably conservative to limit the shell length to not less than five times the band width and not less than twice the shell radius.

It may be noted that the greatest difference between fluid and ring buckling pressures in Fig. 5 is not more than about 30 per cent.

References

[1] Timoshenko, S., *Theory of Plates and Shells*, pp. 397–405, McGraw-Hill Book Company, Inc., New York, 1940.

[2] Flügge, W., *Statik und Dynamik der Schalen*, 2nd Ed., p. 324, Springer, Berlin, 1957.

[3] Langhaar, H. L., and Boresi, A. P., *Buckling and Post-Buckling Behavior of a Cylindrical Shell Subjected to External Pressure*, T. & A.M. Report No. 93, Univ. of Illinois, April, 1956.

[4] Hahne, H. V., *A Stability Problem of a Cylindrical Shell Subject to Direct and Bending Stresses*, Ph.D. Thesis, Stanford University, July, 1954.

[5] Hoff, N. J., *Buckling of Thin Cylindrical Shells under Hoop Stresses Varying in Axial Direction*, J. Appl. Mech., Vol. 24, No. 3, pp. 405–412, September, 1957.

[6] Marguerre, K., *On the Application of the Energy Method to Stability Problems*, NACA TM 1138, 1947.

[7] Timoshenko, S., *Theory of Elastic Stability*, McGraw-Hill Book Company, Inc., New York, 1936.

[8] Novozhilov, V. V., *Foundations of the Nonlinear Theory of Elasticity*, Greylock Press, Rochester, N.Y., 1953.

A New Reprint

Journal of the Aeronautical Sciences

Now entitled Journal of the Aero/Space Sciences

Available Since September 1959

Volumes 1–5, 1934–1937/1938, paper bound set.....$140.00
Volumes 1–2, 1934–1935, single volumes, paper bound..... 20.00
Volumes 3–5, 1935/1936–1937/1938, single volumes, paper bound..... 35.00

In Preparation

Volumes 6–8, 1938/1939–1940/1941

(Reproduced with the permission of the original publisher, Institute of the Aeronautical Sciences, Inc.)

Please address orders and inquiries to:

Johnson Reprint Corporation
111 Fifth Avenue, New York 3, N.Y.

Readers' Forum

BRIEF REPORTS of investigations in the aerospace sciences and discussions of papers published in the JOURNAL are presented in this special department. Entries must be restricted to a maximum of 1,300 words or the equivalent of one JOURNAL page including formulas and illustrations. Publication is completed as soon as possible after receipt of the material. The Editorial Committee does not hold itself responsible for the opinions expressed by the correspondents.

Contents

Comments on "Concise, Systematic Jacobian Thermodynamics for High-Temperature Real Gases" ..... WILLIAM SQUIRE 831

Author's Reply ..... RUSSELL J. ARAVE 832

Comment on "A Note on Blast-Wave Theory" ..... J. LOCKWOOD TAYLOR 832

Aerodynamic Influence Coefficients From Strip Theory ..... WILLIAM P. RODDEN 833

On the Frozen Flow of a Dissociated Gas ..... R. E. GEIGER 834

Determination of Air Stagnation Properties in a High-Enthalpy Test Facility ..... WALTER R. WARREN 835

The Yield Strength and Deflection of Circular Bars Subjected to Torsion ..... ROBERT M. RIVELLO 836

A Note on the Normal Force of a Multifinned Tail Assembly ..... JOHN D. MULHOLLAND 837

Aerodynamic Heating of Simple Geometries in the Slip- and Intermediate-Flow Regimes ..... BARRY L. REEVES AND WILLIAM M. VAN CAMP 838

Boundary-Layer Interaction on a Yawed Infinite Wing in Hypersonic Flow ..... ROBERT J. WHALEN 839

A Simple Method for Determining Turbulent Skin Friction From Velocity Profiles ..... P. BRADSHAW 841

Two-Dimensional Hypersonic Flow of an Ideal Gas With Infinite Electric Conductivity Past a Two-Dimensional Magnetic Dipole ..... TAKEO SAKURAI 841

Reduction of Strain Rosettes in the Plastic Range ..... T. H. H. PIAN 842

On the Effect of a Narrow Band of Distributed Roughness Upon Boundary-Layer Transition ..... J. C. GIBBINGS 843

Some Remarks on the Controversy Regarding Boundary Layers in Shear Flow ..... GÜNTHER JUNGCLAUS 844

Spinning Ballistic Missiles ..... W. H. T. LOH 844

A Closed-Form Solution for Laminar Free Convection on a Vertical Plate With Prescribed, Nonuniform, Wall Heat Flux ..... RICHARD P. BOBCO 846

Behavior of Liquids in Free Fall ..... WILLIAM C. REYNOLDS 847

On the Use of a Spark-Driven Shock Tube to Prepare Nonequilibrium Gas Samples ..... MYRON S. WECKER 848

The Use of the WKBJ Method to Estimate Transient Effects on Structural Response ..... ROBERT E. KELLY 850

Some Aspects of the Modified Newtonian and Prandtl-Meyer-Expansion Method for Axisymmetric Blunt Bodies at Zero Angle of Attack ..... RICHARD D. WAGNER, JR. 851

Comments on "Concise, Systematic Jacobian Thermodynamics for High-Temperature Real Gases"

William Squire*
Southwest Research Institute, San Antonio, Texas

May 26, 1959

ARAVE'S "generalization"[1] of Shaw's Jacobian[2] system for a real—i.e., dissociating—gas was made necessary only by his interpretation of Shaw's formulas. A dissociating gas in chemical equilibrium is still a simple system in the thermodynamic sense. Therefore, if the various extensive quantities such as enthalpy and entropy are taken to refer to a constant mass of material, the tables given by Shaw are valid for a dissociating gas. Modification is only necessary when extensive quantities are taken as being on a per-mole basis. The mole is obviously an unsuitable unit of mass when dealing with a dissociating gas as it no longer represents a fixed mass of material. While practice has not been standardized, there are tabulations[2–6] of the properties of air at high temperature on a per-unit-mass basis. Some tables[6] are on a per-*original*-mole basis, but this also represents a fixed mass.

The earliest table for determining thermodynamic partial derivatives in terms of three reference derivatives was given by Bridgman,[7, 8] who used C_p, $(\partial V/\partial T)_p$ and $(\partial V/\partial p)_T$ as the reference derivatives. The Bridgman table is reproduced in several texts but, unfortunately, two typographical errors[8, 9] in reference 7 have sometimes carried over.[10, 11] These errors are in $(\partial A)_E$ and $(\partial A)_H$. In the first case, the term corresponding to $-S(\partial T)_E$ has been left out, and in the second case a C_p factor has been omitted in one term.

Shaw's contribution is a table which can be memorized easily and which makes it possible to construct tables such as Bridg-

* Formerly of Bell Aircraft Corporation, Buffalo, N.Y.

Contributors Please Note

Readers' Forum items must be confined to the equivalent of one page in the *Journal*. Contributions that exceed this limit will be returned to the authors for condensation and rewrite. To avoid inconvenience and delay, please adhere to the following specifications:

(1) Five, double-spaced, typewritten, manuscript pages (8½ by 11 in.), including wide margins, formulas, and headings, equal one printed page.

(2) For every illustration, deduct at least one-half or as much as one manuscript page, depending on the size of the illustration.

man's for any suitable set of reference derivatives. The usual tables for air list three properties which are thermodynamic derivatives: C_p, C_v, and the speed of sound. A table expressing the other thermodynamic derivatives in terms of these three quantities would be easy to prepare, but the author has not felt any need for it.

The equilibrium speed of sound can be expressed either as

$$a^2 = (H - E)(\partial H/\partial E)_s \cong (H - E)(H/E) = pH/\rho E \quad (1)$$

or

$$a^2 = (\partial p/\partial \rho)_S = -V^2(\partial p/\partial V)_S \quad (2)$$

since $\rho = V^{-1}$. The author has found the approximation indicated in Eq. (1) useful in the past when adequate tables of the velocity of sound were not available.

References

[1] Arave, R. J., *Concise, Systematic Jacobian Thermodynamics for High-Temperature Real Gases*, Readers' Forum, Journal of the Aero/Space Sciences, Vol. 26, No. 4, pp. 250–53, April, 1959.

[2] Shaw, A. N., *The Derivation of Thermodynamical Relations for a Simple System*, Philos. Trans. Royal Soc. (London), Ser. A, Vol. 234, pp. 229–328, May 31, 1935.

[3] Predvoditelev, A. S., et al., *Tables of Thermodynamic Functions of Air*, Infosearch, London, 1958, (translation of a Russian table issued in 1957).

[4] McKowen, P. M., *The Equilibrium Composition and Flow Variables for Air Dissociated by a Strong Shock Wave*, Bell Aircraft Corporation Report 02-984-040, March 8, 1957.

[5] Logan, J. G., Jr., and Treanor, C. E., *Table of Thermodynamic Properties of Air from 3,000°K. to 10,000°K. at Intervals of 100°K.*, Cornell Aeronautical Laboratory Report BE-1007-A-3, January, 1957.

[6] Hilsenrath, J., and Beckett, C. W., *Tables of Thermodynamic Properties of Argon Free Air to 15,000°K.*, AEDC-TN-56-12, September, 1956.

[7] Bridgman, P. W., *A Collection of Thermodynamic Formulas*, Phys. Rev., Vol. 3, No. 4, pp. 273–81, April, 1914.

[8] Bridgman, P. W., *A Condensed Collection of Thermodynamic Formulas*, (1st Ed.), Harvard University Press, Cambridge, Massachusetts, 1925.

[9] Skotnicky, J., *The Dependence of the Melting Point on the Pressure*, Czech. J. Phys., Vol. 3, No. 3, pp. 225–31, September, 1953. See also, Appl. Mech. Rev., Vol. 7, No. 11, p. 507, Rev. 3711, November, 1954.

[10] Steiner, L. E., *Introduction to Chemical Thermodynamics*, First, Ed., p. 223, McGraw-Hill Publishing Co., Inc., New York, 1941.

[11] Penner, S. S., *Chemistry Problems in Jet Propulsion*, (1st Ed.), p. 131, Pergamon Press, Inc., New York, 1957.

Author's Reply

Russell J. Arave
Thermodynamics Group, Convair, A Division of General Dynamics Corp., San Diego, Calif.

July 12, 1959

OBVIOUSLY, a dissociating gas is a simple system in the thermodynamic sense,[1] and likewise the Bridgman table[2] is well known to thermodynamicists; however, the author feels that the necessary up-to-date changes contained in reference 3 are, nevertheless, very useful. In the first place, the compressibility term ($Z = PV/RT$) has come into wide use. It first came into being due to the virial equation of state. Compressibility is a good physical interpretation of the degree of dissociation or ionization[4] in a gas. For example, if a diatomic gas at room temperature having $Z \approx 1$ is heated until $Z \approx 2$, the gas is completely dissociated. Reference 3, like reference 5, is on a per-original-mole basis.

Due to the convenience and usefulness of the compressibility, it and other useful quantities (such as internal energy) have been tabulated for air for a wide range of temperatures and densities.[5,6,7] These values are arrived at by making use of spectroscopic measurements of the atomic energy levels[8] from which partition functions can be calculated. Then equilibrium constants can be found, and the system of gaseous species can be solved.[7] Values for the partial derivatives of compressibility and dimensionless internal energy with respect to temperature and density are contained in references 6, 9, and 10. These are precisely the reference quantities used in the table in reference 3. The reference quantity C_p, as used by Bridgman, is a complex arrangement of the reference quantities G, Z, G_ρ, G_T, and $Z\rho$ and would therefore be of less numerical accuracy. To compute C_p experimentally to a high degree of accuracy (for a high-temperature real gas) would be extremely difficult.

Another feature of reference 3 is that all the quantities are in dimensionless forms, thus avoiding any difficulty with units and conversion factors. Note that ln P, for example, is dimensionless in the table because $\partial \ln P$ is equal to $\partial(\ln P/\ln P_0)$, where P_0 is a reference constant. If it is desired to have the quantities in dimensional form, this may be accomplished by an easy transformation. For example,

$$(\partial X/\partial x)_y = RT[\partial(X/RT)/\partial x]_y + X(\partial \ln T/\partial x)_y$$

where X is a thermodynamic quantity, and (X/RT) is that quantity in dimensionless form.

The numerical values for the approximate formula for the equilibrium speed of sound given in reference 1, as well as the exact values for the speed of sound (over a range of densities and temperatures), are given in references 9 and 10. It is readily seen that this approximation for the speed of sound is accurate for air that is undissociated or only slightly dissociated. These data show, however, that the approximate speed of sound is in error by marked amounts for a highly dissociated and ionized gas such as might be found behind a normal shock at hypersonic velocities.

It might be well to add that Jacobian methods apply very well to other systems. Besides the special and simple thermodynamic cases, they can be applied with advantage to black-body radiation, the general (relativistic and nonrelativistic) quantum gas, the general degenerate Bose-Einstein and Fermi-Dirac gases, thermodynamic fluctuation,[11] etc.

References

[1] Squire, W., *Comments on "Concise, Systematic Jacobian Thermodynamics for High-Temperature Real Gases,"* Readers' Forum, Journal of the Aero/Space Sciences, Vol. 26, No. 11, pp. 831–832, December, 1959.

[2] Bridgman, P. W., *A Collection of Thermodynamic Formulas*, Phys. Rev., Vol. 3, No. 4, pp. 273–281, April, 1914.

[3] Arave, R. J., *Concise, Systematic Jacobian Thermodynamics for High-Temperature Real Gases*, Readers' Forum, Journal of the Aero/Space Sciences, Vol. 26, No. 4, pp. 250–253, April, 1959.

[4] Hochstim, A. R., *Introduction to General Thermodynamics of a Real Gas*, Convair, San Diego, Physics Gr. Report No. ZPh-003, May 15, 1959.

[5] Hilsenrath, J. and Beckett, C. W., *Tables of Thermodynamic Properties of Argon Free Air to 15,000°K.*, AEDC TN-56-12, September, 1956.

[6] Logan, J. G., Jr., and Treanor, C. E., *Tables of Thermodynamic Properties of Air from 3,000°K. to 10,000°K.*, Cornell Aeronautical Laboratory Report BE-1007-A-3, January, 1957.

[7] Gilmore, F. R., *Equilibrium Composition and Thermodynamic Properties of Air to 24,000°K.*, Rand Report RM-1543, August 24, 1955.

[8] Moore, C. E., *Atomic Energy Levels*, NBS 467, Vols. I and II, August 15, 1952.

[9] Hochstim, A. R., and Arave, R. J., *Various Thermodynamic Properties of Air*, Convair, San Diego, Physics Gr. Report No. ZPh-004, June 14, 1957.

[10] Hochstim, A. R., *Tables and Graphs of Thermodynamical Properties of Air*, Convair, San Diego, Physics Gr. Report No. ZPh-004, (revised), August 1, 1958.

[11] Einbinder, H., *The Application of Jacobians to Statistical Thermodynamics*, J. Chem. Phys., Vol. 21, No. 12, pp. 2134–2143, December, 1953.

Comment on "A Note on Blast-Wave Theory"

J. Lockwood Taylor
Professor, Norges Tekniske Hogskole, Institutt for Flyteknikk, Trondheim, Norway

May 4, 1959

I REFER to Harvey Einbinder's letter on the above subject (Readers' Forum, Journal of the Aero/Space Sciences, Vol. 26, No. 3, pp. 191–192, March, 1959) in which he attributes the analytical solution for a spherical blast wave to Richard Latter, the reference being *Similarity Solution for a Spherical Shock Wave*, J. Appl. Phys., Vol. 26, No. 8, pp. 954–960, August, 1955.

May I point out that I published such a solution in *An Exact Solution of the Spherical Blast Wave Problem*, Phil. Mag., Vol. 46, 7th Series, No. 374, pp. 317–320, March, 1955.

Aerodynamic Influence Coefficients From Strip Theory

William P. Rodden*
Research Specialist, Vibration, Flutter, and Acoustics Group, North American Aviation, Inc., Los Angeles, Calif.
May 21, 1959

IN ANY AEROELASTIC ANALYSIS by collocation methods, both structural and aerodynamic influence coefficients must be known. We consider here the derivation of the aerodynamic influence coefficients (AICs) from the simplest of the aerodynamic theories—that of strip theory in which the flow along any section of the wing can be considered as two-dimensional. The type of AICs necessary in an aeroelastic analysis must relate the control-point forces, F (rather than pressures) to the deflections, h, or streamwise slopes. In the present treatment, we prefer the deflections rather than streamwise slopes as the generalized coordinates because the deflections have a more general meaning on a cambered surface and deflection influence coefficients are more readily obtained from a structural analysis than slope influence coefficients. Accordingly, we define a steady matrix of AICs, $[C_{hs}]$, by

$$\{F\} = (qS/\bar{c})[C_{hs}]\{h\} \tag{1}$$

where the forces and deflections are positive up (aerodynamic convention), and q is the dynamic pressure, S is the area of one wing, and $\bar{c}$ is the mean aerodynamic chord; we define a matrix of oscillatory AICs, $[C_h]$, by

$$\{F\} = \rho\omega^2 b_r^2 s[C_h]\{h\} \tag{2}$$

where the forces and deflections are positive down (flutter convention), and ρ is the density, ω is the frequency, b_r is the reference semi-chord, and s is the span of one wing. We note that the definitions of Eqs. (1) and (2) are completely general, being equally applicable to an aerodynamic lifting surface theory or to a strip theory. However, in the case of strip theory, the matrix of AICs appears in a partitioned form. For example, the AICs for a two strip wing appear as

$$[C_h] = \left[\begin{array}{c|c} C_{h1} & 0 \\ \hline 0 & C_{h2} \end{array}\right] \tag{3}$$

where the C_{hi} are the AICs for each strip. Hence, we need only derive the AICs for one strip.

We begin by deriving the steady AICs. The given and the equivalent force systems and geometry are shown in Fig. 1. We have assumed that the given aerodynamic coefficients have been referred to the local quarter-chord, as is usually the case with flutter coefficients. We arbitrarily choose the forward control point at the quarter-chord, the intermediate control point at the control-surface hinge line, and the aft control point at the trailing edge. It should be noted that the chord is considered to be rigid. The strip aerodynamic coefficients are usually defined by

$$\begin{Bmatrix} L \\ M \\ T \end{Bmatrix} = q\Delta y \begin{bmatrix} c & 0 & 0 \\ 0 & c^2 & 0 \\ 0 & 0 & c_a{}^2 \end{bmatrix} \begin{bmatrix} C_{l_\alpha} & C_{l_\delta} \\ C_{m_\alpha} & C_{m_\delta} \\ C_{h_\alpha} & C_{h_\delta} \end{bmatrix} \begin{Bmatrix} \alpha \\ \delta \end{Bmatrix} \tag{4}$$

The force equivalence is given by

$$\begin{bmatrix} 1 & 1 & 1 \\ 0 & -d & -(d+c_a) \\ 0 & 0 & -c_a \end{bmatrix} \begin{Bmatrix} F_1 \\ F_2 \\ F_3 \end{Bmatrix} = \begin{Bmatrix} L \\ M \\ T \end{Bmatrix} \tag{5}$$

* Now Engineering Specialist, Dynamics Branch, Norair Division of Northrop Corporation, Hawthorne, Calif.

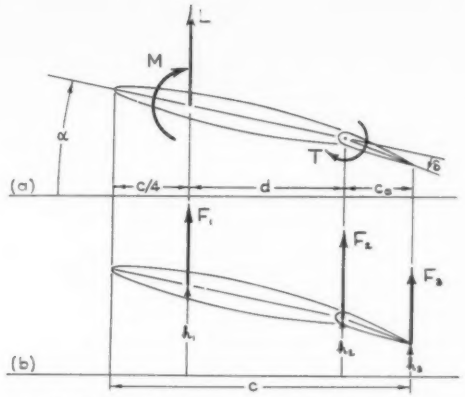

FIG. 1. Original (a) and equivalent (b) force systems and geometry for the steady case.

and the geometrical equivalence is given by

$$\begin{Bmatrix} \alpha \\ \delta \end{Bmatrix} = \begin{bmatrix} 1/d & -1/d & 0 \\ -1/d & (1/d+1/c_a) & -1/c_a \end{bmatrix} \begin{Bmatrix} h_1 \\ h_2 \\ h_3 \end{Bmatrix} \tag{6}$$

Solving for $\{F\}$ in terms of $\{h\}$ by combining Eqs. (4)–(6) and identifying the result with Eq. (1) yields the steady strip AIC matrix.

$$[C_{hs}] = (\bar{c}\Delta y/S) \begin{bmatrix} 1 & c/d & -c_a{}^2/cd \\ 0 & -c/d & (c_a{}^2/cd + c_a/c) \\ 0 & 0 & -c_a/c \end{bmatrix} \times \begin{bmatrix} C_{l_\alpha} & C_{l_\delta} \\ C_{m_\alpha} & C_{m_\delta} \\ C_{h_\alpha} & C_{h_\delta} \end{bmatrix} \begin{bmatrix} c/d & -c/d & 0 \\ -c/d & c/d + c/c_a & -c/c_a \end{bmatrix} \tag{7}$$

In the absence of the control surface, this reduces to

$$[C_{hs}] = (\bar{c}\Delta y/S) \begin{bmatrix} 1 & c/d \\ 0 & -c/d \end{bmatrix} \begin{Bmatrix} C_{l_\alpha} \\ C_{m_\alpha} \end{Bmatrix} [c/d \quad -c/d] \tag{8}$$

We next consider the oscillatory case. The given and the equivalent force systems and geometry are shown in Fig. 2. The oscillatory aerodynamic coefficients are defined by

$$\begin{Bmatrix} L \\ M \\ T \end{Bmatrix} = \pi \cos\Lambda \rho\omega^2 b^2 \Delta y \begin{bmatrix} 1 & 0 & 0 \\ 0 & b & 0 \\ 0 & 0 & b \end{bmatrix} \begin{bmatrix} L_h & L_\alpha & L_\beta \\ M_h & M_\alpha & M_\beta \\ T_h & T_\alpha & T_\beta \end{bmatrix} \begin{Bmatrix} h \\ b\alpha \\ b\beta \end{Bmatrix} \tag{9}$$

(N.B., the factor $\pi \cos\Lambda$ is used with subsonic coefficients where Λ is the sweep of the quarter-chord. Usually, the factor 4 is used in its place with supersonic coefficients). The force equivalence is given by

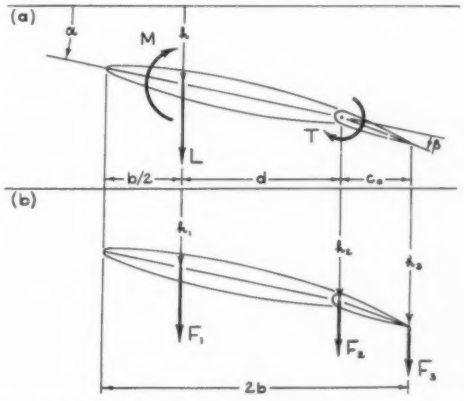

FIG. 2. Original (a) and equivalent (b) force systems and geometry for the oscillatory case.

$$\begin{bmatrix} 1 & 1 & 1 \\ 0 & d & d + c_a \\ 0 & 0 & c_a \end{bmatrix} \begin{Bmatrix} F_1 \\ F_2 \\ F_3 \end{Bmatrix} = \begin{Bmatrix} L \\ M \\ T \end{Bmatrix} \tag{10}$$

The geometrical equivalence is

$$\begin{Bmatrix} h \\ b\alpha \\ b\beta \end{Bmatrix} = \begin{bmatrix} 1 & 0 & 0 \\ -b/d & b/d & 0 \\ b/d & -(b/d + b/c_a) & b/c_a \end{bmatrix} \begin{Bmatrix} h_1 \\ h_2 \\ h_3 \end{Bmatrix} \tag{11}$$

Again, placing $\{F\}$ in terms of $\{h\}$ by combining Eqs. (9)–(11) and identifying the result with Eq. (2) yields the oscillatory strip AIC matrix.

$$[C_h] = \pi \cos \Lambda (b/b_r)^2 (\Delta y/s) \begin{bmatrix} 1 & -b/d & b/d \\ 0 & b/d & -(b/d + b/c_a) \\ 0 & 0 & b/c_a \end{bmatrix} \begin{bmatrix} L_h & L_\alpha & L_\beta \\ M_h & M_\alpha & M_\beta \\ T_h & T_\alpha & T_\beta \end{bmatrix} \begin{bmatrix} 1 & 0 & 0 \\ -b/d & b/d & 0 \\ b/d & -(b/d + b/c_a) & b/c_a \end{bmatrix} \tag{12}$$

In the absence of the control surface, this reduces to

$$[C_h] = \pi \cos \Lambda (b/b_r)^2 (\Delta y/s) \begin{bmatrix} 1 & -b/d \\ 0 & b/d \end{bmatrix} \begin{bmatrix} L_h & L_\alpha \\ M_h & M_\alpha \end{bmatrix} \begin{bmatrix} 1 & 0 \\ -b/d & b/d \end{bmatrix} \tag{13}$$

Once the AIC partitions are obtained for each strip, the total AIC matrix is formed as in Eq. (3).

On the Frozen Flow of a Dissociated Gas

R. E. Geiger
Hypersonic Research Specialist,
Missile and Space Vehicle Department,
General Electric Company, Philadelphia, Pa.
June 9, 1959

Introduction

Very little is known about the extent of departures from thermodynamic equilibrium in many hot-gas flow problems. In an investigation of such a flow, it is desirable to know the possible range of values of flow variables that might be encountered. A calculation of a completely frozen flow is useful for this purpose. This note demonstrates that the usual equations for a constant specific-heat ratio are valid for a completely frozen gas, provided an appropriate effective specific heat ratio is used.

The frozen gas considered here is one in which only the rotational and translational portions of the molecular energy are allowed to change during the flow process. All other gas energy components, such as vibration, dissociation and ionization, remain constant. Furthermore, the composition of the gas remains fixed, and no chemical reactions are permitted. The gas internal energy for this gas may be expressed as

$$\left.\begin{aligned} e &= e_f + e_a \\ &= e_f + C_v T \end{aligned}\right\} \tag{1}$$

where e_f is the frozen component of the energy gas; e_a is the active component (i.e., translational plus rotational energy); and C_v is the specific heat at constant volume and is constant, computed as if the components of the hot gas constituted a mixture of ideal gases.

The equation of state for this frozen gas is

$$P = Z\rho RT \tag{2}$$

or

$$Pv = ZRT \tag{2a}$$

where P, ρ, v, R, T have their usual meaning, and Z is the number of particles in the hot gas per particle of the same gas at normal temperatures and pressures. In the present case, Z remains fixed throughout the flow process.

Since C_v and Z are constant, Eqs. (1) and (2) have precisely the same form as for an ideal gas. It is then possible to go through the standard derivation for an isentropic flow. From the first and second laws of thermodynamics,

$$Tds = de + Pdv \tag{3}$$

From Eq. (1),

$$Tds = C_v dT + Pdv \tag{4}$$

Using Eq. (2a),

$$ds = (C_v dT/T) + (ZR dv/v) \tag{5}$$

For an isentropic process,

$$(dT/T) + (ZR/C_v)(dv/v) = 0 \tag{6}$$

or

$$\log T + (ZR/C_v) \log v = \log \lambda \tag{6a}$$

where $\log \lambda$ is the integration constant.

Using Eq. (2a),

$$v^{(ZR/C_v)} Pv = \lambda ZR \tag{7}$$

or

$$Pv^{[1 + (ZR/C_v)]} = \text{constant} \tag{7a}$$

which has the same form as the isentropic pressure-density relation for an ideal gas if we define

$$\Gamma = 1 + (ZR/C_v) \tag{8}$$

At low temperatures where dissociation and vibration are negligible, this reduces to the usual specific-heat ratio.

If we further adopt the sonic-velocity definition,

$$a^2 = (\partial P/\partial \rho)_s$$

we have, for our frozen flow,

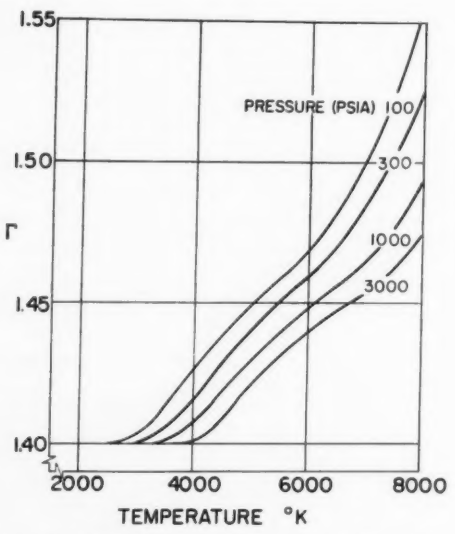

Fig. 1. Effective specific-heat ratio for frozen air.

$$a^2 = \Gamma(P/\rho) \tag{9}$$

which again has the same form as the usual ideal-gas result.

All of the usual ideal-gas isentropic-flow equations now can be derived. Thus, for a completely frozen isentropic flow, the standard ideal-gas equations may be used if we replace γ with Γ. Note that in the present case

$$\left.\begin{aligned} h &= (P/\rho) + C_v T + e_f \\ &= (C_v + ZR)T + e_f \end{aligned}\right\} \tag{10}$$

and

$$C_p = (\partial h/\partial T)_p = C_v + ZR \tag{11}$$

Computation of Γ

According to classic kinetic theory the energy of translation and rotation of a gas at the temperatures of interest here is $(1/2)RT$ per mole per degree of freedom. For a mixture of gases (diatomic and/or monatomic), the active internal energy is given by

$$e_a = (R_0 T/2)\Sigma_j(m_j D_j/M_j) \tag{12}$$

where

R_0 = universal gas constant
D_j = number of active degrees of freedom (rotation and translation) of jth species
m_j = mole fraction of jth species
M_j = molecular weight of jth species

Thus,

$$C_v = (R_0/2)\Sigma_j(m_j D_j/M_j) \tag{13}$$

Such computations have been carried out for air over a range of temperatures and pressures using the data of reference 1. The results are presented in Fig. 1.

Reference

[1] Gilmore, F. R., *Equilibrium Composition and Thermodynamic Properties of Air to 24,000°K.*, Rand Rpt. RM-1543, August, 1955.

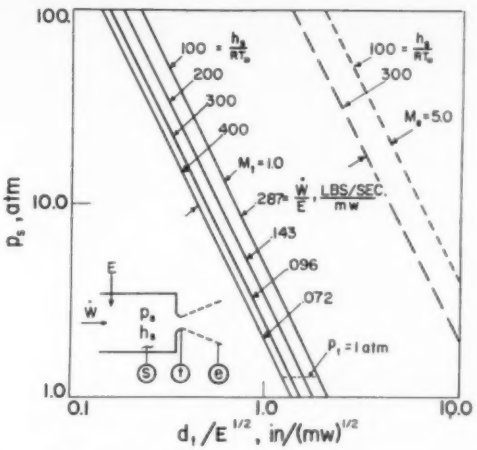

FIG. 1. Relationship between properties in high-enthalpy air flow system, RT_0 = 33.86 B.t.u./lb.

Determination of Air Stagnation Properties in a High-Enthalpy Test Facility*

Walter R. Warren
Consulting Aerodynamics Engineer,
Missile and Space Vehicle Department,
General Electric Company, Philadelphia, Pa.
June 15, 1959

Symbols

d = diameter
E = power added to test gas
h = enthalpy
M = Mach Number
p = pressure
R = universal gas constant
T = temperature
$\dot{W}$ = weight flow of air

Subscripts

e = nozzle exit
0 = reference conditions
s = plenum or stagnation chamber
t = throat

THE AVAILABILITY of high-temperature equilibrium air properties[1] in a convenient-to-use form[2] permits the simple determination of the gas stagnation conditions in test facilities such as an air arc-heated wind tunnel.[3] The method depends upon the measurement of two test parameters: the mass-flow rate through the facility and the plenum-chamber pressure. The assumptions are made that at the throat of the plenum chamber the flow is choked (although this is not necessary as shown in reference 3) and that the flow from the plenum chamber to the throat is one-dimensional with negligible boundary-layer thickness. It is also assumed that the gas is in thermodynamic and chemical equilibrium as it expands from plenum conditions to throat conditions.

The flow system is sketched in Fig. 1. It is characterized by four unknowns—i.e., three state properties and an axial velocity—and four equations—i.e., the equation of state and the conservation equations for mass, energy, and axial momentum. Once the equation of state is used, the system is reduced to three unknowns and three equations, so that the three easily measured test properties of mass-flow rate, plenum-chamber pressure, and nozzle-throat diameter specify the flow system and lead to the determination of test-gas properties in the plenum chamber or at the throat.

A universal chart which summarizes the results of calculations for this flow system over a useful range of operating conditions is shown in Fig. 1. This chart is difficult to use directly; therefore, an example of a more useful display of the results for a particular nozzle-throat diameter is shown in Fig. 2. Only the power added to the gas, E, and its stagnation enthalpy are given in Fig. 2. If other stagnation chamber or throat properties are desired, they can be obtained through the use of the Mollier chart.[2] It is pointed out that a curve of the type shown in Fig. 1 can be extended to describe the flow in an expanded supersonic nozzle.

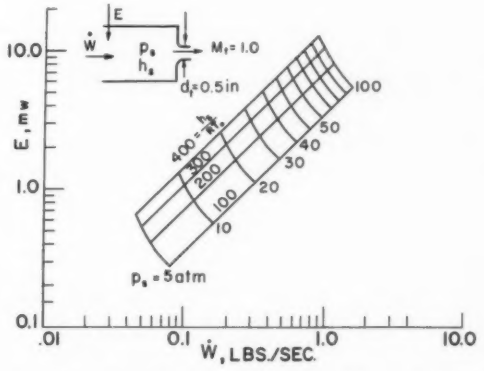

FIG. 2. Stagnation properties of air in high-enthalpy flow system, RT_0 = 33.86 B.t.u./lb.

* This work was supported by the Air Force Ballistic Missile Division under Contract AF 04 (647)269.

For example, curves have been sketched on Fig. 1 for a Mach 5 test flow.

REFERENCES

[1] Hilsenrath, J., and Beckett, C. W., *Tables of Thermodynamic Properties of Argon-Free Air to 15,000°K.*, AEDC TN-56-12, September, 1956.

[2] Feldman, S., *Hypersonic Gas Dynamic Charts for Equilibrium Air*, AVCO Research Laboratory, January, 1957.

[3] Warren, W. R., *Determination of Properties of High Temperature Air Jets*, MSVD Advanced Aerodynamics TM No. 6, General Electric Co., January 8, 1958.

The Yield Strength and Deflection of Circular Bars Subjected to Torsion

Robert M. Rivello*
University of Maryland, College Park, Md.

June 4, 1959

WHEN A CIRCULAR BAR is subjected to torsion, the shear strain at any point a distance r from the center of the section is given by

$$\gamma = r\theta \tag{1}$$

where θ is the angle of twist per unit length. This relationship holds even though the stresses exceed the proportional limit if the angle of twist is small and the material is isotropic.[1] The condition of equilibrium between the applied torsional moment T and shear stress τ at any point is

$$T = 2\pi \int_b^a \tau\, r^2\, dA \tag{2}$$

where a and b are the outer and inner radii, respectively (Fig. 1). Eqs. (1) and (2), together with the appropriate shear stress-strain relation, are sufficient to determine τ and θ for a given torque. The problem is usually solved by numerical integration using the actual stress-strain curve of the material. When the surface of the shaft is stressed to the yield stress, a case of considerable practical importance, it is possible to obtain closed-form solutions for both the yield torque and angle of twist in terms of the Hill parameters of the material. It is the purpose of this note to present these relationships. The development of the equation parallels that of the yield strength of beams in pure bending, which was previously given by the author.[2]

For stresses up to slightly greater than the yield, the stress-strain curve for uniaxial stress may be accurately expressed by the Hill equation[3]

$$\epsilon = (\sigma/E) + 0.002(\sigma/\sigma_y)^n \tag{3}$$

where σ_y is the 0.2 per cent offset yield stress and n is the Hill shape parameter. By using the principal-shear-stress theory, it is possible to derive a stress-strain diagram for pure shear from a uniaxial stress-strain diagram.[4] If this method is applied to the stress-strain relationship of Eq. (3), the following shear stress-strain equation results:

$$\gamma = (\tau/G) + 0.002(2^n + 1)(\tau/\sigma_y)^n \tag{4}$$

where G is the shear modulus which is equal to $E/2(1 + \nu)$.

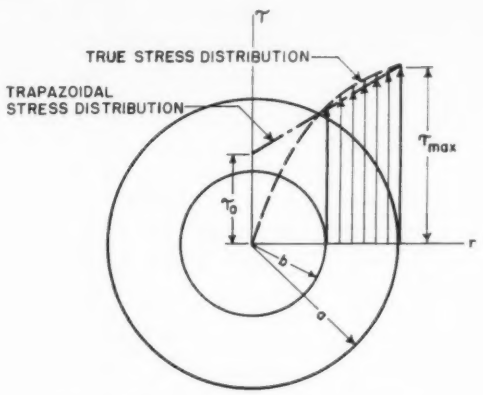

FIG. 1. Geometry and stress distributions.

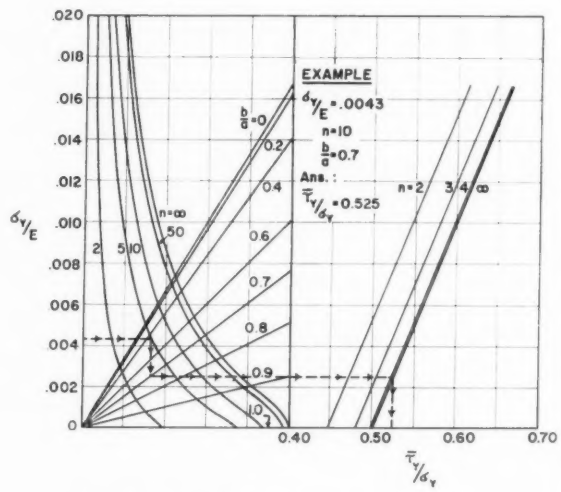

FIG. 2. Nomogram for determination of $\bar{\tau}_y\sigma_y$.

In general, if Eq. (4) is used with Eqs. (1) and (2), the resulting expressions relating T, τ, and θ are lengthy and offer no simplification over numerical integration. If we restrict ourselves to the condition of the maximum stress equal to the 0.2 per cent offset yield shear stress, the yield angle of twist per unit length θ_y in terms of the Hill parameters becomes

$$\theta_y = (1/a)\{0.002 + [2.6/(2^n + 1)^{1/n}](\sigma_y/E)\} \tag{5}$$

I
in Eq. (5) and those involving the Hill parameters which follow, t has been assumed that ν equals 0.3. The yield torque T_y may be related to the torsional modulus of yield $\bar{\tau}_y$ by the equation

$$\bar{\tau}_y \equiv T_y a/J \tag{6}$$

where J is the polar moment of inertia of the cross section. For the solid bar (b equal to zero), the following relationship can be shown to exist between $\bar{\tau}_y$ and the Hill parameters:

$$\left(\frac{\bar{\tau}_y}{\sigma_y}\right)_{b/a=0} = \frac{4}{[0.002(2n+1)^{1/n} + 2.6(\sigma_y/E)]^3}\left[\frac{4.394}{(2^n+1)^{1/n}}\left(\frac{\sigma_y}{E}\right)^3 + \frac{1.352\times10^{-2}(n+2)}{(n+3)}\left(\frac{\sigma_y}{E}\right)^2 + \frac{5.2\times10^{-6}(2n+1)(2^n+1)^{1/n}}{(n+1)}\left(\frac{\sigma_y}{E}\right) + \frac{8\times10^{-9}n(2^n+1)^{2/n}}{(3n+1)}\right] \tag{7}$$

* Associate Professor of Aeronautical Engineering.

A simple relationship similar to Eq. (7) is not possible for the case of the hollow circular bar because of the complexity of the expression for the stress at the inside radius. To circumvent this difficulty, a method similar to that used by Cozzone for plastic bending[5] may be used. Following this approach, the shear-stress distribution in the plastic range will be assumed to be trapezoidal (Fig. 1), so that

$$\tau = \tau_0 + (\tau_{max} - \tau_0)(r/a) \tag{8}$$

where τ_0 is a stress such that the trapezoidal distribution will produce the same torque as the true distribution. For exact solutions, it is necessary to obtain a τ_0 for each ratio of inside to outside radii, and there is no advantage in using the trapezoidal distribution. Cozzone has shown, however, that the minimum stress of a trapezoidal bending-stress distribution determined for a rectangular cross section is sufficiently accurate for other beam sections. Such an assumption is even more justified in the torsion problem because the stresses are weighted by the square of their distance from the center of the shaft. For the solid bar, the value of τ_0 is given by

$$\tau_0 = 3[(Ta/J) - \tau_{max}] \tag{9}$$

Taking τ_{max} equal to the yield shear stress and designating the value of τ_0 associated with this condition by τ_{0y} gives

$$\tau_{0y}/\sigma_y = 3\{(\bar{\tau}_y/\sigma_y)_{b/a=0} - [1/(2^n + 1)^{1/n}]\} \tag{10}$$

Using this same value of τ_{0y} for the hollow section, the torsion modulus of yield for a section of any b/a becomes

$$\bar{\tau}_y/\sigma_y = [1/(2^n + 1)^{1/n}] + K(\tau_{0y}/\sigma^y) \tag{11}$$

where

$$K = (1/3)[(a^4 - 4ab^3 + 3b^4)/(a^4 - b^4)] \tag{12}$$

Eqs. (9), (10), and (11) are plotted in Fig. 2 in the form of a nomogram for a range of the Hill parameters which should cover all practical cases. It may be used for the full range of sections varying from the solid shaft to the thin-walled tube if it is assumed that yielding occurs before buckling. A sample problem is shown on the nomogram.

References

[1] Nadai, A., *Theory of Flow and Fracture of Solids*, 2nd Ed., Vol. 1, pp. 347–352, McGraw-Hill Book Co., Inc., New York, 1950.

[2] Rivello, R. M., *The Yield Strength of Beams in Pure Bending*, Journal of the Aero/Space Sciences, Vol. 26, No. 6, pp. 393–394, June, 1959.

[3] Hill, H. N., *Determination of Stress-Strain Relations from "Offset" Yield Strength Values*, NACA TN 927, 1944.

[4] Shanley, F. R., *Strength of Materials*, pp. 183–190, McGraw-Hill Book Co., Inc., New York, 1957.

[5] Cozzone, F. P., *Bending Strength in the Plastic Range*, Journal of the Aeronautical Sciences, Vol. 10, No. 5, pp. 137–151, May, 1943.

A Note on the Normal Force of a Multifinned Tail Assembly*

John D. Mulholland
Department of Aeronautical Engineering, University of Cincinnati, Cincinnati, Ohio

June 19, 1959

THE AUTHORS of reference 1 presented a supersonic interference parameter for multifinned tail assemblies. This parameter was defined by

$$I = C_r/\beta D \sin \pi/n$$

where

C_r = fin root chord
$\beta = \sqrt{M^2 - 1}$
D = body diameter
n = number of fins (≥ 2)

and represented, physically, the ratio of a particular Mach cone to the distance between adjacent fin root chords. This parameter was used to correlate an "adjusted" tail normal-force slope based on average angles of attack and "effective" fin areas. This method was revised in reference 2 such that the normal-force parameter to be correlated was given by

$$\overline{C_{NT_\alpha}} = C_{NT_\alpha}(\pi D^2/4S_f)(\alpha S_f/\alpha_e S_e)$$

where

$C_{NT_\alpha} = (C_{N_\alpha})_{\text{total}} - (C_{N_\alpha})_{\text{body alone}}$
S_f = exposed area of one fin

and

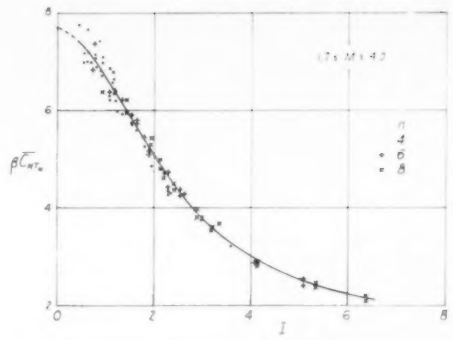

FIG. 1. Normal-force slope of tail assembly with clipped-delta fins. $\lambda = 1/3$, $b/D = 2$, $n = 4, 6, 8$.

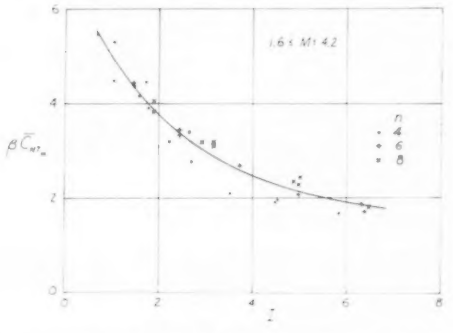

FIG. 2. Normal-force slope of tail assembly with rectangular fins. $b/D = 2$, $n = 4, 6, 8$.

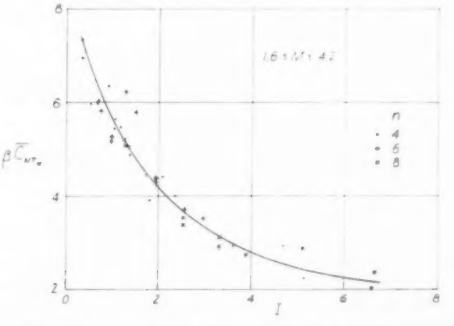

FIG. 3. Normal-force slope of tail assembly with rectangular fins. $b/D = 3$, $n = 4, 6, 8$.

* This study is part of a project sponsored by the Air Proving Ground Center, Eglin AFB, Florida, under Contract AF 08(603)-4491.

$$\alpha_e S_e/\alpha S_f = \int_0^{\pi/n} (1/\pi) \times \left\{ \sum_{k=1}^{n} |\cos [(2\pi k/n) - \psi]| \right\}^2 d\psi, \quad (n/2) \text{ even}$$

$$\alpha_e S_e/\alpha S_f = \int_0^{\pi/n} (1/\pi) \times \left\{ \sum_{k=1}^{n} |\sin [(2\pi k/n) - \psi]| \right\}^2 d\psi, \quad (n/2) \text{ odd}$$

where ψ = roll angle. The roll angle is assumed zero when one pair of fins lies in the pitch plane. Values of $\alpha_e S_e/\alpha S_f$ for common n are

n	2	4	6	8
$S_e\alpha_e/\alpha S_f$	1.00	1.63	2.43	3.24

It was shown rather conclusively in reference 2 that, for a given Mach Number M, taper ratio λ, and span-to-body-diameter ratio b/D, $\overline{C_{NT_\alpha}}$ is a function of I only, independent of the number of fins. The purpose of the present note is to point out that this correlation can be made independent of Mach Number also, by the simple expedient of plotting $\beta\overline{C_{NT_\alpha}}$ versus I.

The result of applying this procedure to the clipped-delta-fin data of reference 2 is shown in Fig. 1. It is seen that excellent correlation is achieved. Figs. 2 and 3 show a somewhat poorer correlation for the rectangular-fin data of references 3–5, but it is felt that even this is sufficiently good to indicate that supersonic multifin normal-force data can be estimated with reasonable accuracy from cruciform-fin data at the same values of λ and b/D.

References

[1] Potter, J. L., Murphree, W. D., and Shapiro, N. M., *On the Normal Force Produced by Multifinned Tail Assemblies in Supersonic Flow*, Journal of the Aeronautical Sciences, Vol. 22, No. 7, pp. 511–513, July, 1955.

[2] Potter, J. L., Shapiro, N. M., and Murphree, W. D., *An Interference Factor for Multifinned Tail Assemblies in Supersonic Flow*, Ordnance Missile Laboratories, Redstone Arsenal, Report 2R12F, May, 1956.

[3] Luther, M. L., and Jaeger, B. F., *Effects of Varying the Number of Fins on Fin-Stabilized Supersonic Rockets*, U.S. Naval Ordnance Test Station, China Lake, NAVORD Report 1900, August, 1951.

[4] Jaeger, B. F., and DeLancey, L. M., *The Aerodynamic Characteristics at Mach Number 1.87 of 14- and 18-Caliber Fin-Stabilized Rocket Models with Varying Fin Parameters*, U.S. Naval Ordnance Test Station, China Lake, NAVORD Report 1918, October, 1951.

[5] Jaeger, B. F., and DeLancey, L. M., *The Aerodynamic Characteristics at Mach Number 4.24 of 10-, 14-, and 18-Caliber Fin-Stabilized Rocket Models with Varying Fin Parameters*, U.S. Naval Ordnance Test Station, China Lake NAVORD Report 1950, March, 1952.

Aerodynamic Heating of Simple Geometries in the Slip- and Intermediate-Flow Regimes

Barry L. Reeves* and William M. Van Camp

Research Associate and Associate Scientist, Respectively, McDonnell Aircraft Corporation, St. Louis, Mo.

June 23, 1959

Because of the complex interactions of viscous, compressibility, and rarefaction effects, only a limited number of theoretical aerodynamic-heating solutions have been formulated for the flow regimes most commonly described in the literature as the slip and intermediate regimes. Most of these theoretical solutions apply only to a very limited region of slip flow bordering the continuum-flow regime. Since few experimental heat-transfer data are available in slip and intermediate flows, the design engineer has very little information at his disposal for predicting vehicle temperatures.

This brief paper presents empirical relationships for determining the aerodynamic heating rates and temperature recovery factors for the flow of a moderately rarefied gas over flat plates, cones, spheres, and transverse cylinders.

* Now, National Science Foundation Fellow, Mechanical Engineering Dept., Washington University.

In establishing the heat-transfer and temperature-recovery-factor relations, it is assumed that (a) the aerodynamic and heat-transfer variables are continuous monotonic functions of gas rarefaction, and (b) the ratio of the number of molecular collisions with the surface to the number of intermolecular collisions is equal to the Knudsen Number, Kn. Thus, if λ represents an aerodynamic or heat-transfer variable in the slip- and intermediate-flow regimes, it is reasonable to assume that

$$\lambda = P\lambda_{fm} + (1 - P)\lambda_c \tag{1}$$

as originally suggested by Martino[1] in a study of temperature-recovery factors on circular cylinders. Here, λ_{fm} and λ_c are the values of the variable λ in the free-molecule and continuum regimes, respectively, and P is the probability that a molecule will collide with the adjacent surface before colliding with another molecule. Since the Knudsen Number (ratio of the mean-free path length to the significant flow dimension) is an indication of the degree of gas rarefaction, P must be some function of Kn, such that

$$\lim_{Kn \to 0} P = 0 \quad \text{and} \quad \lim_{Kn \to \infty} P = 1$$

The probability function for the flow of a gas through a duct is $P = Kn/(1 + Kn)$. Substituting P from this relation into Eq. (1) yields

$$\lambda = (\lambda_c + Kn\lambda_{fm})/(1 + Kn) \tag{2}$$

In the slip and intermediate regimes, the significant flow dimension in the Knudsen Number is the boundary-layer thickness. Because of the low Reynolds Number usually associated with the flow of a rarefied gas, boundary layers are predominantly laminar. For laminar boundary layers, the Knudsen Number may be expressed[2] in terms of the Mach Number, M, Reynolds Number, Re, and specific-heat ratio, γ. Substituting the appropriate relation for Kn into Eq. (2) yields

$$\lambda = \frac{\lambda_c + 1.252\sqrt{\gamma}(M/\sqrt{Re})\lambda_{fm}}{1 + 1.252\sqrt{\gamma}(M/\sqrt{Re})} \tag{3}$$

If it is assumed that the probability function for flow through a duct is applicable to external flows, Eq. (3) becomes the basis for establishing the heat-transfer and temperature-recovery-factor relations for slip and intermediate flows. The case of the flow over a flat plate will be considered.

Oppenheim[3] has shown that for free-molecule flow past a flat plate and for $M > 3$, the Nusselt Number, Nu, is given by

$$Nu = 0.169\ \alpha(\gamma + 1)\ [(Re \cdot Pr)/\gamma M] \tag{4}$$

where α is the accommodation coefficient and Pr is the Prandtl Number. Assuming that the boundary between the free-molecule and intermediate-flow regimes[2] is given by $M/Re = 10$, and substituting this relation into Eq. (4), gives

$$(Nu/\sqrt{Re})_{fm} = 0.0535\ [\alpha(\gamma + 1)Pr/\gamma\sqrt{M}] \tag{5}$$

In the continuum regime, the Nusselt Number may be expressed

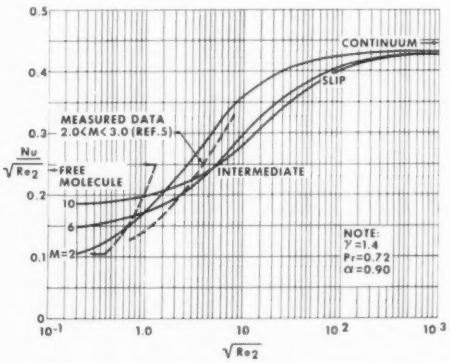

FIG. 1. Aerodynamic heating of transverse circular cylinders in slip and intermediate flow.

as[4]

$$(Nu)_c = 0.332\sqrt{Re^3}\sqrt{Pr} \tag{6}$$

The properties are evaluated at the continuum reference temperature[4], T_c^*.

$$T_c^* = 0.58\,T_w + 0.42\,T_\delta(1 + 0.0762\,M_\delta^2) \tag{7}$$

where the subscripts w and δ refer to conditions at the wall and at the edge of the boundary layer, respectively.

Using the $Nu/\sqrt{Re}$ relations of Eqs. (5) and (6) as the parameter λ in Eq. (3) yields

Flat Plate

$$\frac{Nu}{\sqrt{Re^*}} = \frac{0.332\,(Pr^*)^{1/3} + 0.067\alpha\sqrt{\gamma}[(\gamma+1)/\gamma]\sqrt{M/Re}\,Pr}{1 + 1.252\,\sqrt{\gamma}(\sqrt{M/Re})} \tag{8}$$

where Re^* and Pr^* are evaluated at a modified reference temperature found from Eq. (3)

$$T^* = \frac{T_c^* + 1.252\,\sqrt{\gamma}(M/\sqrt{Re})T_0}{1 + 1.252\,\sqrt{\gamma}(M/\sqrt{Re})} \tag{9}$$

T_0 is the free-stream temperature of the gas.

The following slip and intermediate heat-transfer relations for flow over cones, cylinders, and spheres have been formulated using the above procedure:

Cone

$$\frac{Nu}{\sqrt{Re^*}} = \frac{0.575\,(Pr^*)^{1/3} + 0.20\alpha\sqrt{\gamma}\sin\theta(M^{3/2}/\sqrt{Re})\,[(\gamma+1)/\gamma]\,Pr}{1 + 1.252\,\sqrt{\gamma}\,(M/Re)} \tag{10}$$

for $\theta > 10°$, where θ is the half angle of the cone.

Cylinder

$$\frac{Nu}{\sqrt{Re_2}} = \frac{0.48\,Pr_2^{0.3} + 0.064\,\alpha\,\sqrt{\gamma}(M^{3/2}/\sqrt{Re_2})\,[(\gamma+1)/\gamma]\,Pr}{1 + 1.252\,\sqrt{\gamma}\,(M/\sqrt{Re_2})} \tag{11}$$

Sphere

$$\frac{Nu}{\sqrt{Re_2}} = \frac{0.672\,M^{0.3} + 0.049\,\alpha\,\sqrt{\gamma}(M^{3/2}/\sqrt{Re_2})[(\gamma+1)/\gamma]Pr}{1 + 1.252\,\sqrt{\gamma}\,(M/\sqrt{Re_2})} \tag{12}$$

The subscript 2 in Eqs. (11) and (12) indicates that the gas properties are to be evaluated behind the normal shock. The relations for flat plates and cones yield local convection coefficients, whereas the relations for cylinders and spheres yield average values for the entire surface.

A study[7] of recent experimental data for spheres and cylinders indicates that the slip-continuum boundary is more accurately expressed by $M/\sqrt{Re} = 0.05$ compared to the value of $M/\sqrt{Re} = 0.01$ previously proposed by Tsien[2]. Eqs. (11) and (12) were developed using $M/\sqrt{Re} = 0.05$.

The parameter $Nu/\sqrt{Re}$ is shown in Fig. 1 for flow over transverse cylinders.

From Eq. (3), the temperature recovery factor in the slip and intermediate regimes is

$$r = \frac{r_c + 1.252\,\sqrt{\gamma}(M/\sqrt{Re})r_{fm}}{1 + 1.252\,\sqrt{\gamma}(M/\sqrt{Re})} \tag{13}$$

where r_c and r_{fm} are the continuum and free-molecule values, respectively, of the temperature recovery factor for a particular geometry. Oppenheim[3] has shown that the temperature recovery factor in free-molecule flow for $M > 3$ has a constant value of 1.17 for flat plates, cones, spheres, and transverse cylinders.

The variation of temperature recovery factor in the slip- and intermediate-flow regimes for cylinders and spheres is shown in Fig. 2.

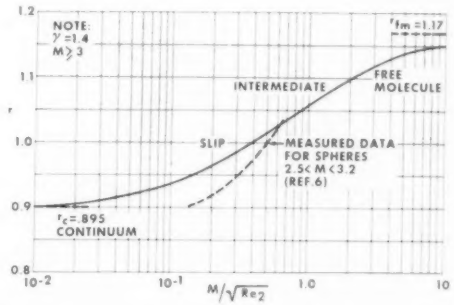

FIG. 2. Temperature recovery factors for transverse circular cylinders and spheres in slip and intermediate flows.

Boundary-Layer Interaction on a Yawed Infinite Wing in Hypersonic Flow

Robert J. Whalen
Principal Scientist, Flight Sciences Laboratory, Inc., Buffalo, N.Y.
July 3, 1959

UNDER the combined Howarth and Mangler transformation, the laminar boundary-layer equations on a yawed infinite wing, for $P_r = 1$, constant wall temperature, linear viscosity-temperature law, may be written

$$f''' + ff'' = \beta\{(f'^2 - 1) + \tan^2\Lambda(g^2 - 1) + \sec^2\Lambda[(T_w/T_0) - 1](g - 1)\} \tag{1}$$

$$g'' + fg' = 0 \tag{2}$$

for $M_\infty^2\cos^2\Lambda \gg 1$. Here,

$$f' = u/u_\delta, \quad g = v/v_\delta = \frac{H/H_\infty - H_w/H_\infty}{1 - H_w/H_\infty},$$

$\beta = (\gamma - 1)/\gamma$ ("strong" interaction), Λ = yaw angle. The boundary conditions for Eqs. (1) and (2) are taken as $f = f' = g = 0$ at $\eta = 0$, and $f' = g = 1$ as $\eta \to \infty$. Tabulated numerical

REFERENCES

[1] Martino, R. L., *Heat Transfer in Slip Flow*, Institute of Aerophysics, University of Toronto, UTIA Report 35, October, 1955.

[2] Tsien, H. S., *Superaerodynamics, Mechanics of Rarefied Gases*, Journal of the Aeronautical Sciences, Vol. 13, No. 12, pp. 653–664, December, 1946.

[3] Oppenheim, A. K., *Generalized Theory of Convective Heat Transfer in a Free Molecule Flow*, Journal of the Aeronautical Sciences, Vol. 20, No. 1, pp. 49–58, January, 1953.

[4] Rubesin, M., and Johnson, H. A., *A Critical Review of Skin-Friction and Heat Transfer Solutions of the Laminar Boundary Layer on a Flat Plate*, Trans. ASME, Vol. 71, pp. 383–388, 1949.

[5] Stalder, J., Goodwin, G., and Creager, M., *Heat Transfer to Bodies in a High-Speed Rarefied-Gas Stream*, NACA Report No. 1093, 1952.

[6] Drake, R. M., and Backer, G. H., *Heat Transfer from Spheres to a Rarefied Gas in Supersonic Flow*, Trans. ASME, Vol. 74, No. 7, pp. 1241–1249, October, 1952.

[7] Reeves, B. L., *Aerodynamic Heating in the Slip, Intermediate and Free Molecule Flow Regimes*, McDonnell Aircraft Corporation Research Department Report No. 6859, February, 1959.

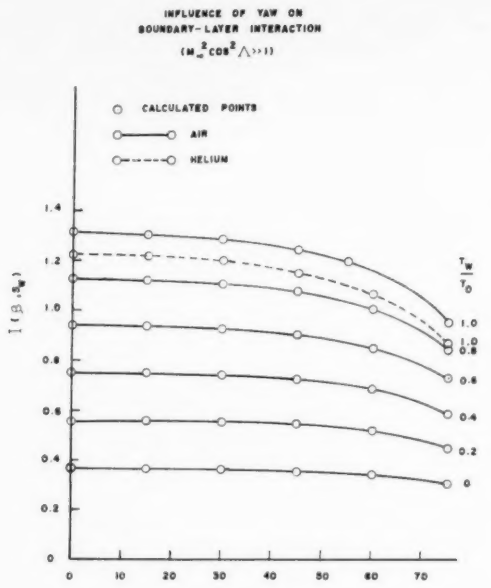

FIG. 1. Yaw angle $\sim \Lambda$.

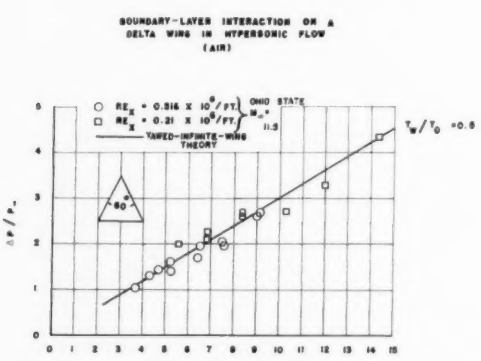

FIG. 2. Hypersonic interaction parameter $\sim \chi$.

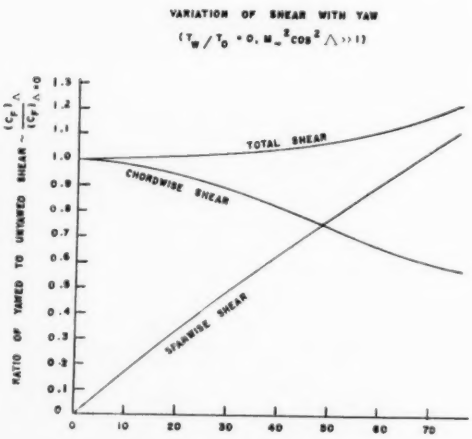
VARIATION OF SHEAR WITH YAW
(T_w / T_0 = 0, $M_\infty^2 \cos^2 \Lambda \gg 1$)
RATIO OF YAWED TO UNYAWED SHEAR $\sim \frac{(c_f)_\Lambda}{(c_f)_{\Lambda=0}}$
TOTAL SHEAR
CHORDWISE SHEAR
SPANWISE SHEAR

FIG. 5. Yaw angle $\sim \Lambda$.

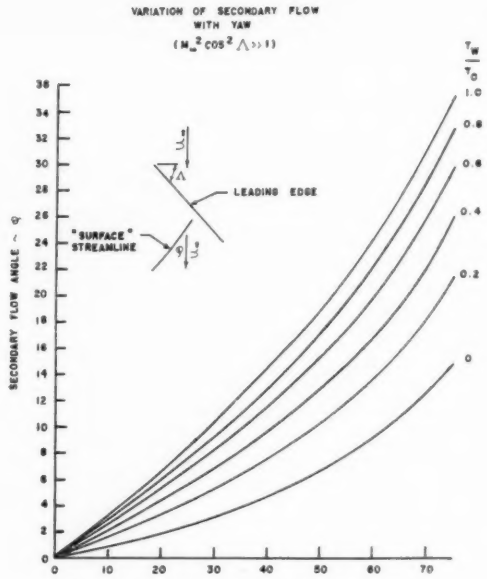

FIG. 3. Sweep angle $\sim \Lambda$.

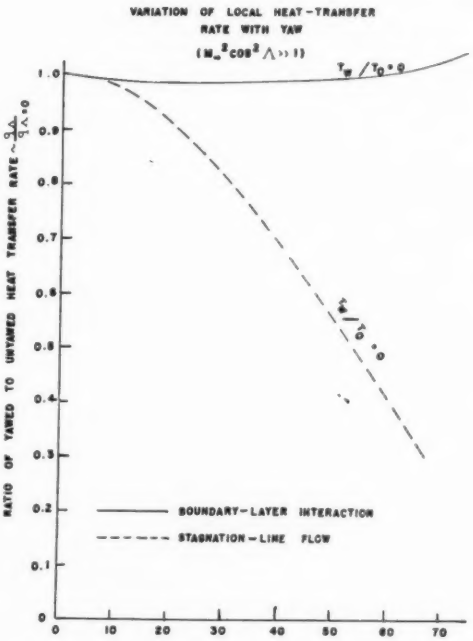
VARIATION OF LOCAL HEAT-TRANSFER
RATE WITH YAW
($M_\infty^2 \cos^2 \Lambda \gg 1$)
$T_w / T_0 = 0$
$T_w / T_0 = 0$
RATIO OF YAWED TO UNYAWED HEAT TRANSFER RATE $\sim \frac{q_\Lambda}{q_{\Lambda=0}}$
BOUNDARY-LAYER INTERACTION
STAGNATION-LINE FLOW

FIG. 4. Yaw angle $\sim \Lambda$.

solutions of Eqs. (1) and (2) for $\gamma = 7/5, 0 \leq T_w/T_0 \leq 1$ and for $\gamma = 5/3, T_w/T_0 = 1, 0° \leq \Lambda \leq 75°$, are presented in reference 1.

The ratio of the local pressure (p_Λ) to that at zero yaw ($p_{\Lambda=0}$) may be written

$$(\Delta p/p_\infty)_\Lambda/(\Delta p/p_\infty)_{\Lambda=0} = I(\beta, S_w)_\Lambda/I(\beta, S_w)_{\Lambda=0} \qquad (3)$$

where

$$I(\beta, S_w) = \int_0^\infty \{1 + [(T_w/T_0) - 1](1 - g) - f'^2 \cos^2 \Lambda - g^2 \sin^2 \Lambda\} d\eta$$

The relative small influence of yaw on $I(\beta, S_w)$ is presented in Fig. 1. Thus, for $\Lambda \leq 75°$, the pressure induced as a result of the interaction of the boundary layer with the external flow, is only slightly dependent on yaw. Experimental results for air in the Ohio State hypersonic tunnel are presented in Fig. 2. The tests were conducted at $M_\infty = 11.5$ for two Reynolds Number conditions corresponding to a $3.5 \leq \chi \leq 14.5$ range, (based on conditions in the free-stream direction). The favorable correlation of the data with the theoretical prediction, for a wall-to-stagnation temperature ratio of 0.5 (the approximate equilibrium temperature during the test), can be observed in Fig. 2.

The increase of boundary-layer secondary flow with yaw is illustrated in Fig. 3. Here, φ is defined as the angle between the velocity vector external to the boundary layer (which, according to the hypersonic small-disturbance assumption, is the direction of the free-stream velocity vector) and the streamline direction in the vicinity of the surface.

The variation of the local heat-transfer rate with yaw for conditions associated with re-entry vehicles, $T_w/T_0 \sim 0$, may be observed in Fig. 4. The variation for the range $0 \leq T_w/T_0 \leq 1$ may be obtained from the results of reference 1. By way of reference, the large decrease in local heat transfer, with yaw, in the neighborhood of the stagnation line is also presented.

The variation of the chord and spanwise shear with yaw is shown in Fig. 5. Again, the variation in the range $0 \leq T_w/T_0 \leq 1$ can be obtained from the results of reference 1. The relatively small influence of yaw on total skin friction is also indicated.

Reference

[1] Whalen, R. J., *Boundary Layer Interaction on a Yawed Infinite Wing in Hypersonic Flow*, Flight Sciences Laboratory Research Report No. 4, December, 1958.

A Simple Method for Determining Turbulent Skin Friction From Velocity Profiles

P. Bradshaw
Aerodynamics Division, National Physical Laboratory, Teddington, Middlesex, England
July 6, 1959

CLAUSER[1] has given a method of finding turbulent skin friction from velocity profiles, once the "inner law" is known. This method involves plotting the velocity profile on axes log $U_0 y/\nu$, u/U_0 and comparing it with plots of the inner law $u/u_\tau = f(u_\tau y/\nu)$ on the same axes for various values of $U_0/u_\tau \equiv \sqrt{2/c_f}$.

A simpler method is to choose *one* suitable reference point on the inner-law curve and to plot this on the axes y, u/U_0 (which are those on which a velocity profile is normally plotted) for different values of U_0/u_τ. The resulting single curve on the y, u/U_0 axes, which replaces Clauser's family of curves on the log $U_0 y/\nu$, u/U_0 axes, has a well-defined intersection with the velocity profile in the region of $u/U_0 = 0.6$ for the more usual values of U_0/u_τ. The value of u/U_0 at the intersection point can then be read off, and U_0/u_τ follows from this and the value of u/u_τ at the chosen reference point. With a little practice, only two or three points need be plotted to find the intersection.

For instance, let us take as the reference the point on the inner law $u/u_\tau = f(u_\tau y/\nu)$ where $u_\tau y/\nu = 100$. If we take $u/u_\tau =$ 16 at this point, which seems to be approximately the correct value for boundary layers with small pressure gradient, the coordinates of the points to be plotted on the y, u/U_0 axes are as shown in Table 1, where ν/U_0 is known from the velocity-traverse measurements.

TABLE 1

U_0/u_τ	16	20	25	30	35	General form
y	1600 $\times(\nu/U_0)$	2000 $\times(\nu/U_0)$	2500 $\times(\nu/U_0)$	3000 $\times(\nu/U_0)$	3500 $\times(\nu/U_0)$	$U_0/u_\tau(\nu/U_0)(u_\tau y/\nu)$ ref.
u/U_0	1.00	0.80	0.64	0.533	0.457	$(u/u_\tau)/(u_0/u_\tau)$ ref.
c_f	0.0078	0.0050	0.0032	0.0022	0.0016	...

Given the value of u/U_0 at the intersection point, the skin friction follows from

$$C_f = \tau_0/(1/2)\rho U_0^2 = 2(u_\tau/U_0)^2 = 2[(u/U_0)/(u/u_\tau) \text{ ref.}]^2 = 1/128(u/U_0)^2$$

with the present reference point.

This method avoids re-plotting the velocity profile on special axes. Like Clauser's method and the surface-tube method of Preston,[2] to both of which it is closely allied, it requires foreknowledge of the inner law for the flow in question, as it now appears that the inner law is not truly universal. The method should, however, prove useful for routine skin-friction determination where no instrument for direct measurement is available or where it is desired to re-analyze old data.

References

[1] Clauser, F. H., *Turbulent Boundary Layers in Adverse Pressure Gradients*, Journal of the Aeronautical Sciences, Vol. 21, p. 91, February, 1954.

[2] Preston, J. H., *The Determination of Turbulent Skin Friction by Means of Pilot Tubes*, J. RAeS., Vol. 58, p. 109, February, 1954.

Two-Dimensional Hypersonic Flow of an Ideal Gas With Infinite Electric Conductivity Past a Two-Dimensional Magnetic Dipole

Takeo Sakurai
Department of Aeronautical Engineering, Faculty of Engineering, Kyoto University, Kyoto, Japan
July 6, 1959

A FEW YEARS AGO, Burgers[1] investigated the flow of an ideal gas with electric conductivity past a magnetic dipole. He speculated that the magnetic field strength is so strong in the immediate neighborhood of the dipole that the flow may not penetrate into a certain region around the dipole, and that the gas flows around the region as if it passed around a rigid body. Recently, Tamada[5] investigated the steady two-dimensional flow of an incompressible fluid with infinite conductivity around a two-dimensional magnetic dipole and found that there exists in actuality the region as Burgers speculated. He discussed several other examples of the "frozen region" (as Tamada said) and, moreover, considered the effect of finite conductivity and viscosity on the "frozen region." In this paper we discuss the possibility of the "frozen region" in hypersonic flow. The problem seems to be interesting from the practical viewpoint because the "frozen region" may serve to protect the re-entering satellite from the high-temperature flow behind a strong shock wave.

Let us consider steady two-dimensional hypersonic flow of an ideal gas with infinite electric conductivity around a two-dimensional magnetic dipole, the axis of which is perpendicular to the direction of the uniform flow. The "frozen region" is assumed to occur in a circle with its center at the dipole. The outer flow is assumed to be the so-called "shock layer" behind a strong circular shock wave. The problem is whether the hydrodynamic pressure in the outer flow can be balanced by the hydrodynamic

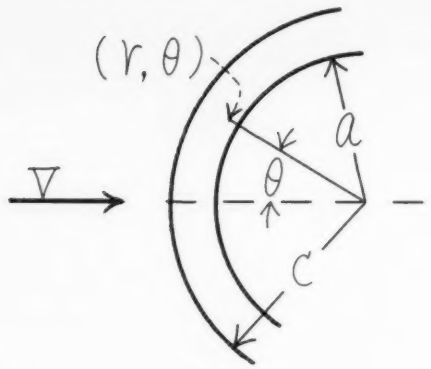

FIG. 1.

plus the magnetic pressure in the "frozen region." The analysis is performed in the neighborhood of the stagnation streamline by applying the Hida-Lighthill method[2, 3] to the outer flow and the usual theory of static magnetic field to the "frozen region."

(1) The Outer Flow

The shock wave is assumed to be a circle of radius C around the dipole with the center at the dipole. The shock conditions are as follows[3] (see Fig. 1):

$$\left.\begin{aligned} v_{r1} &= -V\cos\theta/K, \quad v_{\theta 1} = V\sin\theta, \quad K = \rho_1/\rho_0, \\ p_1 &= [1-(1/K)]\rho_0 V^2\cos^2\theta, \\ \omega_{z1} &= (K-1)^2 V\sin\theta/KC \end{aligned}\right\} \tag{1}$$

where the strong-shock approximation is used. As Hida and Lighthill considered, the shock wave is so strong near the stagnation streamline that compressibility may be neglected. Then the basic equations may be approximated as follows:[3]

$$\left.\begin{aligned} v_r &= -(\partial\psi/r\partial\theta), \quad v_\theta = \partial\psi/\partial r, \\ \omega_z &= (\partial^2\psi/\partial r^2) + (\partial\psi/r\partial r) + (\partial^2\psi/r^2\partial\theta^2) \end{aligned}\right\} \tag{2}$$

where the vorticity due to the entropy jump across the shock wave is considered. Taking into account the shock condition together with the fact that the vorticity is conserved along streamlines, we may obtain an initial-value problem for the Helmholz equation (details are omitted for brevity), the solution of which may be written in the form:

$$\left.\begin{aligned} \psi &= \Psi(r)\sin\theta, \\ \Psi(r) &= \alpha K_1\{[(K-1)/C]r\} + \beta I_1\{[(K-1)/C]r\}, \\ \alpha &= -(K-1)CV\{[(K+1)/K(K-1)]I_1(K-1) - [I_0(K-1)/K]\}, \\ \beta &= (K-1)CV\{[(K+1)/K(K-1)]K_1(K-1) + [K_0(K-1)/K]\} \end{aligned}\right\} \tag{3}$$

where K_1 and I_1 are the modified Bessel functions of the first order. The stream function ψ becomes zero at $r = a$ which is smaller than C. This circle $r = a$ is to be considered as the boundary of the "frozen region."

(2) The "Frozen Region"

The static magnetic field confined within the circle $r = a$ (a magnetic line), due to a magnetic dipole at the center with its axis perpendicular to the uniform flow, is easily obtained from the usual theory of static magnetic field. Thus, the strength of the magnetic field on the boundary is found to be

$$B^2 = 4B_0^2(1-\sin^2\theta) \tag{4}$$

(3) Matching of the Outer and the Inner Regions

The forces acting from each side of the boundary must balance. The force from the outer flow is the pure hydrodynamic pressure, while the force from the "frozen region" is the hydrodynamic plus the magnetic pressure. Bernoulli's equation holds for the stagnation streamline, so that the pressure of the outer flow is

TABLE 1

K	$(C-a)/a$	$K\{\Psi'(a)/V\}^2$
4	0.379	3.57
6	0.260	3.44
8	0.203	3.37
10	0.168	3.32
12	0.144	3.28
14	0.127	3.26

$$p = \rho_0 V^2[1-(1/2K) - K\{\Psi'(a)/V\}^2\sin^2(\theta/2)] \tag{5}$$

The strength of the magnetic field is given in Eq. (4), and the total pressure in the "frozen region" is, in MKS units

$$p_i + (B^2/2\mu_e) = p_i + (B_0^2/2\mu_e)\cdot(1-\sin^2\theta) \tag{6}$$

Equating Eqs. (5) and (6), we obtain the following equations:

$$\left.\begin{aligned} p_i &= \rho_0 V^2[1-(1/2K)] - (B_0^2/2\mu_e) \\ a^4 &= \kappa/\mu_e\rho_0 V^2 K\{\Psi'(a)/V\}^2, \quad \kappa = B_0 a^2 \end{aligned}\right\} \tag{7}$$

where κ is the strength of the magnetic dipole.

The above results show that the Burgers-Tamada "frozen region" can exist even in the hypersonic flow. It seems to be interesting from the practical viewpoint. If, in the future, we can have a sufficiently strong magnet on a satellite, we can protect the re-entering satellite body from the high-temperature flow behind the strong shock wave, using the so-called seeding technique[4] and producing the "frozen region" in front of the satellite.

In conclusion, the author wishes to express his cordial thanks to Professor Ko Tamada for his continual guidance and encouragement.

References

[1] Landshoff, R. K. M. (Ed.), *Magnetohydrodynamics*, Burgers, J., "Penetration of a Shock Wave Into a Magnetic Field," pp. 36–56, Stanford University Press, Stanford, Calif., 1957.

[2] Hida, K., *An Approximate Study on the Detached Shock Wave in Front of a Circular Cylinder and a Sphere*, J. Phys. Soc. Japan, Vol. 10, No. 1, pp. 79–81, January, 1955.

[3] Lighthill, M. J., *Dynamics of a Dissociating Gas, Part 1, Equilibrium Flow*, J. Fluid Mech., Vol. 2, Part 1, pp. 1–32, January, 1957.

[4] Resler, E. L., Jr., and Sears, W. R., *The Prospects for Magnetoaerodynamics*, Journal of the Aero/Space Sciences, Vol. 25, No. 4, pp. 235–246, April, 1958.

[5] Tamada, K., *The Flow of an Incompressible Fluid With Electric Conductivity Around a Magnetic Dipole* (to be published).

Reduction of Strain Rosettes in the Plastic Range

T. H. H. Pian
Associate Professor of Aeronautics and Astronautics, Massachusetts Institute of Technology, Cambridge, Mass.
July 6, 1959

IN A RECENT COMMUNICATION, Ades[1] presented an iteration procedure for evaluating principal stresses in the plastic range when the principal strains have been determined by strain-rosettes measurement. In this proposed method, the expression of the dilatation δ was assumed to be constant in the plastic range. This assumption should really be restricted only to perfectly plastic materials.

It appears to the writer that the change in dilatation for strain-hardening materials can be easily taken into account by the usual method of separation of elastic and plastic strains.[2] One can write the total strains as

$$\epsilon_{max} = (\epsilon_{max})_e + (\epsilon_{max})_p \tag{1}$$

$$\epsilon_{min} = (\epsilon_{min})_e + (\epsilon_{min})_p \tag{2}$$

where

$$(\epsilon_{max})_e = (1/E)(\sigma_{max} - \mu\sigma_{min}) \tag{3}$$

$$(\epsilon_{min})_e = (1/E)(\sigma_{min} - \mu\sigma_{max}) \quad (4)$$

$$(\epsilon_{max})_p = (1/E_p)[\sigma_{max} - (1/2)\sigma_{min}] \quad (5)$$

$$(\epsilon_{min})_p = (1/E_p)[\sigma_{min} - (1/2)\sigma_{max}] \quad (6)$$

E = Young's modulus

μ = Poisson's ratio in the elastic range

$E_p = \dfrac{\text{Effective Stress}}{\text{Effective Plastic Strain}} = \dfrac{\sigma_i}{(e_i)_p}$

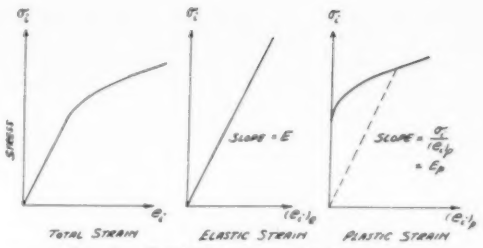

FIG. 1. Typical stress-strain diagrams.

and

$$(e_i)_p = \sqrt{(4/3)[(\epsilon_{max})_p^2 + (\epsilon_{max})_p(\epsilon_{min})_p + (\epsilon_{min})_p^2]} \quad (7)$$

The modulus E_p is obtained from the stress-strain diagram (Fig. 1). Based on the above relation, it can be shown that

$$(\epsilon_{max})_p + (\epsilon_{min})_p = [E/2(1-\mu)E_p + E](\epsilon_{max} + \epsilon_{min}) \quad (8)$$

$$(\epsilon_{max})_p - (\epsilon_{min})_p = [3E/2(1+\mu)E_p + 3E](\epsilon_{max} - \epsilon_{min}) \quad (9)$$

Thus,

$$(\epsilon_{max})_p = (1/2)\{[E/\{2(1-\mu)E_p + E\}](\epsilon_{max} + \epsilon_{min}) + [3E/\{2(1+\mu)E_p + 3E\}](\epsilon_{max} + \epsilon_{min})\} \quad (10)$$

$$(\epsilon_{min})_p = (1/2)\{[E/\{2(1-\mu)E_p + E\}](\epsilon_{max} + \epsilon_{min}) - [3E/\{2(1+\mu)E_p + 3E\}](\epsilon_{max} - \epsilon_{min})\} \quad (11)$$

With the separation of elastic and plastic strain components thus obtained, one can evaluate the principal stresses by solving either Eqs. (3) and (4) or Eqs. (5) and (6).

Substituting Eqs. (10) and (11) into Eq. (7), we obtain one expression of effective strain $(e_i)_p$ in terms of total principal strains

$$(e_i)_p = \sqrt{[E/\{2(1-\mu)E_p + E\}]^2(\epsilon_{max} + \epsilon_{min})^2 + 3[E/\{2(1+\mu)E_p + 3E\}]^2(\epsilon_{max} - \epsilon_{min})^2} \quad (12)$$

This solution, of course, is dependent on the value of the plastic modulus E_p. This quantity can be determined by an iteration process. A certain value of effective plastic strain $(e_i)_p$ is assumed first, and the corresponding value of E_p can be determined from the σ_i vs. $(e_i)_p$ diagram. Eq. (12) can then be used to obtain a more accurate value of $(e_i)_p$ and to establish the iteration procedure.

It should be remarked that the present procedure, as well as that given in reference 1, is based on the deformation theory of plasticity, hence, they are applicable only when the ratio of stresses remains constant while the applied combined stress is increasing gradually.

REFERENCES

[1] Ades, C. S., *Reduction of Strain Rosettes in the Plastic Range*, Journal of the Aero/Space Sciences, Vol. 26, No. 6, pp. 392–393, June, 1959.

[2] Nadai, A., *Theory of Flow and Fracture of Solids*, 2nd Ed., McGraw-Hill Book Co., Inc., New York, 1950.

On the Effect of a Narrow Band of Distributed Roughness Upon Boundary-Layer Transition

J. C. Gibbings
Department of Fluid Mechanics, University of Liverpool, England
July 6, 1959

SYMBOLS

k = height of roughness
$R_k = u_\infty k/\nu_\infty$
u_∞ = stream velocity
x_k = distance of mid-point of roughness band from plate leading edge
x_t = distance of transition from plate leading edge
ν_∞ = stream kinematic viscosity

IT HAS BEEN SHOWN[1] that existing experimental results for the effect of a single spanwise wire upon the position of transition on a flat plate in incompressible flow can be correlated using the two non-dimensional groups R_k and x_t/x_k; here, R_k is the Reynolds Number based upon the wire diameter and the free-stream velocity, while x_t and x_k are the distances from the plate leading edge of the transition and wire positions, respectively. In particular, for incompressible flow, it was found that $1/R_k$ varied linearly over most of the range of x_t/x_k, a linearity that was roughly repeated by the existing results for compressible flow.

R. A. Jones[2] has reported the results of experiments upon the effects of narrow bands of distributed roughness upon transition. These bands were fixed at various positions on a flat plate in a stream of Mach Number 3.05. For a band width, small compared with distance from the leading edge, one might expect the correlation of the results not to be dissimilar from that for the wire results. With this possibility in mind, some of R. A. Jones' results have been plotted as was done with the wire results. The result is shown in the accompanying Fig. 1. Only results for the lowest turbulence level have been used; and, of these, the results for transition close to the wire and close to the natural transition position have been excluded. The results are seen

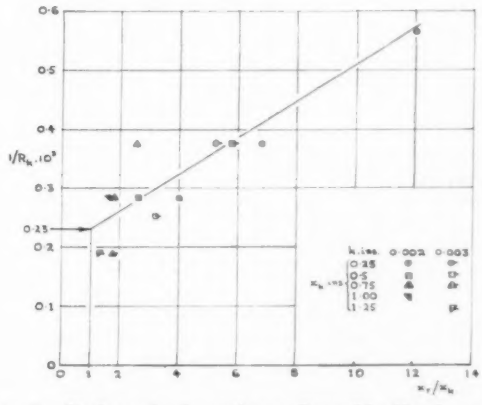

FIG. 1. Reciprocal of roughness Reynolds Number as a function of transition position. Plot of some of R. A. Jones' results (reference 2). $u'/U = 0.7$ per cent, $M = 3.05$. Here, $R_k = u_\infty k/\nu_\infty$.

to be rather scattered, but a mean straight line gives the value, when $x_t/x_k = 1.0$, of $1/R_k = 0.23.10^{-3}$ or $R_k = 4{,}400$.

If now this value is compared with the corresponding value for a transition wire at $M = 3.05$, as given in Fig. 10 of reference 1, it is seen that both are of the same order.

Further detailed experiment is required to confirm or deny this result and also to provide a detailed explanation; but, accepting the arguments of reference 1, it is not considered unreasonable that explanation might take the following lines.

Extending a blunt body rearward when it is immersed in a uniform stream does not greatly alter its separation drag, and so the resistance of a streamwise length of roughness might not be so different from that of a wire of the same height. Thus, the ΔR_θ added to the boundary layer by their presence might not be so different in the two cases; and, hence, if the disturbance to the boundary layer is satisfactorily indicated by ΔR_θ, the transition characteristics at subsonic speeds might be similar. Again, reasoning on similar lines, one might expect the wave drag of a roughness strip to be comparable to that of a wire, even though the irregular leading edge of the roughness band might prevent a single sharp shock forming. Thus, the effect of a narrow band of roughness upon transition close to it at supersonic speeds might be similar to that of a wire.

References

[1] Gibbings, J. C., *On Boundary Layer Transition Wires*, unpublished ARCR, December, 1958 (to be published as ARC CP).

[2] Jones, R. A., *An Experimental Study at a Mach Number of 3 of the Effect of Turbulence Level and Sandpaper Type Roughness on Transition on a Flat Plate*, NASA Memo 2-9-59L, March, 1959.

Some Remarks on the Controversy Regarding Boundary Layers in Shear Flow

Günther Jungclaus
Institute for Applied Mathematics and Mechanics, DVL, Freiburg in Breisgau, Germany

July 6, 1959

THE PROBLEM of boundary layers in shear flow has in the past few years been treated by Li[1, 2, 5] and by the author.[3] In all the mentioned papers, the assumption is made that the external flow is not influenced by the boundary layer, the condition at the outer edge of the boundary layer being $u \to u_0 + \omega_0 y$, with u_0, the velocity at the wall and ω_0, the constant vorticity of the inviscid flow. In contrast, Glauert[4] postulates that the shearing portion $\omega_0 y$ of the external flow is shifted through a distance equivalent to the displacement thickness of the boundary layer δ^*. His outer boundary condition therefore becomes $u \to u_0 + \omega_0(y - \delta^*)$.

Recently Stuart[6] has put forth an exact solution of the Navier-Stokes equations which lends support to Glauert's postulation. Almost at the same time using linearization of the Navier-Stokes equations by means of a development in terms of $\sqrt{\nu}$ for the external flow, and through the usual transformations for the boundary layer, Li has demonstrated in another paper[7] that the boundary layer exerts no influence on the external flow, at least with respect to the first-order terms in the case of flow over a flat plate. This result apparently controverts Glauert's postulation.

A careful study shows, however, that the results obtained by Stuart[6] and Li[7] need not be contradictory to each other. If the postulation by Glauert should be true, it would follow that the effect of an arbitrarily small viscosity is not confined to the vicinity of the wall but will substantially change the entire flow field, whenever ω_0 is sufficiently large. Consequently, the fundamental assumption of the boundary-layer theory would no longer be justified. In view of this, the separation of the flow field by Li[7] into regions of external flow and boundary layer as well as his expansion in $\sqrt{\nu}$ and the subsequent linearization for the external flow will probably not be allowable. His result will mark a step forward in the mathematical treatment of shear flow, granting that the boundary layer conditions are fulfilled, but as such it cannot serve as an argument against Glauert's postulation. On the other hand, the results derived by Glauert[4] with the assumption of the external flow in the form $u_\infty = u_0 + \omega_0(y - \delta^*)$ will also be incorrect, since the assumed external flow conditions are applied to the boundary-layer equations, the validity of which no longer exists.

In the opinion of the author, further investigations in the field of shear flow should be preceded by a clarification of the necessary conditions under which the solutions of the Navier-Stokes equations for shear flow possess the character of a boundary layer. A mere assumption of small viscosity is definitely not sufficient, as is shown by the example provided by Stuart.[6] On the other hand, the good agreement obtained by the author[3] between the boundary-layer theory and the experimental results for a flat plate in Couette flow tends to confirm that in this case the boundary-layer conditions are fulfilled.

References

[1] Li, T. Y., *Simple Shear Flow Past a Flat Plate in an Incompressible Fluid of Small Viscosity*, Readers' Forum, Journal of the Aeronautical Sciences, Vol. 22, No. 9, pp. 651–2, September, 1955.

[2] Li, T. Y., *Effects of Free-Stream Vorticity on the Behavior of a Viscous Boundary Layer*, Readers' Forum, Journal of the Aeronautical Sciences, Vol. 23, No. 12, pp. 1128–9, December, 1956.

[3] Jungclaus, G., *Grenzschichtuntersuchungen in rotierenden Kanälen und bei scherenden Strömungen*, Mitteilung aus dem Max-Planck-Institut für Strömungsforschung, Nr. 11, Göttingen, 1955.

[4] Glauert, M. B., *The Boundary Layer in Simple Shear Flow Past a Flat Plate*. Readers' Forum, Journal of the Aeronautical Sciences, Vol. 24, No. 11, pp. 848–9, November, 1957.

[5] Li, T. Y., *Author's Reply*, Readers' Forum, Journal of the Aeronautical Sciences, Vol. 24, No. 11, pp. 849–50, November, 1957.

[6] Stuart, J. T., *The Viscous Flow Near a Stagnation Point When the External Flow Has Uniform Vorticity*, Readers' Forum, Journal of the Aero/Space Sciences, Vol. 26, No. 2, pp. 124–5, February, 1959.

[7] Li, T. Y., *Simple Shear Flow Past a Flat Plate in an Incompressible Fluid of Small Viscosity*, Rensselaer Polytechnic Institute, Troy, N.Y., TR AE 5813, AFOSR TN-718, AD 162 253, July, 1958.

Spinning Ballistic Missiles

W. H. T. Loh
Chance Vought Aircraft, Dallas, Texas

July 9, 1959

Symbols

C_D	=	drag coefficient
C_N	=	normal-force coefficient
C_{Np}	=	Magnus-force coefficient
C_M	=	pitching-moment coefficient
C_{Mp}	=	magnus-moment coefficient
C_s	=	spin-deceleration coefficient
C_Y	=	yaw-damping coefficient
d	=	maximum body diameter
I_a	=	axial moment of inertia of missile
I_T	=	transverse moment of inertia of missile
m	=	mass of missile
t	=	time
v	=	velocity of the missile in the (x, y, z) coordinate system
V	=	velocity of the missile in the (X, Y, Z) coordinate system
ω	=	angular velocity of the missile
α	=	angle of attack or angle of yaw
P	=	any vector

Subscripts

x, y, z	=	components along the x, y, z axes, respectively, in the (x, y, z) coordinate system
X, Y, Z	=	components along the X, Y, Z axes, respectively in the (X, Y, Z) coordinate system

DYNAMICS of aircraft and missiles have been analyzed differently by aerodynamicists and ballisticians. Aerodynamicists deal with a configuration, essentially non-rolling, nonsymmetrical, and controlled by forces and moments generated

by control-surface deflections, while ballisticians deal with a configuration essentially axially symmetric, rapidly spinning, and controlled by the gyroscopic and Magnus effects. At small angles of yaw, linearized theories have been used by ballisticians. At large angles of yaw, considerable inaccuracy sometimes results from the use of linearized theory. When ballistic missiles are launched in a high wind or when they are launched from a flying platform such as an aircraft, the angle of yaw introduced either by high wind velocity or by aircraft velocity may be quite large. In such cases, nonlinear equations must be used. It is the purpose of this note to present such a set of equations. When aerodynamic coefficients at large angles of yaw are available, these equations may conveniently be solved on a digital computer.

The motion of the ballistic missile is usually analyzed as the combination of translation of the c.g. and rotation about the c.g. Two sets of coordinate systems are usually used. One set (X, Y, Z) is a right-hand coordinate system fixed to earth. Another set (x, y, z) is a right-hand coordinate system with origin on the missile c.g. and coincides with the principal axis of the missile and rotates with it. The missile's instantaneous attitude (θ, ψ, ϕ) is defined by the following three consecutive rotations from an attitude (x, y, z) originally parallel to the fixed inertia axis (X, Y, Z): (1) rotate an angle θ about the Z-axis, (2) rotate an angle ψ about the Y-axis at the end of step (1), (3) rotate an angle ϕ about the X-axis at the end of step (2). The equations of transformation from one set of coordinates to the other may best be expressed by the following matrices:

$$\begin{bmatrix} P_X \\ P_Y \\ P_Z \end{bmatrix} = \begin{bmatrix} \cos\theta & -\sin\theta & 0 \\ \sin\theta & \cos\theta & 0 \\ 0 & 0 & 1 \end{bmatrix} \begin{bmatrix} \cos\psi & 0 & \sin\psi \\ 0 & 1 & 0 \\ -\sin\psi & 0 & \cos\psi \end{bmatrix} \begin{bmatrix} 1 & 0 & 0 \\ 0 & \cos\phi & -\sin\phi \\ 0 & \sin\phi & \cos\phi \end{bmatrix} \begin{bmatrix} P_x \\ P_y \\ P_z \end{bmatrix} =$$

$$\begin{bmatrix} (\cos\theta\cos\psi) & (-\sin\theta\cos\phi + \cos\theta\sin\psi\sin\phi) & (\sin\theta\sin\phi + \cos\theta\sin\psi\cos\phi) \\ (\sin\theta\cos\psi) & (\cos\theta\cos\phi + \sin\theta\sin\psi\sin\phi) & (-\cos\theta\sin\phi + \sin\theta\sin\psi\cos\phi) \\ (-\sin\psi) & (\cos\psi\sin\phi) & (\cos\psi\cos\phi) \end{bmatrix} \begin{bmatrix} P_x \\ P_y \\ P_z \end{bmatrix}$$

By the method of inverting matrices, the following reverse transformation may be obtained:

$$\begin{bmatrix} P_x \\ P_y \\ P_z \end{bmatrix} = \begin{bmatrix} (\cos\theta\cos\psi) & (\sin\theta\cos\psi) & (-\sin\psi) \\ (\cos\theta\sin\psi\sin\phi - \sin\theta\cos\phi) & (\sin\theta\sin\psi\sin\phi + \cos\theta\cos\phi) & (\cos\psi\sin\phi) \\ (\cos\theta\sin\psi\cos\phi + \sin\theta\sin\phi) & (\sin\theta\sin\psi\cos\phi - \cos\theta\sin\phi) & (\cos\psi\cos\phi) \end{bmatrix} \begin{bmatrix} P_X \\ P_Y \\ P_Z \end{bmatrix}$$

Similarly, the following matrices may be written:

$$\begin{bmatrix} \omega_x \\ \omega_y \\ \omega_z \end{bmatrix} = \begin{bmatrix} -\sin\psi & 0 & 1 \\ \cos\psi\sin\phi & \cos\phi & 0 \\ \cos\psi\cos\phi & -\sin\phi & 0 \end{bmatrix} \begin{bmatrix} \dot{\theta} \\ \dot{\psi} \\ \dot{\phi} \end{bmatrix}$$

$$\begin{bmatrix} \omega_X \\ \omega_Y \\ \omega_Z \end{bmatrix} = \begin{bmatrix} 0 & -\sin\theta & \cos\theta\cos\psi \\ 0 & \cos\theta & \sin\theta\cos\psi \\ 1 & 0 & -\sin\psi \end{bmatrix} \begin{bmatrix} \dot{\theta} \\ \dot{\psi} \\ \dot{\phi} \end{bmatrix}$$

$$\begin{bmatrix} \dot{\theta} \\ \dot{\psi} \\ \dot{\phi} \end{bmatrix} = \begin{bmatrix} 0 & \sin\phi/\cos\psi & \cos\phi/\cos\psi \\ 0 & \cos\phi & -\sin\phi \\ 1 & \tan\psi\sin\phi & \tan\psi\cos\phi \end{bmatrix} \begin{bmatrix} \omega_x \\ \omega_y \\ \omega_z \end{bmatrix}$$

The aerodynamic forces and moments in the (x, y, z) coordinate system* may best be resolved into the following:

Axis	*Forces*	*Moments*
x	Drag Force $-C_D(1/2)\rho v^2[(\pi/4)d^2](v_x/v)$ Gravitational Force $-mg\sin\theta\cos\psi$	Spin-Deceleration Moment $-C_x(1/2)\rho v^2[(\pi/4)d^2]d(\omega_x d/2v)$
y	Drag Force $-C_D(1/2)\rho v^2[(\pi/4)d^2](v_y/v)$ Gravitational Force $-mg(\sin\theta\sin\psi\sin\phi + \cos\theta\cos\phi)$ Normal Force $-C_N(1/2)\rho v^2[(\pi/4)d^2](v_y/\sqrt{v_y^2 + v_z^2})$ Magnus Force $+C_{N_p}(1/2)\rho v^2[(\pi/4)d^2](\omega_x d/2v)(v_z/\sqrt{v_y^2 + v_z^2})$	Pitching Moment $+C_M(1/2)\rho v^2[(\pi/4)d^2]d(v_z/\sqrt{v_y^2 + v_z^2})$ Magnus Moment $+C_{M_p}(1/2)\rho v^2[(\pi/4)d^2]d(\omega_x d/2v)(v_y/\sqrt{v_y^2 + v_z^2})$ Yaw-Damping Moment $-C_Y(1/2)\rho v^2[(\pi/4)d^2]d(\sqrt{\omega_y^2 + \omega_z^2})(d/2v)(\omega_y/\sqrt{\omega_y^2 + \omega_z^2})$
z	Drag Force $-C_D(1/2)\rho v^2[(\pi/4)d^2](v_z/v)$ Gravitational Force $-mg(\sin\theta\sin\psi\cos\theta - \cos\theta\sin\phi)$ Normal Force $-C_N(1/2)\rho v^2[(\pi/4)d^2](v_z/\sqrt{v_y^2 + v_z^2})$ Magnus Force $-C_{N_p}(1/2)\rho v^2[(\pi/4)d^2](\omega_x d/2v)(v_y/\sqrt{v_y^2 + v_z^2})$	Pitching Moment $-C_M(1/2)\rho v^2[(\pi/4)d^2]d(v_y/\sqrt{v_y^2 + v_z^2})$ Magnus Moment $+C_{M_p}(1/2)\rho v^2[(\pi/4)d^2]d(\omega_x d/2v)(v_z/\sqrt{v_y^2 + v_z^2})$ Yaw-Damping Moment $-C_Y(1/2)\rho v^2[(\pi/4)d^2]d(\sqrt{\omega_y^2 + \omega_z^2})(d/2v)(\omega_z/\sqrt{\omega_y^2 + \omega_z^2})$

* From proper application of equations of transformation from (X, Y, Z) system to (x, y, z) system.

The motion of the axially symmetrical missile after cessation of thrust, in terms of the (x, y, z) coordinate system, may now be written as:

$$(dv_x/dt) + \omega_y v_z - \omega_z v_y = -C_D(1/2)\rho v^2[(\pi/4)d^2](v_x/v)(1/m) - g\sin\theta\cos\psi \quad (1)$$

$$(dv_y/dt) + \omega_z v_x - \omega_x v_y = -C_D(1/2)\rho v^2[(\pi/4)d^2](v_y/v)(1/m) - g(\sin\theta\sin\psi\sin\phi + \cos\theta\cos\phi) - C_N(1/2)\rho v^2[(\pi/4)d^2](v_y/\sqrt{v_y^2+v_z^2})(1/m) + C_{N_p}(1/2)\rho v^2[(\pi/4)d^2](\omega_x d/2v)(v_z/\sqrt{v_y^2+v_z^2})(1/m) \quad (2)$$

$$(dv_z/dt) + \omega_x v_y - \omega_y v_x = -C_D(1/2)\rho v^2[(\pi/4)d^2](v_z/v)(1/m) - g(\sin\theta\sin\psi\cos\phi - \cos\theta\sin\phi) - C_N(1/2)\rho v^2[(\pi/4)d^2](v_z/\sqrt{v_y^2+v_z^2})(1/m) - C_{N_p}(1/2)\rho v^2[(\pi/4)d^2](\omega_x d/2v)(v_y/\sqrt{v_y^2+v_z^2})(1/m) \quad (3)$$

$$I_a(d\omega_x/dt) = -C_s(1/2)\rho v^2[(\pi/4)d^2]d(\omega_x d/2v) \quad (4)$$

$$I_T(d\omega_y/dt) - (I_T - I_a)\omega_z\omega_x = C_M(1/2)\rho v^2[(\pi/4)d^2]d(v_z/\sqrt{v_y^2+v_z^2}) + C_{M_p}(1/2)\rho v^2[(\pi/4)d^2]d(\omega_x d/2v)(v_y/\sqrt{v_y^2+v_z^2}) - C_Y(1/2)\rho v^2[(\pi/4)d^2]d(\sqrt{\omega_y^2+\omega_z^2})(d/2v)(\omega_y/\sqrt{\omega_y^2+\omega_z^2}) \quad (5)$$

$$I_T(d\omega_z/dt) + (I_T - I_a)\omega_x\omega_y = -C_M(1/2)\rho v^2[(\pi/4)d^2]d(v_y/\sqrt{v_y^2+v_z^2}) + C_{M_p}(1/2)\rho v^2[(\pi/4)d^2]d(\omega_x d/2v)(v_z/\sqrt{v_y^2+v_z^2}) - C_Y(1/2)\rho v^2[(\pi/4)d^2]d(\sqrt{\omega_y^2+\omega_z^2})(d/2v)(\omega_z/\sqrt{\omega_y^2+\omega_z^2}) \quad (6)$$

$$d\theta/dt = (\sin\phi/\cos\psi)\omega_y + (\cos\phi/\cos\psi)\omega_z \quad (7)$$

$$d\psi/dt = (\cos\phi)\omega_y - (\sin\phi)\omega_z \quad (8)$$

$$d\phi/dt = w_x + (\tan\psi\sin\phi)w_y + (\tan\psi\cos\phi)\omega_z \quad (9)$$

$$V_X = (\cos\theta\cos\psi)v_x + (\cos\theta\sin\psi\sin\phi - \sin\theta\cos\phi)v_y + (\cos\theta\sin\psi\cos\phi + \sin\theta\sin\phi)v_z \quad (10)$$

$$V_Y = (\sin\theta\cos\psi)v_x + (\sin\theta\sin\psi\sin\phi + \cos\theta\cos\phi)v_y + (\sin\theta\sin\psi\cos\phi - \cos\theta\sin\phi)v_z \quad (11)$$

$$V_Z = (-\sin\psi)v_x + (\cos\psi\sin\phi)v_y + (\cos\psi\cos\phi)v_z \quad (12)$$

$$\alpha = \sin^{-1}\{\sqrt{v_z^2+v_z^2}/v\} \quad (13)$$

$$X = X_0 + \int_0^t V_X dt \quad (14)$$

$$Y = Y_0 + \int_0^t V_Y dt \quad (15)$$

$$Z = Z_0 + \int_0^t V_Z dt \quad (16)$$

$$V^2 = V_X^2 + V_Y^2 + V_Z^2 \quad (17)$$

$$v^2 = v_x^2 + v_y^2 + v_z^2 \quad (18)$$

$$\theta = \theta_0 + \int_0^t \dot{\theta} dt \quad (19)$$

$$\psi = \psi_0 + \int_0^t \dot{\psi} dt \quad (20)$$

$$\phi = \phi_0 + \int_0^t \dot{\phi} dt \quad (21)$$

When the Y axis is taken as the altitude axis, density variation becomes approximately

$$\rho = C_1 e^{c_2 Y} \quad (22)$$

Eqs. (1)-(22) are independent equations and contain twenty-two unknowns: v_x, v_y, v_z, ω_x, ω_y, ω_z, θ, ψ, ϕ, $\dot{\theta}$, $\dot{\psi}$, $\dot{\phi}$, V_X, V_Y, V_Z, X, Y, Z, v, V, α, and ρ. Consequently, they may be solved.

References

[1] McShane, E. J., Kelley, J. L., and Reno, F., *Exterior Ballistics*, University of Denver Press, 1953.

A Closed-Form Solution for Laminar Free Convection on a Vertical Plate With Prescribed, Nonuniform, Wall Heat Flux

Richard P. Bobco
Senior Engineer, Nortronics Division, Northrop Corporation, Hawthorne, Calif.
July 9, 1959

Using the integral technique formalized by Tribus,[1] it is possible to obtain an approximate closed-form solution to the problem of laminar free convection on a vertical plate with the nonuniform wall heat flux prescribed by Sparrow.[2] The approximate solution given here is found to be in good agreement with the series solution described in reference 2. Although this brief note considers only one type of nonuniform wall heat flux, the method may be used for many other types of heat flux without any great loss in accuracy.

In reference 1, an integral method is used to derive expressions for Nusselt modulus, nonuniform wall temperature, etc., for an arbitrary prescribed wall heat flux $q/q_0 = f(x)$. The numerical constants in Tribus' solution depend on the usual assumed boundary-layer velocity and temperature distributions, $u/u_1 = (y/\delta)[1 - (y/\delta)]^2$ and $(T - T_\infty) = (T_w - T_\infty)[1 - (y/\delta)]^2$. The following expressions can be developed for the boundary-layer parameters, wall temperature, and Nusselt modulus:

$$u_1\left(\frac{g\beta q_0\nu}{k}\right)^{-(1/4)} \equiv \Omega = \frac{60A^{3/5}q^{1/3}}{Pr^{1/5}}\left[\frac{7I_1(x)}{864q_0Q^{c-(1/2)}}\right]^{2/5} \quad (1)$$

$$\left(\frac{g\beta q_0}{k\nu^2}\right)^{1/4}\delta \equiv \Delta = \frac{1}{q^{2/3}Pr^{2/5}}\left[\frac{864q_0AQ^{c+2}}{7I_1(x)}\right]^{1/5} \quad (2)$$

$$T_w - T_\infty = \frac{q^{1/3}}{kPr^{2/5}}\left[\frac{27}{7}\frac{q_0Q^{c+2}}{A^4I_1(x)}\right]^{1/5} \quad (3)$$

$$\frac{Nu}{(Gr)^{1/4}} = \sqrt{2}\,Pr^{1/2}\left[\frac{28}{27}\frac{q^{7/3}}{Q^{c+2}}\frac{x\ I_1(x)}{}\right]^{1/4} \quad (4)$$

where

$$Q = \int_0^x q\,dx$$

$I_1(x) = \int Q^c q^{-(1/3)}\,dx$, an indefinite integral

$c = (35/12)Pr + (4/3)$

$A = (g\beta q_0/k\nu^2)^{1/4}$

In principle, the problem is completely solved with the presentation of Eqs. (1)-(4). Unfortunately, the integral, $I_1(x)$ cannot readily be evaluated except for the simple wall heat flux $q = q_0x^n$, for which a similarity solution also exists.[3] For more complex heat-flux relationships, an approximate integration of $I_1(x)$ may be carried out with accuracies suitable for many engineering applications.

A technique commonly used to evaluate difficult integrals arising in forced-convection problems was utilized here. The integral $I_1(x)$ was evaluated by integrating by parts once, and the residual integral was neglected. The magnitude of the re-

sulting error was estimated algebraically. For other cases, the error can be estimated by numerical and/or graphical techniques.

The heat flux considered in reference 2 is

$$q = q_0[1 + \epsilon(x/L)^r] \tag{5}$$

where q_0 and L are reference values of heat flux and wall height, respectively, and ϵ is the per cent deviation of q/q_0 at $x = L$. Then

$$Q = q_0 x[1 + \lambda(x/L)^r] \tag{6}$$

where $\lambda = \epsilon/(r + 1)$

For simplicity, let $\eta = x/L$, then the integral $I_1(x)$ may be written as

$$I_1(x) = L \int \frac{Q^c}{q^{1/3}} d\eta = L^{c+1}\, q_0{}^{c-(1/3)} \int \frac{\eta^c(1 + \lambda\eta^r)^c}{(1 + \epsilon\eta^r)^{1/3}} d\eta \tag{7}$$

Eq. (7) was evaluated for two cases: (1) $Pr = 0.915$ for which $c = 4$, and (2) arbitrary Pr. In the first instance, it was possible to expand the numerator of the integrand in Eq. (7) and integrate each term by parts. Then, to a close approximation, it is found that

$$I_1(x) = \frac{L^{c+1}\, q_0{}^{c-(1/3)}\, \eta^5}{(1 + \epsilon\eta^r)^{1/3}} \times \left[\frac{1}{5} + \frac{4\lambda}{r + 5}\eta^r + \frac{6\lambda^2}{2r + 5}\eta^{2r} + \frac{4\lambda^3}{3r + 5}\eta^{3r} + \frac{\lambda^4}{4r + 5}\eta^{4r}\right] \tag{8}$$

$(T_w - T_\infty)$ and N_u may be found from Eqs. (3) and (4), but it is of greater interest to present a solution which may be compared to the results of reference 2. Sparrow presents his solution in graphical form by plotting $(T_w - T_\infty)/(T_w - T_\infty)_{q_0}$ versus q/q_0 using the Prandtl Number as the parameter. The wall temperature distribution for a wall with a uniform heat flux can be found from reference 2 or Eq. (3) to be

$$(T_w - T_\infty)_{q_0} = 1.622(q_0 x/k)[(0.8 + Pr)/Pr^2 Gr_x{}^*]^{1/5} \tag{9}$$

where $Gr_x{}^* = g\beta q_0 x^4/k\nu^2$. Using Eq. (9) to normalize the wall temperature resulting from the heat flux of Eq. (12) leads to the expression

$$\frac{T_w - T_\infty}{(T_w - T_\infty)_{q_0}} = \frac{0.725\left[1 + \epsilon\left(\frac{x}{L}\right)^r\right]^{0.4}\left[1 + \lambda\left(\frac{x}{L}\right)^r\right]^{1.2}}{\left[\frac{1}{5} + \frac{4\lambda}{r + 5}\left(\frac{x}{L}\right)^r + \frac{6\lambda^2}{2r + 5}\left(\frac{x}{L}\right)^{2r} + \frac{4\lambda^3}{3r + 5}\left(\frac{x}{L}\right)^{3r} + \frac{\lambda^4}{4r + 5}\left(\frac{x}{L}\right)^{4r}\right]^{0.2}} \tag{10}$$

Eq. (10) and the results of reference 2 for the case $Pr = 1.0$ are compared in Table 1 for several different values of r and q/q_0. The largest deviation between the two results is less than 1.5 per cent. The solution given by Eq. (10) can be found for other values of r, subject to the restriction $r > -1.0$.

A less accurate, though more general, solution to Eq. (7) can also be found. This solution also depends on integrating by parts, then neglecting the residual integral. The result is

$$I_1(x) = \frac{L^{c+1}\, q_0{}^{c-(1/3)}\, \eta^{c+1}(1 + \lambda\eta^r)^c}{(c + 1)(1 + \epsilon\eta^r)^{1/3}} \tag{11}$$

The normalized wall temperature can then be written as

$$(T_w - T_\infty)/(T_w - T_\infty)_{q_0} = \{[1 + \epsilon(x/L)^r] \times [1 + \lambda(x/L)^r]\}^{0.4} = \{q/q_0[1 + \lambda(x/L)^r]\}^{0.4} \tag{12}$$

The loss in accuracy is apparent inasmuch as the dimensionless temperature of Eq. (12) is independent of the Prandtl modulus.* Although this expression compares favorably with the results of Eq. (10) and reference 2 for the case $Pr = 1$ (the deviation is less than 4 per cent), the error for Pr different from unity could exceed 9 per cent for certain combinations of Pr, q/q_0, and r considered in reference 2.

Some insight into the magnitude of the error in $I_1(x)$, and the subsequent errors in Δ, $(T_w - T_\infty)$, etc., may be gained by considering some integral $[i] = \int udv = uv - \int vdu$. If it is assumed that $[i] = uv$, the per cent error introduced by this assumption may be expressed as

$$\%E_i = 100/[1 - (uv/\int vdu)] \tag{13}$$

* The Pr dependence in Eq. 10 is submerged in the numerical constants $1/5$, $1/(r + 5)$, etc., appearing in the denominator.

TABLE 1

r	q/q_0	$(T_w - T\infty)/(T_w - T\infty)_{q_0}$ Reference 2, $Pr = 1$	Eq. 10	Eq. 12
0	1.50	1.383	1.386	1.383
1/2	1.50	1.345	1.350	1.330
1.0	1.50	1.321	1.321	1.287
1.0	1.00	1.000	1.000	1.000
1.0	0.50	0.645	0.645	0.675
2.0	1.50	1.295	1.296	1.252
3.0	1.50	1.278	1.285	1.233

For the first case considered above it can be shown that for $0 \leq \eta \leq 1$, the maximum per cent error can be expressed as

$$\%E_{I_1} \leq 100r/[(r + 3) + (3/\epsilon\eta^{r+1})] \tag{14}$$

As an example, for $\eta = 1.0$, $\epsilon = 0.5$, $r = 1$, $\%E_{I_1} \leq 10\%$. Then, if $I_1(x)$ is too small by 10 per cent, from Eq. (1)–(4) it can be found that Δ and $T_w - T_\infty$ will be too large by 2 per cent, Ω too small by 4 per cent, etc.

A comparable expression for the maximum expected error cannot be given at this time for the less accurate integration of Eq. (11). The general expression has a strong dependence on Prandtl modulus as well as the parameters, ϵ and r, and the dimensionless height, η. However, if Pr, ϵ, r, and η are specified, the per cent error can be determined by numerical techniques.

The author happily acknowledges the encouragement and guidance of Professor D. Harmon of U.C.L.A. in preparing this note.

REFERENCES

[1] Tribus, M., *Comments on the Paper "Similar Solutions for Free Convection From a Nonisothermal Vertical Plate"* by Sparrow and Gregg, ASME Transactions, Vol. 80, pp. 1180–1, July, 1958.

[2] Sparrow, E. M., *Laminar Free Convection on a Vertical Plate With Prescribed Nonuniform Wall Heat Flux or Prescribed Nonuniform Wall Temperature*, NACA TN 3508, July, 1955.

[3] Sparrow, E. M., and Gregg, J. L., *Similar Solutions for Free Convection from a Nonisothermal Vertical Plate*, ASME Transactions, Vol. 80, pp. 379–86, February, 1958.

Behavior of Liquids in Free Fall*

William C. Reynolds
Assistant Professor of Mechanical Engineering, Stanford University, Stanford, Calif.
July 10, 1959

RECENT rocket and satellite activities have brought into focus a number of important problems involving the behavior of

* In the preparation of this note, the assistance of Stanford students, G. A. McKinzie, J. Gerstley, H. Munson, A. Lindsay, N. Wooldridge, O. Kyte, and A. Hill is gratefully acknowledged.

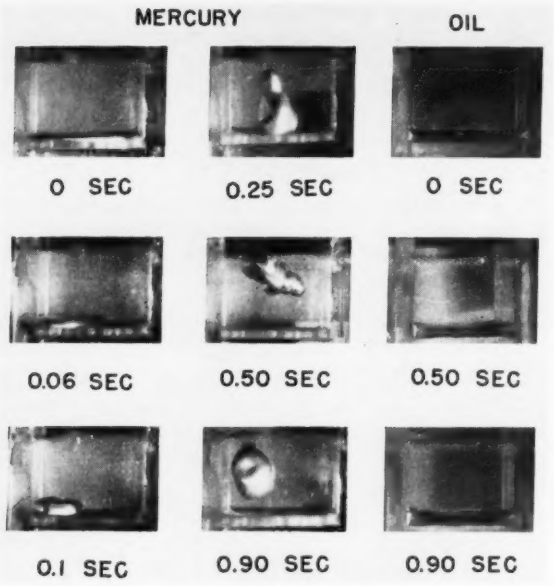

FIG. 1. Liquids in free fall.

liquids under weightless conditions. If a suitable criteria for weightlessness is the absence of any hydrostic pressures, then a liquid in a freely falling container may be considered weightless. Study of the behavior of liquids in free fall, therefore, can give considerable insight into the behavior of liquids in space. A photographic study of boiling during 8 ft. of free fall[1] clearly demonstrated the existence of differences between earthbound and weightless fluid behavior. An analysis of the relative orders of magnitudes of surface tensile, viscous, and inertia forces acting on weightless liquid[2] allows estimation of the approximate time required for deformation due to surface tension after removal of gravity forces. In the present note, some photographs of fluids in free fall are included. It should be noted that this study was entirely qualitative and of a very preliminary nature. For these experiments, a free-fall vehicle consisting of a 2-in. square lucite box and a heavy steel weight was constructed. The vehicle was dropped from heights up to 16 ft. and caught by an arresting system. Liquids placed in the lucite box were photographed at the bottom of their fall by a 3-microsecond exposure flash camera. While the container was dropped from successively greater heights, a series of photographs was taken which show the progress of the fluid in free fall. It is important to remember that the photographs were taken during different drops and, therefore, are not quite what would appear in a series of motion-picture frames. The deceleration due to wind resistance was estimated at a maximum of $0.01g$, and, therefore, the fluids were almost exactly weightless.

In the first series of drops, the floor of the lucite box was lined with paraffin, and a small amount of mercury placed on the paraffin. The box and the mercury, before the drop, can be seen in the upper left corner of Fig. 1. Note that the mercury is off to the left side of the box. Photographs taken after increased durations of free fall are shown. Note that the surface forces act very quickly to pull the mercury together, once the gravity forces are removed. In fact, the surface energy is sufficient to lift the mercury glob completely off the surface, where it hangs in space, as shown. For a short time the glob retains an irregular shape, but before long the surface forces start to reshape the glob into a sphere. The time estimates for deformation are consistent with those predicted by Benedikt.[2] A similar series of tests with mercury on the lucite floor yielded essentially the same results.

Photographs taken during a series of drops with oil on the lucite floor are shown in Fig. 1. Because of the relatively low surface tension for the oil, the time required for motion is somewhat longer than for the mercury; but even in the short time available, some motion occurs. Note that the oil does not tend to globulate, but instead starts immediately to climb up the wall.

The difference between the behavior of mercury and oil can be attributed to the type of wetting. Mercury does not wet the floor, and therefore surface forces tend to pull it together. Oil does wet the wall, and the surface forces tend to pull it up the wall.

On the basis of these experiments, it is concluded that fluids which wet their container will crawl around the wall, leaving the gas pocket in the center. Fluids which do not wet will kick themselves off the wall, leaving the gas in contact with the wall. However, from energy considerations, it is evident that the wetting fluids cannot crawl forever; the surface area is limited by the energy available for stretching it, and therefore a wetting fluid may not completely cover its container. Similarly, a nonwetting fluid may tend to form more than one glob; the energy available for moving the mass off the floor may not raise the centroid enough to allow a sphere to form, in which case the ultimate shape would probably be two or more spheres.

REFERENCES

[1] Siegel, R., and Usiskin, C., *A Photographic Study of Boiling in the Absence of Gravity*, J. Heat Transfer, Vol. 81, Series C, No. 3, p. 230, August, 1959.

[2] Benedikt, E. T., *Scale of Separation Phenomena in Liquids Under Conditions of Nearly Free Fall*, J. ARS, February, 1959.

On the Use of a Spark-Driven Shock Tube to Prepare Nonequilibrium Gas Samples†

Myron S. Wecker*
Cornell University, Ithaca, New York
July 13, 1959

CERTAIN chemical species of interest in gas reactions only occur at extremely high temperatures. If, however, a sample of gas is heated to extremely high temperatures, and then very rapidly cooled, it is possible to "freeze" into the gas the constituents which would not ordinarily exist at lower temperatures. Thus, the gas will persist in a nonequilibrium state. The purpose of the present note is to bring to the readers' attention a mechanism with which to "freeze" nonequilibrium conditions into a sample of gas. The basic requirements of the mechanism are: (1) production of a high temperature in a sample of gas, and (2) rapid cooling of the sample once the desired high temperature is attained. Such a mechanism can be achieved by utilizing nonsteady waves moving through the gas, since a shock wave increases the temperature of the medium through which it moves, and an expansion, or rarefaction wave decreases the temperature of the medium. A spark-driven shock tube[1, 2] is ideally suited for the production of the required wave patterns. In a spark-driven shock tube, both the driver and driven gases are initially at the same pressure (no diaphragm separating the two sections of the tube). The pressure ratio, necessary for initiating the shock, is obtained by heating the driver gas, essentially at constant volume, through the mechanism of an electrical discharge. After the driver gas temperature, and thus the pressure, has been increased by means of the spark, the usual shock tube relations can be applied to the flow.[3] Thus, the pressure ratio after the discharge is determined by

† This research was partially supported by the Mechanics Branch of the Office of Naval Research under contract Nonr 401(25). Reproduction in whole or in part is permitted for any purpose of the United States Government. The author is indebted to Professor E. L. Resler, Jr., for advice concerning this research.

* Douglas Aircraft Corporation Fellow.

$$\frac{p_4}{p_1} = \left[\frac{2\gamma_1 M_1^2 - (\gamma_1 - 1)}{\gamma_1 + 1}\right] \times \left\{\frac{1}{1 - [(\gamma_4 - 1)/(\gamma_1 + 1)]\,(a_1/a_4)\,[M_1 - (1/M_1)]}\right\}^{2\gamma_4/(\gamma_4 - 1)}$$

where the subscripts (1) and (4) refer to driven and driver sections, respectively. If we assume strong shocks ($M_1 \gg 1$) as well as perfect gases and constant volume heating, we find

$$m_4/m_1 = [2\gamma_4/(\gamma_1 + 1)]\,[(a_1/a_4)M_1]^2 \times \left[\frac{1}{1 - [(\gamma_4 - 1)/(\gamma_1 + 1)]\,[(a_1/a_4)M_1]}\right]^{2\gamma_4/(\gamma_4 - 1)}$$

Thus

$$(a_1/a_4)M_1 = K(\gamma_1, \gamma_4, m_4/m_1)$$

In Fig. (1), K is plotted vs. m_4/m_1 with γ_1 and γ_4 as parameters. Now

$$(a_1/a_4)M_1 = (a_{4i}/a_4)M_1 \sqrt{(\gamma_1/\gamma_4)(m_4/m_1)}$$

where subscript (i) denotes conditions before discharge. In Fig. 1, $(a_{4i}/a_4)M_1$ is plotted vs. m_4/m_1, with γ_1 and γ_4 as parameters. From this figure it can be seen, as is usually the case, that the strongest shocks would be produced by a light driver gas and a heavy driven gas.

If we consider the energy transfer from the condenser to the driver gas, we find

$$M_1 = (\gamma_1 + 1)/(\gamma_4 - 1) \sqrt{(k/2C_V)(\eta/S)(\gamma_4/\gamma_1)(VC)(m_1/m_4)}$$

where η is discharge efficiency, S is tube cross-sectional area, V is discharge potential, and C is capacitance. It is known (see, for example, reference 4) that $V/p_{4i}l_4$ is approximately constant for different values of the variables. Thus, we see the Mach Number varies with $\sqrt{VC}$ and, as previously determined, with $\sqrt{m_1/m_4}$. Strong shock waves, and thus high temperatures, are produced using the spark-driven shock tube. By reflecting the initial shock wave off the end of the tube, a reflected shock wave is generated which further increases the temperature of the gas.

Contact-Surface Reflected Expansion

One of the most significant differences between the pressurized driver shock tube and the spark-driven shock tube is that, in the former, the hottest gas is in region (5), and $T_2 > T_3$, while in the latter the hottest gas is in region (4), the driver, due to the presence of the electrical discharge, and $T_2 < T_3$.

In the head-on collision of the shock wave and the contact surface, the transmitted wave is a shock, and the reflected wave may be either a compression or an expansion, depending on the acoustic impedance, ρa, on either side of the contact surface. In the spark-driven shock tube, due to the high temperature in

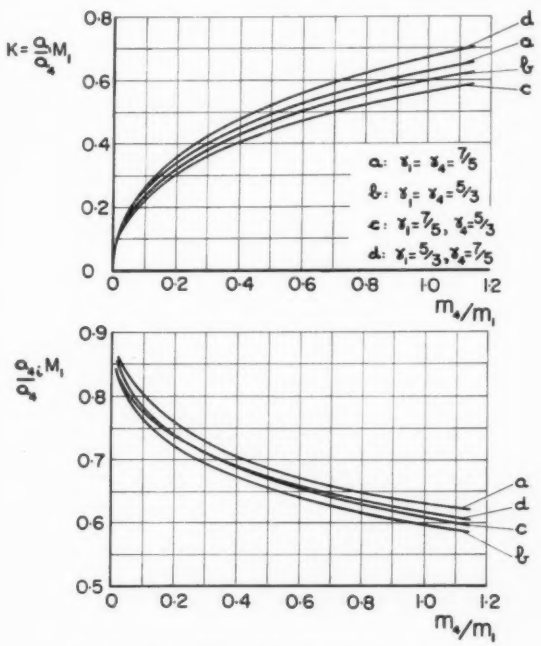

FIG. 1. $(a_1/a_4)M_1$ and $(a_{4_i}/a_4)M_1$ vs. m_4/m_1.

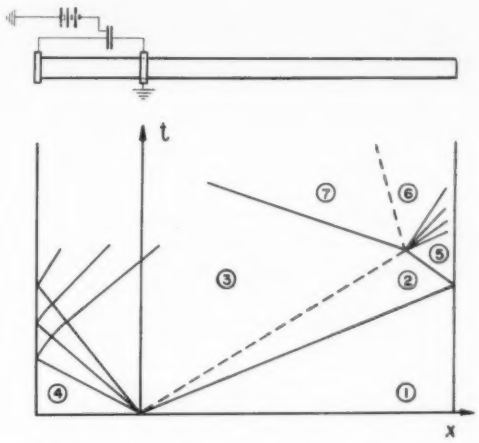

FIG. 2. Shock tube schema and wave diagram.

FIG. 3. Drum-camera photograph of the wave pattern in a spark-driven shock tube.

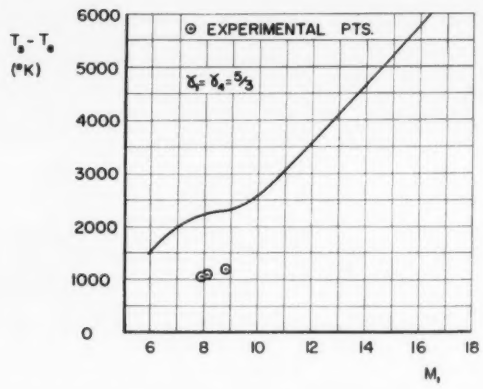

FIG. 4. Temperature drop across reflected expansion.

region (3), the acoustic impedance is such that the reflected wave is an expansion. Thus, the reflected expansion will propagate into region (5), cooling the hot gas there. A typical diagram for this type of flow is shown in Fig. 2.

APPARATUS

A schema of the shock tube constructed for and used in this research is shown in Fig. 2. The tube was constructed of 1 in. I.D. Pyrex pipe, and the end and ring electrodes were made of aluminum.

Tests were conducted at pressures ranging from a few millimeters to several centimeters of mercury, using air, argon, and helium, both individually and in combination.

A variable d.c. source was used in conjunction with two 4,000-volt, 100-microfarad condensers. A rotating drum camera was used to photograph the wave pattern in the tube. The gas was made luminous by the combination of high temperature after discharge and high Mach Number, and was photographed in its own light.

DISCUSSION OF RESULTS

In Fig. 3 is shown a photograph of the wave pattern in the shock tube. From the slope of the contact surface originating at the intersection of the reflected shock and initial contact surface, we see that the flow is directed away from the end wall. Thus, the reflected wave from the initial contact surface is indeed an expansion. This expansion, since it originates in the hot region (5), is very effective in rapidly cooling the gas. That this is so can be seen in Fig. 4, which indicates the theoretical and experimental temperature decrease a particle undergoes in passing through the reflected expansion, as calculated in reference 5. It will be noticed that $T_5 - T_6$ is a function of Mach Number of the initial shock wave. This allows us to control the cooling rate in the shock tube by varying the Mach Number.

For the conditions indicated in Fig. 3, the initial cooling rate near the end of the tube is approximately 2×10^7 °K./sec. In this figure, the distance between the contact-surface-reflected-shock intersection point is 1.5 in.

REFERENCES

[1] Fowler, R. G., Goldstein, J. S., and Clotfelter, B. E., *Luminous Fronts in Pulsed Gas Discharges*, Phys. Rev., Vol. 82, No. 6, June, 1951.

[2] Fowler, R. G., Atkinson, W. R., Compton, W. D., and Lee, R. J., *Shock Waves in Low-Pressure Spark Discharges*, Phys. Rev., Vol. 88, No. 1, October, 1952.

[3] Resler, E. L., Lin, S. C., and Kantrowitz, A., *The Production of High Temperature Gases in Shock Tubes*, J. Appl. Phys., Vol. 23, No. 12, December, 1952.

[4] Llewellyn-Jones, F., *Ionization and Breakdown in Gases*, Methuen & Co., London, 1957.

[5] Wecker, M. S., *On the Use of a Spark-Driven Shock Tube to Prepare Non-equilibrium Gas Samples*, M. Aero. E. Thesis, Cornell University, June, 1959.

The Use of the WKBJ Method to Estimate Transient Effects on Structural Response

Robert E. Kelly*

Fulbright Scholar, Imperial College, London, England, on leave from Fluid Dynamic Research Group, Massachusetts Institute of Technology, Cambridge, Mass.

July 13, 1959

DUE to an increasing number of problems involving differential equations with time-dependent coefficients, the WKBJ method has been called on with increasing frequency as a means to obtain an accurate, approximate solution. Most recently, the method has been applied by Garber[1] and discussed by Squire.[2] Also, the assumptions required for its validity can be shown to be identical to those of Allen[3] and Reed[4] in their own methods of solution. Thus, the applicability of the WKBJ method is quite wide, and comparison with other methods employed to date will indicate its simplicity.

Briefly, the WKBJ method claims that an approximate solution of

$$\ddot{u} + G^2(t)u = 0 \tag{1}$$

where $(\dot{}) = d/dt$ is

$$u(t) = [G(t)]^{-(1/2)} \{C_1 \exp [i\phi(t)] + C_2 \exp [-i\phi(t)]\} \tag{2}$$

where

$$\phi(t) = \int G(t)dt$$

The criterion is established by substituting Eq. (2) into Eq. (1):

$$\ddot{u} + \{G^2(t) + (1/2)[\ddot{G}(t)/G(t)] - (3/4)[\dot{G}(t)/G(t)]^2\} u = 0 \tag{3}$$

Thus, the approximation is very good if

$$G^2(t) >> -(1/2)[\ddot{G}(t)/G(t)] + (3/4)[\dot{G}(t)/G(t)]^2 \tag{4}$$

The method is now applied in order to estimate the effect of a continuous variation in stiffness on the impulsive pitch response of a two-dimensional airfoil. The system might simulate the pitch response of a supersonic airfoil to a sharp-edged gust after instantaneous acceleration to a high Mach Number. In such a case, as Fig. 4 of reference 5 indicates, the rate of decrease of torsional stiffness is much greater than that of bending stiffness and also occurs on a nearly linear basis. Hence, the equation of interest is:

$$I\ddot{\alpha} + d\dot{\alpha} + (c_0 - c_1 t)\alpha = 0 \tag{5}$$

By using the familiar substitution

$$\alpha = u(t) \exp [-(1/2)(d/I)t]$$

Eq. (5) is placed in the form of Eq. (1). Applying the initial conditions:

$$\alpha_I(0, 0) = 0, \quad \dot{\alpha}_I(0, 0) = 1/I$$

The resulting WKBJ solution is

$$\alpha_{I,\,r}(t, 0) = [e^{-(d/2I)t}/I\sqrt{\omega_{d_0}(t)}\,\sqrt{\omega_{d_0}}] \times \{\sin (2I/3c_1)\,[\omega_{d_0}{}^3 - \omega_{d_0}{}^3(t)]\} \tag{6}$$

where

$$\omega_{d_0}(t) = \sqrt{(c_0 - c_1 t)/(I) - (d^2/4a^2)}$$

$$\omega_{d_0} = \sqrt{(c_0/I) - (d^2/4a^2)}$$

The constant stiffness solution ($c_1 = 0$) is, of course

$$\alpha_{I,\,c}(t, 0) = (e^{-(d/2I)t}/I\,\omega_{d_0}) \sin \omega_{d_0} t \tag{7}$$

The ratio of envelopes is

$$\frac{|\alpha_{I,\,r}(t, 0)|}{|\alpha_{I,\,c}(t, 0)|} = \sqrt{\frac{\omega_{d_0}}{\omega_{d_0}(t)}} \tag{8}$$

* Formerly, graduate student, Dept. of Aeronautics and Astronautics, M.I.T.

The instants of zero amplitude ($\alpha_{I,\,v} = 0$) may be found from the condition

$$(2I/3c_1)[\omega_{d_0}^2 - \omega_{d_0}^2(t)] = n\pi \tag{9}$$

or

$$\{1 - [(c_1/I)t/\omega_{d_0}^2]\}^{3/2} = 1 - (3c_1 n\pi/2I\,\omega_{d_0}^2) \tag{10}$$

If $(c_1/I) \ll (c_0/I) - (d^2/4I^2)$, which is certainly true for the lightly damped supersonic airfoil, the left-hand side of Eq. (10) may be expanded in a two-term binomial expansion:

$$1 - (3/2)(c_1/I)(t/\omega_{d_0}^2) = 1 - (3c_1 n\pi/2I\omega_{d_0}^3)$$

or $t = n\pi/\omega_{d_0}$, which is identical to the constant stiffness result. Hence, to this order of approximation, the inclusion of continuous stiffness variation has a higher-order effect on the period. An identical result was obtained in the case of a stiffness which was a quadratic function of time. Thus, considering the peak response in both cases to occur at the initial quarter-cycle point—i.e., small damping—and using $t = n\pi/2\omega_{d_0}$ in Eq. (8):

$$\left.\frac{\alpha_{I,\,v}}{\alpha_{I,\,c}}\right|_{max} = \frac{1}{[1 - (\pi c_1/2I\omega_{d_0}^2)]^{1/4}} \tag{11}$$

As one might expect, the additional accuracy obtained by including the continuous variation of stiffness is very small. The example shows, however, the usefulness of the WKBJ method in achieving such qualitative measures. Also, in an application to a hypothetical case, Eq. (11) gave much better quantitative results than those obtained through the use of Laitone's bounds,[6] as compared to a higher order approximation calculated by the use of an Airy integral solution.[7]

Although Merrick[8] recently developed the method independently, his extension to a coupled set of differential equations with arbitrary time-dependent operators is invalid because he assumes the same linear combination of time-dependent functions as a solution for each variable. As Hildebrand shows,[9] this assumption depends on the commutability of the linear operators, which property is not present in Merrick's case.

Two types of problems involving multi-degree of freedom systems may be solved by utilization of the WKBJ method. These are:

(1) Separable systems, such as a beam undergoing uniform heating with time, thus having a stiffness which is a product of a time function and a length function. The governing partial differential equation is still separable, and the ordinary differential equation involving time may be solved by the WKBJ method.

(2) Nonseparable systems, where a one-term Rayleigh-Ritz solution is assumed for one coordinate, and the WKBJ method is utilized for the other coordinate solution. Nonuniform heating of a beam serves as an example.

References

[1] Garber, T. B., *On the Rotational Motion of a Body Re-Entering the Atmosphere*, Journal of the Aero/Space Sciences, Vol. 26, No. 3, p. 443, July, 1959.

[2] Squire, W., *Approximate Solution of Linear Second-Order Differential Equations*, Journal of the Royal Aeronautical Society, Vol. 63, No. 582, p. 368, June, 1959.

[3] Allen, H. J., *Motion of a Ballistic Missile Angularly Misaligned With the Flight Path Upon Entering the Atmosphere*, NACA TN 4048, October, 1957.

[4] Reed, W. H., *Effects of a Time-Varying Test Environment on the Evaluation of Dynamic Stability With Application to Flutter Testing*, Journal of the Aero/Space Sciences, Vol. 25, No. 7, p. 435, July, 1958.

[5] Hoff, N. J., (Ed.), *High Temperature Effects in Aircraft Structures*, Bisplinghoff, R. L., and Dugundji, J., "Aerodynamic Heating on Aeroelastic Phenomena," p. 288, Pergamon Press, New York, 1958.

[6] Laitone, E. V., *On the Damped Oscillations Equation With Variable Coefficients*, Quarterly of Applied Mathematics, Vol. 16, No. 1, p. 90, April, 1958.

[7] Pipes, L. A., *Matrix Analysis of Linear Time-Varying Systems*, Journal of Applied Physics, Vol. 25, No. 9, p. 1179, September, 1954

[8] Merrick, V. K., *The Influence of Rate of Change of Altitude and Acceleration on the Longitudinal Dynamic Stability of Aircraft and Missiles*, Proc. of the National Specialists Meeting on Dynamics and Aeroelasticity, p. 118, November, 1958.

[9] Hildebrand, F. B., *Advanced Calculus for Engineers*, p. 21, Prentice-Hall, Inc., New York, 1949.

Some Aspects of the Modified Newtonian and Prandtl-Meyer-Expansion Method for Axisymmetric Blunt Bodies at Zero Angle of Attack

Richard D. Wagner, Jr.
Aeronautical Research Engineer,
Langley Research Center, NASA, Langley Field, Va.

July 14, 1959

In a recent article on hypersonic flow,[1] Lees and Kubota suggested a modification of the local-expansion method to predict the surface pressures in the region of a nose-cylinder junction where Newtonian theory fails. The modification consists of matching the Newtonian pressure distribution

$$C_p = C_{p,\,max} \sin^2 \theta \tag{1}$$

and the Prandtl-Meyer relation

$$(1/p)(dp/d\theta) = \gamma M^2/\sqrt{M^2 - 1} \tag{2}$$

at the point on the nose surface where both the pressure and the pressure gradient, predicted by these two solutions, are equal. With this approximation, the pressure distribution can be predicted quite accurately up to the nose-cylinder junction for blunt-nosed bodies of continuous curvature, provided centrifugal-force effects are negligible.

The purpose of this note is to facilitate the application of Lees' suggestion and to draw attention to some of its consequences.

With this aim, the matching-point location (in terms of the angle between the tangent to the body surface and the body centerline) and corresponding local matching-point Mach Number were determined as functions of the free-stream Mach Number and are presented in Fig. 1(a) and (b). Due to the current interest in helium, the results are presented for both helium and air. The curves were obtained using Eqs. (1) and (2) and the isentropic relation

$$p/p_t = \{1 + [(\gamma - 1)/2]M^2\}^{-[\gamma/(\gamma-1)]} \tag{3}$$

assuming that the stagnation pressure immediately downstream of the normal portion of the bow shock exists over the entire nose of the body.

Having obtained the matching-point location and the local matching-point Mach Number, the Prandtl-Meyer expansion can be used to predict the pressure coefficient at the nose-cylinder

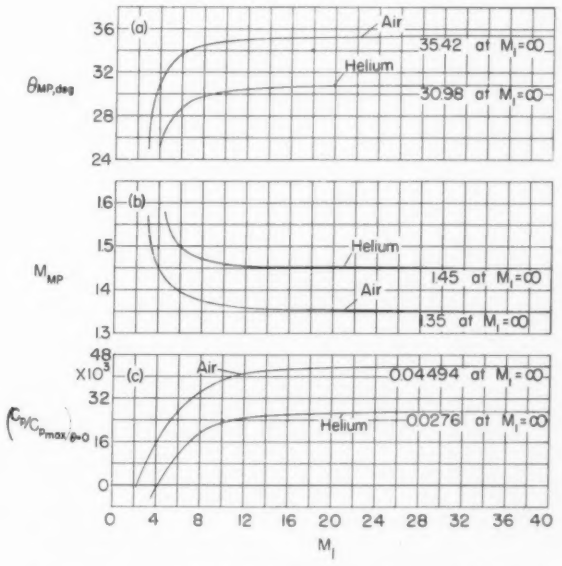

Fig. 1. Variation of (a) matching-point location, (b) matching-point Mach Number, and (c) nose-cylinder-junction pressure coefficient with Mach Number.

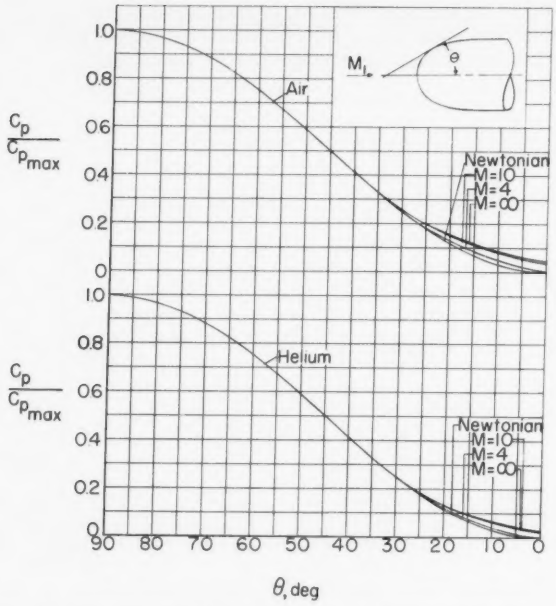

FIG. 2. Pressure coefficient distribution for various free-stream Mach Numbers.

junction. (See Fig. 1(c).) It is interesting to note that the pressure coefficient at the initial point of induced pressure effects can be predicted quite accurately by the following equations:

$$C_{p\theta} = 0^\circ = C_{p\theta} = 0^\circ (M_1 = \infty) - (0.827/M_1^2) \quad \text{(air)} \qquad (4)$$

$$C_{p\theta} = 0^\circ = C_{p\theta} = 0^\circ (M_1 = \infty) - (1.005/M_1^2) \quad \text{(helium)} \qquad (5)$$

The form of these equations was suggested in the results of reference 2.

The matching-point location and the corresponding local Mach Number are seen to be essentially independent of the free-stream Mach Number at hypersonic speeds. As a result of this Mach Number freeze, the following observations can be made in regard to hypersonic flight speeds:

(1) The Prandtl-Meyer expansion predicts that the pressure-coefficient distribution from the matching point to the nose-cylinder junction will also be essentially invariant.

(2) The pressure coefficient at the initial point of induced pressure effects on the cylindrical afterbody will be independent of Mach Number. (See Fig. 1(c).)

Since no geometrical restrictions have been made, the matching-point location and corresponding local Mach Number, the pressure distribution from the matching point to the nose-cylinder junction, and the pressure coefficient at the initial point of induced pressure effects on the cylindrical afterbody will be independent of body geometry.

In Fig. 2 is shown the complete pressure distribution (in terms of $C_p/C_{p,\,max}$ vs. the surface incidence angle) for various free-stream Mach Numbers. Note that as the free-stream Mach Number increases, the pressure distribution downstream of the matching point rapidly approaches the limiting case of an infinite Mach Number. Therefore, a universal curve of $C_p/C_{p,\,max}$ vs. θ is obtained which will apply to any blunt-nose body with constant curvature at any Mach Number above approximately 10, provided centrifugal-force effects are negligible.

REFERENCES

[1] Lees, L., and Kubota, T., *Inviscid Hypersonic Flow Over Blunt-Nosed Slender Bodies*, Journal of the Aeronautical Sciences, Vol. 24, No. 3, pp. 195–202, March, 1957.

[2] Bertram, M. H., and Baradell, D. L., *A Note on the Sonic-Wedge Leading-Edge Approximation in Hypersonic Flow*, Readers' Forum, Journal of the Aeronautical Sciences, Vol. 24, No. 8, pp. 627–628, August, 1957.

An Authorized Binding for
Journal of the Aero/Space Sciences

Arrangements have been made by the Institute of the Aeronautical Sciences for members and subscribers to have their Journals bound carefully and economically. Simply write for details to:

Publisher's Authorized Bindery Service, 5809 West Division St., Chicago 51, Ill.

Advances in Aeronautical Science

Proceedings of the First International Congress of the Aeronautical Sciences, Madrid, 1958 (2 Vols.)

In these two volumes are published the 46 papers presented by the world's outstanding specialists in the field of aeronautics and astronautics at the First International Congress of the Aeronautical Sciences held in Madrid in September, 1958, under the leadership of Prof. Theodore von Kármán. Some 600 delegates from 25 countries, including an official delegation from the U.S.S.R., attended, and the meeting was so successful that it was decided to hold similar congresses at 2-year intervals in future.

The volumes have a full author and subject index and number 1,200 pages. The *Proceedings*, edited by Th. von Kármán, A. M. Ballantyne, H. Blenk, R. R. Dexter, M. Roy, and H. L. Dryden, are of special interest to aerodynamicists, aeronautical engineers, rocketry research workers, and propulsion engineers.

The *Proceedings* (price, $30.00) may be obtained by writing to: *Sales Director, Pergamon Press, Inc., 122 East 55 St., New York 22, N.Y.*

REQUIREMENTS *for* CONTRIBUTIONS
to the publications of the
INSTITUTE *of the* AERONAUTICAL SCIENCES

The Institute of the Aeronautical Sciences invites both members and nonmembers from any country to submit papers for publication in the JOURNAL OF THE AERO/SPACE SCIENCES and AERO/SPACE ENGINEERING. The Institute, following the practice of other societies, does not pay for contributions.

The following directions for the preparation of papers, if followed by authors, will save correspondence, avoid the return of papers for changes, minimize the work of preparation for the printer, and save the expense due to the charges made for "author's corrections."

MANUSCRIPTS: The original typewritten copy of the paper is desired. **To expedite review, an additional copy of both the manuscript and figures should be submitted.** The manuscript must be double or triple spaced on one side of white paper sheets, consecutively numbered. There should be wide margins to allow for the marking of directions to the printer. Correcting, changing, or adding to papers after they are in type is costly. It is, therefore, imperative that papers submitted be in final form. Typographical errors may be corrected on proofs, but if authors wish to add material, they may do so at their own expense. In mailing, drawings may be rolled, but manuscripts should be sent flat. Send by first-class mail (register if you wish for your own protection) to the Editorial Office, Institute of the Aeronautical Sciences, 2 East 64th Street, New York 21, N.Y. All manuscripts will be examined by the Editorial Committee and by the Editor. Authors will be advised as promptly as possible whether the paper is acceptable for publication.

TITLES: The title of the paper should be brief. The name and initials of the author should be written as he prefers. The use of the full name of an author is advocated because of the frequent duplication of initials and surnames which sometimes makes it difficult to establish the identity of the author. This is particularly important for large annual indexing and abstracting services. All titles and degrees or honors are omitted. The name of the organization with which the author is associated should be placed after his name on a separate line. The date on which the paper is received will be inserted by the Editor. The author's title or position should be indicated in a footnote.

SUMMARIES OR ABSTRACTS: An abstract to be printed at the beginning should accompany each article. It should be adequate as an *index* and as a *summary*. It should contain a statement of major conclusions reached, since summaries in many cases constitute the only source of information used in compiling scientific reference indexes. Abstracts printed in other journals, especially foreign, in most cases consist of summaries from printed papers. The summary should explain as adequately as possible the major conclusions to a nonspecialist in the subject and should contain from 100 to 300 words, depending on the length of the paper.

SUBHEADINGS: Subheadings should be inserted by the author at frequent intervals. The work of editorial preparation will be simplified by the author's provision of many subheadings.

MATTER USUALLY DELETED: Photographs or illustrations of little technical interest and not showing advances in general practice. Too detailed tabular matter (general results of such tables may be included in the text). Lengthy descriptions of materials or processes or of preliminary experiments or theories that preceded final results; salient features only are of interest.

REFERENCES: References should be numbered consecutively and grouped together at the end of the manuscript, with only the corresponding number being mentioned in the text. The arrangement should be as follows. For books: [1] Durand, W. F., *Aerodynamic Theory*, 1st Ed., Vol. 1, p. 23; Julius Springer, Berlin, 1934. For magazines: [1]England, C. R., Crawford, A. B., and Mumford, W. W., *Some Results of a Study of Ultra-Short-Wave Transmission Phenomenon*, Proc. IRE, Vol. 20, No. 12, pp. 481–482, March, 1933. Please give author, title, edition, volume, number, page, publisher, and place and date of publication as indicated. Omission of one required fact causes much extra editorial work and possible inaccuracies.

ILLUSTRATIONS: Illustrations should accompany manuscripts, and each should always be referred to in the text by number. Drawings or graphs should not be larger than 12 × 16 inches, and must be made with jet black India ink on white paper or tracing cloth, the latter being preferred. *Do not use typewriter for lettering.* The smallest lettering on 8 × 10 inch figures should be no less than $^1/_4$ inch high. Cross-section paper (white with black lines) may be used, but it should not have more than 4 lines per inch. If finer ruled paper is used, the major division lines should be drawn in with black ink, omitting the finer divisions. In the case of finely ruled paper, only blue-lined paper can be accepted. *Tracing paper and blueprints* are not acceptable. Lettering and all markings must be large enough to be readable after reduction to single-column width ($3^5/_{16}$ in.). Mail rolled or flat; never fold. Drawings that cannot be reproduced (including pencil drawings) will be returned to the author for redrawing, thus delaying publication of the paper. Photographs should be distinct and show clear black and white contrasts. They must be on glossy white paper. Avoid round or oval photographs.

CAPTIONS AND LEGENDS: Legends or captions must accompany each drawing or photograph submitted. If written on the drawing or photograph, they should be placed below and well outside the part to be reproduced. Each table should have a caption such as Table 1, Table 2, Table 3, etc. Captions should be complete in themselves so as to make the data intelligible to the reader without reference to the text. A duplicate list of captions for figures should be included as the last page of the manuscript. Use "Fig. 1" (not Figure 1), "Figs. 3 and 4," etc., in both the text and the numbering of illustrations. In the text, "Eq. (1)" or "Eqs. (1) and (2)" is used, not "Equation (1)." In captions, legends, and in table headings, write all words in full; do not abbreviate, except for "Fig." and "Eq."

MATHEMATICAL WORK: Formulas may be typewritten or carefully written in pen and ink, the writing to be large enough so that it can be marked for the printer. Considerable space for marking should be allowed above and below all equations. All complicated equations should be repeated on separate sheets with plenty of space left for marking. The solidus should be used for simple fractions appearing within the text. Make all expressions clear to the typesetter. Greek letters used in formulas should be clearly designated by name in the margin of the manuscript. The difference between capital and lower-case letters should be clearly distinguished and care taken to avoid confusion between zero (0) and the letter (o), between the numeral (one) and the letter (ell) and the prime ($'$), between alpha and a, kappa and k, u and mu, v and nu, n and eta. All subscripts and exponents should be clearly distinguished. Avoid complicated exponents and subscripts. Dots and bars over letters or mathematical expressions should also be avoided. When it is necessary to repeat a complicated expression, it should be represented by some convenient symbol.

SYMBOLS AND ABBREVIATIONS: The symbols recommended in the American Standard Association "Letter Symbols for Aeronautical Sciences," ASA Y10.7—1954, should be used wherever practicable. All symbols should be clearly written and carefully checked. Standard abbreviations should be used, and it should be noted that most abbreviations are lower case, such as m.p.h., b.m.e.p., i.h.p b.hp., hp., etc.

CORPORATE MEMBERS

OF THE

INSTITUTE OF THE AERONAUTICAL SCIENCES

AC SPARK PLUG DIVISION, GENERAL MOTORS CORPORATION
ACADEMY OF AERONAUTICS
ADAMS RITE MANUFACTURING COMPANY
AEROJET-GENERAL CORPORATION
AEROLAB DEVELOPMENT COMPANY
AERONCA MANUFACTURING CORPORATION
AERONUTRONIC SYSTEMS, INC.
AEROQUIP CORPORATION
AGAWAM AIRCRAFT PRODUCTS, INC.
ALLIED RESEARCH ASSOCIATES, INC.
ALLISON DIVISION, GENERAL MOTORS CORPORATION
ALUMINUM COMPANY OF AMERICA
AMERICAN AIRLINES, INC.
AMERICAN BOSCH ARMA CORPORATION
AMERICAN STEEL & WIRE DIVISION, UNITED STATES STEEL CORPORATION
AMOCO CHEMICALS CORPORATION
AMPHENOL-BORG ELECTRONICS CORPORATION
ANDERSON, GREENWOOD & CO.
ARDE ASSOCIATES
ASSOCIATED AVIATION UNDERWRITERS
AVCO RESEARCH LABORATORY
AVIEN, INC.
AVRO AIRCRAFT LIMITED
BAKER STEEL & TUBE COMPANY
BEECH AIRCRAFT CORPORATION
BELL AIRCRAFT CORPORATION
BENDIX AVIATION CORPORATION
BOEING AIRPLANE COMPANY
BOOZ, ALLEN & HAMILTON
THE BRISTOL AEROPLANE COMPANY (U.S.A.) INC.
BULOVA RESEARCH AND DEVELOPMENT LABORATORIES, INC.
CANADAIR, LTD.
THE CESSNA AIRCRAFT COMPANY
CHANCE VOUGHT AIRCRAFT, INCORPORATED
THE CHASE MANHATTAN BANK
CHICAGO AERIAL INDUSTRIES, INC.
THE CLEVELAND PNEUMATIC INDUSTRIES, INC.
CONSOLIDATED CONTROLS CORPORATION
CONTINENTAL MOTORS CORPORATION
CORNELL AERONAUTICAL LABORATORY, INC.
CURTISS-WRIGHT CORPORATION
DANIEL, MANN, JOHNSON, & MENDENHALL
DAYSTROM, INC.
DAYSTROM-WESTON SALES DIVISION
THE DECKER CORPORATION
DEL MAR ENGINEERING LABORATORIES
DELCO-REMY DIVISION, GENERAL MOTORS CORPORATION
DOAK AIRCRAFT COMPANY, INC.
DOUGLAS AIRCRAFT COMPANY, INC.
DZUS FASTENER COMPANY, INC.
EASTERN AIR LINES, INC.
EATON MANUFACTURING COMPANY
EDO CORPORATION
ELASTIC STOP NUT CORPORATION OF AMERICA
ELECTROL INCORPORATED
ENGINEERING SUPERVISION COMPANY
ESSO STANDARD OIL COMPANY
FAIRCHILD CAMERA AND INSTRUMENT CORPORATION
FAIRCHILD ENGINE AND AIRPLANE CORPORATION
THE FIRESTONE TIRE & RUBBER COMPANY
THE GARRETT CORPORATION
GENERAL APPLIED SCIENCE LABORATORIES, INC.
GENERAL DYNAMICS CORPORATION
GENERAL ELECTRIC COMPANY
GENERAL PRECISION EQUIPMENT CORPORATION
G. M. GIANNINI & CO., INC.
GIANNINI PLASMADYNE CORPORATION
THE B. F. GOODRICH COMPANY
GOODYEAR AIRCRAFT CORPORATION
GRUMMAN AIRCRAFT ENGINEERING CORPORATION
HYDRO-AIRE CO.
INSURANCE COMPANY OF NORTH AMERICA COMPANIES
INTERNATIONAL BUSINESS MACHINES CORPORATION
THE INTERNATIONAL NICKEL COMPANY, INC.
ITT LABORATORIES, DIVISION OF INTERNATIONAL TELEPHONE AND TELEGRAPH CORPORATION
JANITROL AIRCRAFT DIVISION, SURFACE COMBUSTION CORPORATION
JOHNS-MANVILLE SALES CORPORATION
EARLE M. JORGENSEN CO.
WALTER KIDDE & COMPANY, INC.
KOLLSMAN INSTRUMENT CORPORATION
LAVELLE AIRCRAFT CORPORATION
LEAR, INCORPORATED
C. W. LEMMERMAN, INC.
LIBRASCOPE, INCORPORATED
THE LIQUIDOMETER CORPORATION
LOCKHEED AIRCRAFT CORPORATION
LOEWY-HYDROPRESS DIVISION OF BALDWIN-LIMA-HAMILTON CORPORATION
LONGINES-WITTNAUER WATCH COMPANY, INC.
THE MARQUARDT CORPORATION
THE MARTIN COMPANY
MARTIN STEEL PRODUCTS CORPORATION
McDONNELL AIRCRAFT CORPORATION
MELETRON CORPORATION
MID-CONTINENT MANUFACTURING, INC.
MINNEAPOLIS-HONEYWELL REGULATOR COMPANY
NATIONAL CREDIT OFFICE, INC.
NORTH AMERICAN AVIATION, INC.
NORTHROP CORPORATION
NUCLEAR DEVELOPMENT CORPORATION OF AMERICA
PAN AMERICAN WORLD AIRWAYS, INC.
THE RALPH M. PARSONS COMPANY
PESCO PRODUCTS DIVISION, BORG-WARNER CORPORATION
PHILLIPS PETROLEUM COMPANY
PIASECKI AIRCRAFT CORPORATION
RADIO CORPORATION OF AMERICA
ASTRO-ELECTRONIC PRODUCTS DIVISION
DEFENSE ELECTRONIC PRODUCTS
RAMO-WOOLDRIDGE DIVISION, THOMPSON RAMO WOOLDRIDGE INC.
REPUBLIC AVIATION CORPORATION
ROHR AIRCRAFT CORPORATION
PAUL ROSENBERG ASSOCIATES
RYAN AERONAUTICAL COMPANY
SANDBERG-SERRELL CORPORATION
SHAFER BEARING DIVISION, CHAIN BELT COMPANY
SHELL OIL COMPANY
SIMMONDS AEROCESSORIES, INC.
SOCONY MOBIL OIL COMPANY, INC.
SOLAR AIRCRAFT COMPANY
SOUTHWEST PRODUCTS CO.
SPACE TECHNOLOGY LABORATORIES, INC.
R. DIXON SPEAS ASSOCIATES
SPERRY GYROSCOPE COMPANY DIVISION OF SPERRY RAND CORPORATION
STANDARD OIL COMPANY OF CALIFORNIA
STANDARD OIL COMPANY (INDIANA)
STANDARD-THOMSON CORPORATION
CLIFFORD MANUFACTURING DIVISION
STANLEY AVIATION CORPORATION
THIOKOL CHEMICAL CORPORATION
THOMPSON RAMO WOOLDRIDGE INC.
TRANS WORLD AIRLINES, INC.
TURBO PRODUCTS, INC.
UNION CARBIDE CORPORATION
UNITED AIR LINES, INC.
UNITED AIRCRAFT CORPORATION
UNITED STATES AVIATION UNDERWRITERS, INC.
VARD, INC.
VERTOL AIRCRAFT CORPORATION
VITRO CORPORATION OF AMERICA
WESTERN GEAR CORPORATION
WESTINGHOUSE ELECTRIC CORPORATION
WYMAN-GORDON COMPANY
YOUNG RADIATOR COMPANY

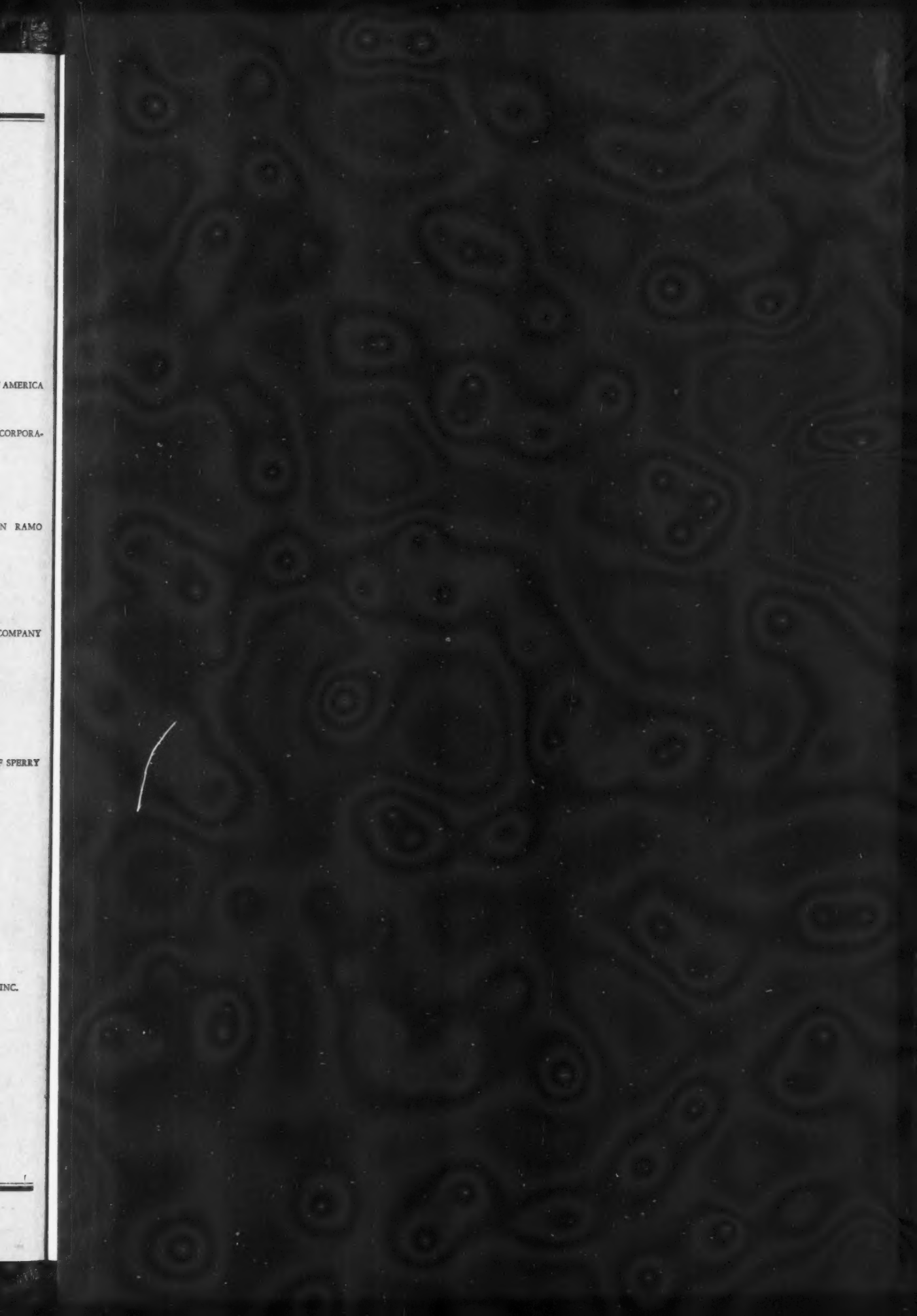

Index to Volume 26

Journal of the Aero/Space Sciences

Numbers 1–12, January–December, 1959

No. 1, January, pages 1–64
No. 2, February, pages 65–128
No. 3, March, pages 129–192
No. 4, April, pages 193–256
No. 5, May, pages 257–320
No. 6, June, pages 321–400
No. 7, July, pages 401–464
No. 8, August, pages 465–544
No. 9, September, pages 545–608
No. 10, October, pages 609–688
No. 11, November, pages 689–768
No. 12, December, pages 769–864

The material has been indexed in two sections: under a subject heading and by author.

*An asterisk following an item identifies it as having appeared in the Readers' Forum section.

Subject Index

AERODYNAMICS

Deduction of Mass-Mean Properties From a Knowledge of Pressure and Mean Density, H. G. Elrod, Jr.* ... 460
The Effect of Slip on Induced Pressures, J. A. Laurmann* ... 53
Further Note on Isentropic Compressible Flow of Air With Variable Specific Heats, K. E. Templemeyer* ... 312
Hydraulic Analogy for Two-Dimensional and One-Dimensional Flows, W. H. T. Loh* ... 389
A Note on Blast-Wave Theory, Harvey Einbinder* ... 191
Comment, J. Lockwood Taylor* ... 832
A Note on the Normal Force of a Multifinned Tail Assembly, John D. Mulholland* ... 837
On the Generalized Prandtl Relation, Rudi S. Ong (Vol. 25 p. 209)*
Comment, S. M. Ramachandra* ... 393
On the Heating Effect in a Resonance Tube, I. M. Hall and C. J. Berry* ... 253
On the Normal Shock Wave Attached to the Curved Surface, Takeo Sakurai* ... 460
On the Viscous Flow Around the Leading Edge of a Flat Plate, Bruno A. Boley and Morton B. Friedman* ... 453
The Problem of Obtaining High Lift-Drag Ratios at Supersonic Speeds, Clinton E. Brown and Francis E. McLean 298
Shock Waves and Dissipation in a Resonance Tube, Ascher H. Shapiro* ... 684
Some Evidence Justifying the Representation of Blasts as Traveling Gusts, Theodore R. Goodman and Theodore P. Sargent* ... 608
Some Significant Developments in Aerodynamics Since 1946 (The First Daniel and Florence Guggenheim Memorial Lecture), Theodore von Kármán ... 129
A Study of the Adiabatic Exponent of the "Hydrodynamical Gas" by Statistical Thermodynamics, Syōgo Matsunaga* 527

AERODYNAMICS—BODIES

Aerodynamics of Wings and Bodies at Transonic Speeds, John R. Spreiter ... 465
Correlation of Base Pressure and Wake Structure of Sharp- and Blunt-Nose Cones With Reynolds Number Based on Boundary-Layer Momentum Thickness, R. Lehnert and V. L. Schermerhorn* ... 185
Design of Missile Bodies for Minimum Drag at Very High Speeds—Thickness Ratio, Lift, and Center of Pressure Given, T. Strand ... 568
Forces and Moments on Oscillating Wing-Body Combinations at Supersonic Speed, Haim Kennet and Holt Ashley* ... 605
Forebody Drag Characteristics of an Ogive Cylinder, W. T. Strike and Jack D. Whitfield* ... 383
Generalized-Newtonian Theory, E. S. Love* ... 314
Hypersonic Viscous Flow Over Slender Cones, L. Talbot, T. Koga, and P. M. Sherman ... 723
An Investigation of a Low-Drag Auxiliary Body Utilizing Favorable Interference, Anthony Martellucci* ... 538
Investigation of Normal Force Distributions and Wake Vortex Characteristics of Bodies of Revolution at Supersonic Speeds, J. F. Mello ... 155
An Investigation of the Pressure Distribution on Conical Bodies in Hypersonic Flows, Victor Zakkay* ... 457
Inviscid Hypersonic Flow Around Spheres and Circular Cylinders, E. Dale Martin* ... 529
Nose Drag in Free-Molecule Flow and Its Minimization, H. S. Tan ... 360
A Note on Conical Flow, Ernest C. Kennedy* ... 59
On an Exact Solution of Incompressible, Inviscid, Hypersonic, Stagnation-Point Flow for a Sphere, Koon-Sang Wan* ... 755
On Flat Plates and Detached Shock Waves, S. S. Sopczak* ... 313
On the Integral of Moment of Pressure in Supersonic Flow, Lu Ting* ... 758
Pressure Distributions for a Two-Dimensional Blunt-Nosed Body at Different Angles of Attack, Antonio Ferri and Victor Zakkay* ... 395
Shroud Tests of Pressure and Heat Transfer Over Short Afterbodies With Separated Wakes, Martin H. Bloom and Adrian Pallone ... 626
Similitude of Hypersonic Real-Gas Flows Over Slender Bodies With Blunted Noses, Hsien K. Cheng ... 575
Some Aspects of the Modified Newtonian and Prandtl-Meyer-Expansion Method for Axisymmetric Blunt Bodies at Zero Angle of Attack, Richard D. Wagner, Jr.* ... 851
Theoretical Pressure Distribution on a Hemisphere-Cylinder Combination, Anthony Casaccio* ... 63

AERODYNAMICS—BOUNDARY LAYER

Analysis of Effects of Diffusion of a Foreign Gas Into the Laminar Boundry Layer of a Supersonic Flow of Air in a Tube, John R. Radbill and Joseph Kaye* ... 602

Application of Generalized Gauss-Laguerre Quadrature to Boundry-Layer Problems, William Squire* 540
The Axisymmetric Free-Convection Temperature Field Along a Vertical Thin Cylinder, Francis R. Hama, John V. Recesso, and Jean Christiaens 335
Boundary-Layer Interaction on a Yawed Infinite Wing in Hypersonic Flow, Robert J. Whalen* 839
Calculation by the Integral Method of the Effect of Fluid Injection Upon an Isothermal Boundary Layer, Milton M. Klein* 686
The Characteristics of Roughness From Insects as Observed for Two-Dimensional, Incompressible Flow Past Airfoils, Walter S. Coleman 264
The Compressible Laminar Boundary Layer With Constant Injected Mass Flux at the Surface, Alan Q. Eschenroeder* 762
Correlation of Base Pressure and Wake Structure of Sharp- and Blunt-Nose Cones With Reynolds Number Based on Boundary-Layer Momentum Thickness, R. Lehnert and V. L. Schermerhorn* 185
Effect of Uniformly Distributed Roughness on Turbulent Skin-Friction Drag at Supersonic Speeds, Frank E. Goddard, Jr. 1
An Experimental Study of Jet-Flap Compressor Blades, Edward L. Clark, Jr. and Donald Earl Ordway 698
Experimental Verification of Boundary-Layer Corrections in Hypersonic Nozzles, Donald L. Baradell* 454
A Generalized Porous-Wall "Couette-Type" Flow, Kenneth R. Cramer* 121
Influence of Shock-Wave Attenuation by Boundary-Layer Growth on Contact-Surface Motion in a Shock Tube, Jan Rosciszewski* 388
The Law of the Wake in Compressible Turbulent Boundary Layers, Paul A. Libby and Marian Visich, Jr.* 541
A New Solution to the Laminar Boundary-Layer Equations, H. A. Hassan* 189
Comment, M. Z. v. Krzywoblocki* 760
A Note on the Blasius Equation With Three-Point Boundary Conditions, William Squire* 678
Note on the Shock-Induced Unsteady Laminar Boundary Layer on a Semi-Infinite Flat Plate, S. H. Lam and L. Crocco* 54
Numerical Solution of the Boundary-Layer Equations Without Similarity Assumptions, R. F. Kramer and H. M. Lieberstein 508
On Panel Flutter in the Presence of a Boundary Layer, John W. Miles 81
On the Continuity of the Schmidt Number at the Interface Between the Laminar Sublayer and the Outer Turbulent Region, Nathan Ness* 396
On the Effect of a Narrow Band of Distributed Roughness Upon Boundary-Layer Transition, J. C. Gibbings* 843
On the Plateau and Peak Pressure of Regions of Pure Laminar and Fully Turbulent Separation in Two-Dimensional Supersonic Flow, William J. Guman* 56
On the Solution of the Laminar Boundary-Layer Equations, Melvin Epstein* 58
Comment, M. Z., v. Krzywoblocki* 455
Preliminary Results of Measurement of Effects of Diffusion of Helium Into the Laminar Boundary Layer of a Supersonic Flow of Air in a Tube at Mach 5, S. William Gouse, Jr., George A. Brown, and Joseph Kaye* 533
A Rapid Method for Estimating Grit Size for Fixing Transition on Wind-Tunnel Models, Jerold M. Bidwell* 118
The Role of Unit Reynolds Number in Boundary-Layer Transition, Jack D. Whitfield and J. Leith Potter* 186
A Semiempirical Relation for Laminar Separation, James L. Amick* 603
Similar Temperature Boundary Layers, Dragutin Stojanović 571
The Smallest Height of Roughness Capable of Affecting Boundary-Layer Transition, A. M. O. Smith and Darwin W. Clutter 229
Some Remarks on the Controversy Regarding Boundary Layers in Shear Flow, Günther Jungclaus* 844
The Stagnation-Point Boundary Layer on a Rotating Hypersonic Body, Sinclaire M. Scala and Joseph B. Workman* 183
A Total-Temperature Probe for High-Temperature Boundary-Layer Measurements, M. Sibulkin* 458
Transformation of the Compressible Turbulent Boundary Layer, A. Mager (Vol. 25, p. 305)
Comment, Michiru Yasuhara* 528
Unsteady Laminar Compressible Boundary Layers on an Infinite Plate With Suction or Injection, Kwang-Tzu Yang 653
The Viscous Flow Near a Stagnation Point When the External Flow Has Uniform Vorticity, J. T. Stuart* 124

AERODYNAMICS—INTERNAL FLOW

An Actuator Disc Analysis of Inlet Distortion and Rotating Stall in Axial Flow Turbomachines, Hsuan Yeh 739
An Approximate Solution for Transonic Flow in Cascades, Albert D. Wood and Joseph H. Clarke* 318
An Exact Solution of the Navier-Stokes Equations, Herbert E. Hunter* 181
A Generalized Porous-Wall "Couette-Type" Flow, Kenneth R. Cramer* 121
Heat Transfer for Laminar Flow in an Annulus With Porous Walls, Robert M. Inman* 532
A Mechanism of Resonance Tubes, J. Wilson and E. L. Resler, Jr.* 461
A Note on the Skin-Friction Coefficient for Compressible Couette Flow, Robert M. Inman* 182
On a Generalized Porous-Wall "Couette-Type" Flow, G. M. Lilley* 685
On the Heating Effect in a Resonance Tube, I. M. Hall and C. J. Berry* 253

AERODYNAMICS—NOZZLES AND JETS

Acoustical Instability of Jets and Wakes for Mach Numbers Above Two, Erik Mollö-Christensen* 765
Experimental Verification of Boundary-Layer Corrections in Hypersonic Nozzles, Donald L. Baradell* 454
On Hypersonic Similarity for Nozzles, Martin H. Bloom* 395
On the Base Pressure Resulting From the Interaction of a Supersonic External Stream With a Sonic or Subsonic Jet, W. L. Chow 176
On the Structure of Jets From Highly Underexpanded Nozzles Into Still Air, T. C. Adamson, Jr., and J. A. Nicholls 16
Comment, S. L. Bragg* 607
A Perturbation Analysis of Shock Flow in a Nozzle, Roy Gundersen* 763
Some Effects of Sound-Reduction Devices on a Turbulent Jet, Gilles M. Corcos 717
An Unusual Aerodynamic Stagnation-Temperature Effect, Irvin Glassman and James E. A. John* 387

AERODYNAMICS—VORTICES

Effect of Air Pressure on Vortex-Shedding Frequency of Cylinders, R. F. Rimoldi, W. D. Clifford, and R. J. Bacigalupi (Vol. 25, p. 532)*
Comment, Anatol Roshko* 121
Author's Reply, William D. Clifford* 121
Investigation of Normal Force Distributions and Wake Vortex Characteristics of Bodies of Revolution at Supersonic Speeds, J. F. Mello 155
A Two-Cell Vortex Solution of the Navier-Stokes Equations, Roger D. Sullivan* 767

Vorticity Effect on the Stagnation-Point Flow of a Viscous Incompressible Fluid, Nicholas Rott and Michael Lenard* 542
Vorticity Interaction at an Axisymmetric Stagnation Point in a Viscous Incompressible Fluid, Nelson H. Kemp* 543

AERODYNAMICS—WINGS AND AIRFOILS

Aerodynamics of Wings and Bodies at Transonic Speeds, John R. Spreiter 465
An Experimental Study of the Flow Field About Swept and Delta Wings With Sharp Leading Edges, Ivan Jaszlics and Leon Trilling 487
The Limiting Circulatory Lift of a Wing of Finite Aspect Ratio, Barnes W. McCormick* 247
A Linearized Analysis of the Forces Exerted on a Rigid Wing by a Shock Wave, F. Edward Ehlers and E. M. Shoemaker 75
A Note on Blast-Wave Theory, Harvey Einbinder* 191
Comment, J. Lockwood Taylor* 832
On a Simple Relation of Exact Airfoil Theory, William T. Evans* 456
On Jones' Criterion for Optimum Lifting Wings, H. Yoshihara and T. Strand, (Vol. 25, p. 600)
Comment, Robert T. Jones* 382
Author's Reply, H. Yoshihara* 383
On the Application of the Ursell-Ward Theorem to Wings With Edge Forces, Joseph H. Clarke* 535
On the Base Pressure Resulting From the Interaction of a Supersonic External Stream With a Sonic or Subsonic Jet, W. L. Chow 176
On the Effect of Flow Discontinuities on Oscillatory-Pressure Measurements in Supersonic Flow, Erik Mollo-Christensen and John R. Martuccelii* 601
On the Flow of a Sonic Stream Past an Airfoil Surface, Colin S. Sinnott 169
The Replacement of Lifting Surfaces by Lifting Lines With Variable Position, A. Van Tuyl* 127
A Similarity Law for the Normal Force on a Delta Wing at Hypersonic Speeds, Arthur F. Messiter* 119
Some Evidence Justifying the Representation of Blasts as Traveling Gusts, Theodore R. Goodman and Theodore P. Sargent* 608

AEROELASTICITY

Accumulative Fatigue Damage Caused by Random Loading, H. C. Schjelderup* 394
Aerodynamic Influence Coefficients From Strip Theory, William P. Rodden* 833
An Alternative Formulation of the Problem of Flutter in Real Fluids, Wen-Hwa Chu and H. Norman Abramson* 683
Analytical Results of Certain Nonlinear Flutter Problems, S. F. Shen and C. C. Hsu (Vo. 25, p. 136)*
Comment, Donald S. Woolston and Robert E. Andrews* 51
Author's Reply, S. F. Shen 52
An Approximate Analysis of Nonlinear Flutter Problems, S. F. Shen 25
A Comparison of Theoretical and Experimental Loads on the B-47 Resulting From Discrete Vertical Gusts, Charles E. Jackson and John E. Wherry 33
Coupled Free Vibrations of a Swept Wing, A. E. Engelbrecht (Vol. 18, p. 329)
Errata, A. E. Engelbrecht and W. P. Rodden* 541
Divergence of Plate Airfoils of Low Aspect Ratio at Supersonic Speeds, G. J. Hancock 495
The Equation of Energy Balance for Fluttering Systems With Some Applications in the Supersonic Regime, John D. C. Crisp 703
Forces and Moments on Oscillating Wing-Body Combinations at Supersonic Speed, Haim Kennet and Holt Ashley* 605
Further Remarks on Matrix Interpolation of Flexibility Influence Coefficients, William P. Rodden* 760
Generalized Spectral Representation in Aeroelasticity, Arthur K. Cross* 766
An Improvement of the Myklestad Method for Flexural-Vibration Problems, S. Mahalingam 46
A Linear Perturbation Method for Stability and Flutter Calculations on Hypersonic Bodies, Maurice Holt 787
The Modified Goodman Diagram and Random Vibration, H. C. Schjelderup* 686
Note on the Determination of Higher Modes of Vibration by the Stodola or Matrix-Iteration Method, Henry E. Fettis* 317
On Panel Flutter in the Presence of a Boundary Layer, John W. Miles 81
On the Supersonic Flutter of Two-Dimensional Infinite Panels, John W. Miles and William P. Rodden* 190
The Oscillating Inboard Flap at Supersonic Speeds, Edmund F. Tyler* 56
A Remark Concerning the Vibration of a Delta Wing in Supersonic Flight, Milomir M. Stanišić* 679
Some Panel-Flutter Studies Using Piston Theory, David J. Johns (Vol. 25, p. 679)
Errata* 192
Theoretical Considerations of Flutter at High Mach Numbers, H. G. Morgan, H. L. Runyan, and Vera Huckel (Vol. 25, p. 371)
Authors' Comment, Harry L. Runyan and Homer G. Morgan* 458
A Theory of the Response of Airplanes to Random Atmospheric Turbulence, B. Etkin 409
The Use of the WKBJ Method to Estimate Transient Effects on Structural Response, Robert E. Kelly* 850

AEROTHERMODYNAMICS

Aerodynamic Heating of Simple Geometries in the Slip- and Intermediate-Flow Regimes, Barry L. Reeves and William M. Van Camp* 838
The Axisymmetric Free-Convection Temperature Field Along a Vertical Thin Cylinder, Francis R. Hama, John V. Recesso, and Jean Christiaens 335
Chemically Frozen Boundary Layers With Catalytic Surface Reaction, Daniel E. Rosner 281
A Comparison of Several Approximate Theories of Melting Ablation, George W. Sutton* 397
Comment, Hans A. Bethe and Mac C. Adams* 768
The Compressible Laminar Boundary Layer With Arbitrary Pressure Gradient and Wall Temperature Distribution, James C. Williams, III* 677
Concise, Systematic Jacobian Thermodynamics for High-Temperature Real Gases, Russell J. Arave* 250
Comment, William Squire* 831
Author's Reply* 832
Determination of Air Stagnation Properties in a High-Enthalpy Test Facility, Walter R. Warren* 835
Determination of Local Skin Friction by Means of Surface Total-Pressure Probes, James A. Martin* 320
Eddy Diffusivities in Forced and Free Convection Boundary Layers, D. E. Bourne* 459
The Effect of Helium Injection at an Axially Symmetric Stagnation Point, H. Hoshizaki and H. J. Smith* 399
Effect of Uniformly Distributed Roughness on Turbulent Skin-Friction Drag at Supersonic Speeds, Frank E. Goddard, Jr. 1
The Effect of Vehicle Deceleration on a Melting Surface, D. M. Tellep* 537
The Effects of Constant-Pressure Sound Fields on Free-Convection Heat Transfer From a Horizontal Cylinder, Jack P. Holman and Tipton P. Mott-Smith* 188
Experimental Investigations of the Effect of Heat Transfer

on Hypersonic Turbulent Boundary-Layer Skin Friction, Eva M. Winkler and Moon H. Cha* ... 123
Forebody Drag Characteristics of an Ogive Cylinder, W. T. Strike and Jack D. Whitfield* ... 383
Free Molecular Flow Forces and Heat Transfer for an Infinite Circular Cylinder at Angle of Attack, L. Talbot (Vol. 24, p. 458)*
Errata* ... 61
Heat Transfer and Recovery Factor in a Laminar Boundary Layer With Arbitrary Pressure Gradient and Wall Temperature Distribution, Bernard Le Fur* ... 682
Heat Transfer in Separated Flows, Howard K. Larson ... 731
Heat Transfer to a Vaporizing, Ablating Surface, Richard G. Fleddermann* ... 604
Heat Transfer to Separated and Reattached Subsonic Turbulent Flows Obtained Downstream of a Surface Step, R. A. Seban, A. Emery, and A. Levy ... 809
An "Insulating" Boundary-Layer Experiment, F. H. Durgin* ... 450
Integration of Some Thermal Differential Equations, B. Saelman* ... 754
Laminar Heat Transfer Around Blunt Bodies in Dissociated Air, Nelson H. Kemp, Peter H. Rose, and Ralph W. Detra ... 421
Nose Drag in Free-Molecule Flow and Its Minimization, H. S. Tan ... 360
Note on the Calculation of Equilibrium Skin Temperatures, Hans C. Vetter* ... 757
A Note on the Skin-Friction Coefficient for Compressible Couette Flow, Robert M. Inman* ... 182
Numerical Solution of the Boundary-Layer Equations Without Similarity Assumptions, R. F. Kramer and H. M. Lieberstein ... 508
On an Exact Solution of Incompressible, Inviscid, Hypersonic, Stagnation-Point Flow for a Sphere, Koon-Sang Wan* ... 755
On Heat Transfer to Laminar Boundary Layers, H. A. Hassan* ... 464
On Similitude in Rarefied-Gas Aerothermodynamics, F. Marcel Devienne* ... 183
On Slip-Flow Heat Transfer to a Flat Plate, Richard A. Oman and Richard A. Scheuing* ... 126
Comment, Donald E. Nestler* ... 687
On the Continuity of the Schmidt Number at the Interface Between the Laminar Sublayer and the Outer Turbulent Region, Nathan Ness* ... 396
On the Contribution of Thermal Creep to the Skin Friction in Slip Flow, A. F. Charwat* ... 120
On the Stable Shape of an Ablating Graphite Body, Daphne Christensen and Rolf D. Buhler* ... 54
Comment, George W. Sutton* ... 681
Preliminary Investigations of Spiked Bodies at Hypersonic Speeds, Seymour M. Bogdonoff and Irwin E. Vas ... 65
Similar Temperature Boundary Layers, Dragutin Stojanović ... 571
A Simple Method for Determining Turbulent Skin Friction From Velocity Profiles, P. Bradshaw* ... 841
The Stagnation-Point Boundary Layer on a Rotating Hypersonic Body, Sinclaire M. Scala and Joseph B. Workman* ... 183
Steady-State Surface Temperatures in Dissociated High-Speed Gas Flows, Daniel E. Rosner* ... 384
Supersonic Airfoil Performance With Small Heat Addition, Artur Mager ... 99
A Theory for the Ablation of Glassy Materials, Hans A. Bethe and Mac C. Adams ... 321
Thermal Analysis of Stagnation Regions With Emphasis on Heat-Sustaining Nose Shapes at Hypersonic Speeds, A. J. Hanawalt, A. H. Blessing, and C. M. Schmidt ... 257
The Viscous Flow Near a Stagnation Point When the External Flow Has Uniform Vorticity, J. T. Stuart* ... 124
Viscous Hypersonic Similitude, Wallace D. Hayes and Ronald F. Probstein ... 815
Vorticity Effect on the Stagnation-Point Flow of a Viscous Incompressible Fluid, Nicholas Rott and Michael Lenard* ... 542
Vorticity Interaction at an Axisymmetric Stagnation Point in a Viscous Incompressible Fluid, Nelson H. Kemp* ... 543

COMPUTERS AND SIMULATORS

Direct-Analog Method of Analysis of the Influence of Aerodynamic Heating on the Static Characteristics of Thin Wings, Michael A. Basin, Richard H. MacNeal, and John H. Shields ... 145
Energy Versus Compatibility Analogs in Electrical Simulators of Structures, Frederick L. Ryder ... 108

CONTROL AND STABILITY

Dynamic Longitudinal Stability Equations for the Re-Entry Ballistic Missile, E. V. Laitone ... 94
A Linear Perturbation Method for Stability and Flutter Calculations on Hypersonic Bodies, Maurice Holt ... 787
Note on a Criterion for Severity of Roll-Induced Instability, Ordway B. Gates and Karlis Minka ... 287
On the Rotational Motion of a Body Re-Entering the Atmosphere, T. B. Garber ... 443

DANIEL AND FLORENCE GUGGENHEIM MEMORIAL LECTURE, 1ST

Some Significant Developments in Aerodynamics Since 1946, Theodore von Kármán ... 129

FLIGHT DYNAMICS

Lagrange Multipliers and Quasi-Steady Flight Mechanics, Angelo Miele ... 592

FLIGHT PROPULSION

Analysis of a Simplified Model of Solid Propellant Resonant Burning, W. Nachbar and L. Green, Jr. ... 518
An Experimental Study of Jet-Flap Compressor Blades, Edward L. Clark, Jr. and Donald Earl Ordway ... 698
Experiments on Porous-Wall Cooling and Flow Separation Control in a Supersonic Nozzle, Leon Green, Jr. and Kenneth L. Nall ... 689
Jet Flap Thrust Recovery, William M. Foley, and Elliott G. Reid* ... 385
Rocket Propulsion Systems for Interplanetary Flight (Minta Martin Aeronautical Lecture, 1959), George Paul Sutton ... 609
Some Effects of Sound-Reduction Devices on a Turbulent Jet, Gilles M. Corcos ... 717
Supersonic Airfoil Performance With Small Heat Addition, Artur Mager ... 99

LANDING GEAR

Landing-Gear Vibration Instability, Frederick L. Ryder and Melvin Zaid ... 303
Relaxation Characteristics of Pneumatic Tires, John Erwin Stevens ... 343

MAGNETOHYDRODYNAMICS

Laminar Jet Mixing of Electrically Conducting Fluid in a Transverse Magnetic Field, S. I. Pai* ... 254
The Matching of the Viscid and Inviscid Regions for the Stagnation Magnetic Flow, Paul S. Lykoudis* ... 315
A Note on Magnetohydrodynamic-Hypersonic Flow Past a Blunt Body, William B. Bush* ... 536

On Hypersonic Stagnation-Point Flow With a Magnetic Field, Nelson H. Kemp (Vol. 25, p. 405)*
Comment, N. C. Freeman* ... 670
Author's Reply* ... 672
On the Concepts of Moving Electric and Magnetic Fields in Magnetohydrodynamics, J. E. McCune and W. R. Sears* 674
On the Flow of a Hydromagnetic Fluid Near an Oscillating Flat Plate, R. S. Ong and J. A. Nicholls* ... 313
The Prospects for Magneto-Aerodynamics—Correction and Addition, E. L. Resler, Jr. and W. R. Sears* ... 318
A Simple Construction for the Determination of the Magnetohydrodynamic Wave Speed in a Compressible Conductor, Nicholas Rott* ... 249
Some Exact Solutions to the Magnetohydrodynamic Equations for Incompressible Flow, F. D. Hains* ... 246
Two-Dimensional Hypersonic Flow of an Ideal Gas With Infinite Electric Conductivity Past a Two-Dimensional Magnetic Dipole, Takeo Sakurai* ... 841

MATERIALS

A Comparison of Several Approximate Theories of Melting Ablation, George W. Sutton* ... 397
Comment, Hans A. Bethe and Mac C. Adams ... 768
On Stress Interaction in Fatigue and a Cumulative Damage Rule, Alfred M. Freudenthal and Robert A. Heller ... 431
On the Stable Shape of an Ablating Graphite Body, Daphne Christensen and Rolf D. Buhler* ... 54
Comment, George W. Sutton* ... 681
A Theory for the Ablation of Glassy Materials, Hans A. Bethe and Mac C. Adams ... 321

MATHEMATICS

Stability Criteria for Systems Having Complex-Coefficient Polynomial Characteristic Equations, Louis G. Kaufman, II* ... 122

MINTA MARTIN AERONAUTICAL LECTURE, 1959

Rocket Propulsion Systems for Interplanetary Flight, George Paul Sutton ... 609

PERFORMANCE

An Investigation of Optimal Zoom Climb Techniques, Henry J. Kelley ... 794
Optimum Path of an Airplane—Minimum Time to Climb, Theodore Theodorsen ... 637

RESEARCH

Means and Examples of Aeronautical Research in France at ONERA (Twenty-Second Wright Brothers Lecture), Maurice Roy ... 193
Discussion, Hugh L. Dryden, A. H. Flax, and John J. Green ... 207

SPACECRAFT

Behavior of Liquids in Free Fall, William C. Reynolds* ... 847
The Determination of Round-Trip Planetary Reconnaissance Trajectories, Richard H. Battin ... 545
Dynamic Longitudinal Stability Equations for the Re-Entry Ballistic Missile, E. V. Laitone ... 94
Flight Mechanics of Low-Thrust Spacecraft, Frank M. Perkins ... 291
On a Class of Variational Problems in Rocket Flight, G. Leitmann ... 586
On the Rotational Motion of a Body Re-Entering the Atmosphere, T. B. Garber ... 443
An Orbital Energy Indicator, Harold E. Bamford, Jr.* ... 452
Space Vehicle Environment, Carl Gazley, Jr., W. W. Kellogg, and E. H. Vestine ... 770
Spinning Ballistic Missiles, W. H. T. Loh* ... 844
Stability Criteria for the Airframe Dynamics of a Liquid-Propellant Rocket, Josef S. Pistiner* ... 678
Steady-State Circular Pitching and Yawing Motion of Symmetric Missiles, Charles H. Murphy, Jr.* ... 600

STRESS ANALYSIS AND STRUCTURES

Accumulative Fatigue Damage Caused by Random Loading, H. C. Schjelderup* ... 394
Approximate Bending Moment Diagrams for Flight Maneuvers, P. W. Sharman* ... 530
Beam Columns on Elastic Supports, Ben A. Neffson* ... 255
Comment, Paul E. Sandorff* ... 759
Buckling of a Cylindrical Shell Under a Circumferential Band Load, D. O. Brush and F. A. Field ... 825
A Creep Instability of Thin-Walled Tubes Under Internal Pressure, Iain Finnie* ... 248
A Critical Strain Approach to Creep Buckling of Plates and Shells, George Gerard and Arthur C. Gilbert (Vol. 25, p. 429)
Comment, Nicholas J. Hoff* ... 117
The Determination of the Shear Center for a Special Solid Symmetrical Airfoil, Alphonse J. Sistino (Vol. 25, p. 402)*
Comment, J. Lockwood Taylor* ... 118
Author's Reply* ... 118
Displacement and Rotation at the Junction of Two Cylinders of Unequal Thickness Due to Axisymmetrical Loadings, G. D. Galletly* ... 60
The Elastic-Plastic Bending of an Eccentrically Loaded Sandwich Column, William E. Boyce* ... 398
Energy Versus Compatibility Analogs in Electrical Simulators of Structures, Frederick L. Ryder ... 108
Equations for Thin Toroidal Shells, T. Au* ... 391
Linear Deformation of Conical Shells, M. D. Mc Ilroy* ... 253
On a Cross-Elasticity Phenomenon in Symmetrically Nonhomogeneous Plates, Yehuda Stavsky* ... 607
On Stress Interaction in Fatigue and a Cumulative Damage Rule, Alfred M. Freudenthal and Robert A. Heller ... 431
On the Local Elastic Stability of Honeycomb Face Plate Subjected to Uniaxial Compression, Raymond C. Weikel and Albert S. Kobayashi* ... 672
On the Optimum Design of an I-Section Beam, S. Krishnan and K. V. Shetty* ... 599
On the Torsion of a Cylindrical Beam Having a Trapezoidal Cross Section, L. K. Shirely and M. M. Stanišić* ... 462
Reduction of Strain Rosettes in the Plastic Range, C. S. Ades* ... 392
Comment, T. H. H. Pian* ... 842
A Simple Method of Matric Structural Analysis: Part IV—Nonlinear Problems, Bertram Klein ... 351
Simultaneous Calculation of Influence Coefficients and Influence Loads for Arbitrary Structures, Bertram Klein* ... 451
Spherical Cap Snapping, Herbert B. Keller and Edward L. Reiss ... 643
Stress Functions for Plates of Convex Polygonal Shape, Hans A. Balmer* ... 675
A Study of Creep Collapse of a Long Circular Cylindrical Shell Under Uniform External Pressure, N. J. Hoff, W. E. Jahsman, and W. Nachbar ... 663
The Yield Strength and Deflection of Circular Bars Subjected to Torsion, Robert M. Rivello* ... 836
The Yield Strength of Beams in Pure Bending, Robert M. Rivello* ... 393

STRESS ANALYSIS AND STRUCTURES—THERMAL STRESSES

Comparison of Approximate Solutions of the Thermoelastic Problem of the Thick-Walled Tube, J. H. Baltrukonis ... 329

Direct-Analog Method of Analysis of the Influence of Aerodynamic Heating on the Static Characteristics of Thin Wings, Michael A. Basin, Richard H. MacNeal, and John H. Shields ... 145
The Heating of Slabs With Arbitrary Heat Inputs, Theodore R. Goodman* ... 187
Comment, William Squire* ... 756
New Thermomechanical Reciprocity Relations With Application to Thermal Stress Analysis, M. A. Biot ... 401
On the Representation of Nonlinear Creep by a Linear Viscoelastic Model, Harry H. Hilton* ... 311
On Thermoelastic Stress-Strain Relations for Thin Isotropic Shells, P. M. Naghdi* ... 125
Photothermoelastic Investigation of Transient Thermal Stresses in a Multiweb Wing Structure, George Gerard and Herbert Tramposch ... 783
Thermal Buckling of Circular Cylindrical Shells Under Circumferential Temperature Gradients, David Abir and S. V. Nardo ... 803
Thermal Buckling of Clamped Cylindrical Shells, W. Zuk (Vol. 24, p. 389)*
Comment, David J. Johns* ... 59
Thermal Stresses and Deflections in Rectangular Sandwich Plates, P. P. Bijlaard ... 210
Thermal Stresses in Rings, Marvin Forray* ... 310

THERMODYNAMICS

A Closed-Form Solution for Laminar Free Convection on a Vertical Plate With Prescribed, Nonuniform, Wall Heat Flux, Richard P. Bobco* ... 846
Further Developments of New Methods in Heat-Flow Analysis, M. A. Biot ... 367
Heat Transfer for Laminar Flow in an Annulus With Porous Walls, Robert M. Inman* ... 532
Heat Transfer in Separated Flows, Howard K. Larson ... 731
Heat Transfer to a Vaporizing, Ablating Surface, Richard G. Fleddermann* ... 604
On the Frozen Flow of a Dissociated Gas, R. E. Geiger* ... 834
Summary of Laminar Heat Transfer Between Parallel Plates With Unsymmetrical Wall Temperatures, R. D. Cess and E. C. Shaffer* ... 538

WIND TUNNELS

A Cool Mercury Plasma Tunnel, Hans U. Eckert ... 515
Determination of Local Skin Friction by Means of Surface Total-Pressure Probes, James A. Martin* ... 320
The Effect of Temperature on Pressures Measured in a Hypersonic Wind Tunnel, Weston M. Howard* ... 764
A High-Temperature, Steady-Flow, Supersonic Tunnel, Robert A. Gross* ... 676
Influence of Shock-Wave Attenuation by Boundary-Layer Growth on Contact-Surface Motion in a Shock Tube, Jan Rosciszewski* ... 388
A Mechanism of Resonance Tubes, J. Wilson and E. L. Resler, Jr.* ... 461
On the Heating Effect in a Resonance Tube, I. M. Hall and C. J. Berry* ... 253
On the Use of a Spark-Driven Shock Tube to Prepare Nonequilibrium Gas Samples, Myron S. Wecker* ... 848
Preliminary Results of Measurement of Effects of Diffusion of Helium Into the Laminar Boundary Layer of a Supersonic Flow of Air in a Tube at Mach 5, S. William Gouse, Jr., George A. Brown, and Joseph Kaye* ... 533
Pressure Fluctuations in a Blowdown Wind Tunnel, James S. Murphy* ... 61
Shock Waves and Dissipation in a Resonance Tube, Ascher H. Shapiro* ... 684
Shock-Tube Testing Time, G. F. Anderson* ... 184
The Tailored-Interface Hypersonic Shock Tunnel, Charles E. Wittliff, Merle R. Wilson, and Abraham Hertzberg ... 219
A Total-Temperature Probe for High-Temperature Boundary-Layer Measurements, M. Sibulkin* ... 458
Transient Analysis of a Two-Chamber Blowdown Process With Critical Flow, C. Forbes Dewey, Jr.* ... 62
Visual Supersonic Flow Patterns by Means of Smoke Lines, V. P. Goddard, J. A. McLaughlin, and F. N. M. Brown* ... 761

WRIGHT BROTHERS LECTURE, 22ND

Means and Examples of Aeronautical Research in France at ONERA (Twenty-Second Wright Brothers Lecture), Maurice Roy ... 193
Discussion, Hugh L. Dryden, A. H. Flax, and John J. Green ... 207

Author Index

ABIR, DAVID, AND S. V. NARDO. Thermal Buckling of Circular Cylindrical Shells Under Circumferential Temperature Gradients ... 803
ABRAMSON, H. NORMAN, AND WEN-HWA CHU. An Alternative Formulation of the Problem of Flutter in Real Fluids* ... 683
ADAMS, MAC C., AND HANS A. BETHE. Comment on: A Comparison of Several Approximate Theories of Melting Ablation, George W. Sutton, p. 397* ... 768
ADAMS, MAC C., AND HANS A. BETHE. A Theory for the Ablation of Glassy Materials ... 321
ADAMSON, T. C., JR., AND J. A. NICHOLLS. On the Structure of Jets From Highly Underexpanded Nozzles Into Still Air ... 16
Comment, S. L. Bragg ... 607
ADES, C. S. Reduction of Strain Rosettes in the Plastic Range* ... 392
Comment, T. H. H. Pian* ... 842
AMICK, JAMES L. A Semiempirical Relation for Laminar Separation* ... 603
ANDERSON, G. F. Shock-Tube Testing Time* ... 184
ANDREWS, ROBERT E., AND DONALD S. WOOLSTON. Comment on: Analytical Results of Certain Nonlinear Flutter Problems, S. F. Shen and C C. Hsu (Vol. 25, p. 136)* ... 51
Author's Reply, S. F. Shen ... 52
ARAVE, RUSSELL J. Concise, Systematic Jacobian Thermodynamics for High-Temperature Real Gases* ... 250
Comment, William Squire* ... 831
Author's Reply* ... 832
ASHLEY, HOLT, AND HAIM KENNET. Forces and Moments on Oscillating Wing-Body Combinations at Supersonic Speed* ... 605
AU, T. Equations for Thin Toroidal Shells* ... 391

BACIGALUPI, R. J., R. F. RIMOLDI, AND W. D. CLIFFORD. Effect of Air Pressure on Vortex-Shedding Frequency of Cylinders (Vol. 25, p. 532)*
Comment, Anatol Roshko* ... 121
Author's Reply, William D. Clifford* ... 121
BALMER, HANS A. Stress Functions for Plates of Convex Polygonal Shape* ... 675
BALTRUKONIS, J. H. Comparison of Approximate Solu-

tions of the Thermoelastic Problem of the Thick-Walled Tube ... 329
BAMFORD, HAROLD E., JR. An Orbital Energy Indicator* ... 452
BARADELL, DONALD L. Experimental Verification of Boundary-Layer Corrections in Hypersonic Nozzles* ... 454
BASIN, MICHAEL A., RICHARD H. MACNEAL, AND JOHN H. SHIELDS. Direct-Analog Methods of Analysis of the Influence of Aerodynamic Heating on the Static Characteristics of Thin Wings ... 145
BATTIN, RICHARD H. The Determination of Round-Trip Planetary Reconnaissance Trajectories ... 545
BERRY, C. J., AND I. M. HALL. On the Heating Effect in a Resonance Tube* ... 253
BETHE, HANS A., AND MAC C. ADAMS. Comment on: A Comparison of Several Approximate Theories of Melting Ablation, George W. Sutton, p. 397* ... 768
BETHE, HANS A., AND MAC C. ADAMS. A Theory for the Ablation of Glassy Materials ... 321
BIDWELL, JEROLD M. A Rapid Method for Estimating Grit Size for Fixing Transition on Wind-Tunnel Models* ... 118
BIJLAARD, P. P. Thermal Stresses and Deflections in Rectangular Sandwich Plates ... 210
BIOT, M. A. Further Developments of New Methods in Heat-Flow Analysis ... 367
BIOT, M. A. New Thermomechanical Reciprocity Relations With Application to Thermal Stress Analysis ... 401
BLESSING, A. H., A. J. HANAWALT, AND C. M. SCHMIDT. Thermal Analysis of Stagnation Regions With Emphasis on Heat-Sustaining Nose Shapes at Hypersonic Speeds ... 257
BLOOM, MARTIN H. On Hypersonic Similarity for Nozzles* ... 395
BLOOM, MARTIN H., AND ADRIAN PALLONE. Shroud Tests of Pressure and Heat Transfer Over Short Afterbodies With Separated Wakes ... 626
BOBCO, RICHARD P. A Closed-Form Solution for Laminar Free Convection on a Vertical Plate With Prescribed, Nonuniform, Wall Heat Flux* ... 846
BOGDONOFF, SEYMOUR M., and IRWIN E. VAS. Preliminary Investigations of Spiked Bodies at Hypersonic Speeds ... 65
BOLEY, BRUNO A., AND MORTON B. FRIEDMAN. On the Viscous Flow Around the Leading Edge of a Flat Plate* ... 453
BOURNE, D. E. Eddy Diffusivities in Forced and Free Convection Boundary Layers* ... 459
BOYCE, WILLIAM E. The Elastic-Plastic Bending of an Eccentrically Loaded Sandwich Column* ... 398
BRADSHAW, P. A Simple Method for Determining Turbulent Skin Friction From Velocity Profiles* ... 841
BRAGG, S. L. Comment on: On the Structure of Jets From Highly Underexpanded Nozzles Into Still Air, T. C. Adamson, Jr., and J. A. Nicholls (p. 16)* ... 607
BROWN, CLINTON E., AND FRANCIS E. MCLEAN. The Problem of Obtaining High Lift-Drag Ratios at Supersonic Speeds ... 298
BROWN, F. N. M., V. P. GODDARD, AND J. A. MCLAUGHLIN. Visual Supersonic Flow Patterns by Means of Smoke Lines* ... 761
BROWN, GEORGE A., S. WILLIAM GOUSE, JR., AND JOSEPH KAYE. Preliminary Results of Measurement of Effects of Diffusion of Helium Into the Laminar Boundary Layer of a Supersonic Flow of Air in a Tube at Mach 5* ... 533
BRUSH, D. O., AND F. A. FIELD. Buckling of a Cylindrical Shell Under a Circumferential Band Load ... 825
BUHLER, ROLF D., AND DAPHNE CHRISTENSEN. On the Stable Shape of an Ablating Graphite Body* ... 54
BUSH, WILLIAM B. A Note on Magnetohydrodynamic-Hypersonic Flow Past a Blunt Body* ... 536

CASACCIO, ANTHONY. Theoretical Pressure Distribution on a Hemisphere-Cylinder Combination* ... 63
CESS, R. D., AND E. C. SHAFFER. Summary of Laminar Heat Transfer Between Parallel Plates With Unsymmetrical Wall Temperatures* ... 538
CHA, MOON H., AND EVA M. WINKLER. Experimental Investigations of the Effect of Heat Transfer on Hypersonic Turbulent Boundary-Layer Skin Friction* ... 123
CHARWAT, A. F. On the Contribution of Thermal Creep to the Skin Friction in Slip Flow* ... 120
CHENG, HSIEN K. Similitude of Hypersonic Real-Gas Flows Over Slender Bodies With Blunted Noses ... 575
CHRISTENSEN, DAPHNE, AND ROLF D. BUHLER. On the Stable Shape of an Ablating Graphite Body* ... 54
CHRISTIAENS, JEAN, FRANCIS R. HAMA AND JOHN V. RECESSO. The Axisymmetric Free-Convection Temperature Field Along a Vertical Thin Cylinder ... 335
CHOW, W. L. On the Base Pressure Resulting From the Interaction of a Supersonic External Stream With a Sonic or Subsonic Jet ... 176
CHU, WEN-HWA, AND H. NORMAN ABRAMSON. An Alternative Formulation of the Problem of Flutter in Real Fluids* ... 683
CLARK, EDWARD L., JR., AND DONALD EARL ORDWAY. An Experimental Study of Jet-Flap Compressor Blades ... 698
CLARKE, JOSEPH H. On the Application of the Ursell-Ward Theorem to Wings With Edge Forces* ... 535
CLARKE, JOSEPH H., AND ALBERT D. WOOD. An Approximate Solution for Transonic Flow in Cascades* ... 318
CLIFFORD, W. D., R. F. RIMOLDI, AND R. J. BACIGALUPI. Effect of Air Pressure on Vortex-Shedding Frequency of Cylinders (Vol. 25, p. 532)*
Comment, Anatol Roshko* ... 121
Author's Reply, William D. Clifford* ... 121
CLUTTER, DARWIN W., AND A. M. O. SMITH. The Smallest Height of Roughness Capable of Affecting Boundary-Layer Transition ... 229
COLEMAN, WALTER S. The Characteristics of Roughness From Insects as Observed for Two-Dimensional, Incompressible Flow Past Airfoils ... 264
CORCOS, GILLES M. Some Effects of Sound-Reduction Devices on a Turbulent Jet ... 717
CRAMER, KENNETH R. A Generalized Porous-Wall "Couette-Type" Flow* ... 121
CRISP, JOHN D. C. The Equation of Energy Balance for Fluttering Systems With Some Applications in the Supersonic Regime ... 703
CROCCO, L., AND S. H. LAM. Note on the Shock-Induced Unsteady Laminar Boundary Layer on a Semi-Infinite Flat Plate* ... 54
CROSS, ARTHUR K. Generalized Spectral Representation in Aeroelasticity* ... 766

DETRA, RALPH W., NELSON H. KEMP, AND PETER H. ROSE. Laminar Heat Transfer Around Blunt Bodies in Dissociated Air ... 421
DEVIENNE, F. MARCEL. On Similitude in Rarefied-Gas Aerothermodynamics* ... 183
DEWEY, C. FORBES, JR. Transient Analysis of a Two-Chamber Blowdown Process With Critical Flow* ... 62
DRYDEN, HUGH L. Discussion of: Means and Examples of Aeronautical Research in France at ONERA (Twenty-Second Wright Brothers Lecture), Maurice Roy (p. 193) ... 207
DURGIN, F. H. An "Insulating" Boundary-Layer Experiment* ... 450

ECKERT, HANS U. A Cool Mercury Plasma Tunnel ... 515
EHLERS, F. EDWARD, AND E. M. SHOEMAKER. A Linearized Analysis of the Forces Exerted on a Rigid Wing by a Shock Wave ... 75
EINBINDER, HARVEY. A Note on Blast-Wave Theory* ... 191
Comment, J. Lockwood Taylor* ... 832

ELROD, H. G., JR. Deduction of Mass-Mean Properties From a Knowledge of Pressure and Mean Density* 460
EMERY, A., R. A. SEBAN, AND A. LEVY. Heat Transfer to Separated and Reattached Subsonic Turbulent Flows Obtained Downstream of a Surface Step 809
ENGELBRECHT, A. E., AND W. P. RODDEN. Errata: Coupled Free Vibrations of a Swept Wing, A. E. Engelbrecht (Vol. 18, p. 329)* 541
EPSTEIN, MELVIN. On the Solution of the Laminar Boundary-Layer Equations* 58
Comment, M. Z. v. Krzywoblocki 455
ESCHENROEDER, ALAN Q. The Compressible Laminar Boundary Layer With Constant Injected Mass Flux at the Surface* 762
ETKIN, B. A Theory of the Response of Airplanes to Random Atmospheric Turbulence 409
EVANS, WILLIAM T. On a Simple Relation of Exact Airfoil Theory* 456

FERRI, ANTONIO, AND VICTOR ZAKKAY. Pressure Distributions for a Two-Dimensional Blunt-Nosed Body at Different Angles of Attack* 395
FETTIS, HENRY E. Note on the Determination of Higher Modes of Vibration by the Stodola or Matrix-Iteration Method* 317
FIELD, F. A., AND D. O. BRUSH. Buckling of a Cylindrical Shell Under a Circumferential Band Load 825
FINNIE, IAIN. A Creep Instability of Thin-Walled Tubes Under Internal Pressure* 248
FLAX, A. H. Discussion of: Means and Examples of Aeronautical Research in France at ONERA (Twenty-Second Wright Brothers Lecture), Maurice Roy (p. 193) 207
FLEDDERMANN, RICHARD G. Heat Transfer to a Vaporizing, Ablating Surface* 604
FOLEY, WILLIAM M., AND ELLIOTT G. REID. Jet Flap Thrust Recovery* 385
FORRAY, MARVIN. Thermal Stresses in Rings* 310
FREEMAN, N. C. Comment on: On Hypersonic Stagnation-Point Flow With a Magnetic Field, N. H. Kemp, (Vol. 25, p. 405)* 670
Author's Reply* 672
FREUDENTHAL, ALFRED M., AND ROBERT A. HELLER. On Stress Interaction in Fatigue and a Cumulative Damage Rule 431
FRIEDMAN, MORTON B., AND BRUNO A. BOLEY. On the Viscous Flow Around the Leading Edge of a Flat Plate* .. 453

GALLETLY, G. D. Displacement and Rotation at the Junction of Two Cylinders of Unequal Thickness Due to Axisymmetrical Loadings* 60
Garber, T. B. On the Rotational Motion of a Body Reentering the Atmosphere 443
GATES, ORDWAY B., AND KARLIS MINKA. Note on a Criterion for Severity of Roll-Induced Instability 287
GAZLEY, CARL, JR., W. W. KELLOGG, AND E. H. VESTINE. Space Vehicle Environment 770
GEIGER, R. E. On the Frozen Flow of a Dissociated Gas* 834
GERARD, GEORGE, AND ARTHUR C. GILBERT. A Critical Strain Approach to Creep Buckling of Plates and Shells (Vol. 25, p. 429)
Comment, Nicholas J. Hoff* 117
GERARD, GEORGE, AND HERBERT TRAMPOSCH. Photothermoelastic Investigation of Transient Thermal Stresses in a Multiweb Wing Structure 783
GIBBINGS, J. C. On the Effect of a Narrow Band of Distributed Roughness Upon Boundary-Layer Transition* .. 843
GILBERT, ARTHUR C., AND GEORGE GERARD. A Critical Strain Approach to Creep Buckling of Plates and Shells (Vol. 25, p. 429)
Comments, Nicholas J. Hoff* 117
GLASSMAN, IRVIN, AND JAMES E. A. JOHN. An Unusual Aerodynamic Stagnation-Temperature Effect* 387
GODDARD, FRANK E., JR. Effect of Uniformly Distributed Roughness on Turbulent Skin-Friction Drag at Supersonic Speeds 1
GODDARD, V. P., J. A. MCLAUGHLIN, AND F. N. M. BROWN. Visual Supersonic Flow Patterns by Means of Smoke Lines* 761
GOODMAN, THEODORE R. The Heating of Slabs With Arbitrary Heat Inputs* 187
Comment, William Squire* 756
GOODMAN, THEODORE R., AND THEODORE P. SARGENT. Some Evidence Justifying the Representation of Blasts as Traveling Gusts* 608
GOUSE, S. WILLIAM, JR., GEORGE A. BROWN, AND JOSEPH KAYE. Preliminary Results of Measurement of Effects of Diffusion of Helium Into the Laminar Boundary Layer of a Supersonic Flow of Air in a Tube at Mach 5* 533
GREEN, JOHN J. Discussion of: Means and Examples of Aeronautical Research in France at ONERA (Twenty-Second Wright Brothers Lecture), Maurice Roy (p. 193) 207
GREEN, L., JR., AND W. NACHBAR. Analysis of a Simplified Model of Solid Propellant Resonant Burning 518
GREEN, LEON, JR., AND KENNETH L. NALL. Experiments on Porous-Wall Cooling and Flow Separation Control in a Supersonic Nozzle 689
GROSS, ROBERT A. A High-Temperature, Steady-Flow, Supersonic Tunnel* 676
GUMAN, WILLIAM J. On the Plateau and Peak Pressure of Regions of Pure Laminar and Fully Turbulent Separation in Two-Dimensional Supersonic Flow* 56
GUNDERSEN, ROY. A Perturbation Analysis of Shock Flow in a Nozzle* 763

HAINS, F. D. Some Exact Solutions to the Magnetohydrodynamic Equations for Incompressible Flow* 246
HALL, I. M., AND C. J. BERRY. On the Heating Effect in a Resonance Tube* 253
HAMA, FRANCIS R., JOHN V. RECESSO, AND JEAN CHRISTIAENS. The Axisymmetric Free-Convection Temperature Field Along a Vertical Thin Cylinder 335
HANAWALT, A. J., A. H. BLESSING, AND C. M. SCHMIDT. Thermal Analysis of Stagnation Regions With Emphasis on Heat-Sustaining Nose Shapes at Hypersonic Speeds .. 257
HANCOCK, G. J. Divergence of Plate Airfoils of Low Aspect Ratio at Supersonic Speeds 495
HASSAN, H. A. A New Solution to the Laminar Boundary-Layer Equations* 189
Comment, M. Z. v. Kryzwoblocki* 760
HASSAN, H. A. On Heat Transfer to Laminar Boundary Layers* 464
HAYES, WALLACE D., AND RONALD F. PROBSTEIN. Viscous Hypersonic Similitude 815
HELLER, ROBERT A., AND ALFRED M. FREUDENTHAL. On Stress Interaction in Fatigue and a Cumulative Damage Rule 431
HERTZBERG, ABRAHAM, CHARLES E. WITTLIFF, AND MERLE R. WILSON. The Tailored-Interface Hypersonic Shock Tunnel 219
HILTON, HARRY H. On the Representation of Nonlinear Creep by a Linear Viscoelastic Model* 311
HOFF, NICHOLAS J. Comment on: A Critical Strain Approach to Creep Buckling of Plates and Shells, George Gerard and Arthur C. Gilbert (Vol. 25, p. 429)* 117
HOFF, N. J., W. E. JAHSMAN, AND W. NACHBAR. A Study of Creep Collapse of a Long Circular Cylindrical Shell Under Uniform External Pressure 663

HOLMAN, JACK P., AND TIPTON P. MOTT-SMITH. The Effects of Constant-Pressure Sound Fields on Free-Convection Heat Transfer From a Horizontal Cylinder* 188
HOLT, MAURICE. A Linear Perturbation Method for Stability and Flutter Calculations on Hypersonic Bodies 787
HOSHIZAKI, H., AND H. J. SMITH. The Effect of Helium Injection at an Axially Symmetric Stagnation Point* 399
HOWARD, WESTON M. The Effect of Temperature on Pressures Measured in a Hypersonic Wind Tunnel* 764
HSU, C. C., AND S. F. SHEN. Analytical Results of Certain Nonlinear Flutter Problems (Vol. 25, p. 136)*
Comment, Donald S. Woolston and Robert E. Andrews* 51
Author's Reply, S. F. Shen* 52
HUCKEL, VERA, H. G. MORGAN, AND H. L. RUNYAN. Theoretical Considerations of Flutter at High Mach Numbers (Vol. 25, p. 371)
Authors' Comment, Harry L. Runyan and Homer G. Morgan* 458
HUNTER, HERBERT E. An Exact Solution of the Navier-Stokes Equations* 181

INMAN, ROBERT M. Heat Transfer for Laminar Flow in an Annulus With Porous Walls* 532
INMAN, ROBERT M. A Note on the Skin-Friction Coefficient for Compressible Couette Flow* 182

JACKSON, CHARLES E., AND JOHN E. WHERRY. A Comparison of Theoretical and Experimental Loads on the B-47 Resulting From Discrete Vertical Gusts 33
JAHSMAN, W. E., N. J. HOFF, AND W. NACHBAR. A Study of Creep Collapse of a Long Circular Cylindrical Shell Under Uniform External Pressure 663
JASZLICS, IVAN, AND LEON TRILLING. An Experimental Study of the Flow Field About Swept and Delta Wings With Sharp Leading Edges 487
JOHN, JAMES E. A., AND IRVIN GLASSMAN. An Unusual Aerodynamic Stagnation-Temperature Effect* 387
JOHNS, DAVID J. Comment on: Thermal Buckling of Clamped Cylindrical Shells, W. Zuk (Vol. 24, p. 389)* 59
JOHNS, DAVID J. Some Panel-Flutter Studies Using Piston Theory (Vol. 25, p. 679)
Errata* 192
JONES, ROBERT T. Comments on: On Jones' Criterion for Optimum Lifting Wings, H. Yoshihara and T. Strand (Vol. 25, p. 600)* 382
Author's Reply, H. Yoshihara* 383
JUNGCLAUS, GÜNTHER. Some Remarks on the Controversy Regarding Boundary Layers in Shear Flow* 844

KAUFMAN, LOUIS G., II. Stability Criteria for Systems Having Complex-Coefficient Polynomial Characteristic Equations* 122
KAYE, JOSEPH, S. WILLIAM GOUSE, JR., AND GEORGE A. BROWN. Preliminary Results of Measurement of Effects of Diffusion of Helium Into the Laminar Boundary Layer of a Supersonic Flow of Air in a Tube at Mach 5* 533
KAYE, JOSEPH, AND JOHN R. RADBILL. Analysis of Effects of Diffusion of a Foreign Gas Into the Laminar Boundary Layer of a Supersonic Flow of Air in a Tube* 602
KELLER, HERBERT B., AND EDWARD L. REISS. Spherical Cap Snapping 643
KELLEY, HENRY J. An Investigation of Optimal Zoom Climb Techniques 794
KELLOGG, W. W., CARL GAZLEY, JR., and E. H. VESTINE. Space Vehicle Environment 770
KELLY, ROBERT E. The Use of the WKBJ Method to Estimate Transient Effects on Structural Response* 850
KEMP, NELSON H. On Hypersonic Stagnation-Point Flow With a Magnetic Field (Vol. 25, p. 405)*
Comment, N. C. Freeman* 670
Author's Reply* 672
KEMP, NELSON H. Vorticity Interaction at an Axisymmetric Stagnation Point in a Viscous Incompressible Fluid* 543
KEMP, NELSON H., PETER H. ROSE, AND RALPH W. DETRA. Laminar Heat Transfer Around Blunt Bodies in Dissociated Air 421
KENNEDY, ERNEST C. A Note on Conical Flow* 59
KENNET, HAIM, AND HOLT ASHLEY. Forces and Moments on Oscillating Wing-Body Combinations at Supersonic Speed* 605
KLEIN, BERTRAM. A Simple Method of Matric Structural Analysis: Part IV—Nonlinear Problems 351
KLEIN, BERTRAM. Simultaneous Calculation of Influence Coefficients and Influence Loads for Arbitrary Structures* 451
KLEIN, MILTON M. Calculation by the Integral Method of the Effect of Fluid Injection Upon an Isothermal Boundary Layer* 686
KOBAYASHI, ALBERT S., AND RAYMOND C. WEIKEL. On the Local Elastic Stability of Honeycomb Face Plate Subjected to Uniaxial Compression* 672
KOGA, T., L. TALBOT, AND P. M. SHERMAN. Hypersonic Viscous Flow Over Slender Cones 723
KRAMER, R. F., AND H. M. LIEBERSTEIN. Numerical Solution of the Boundary-Layer Equations Without Similarity Assumptions 508
KRISHNAN, S., AND K. V. SHETTY. On the Optimum Design of an I-Section Beam* 599
KRZYWOBLOCKI, M. Z. v. Comment on: A New Solution to the Laminar Boundary-Layer Equations, H. A. Hassan* (p. 189) 760
KRZYWOBLOCKI, M. Z. v. Comment on: On the Solution of the Laminar Boundary-Layer Equations, M. Epstein (p. 58)* 455

LAITONE, E. V. Dynamic Longitudinal Stability Equations for the Re-Entry Ballistic Missile 94
LAM, S. H., AND L. CROCCO. Note on the Shock-Induced Unsteady Laminar Boundary Layer on a Semi-Infinite Flat Plate* 54
LARSON, HOWARD K. Heat Transfer in Separated Flows 731
LAURMANN, J. A. The Effect of Slip on Induced Pressures* 53
LE FUR, BERNARD. Heat Transfer and Recovery Factor in a Laminar Boundary Layer With Arbitrary Pressure Gradient and Wall Temperature Distribution* 682
LEHNERT, R., AND V. L. SCHERMERHORN. Correlation of Base Pressure and Wake Structure of Sharp- and Blunt-Nose Cones With Reynolds Number Based on Boundary-Layer Momentum Thickness* 185
LEITMANN, G. On a Class of Variational Problems in Rocket Flight 586
LENARD, MICHAEL, AND NICHOLAS ROTT. Vorticity Effect on the Stagnation-Point Flow of a Viscous Incompressible Fluid* 542
LEVY, A., R. A. SEBAN, AND A. EMERY. Heat Transfer to Separated and Reattached Subsonic Turbulent Flows Obtained Downstream of a Surface Step 809
LIBBY, PAUL A., AND MARIAN VISICH, JR. The Law of the Wake in Compressible Turbulent Boundary Layers* 541
LIEBERSTEIN, H. M., AND R. F. KRAMER. Numerical Solution of the Boundary-Layer Equations Without Similarity Assumptions 508
LILLEY, G. M. On a Generalized Porous-Wall "Couette-Type" Flow* 685
LOH, W. H. T. Hydraulic Analogy for Two-Dimensional and One-Dimensional Flows* 389

Loh, W. H. T. Spinning Ballistic Missiles* 844
Love, E. S. Generalized-Newtonian Theory* 314
Lykoudis, Paul S. The Matching of the Viscid and Inviscid Regions for the Stagnation Magnetic Flow* 315

McCormick, Barnes W. The Limiting Circulatory Lift of a Wing of Finite Aspect Ratio* 247
McCune, J. E., and W. R. Sears. On the Concepts of Moving Electric and Magnetic Fields in Magnetohydrodynamics* 674
Mc Ilroy, M. D. Linear Deformation of Conical Shells* 253
McLaughlin, J. A., V. P. Goddard, and F. N. M. Brown. Visual Supersonic Flow Patterns by Means of Smoke Lines* 761
McLean, Francis E., and Clinton E. Brown. The Problem of Obtaining High Lift-Drag Ratios at Supersonic Speeds 298
MacNeal, Richard H., Michael A. Basin, and John H. Shields. Direct-Analog Method of Analysis of the Influence of Aerodynamic Heating on the Static Characteristics of Thin Wings 145
Mager, Artur. Supersonic Airfoil Performance With Small Heat Addition 99
Mager, Artur. Transformation of the Compressible Turbulent Boundary Layer (Vol. 25, p. 305)
Comment, Michiru Yasuhara* 528
Mahalingam, S. An Improvement of the Myklestad Method for Flexural-Vibration Problems 46
Martellucci, Anthony. An Investigation of a Low-Drag Auxiliary Body Utilizing Favorable Interference* 538
Martin, E. Dale. Inviscid Hypersonic Flow Around Spheres and Circular Cylinders* 529
Martin, James A. Determination of Local Skin Friction by Means of Surface Total-Pressure Probes* 320
Martuccelli, John R., and Erik Mollo-Christensen. On the Effect of Flow Discontinuities on Oscillatory-Pressure Measurements in Supersonic Flow* 601
Matsunaga, Syōgo. A Study of the Adiabatic Exponent of the "Hydrodynamical Gas" by Statistical Thermodynamics* 527
Mello, J. F. Investigation of Normal Force Distributions and Wake Vortex Characteristics of Bodies of Revolution at Supersonic Speeds 155
Messiter, Arthur F. A Similarity Law for the Normal Force on a Delta Wing at Hypersonic Speeds* 119
Miele, Angelo. Lagrange Multipliers and Quasi-Steady Flight Mechanics 592
Miles, John W. On Panel Flutter in the Presence of a Boundary Layer 81
Miles, John W., and William P. Rodden. On the Supersonic Flutter of Two-Dimensional Infinite Panels* 190
Minka, Karlis, and Ordway B. Gates. Note on a Criterion for Severity of Roll-Induced Instability 287
Mollö-Christensen, Erik. Acoustical Instability of Jets and Wakes for Mach Numbers Above Two* 765
Mollö-Christensen, Erik, and John R. Martuccelli. On the Effect of Flow Discontinuities on Oscillatory-Pressure Measurements in Supersonic Flow* 601
Morgan, H. G., H. L. Runyan, and Vera Huckel. Theoretical Considerations of Flutter at High Mach Numbers (Vol. 25, p. 371)
Authors' Comment, Harry L. Runyan and Homer G. Morgan* 458
Mott-Smith, Tipton P., and Jack P. Holman. The Effects of Constant-Pressure Sound Fields on Free-Convection Heat Transfer From a Horizontal Cylinder* 188
Mulholland, John D. A Note on the Normal Force of a Multifinned Tail Assembly* 837
Murphy, Charles H., Jr. Steady-State Circular Pitching and Yawing Motion of Symmetric Missiles* 600
Murphy, James S. Pressure Fluctuations in a Blowdown Wind Tunnel* 61

Nachbar, W., and L. Green, Jr. Analysis of a Simplified Model of Solid Propellant Resonant Burning 518
Nachbar, W., N. J. Hoff, and W. E. Jahsman. A Study of Creep Collapse of a Long Circular Cylindrical Shell Under Uniform External Pressure 663
Naghdi, P. M. On Thermoelastic Stress-Strain Relations for Thin Isotropic Shells* 125
Nall, Kenneth L., and Leon Green, Jr. Experiments on Porous-Wall Cooling and Flow Separation Control in a Supersonic Nozzle 689
Nardo, S. V., and David Abir. Thermal Buckling of Circular Cylindrical Shells Under Circumferential Temperature Gradients 803
Neffson, Ben A. Beam Columns on Elastic Supports*. 255
Comment, Paul E. Sandorff* 759
Ness, Nathan. On the Continuity of the Schmidt Number at the Interface Between the Laminar Sublayer and the Outer Turbulent Region* 396
Nestler, Donald E. Comment on: On Slip-Flow Heat Transfer to a Flat Plate, R. A. Oman and R. A. Scheuing (p. 126)* 687
Nicholls, J. A., and T. C. Adamson, Jr. On the Structure of Jets From Highly Underexpanded Nozzles Into Still Air 16
Comment, S. L. Bragg 607
Nicholls, J. A., and R. S. Ong. On the Flow of a Hydromagnetic Fluid Near an Oscillating Flat Plate* 313

Oman, Richard A., and Richard A. Scheuing. On Slip-Flow Heat Transfer to a Flat Plate* 126
Comment, Donald E. Nestler* 687
Ong, Rudi S. On the Generalized Prandtl Relation (Vol. 25, p. 209)
Ong, R. S., and J. A. Nicholls. On the Flow of a Hydromagnetic Fluid Near an Oscillating Flat Plate* 313
Comment, S. M. Ramachandra 393
Ordway, Donald Earl, and Edward L. Clark, Jr. An Experimental Study of Jet-Flap Compressor Blades 698

Pai, S. I. Laminar Jet Mixing of Electrically Conducting Fluid in a Transverse Magnetic Field* 254
Pallone, Adrian, and Martin H. Bloom. Shroud Tests of Pressure and Heat Transfer Over Short Afterbodies With Separated Wakes 626
Perkins, Frank M. Flight Mechanics of Low-Thrust Spacecraft 291
Pian, T. H. H. Comment on: Reduction of Strain Rosettes in the Plastic Range, C. S. Ades (p. 392)* 842
Pistiner, Josef S. Stability Criteria for the Airframe Dynamics of a Liquid-Propellant Rocket* 678
Potter, J. Leith, and Jack D. Whitfield. The Role of Unit Reynolds Number in Boundary-Layer Transition* . 186
Probstein, Ronald F., and Wallace D. Hayes. Viscous Hypersonic Similitude 815

Radbill, John R., and Joseph Kaye. Analysis of Effects of Diffusion of a Foreign Gas Into the Laminar Boundary Layer of a Supersonic Flow of Air in a Tube* 602
Ramachandra, S. M. Comment on: On the Generalized Prandtl Relation, Rudi S. Ong (Vol. 25, p. 209)* 393
Recesso, John V., Francis R. Hama, and Jean Christiaens. The Axisymmetric Free-Convection Temperature Field Along a Vertical Thin Cylinder 335
Reeves, Barry L., and William M. Van Camp. Aerodynamic Heating of Simple Geometries in the Slip- and Intermediate-Flow Regimes* 838
Reid, Elliott G., and William M. Foley. Jet Flap Thrust Recovery* 385
Reiss, Edward L., and Herbert B. Keller. Spherical Cap Snapping 643
Resler, E. L., Jr., and W. R. Sears. The Prospects for Magneto-Aerodynamics—Correction and Addition* 318
Resler, E. L., Jr., and J. Wilson. A Mechanism of Resonance Tubes* 461

REYNOLDS, WILLIAM C. Behavior of Liquids in Free Fall* 847

RIMOLDI, R. F., W. D. CLIFFORD, AND R. J. BACIGALUPI. Effect of Air Pressure on Vortex-Shedding Frequency of Cylinders (Vol. 25, p. 532)*
Comment, Anatol Roshko* ... 121
Author's Reply, William D. Clifford* ... 121

RIVELLO, ROBERT M. The Yield Strength and Deflection of Circular Bars Subjected to Torsion* ... 836

RIVELLO, ROBERT M. The Yield Strength of Beams in Pure Bending* ... 393

RODDEN, WILLIAM P. Aerodynamic Influence Coefficients From Strip Theory* ... 833

RODDEN, WILLIAM P. Further Remarks on Matrix Interpolation of Flexibility Influence Coefficients* ... 760

RODDEN, W. P., AND A. E. ENGELBRECHT. Errata: Coupled Free Vibrations of a Swept Wing, A. E. Engelbrecht (Vol. 18, p. 329)* ... 541

RODDEN, WILLIAM P., AND JOHN W. MILES. On the Supersonic Flutter of Two-Dimensional Infinite Panels* 190

ROSCISZEWSKI, JAN. Influence of Shock-Wave Attenuation by Boundary-Layer Growth on Contact-Surface Motion in a Shock Tube* ... 388

ROSE, PETER H., NELSON H. KEMP, AND RALPH W. DETRA. Laminar Heat Transfer Around Blunt Bodies in Dissociated Air ... 421

ROSHKO, ANATOL. Comment on: Effect of Air Pressure on Vortex-Shedding Frequency of Cylinders, R. F. Rimoldi, W. D. Clifford, and R. J. Bacigalupi (Vol. 25, p. 532)* ... 121
Author's Reply, William D. Clifford* ... 121

ROSNER, DANIEL E. Chemically Frozen Boundary Layers With Catalytic Surface Reaction ... 281

ROSNER, DANIEL E. Steady-State Surface Temperatures in Dissociated High-Speed Gas Flows* ... 384

ROTT, NICHOLAS. A Simple Construction for the Determination of the Magnetohydrodynamic Wave Speed in a Compressible Conductor* ... 249

ROTT, NICHOLAS, AND MICHAEL LENARD. Vorticity Effect on the Stagnation-Point Flow of a Viscous Incompressible Fluid* ... 542

ROY, MAURICE. Means and Examples of Aeronautical Research in France at ONERA (Twenty-Second Wright Brothers Lecture) ... 193
Discussion, Hugh L. Dryden, A. H. Flax, and John J. Green ... 207

RUNYAN, H. L., H. G. MORGAN, AND VERA HUCKEL. Theoretical Considerations of Flutter at High Mach Numbers (Vol. 25, p. 371)
Authors' Comment, Harry L. Runyan and Homer G. Morgan* ... 458

RYDER, FREDERICK L. Energy Versus Compatibility Analogs in Electrical Simulators of Structures ... 108

RYDER, FREDERICK L., AND MELVIN ZAID. Landing-Gear Vibration Instability ... 303

SAELMAN, B. Integration of Some Thermal Differential Equations* ... 754

SAKURAI, TAKEO. On the Normal Shock Wave Attached to the Curved Surface* ... 460

SAKURAI, TAKEO. Two-Dimensional Hypersonic Flow of an Ideal Gas With Infinite Electric Conductivity Past a Two-Dimensional Magnetic Dipole* ... 841

SANDORFF, PAUL E. Comment on: Beam Columns on Elastic Supports, Ben A. Neffson (p. 255)* ... 759

SARGENT, THEODORE P., AND THEODORE R. GOODMAN. Some Evidence Justifying the Representation of Blasts as Traveling Gusts* ... 608

SCALA, SINCLAIRE M., AND JOSEPH B. WORKMAN. The Stagnation-Point Boundary Layer on a Rotating Hypersonic Body* ... 183

SCHERMERHORN, V. L., AND R. LEHNERT. Correlation of Base Pressure and Wake Structure of Sharp- and Blunt-Nose Cones With Reynolds Number Based on Boundary-Layer Momentum Thickness* ... 185

SCHEUING, RICHARD A., AND RICHARD A. OMAN. On Slip-Flow Heat Transfer to a Flat Plate* ... 126
Comment, Donald E. Nestler* ... 687

SCHJELDERUP, H. C. Accumulative Fatigue Damage Caused by Random Loading* ... 394

SCHJELDERUP, H. C. The Modified Goodman Diagram and Random Vibration* ... 686

SCHMIDT, C. M., A. J. HANAWALT, AND A. H. BLESSING. Thermal Analysis of Stagnation Regions With Emphasis on Heat-Sustaining Nose Shapes at Hypersonic Speeds ... 257

SEARS, W. R., AND J. E. MCCUNE. On the Concepts of Moving Electric and Magnetic Fields in Magnetohydrodynamics* ... 674

SEARS, W. R., AND E. L. RESLER, JR. The Prospects for Magneto-Aerodynamics—Correction and Addition* ... 318

SEBAN, R. A., A. EMERY, AND A. LEVY. Heat Transfer to Separated and Reattached Subsonic Turbulent Flows Obtained Downstream of a Surface Step ... 809

SHAFFER, E. C., AND R. D. CESS. Summary of Laminar Heat Transfer Between Parallel Plates With Unsymmetrical Wall Temperatures* ... 538

SHAPIRO, ASCHER H. Shock Waves and Dissipation in a Resonance Tube* ... 684

SHARMAN, P. W. Approximate Bending Moment Diagrams for Flight Maneuvers* ... 530

SHEN, S. F. An Approximate Analysis of Nonlinear Flutter Problems ... 25

SHEN, S. F., AND C. C. HSU. Analytical Results of Certain Nonlinear Flutter Problems (Vol. 25, p. 136)*
Comment, Donald S. Woolston and Robert E. Andrews* 51
Author's Reply, S. F. Shen* ... 52

SHERMAN, P. M., L. TALBOT, AND T. KOGA. Hypersonic Viscous Flow Over Slender Cones ... 723

SHETTY, K. V., AND S. KRISHNAN. On the Optimum Design of an I-Section Beam* ... 599

SHIELDS, JOHN H., MICHAEL A. BASIN, AND RICHARD H. MACNEAL. Direct-Analog Method of Analysis of the Influence of Aerodynamic Heating on the Static Characteristics of Thin Wings ... 145

SHIRELY, L. K., AND M. M. STANIŠIĆ. On the Torsion of a Cylindrical Beam Having a Trapezoidal Cross Section* 462

SHOEMAKER, E. M., AND F. EDWARD EHLERS. A Linearized Analysis of the Forces Exerted on a Rigid Wing by a Shock Wave ... 75

SIBULKIN, M. A Total-Temperature Probe for High-Temperature Boundary-Layer Measurements* ... 458

SINNOTT, COLIN S. On the Flow of a Sonic Stream Past an Airfoil Surface ... 169

SISTINO, ALPHONSE J. The Determination of the Shear Center for a Special Solid Symmetrical Airfoil (Vol. 25, p. 402)*
Comment, J. Lockwood Taylor* ... 118
Author's Reply* ... 118

SMITH, A. M. O., AND DARWIN W. CLUTTER. The Smallest Height of Roughness Capable of Affecting Boundary-Layer Transition ... 229

SMITH, H. J., AND H. HOSHIZAKI. The Effect of Helium Injection at an Axially Symmetric Stagnation Point* ... 399

SOPCZAK, S. S. On Flat Plates and Detached Shock Waves* ... 313

SPREITER, JOHN R. Aerodynamics of Wings and Bodies at Transonic Speeds ... 465

SQUIRE, WILLIAM. Application of Generalized Gauss-Laguerre Quadrature to Boundary-Layer Problems* ... 540

SQUIRE, WILLIAM. Comment on: Concise, Systematic Jacobian Thermodynamics for High-Temperature Real Gases, Russell J. Arave (p. 250)* ... 831
Author's Reply* ... 832

SQUIRE, WILLIAM. Comment on: The Heating of Slabs With Arbitrary Heat Inputs, T. R. Goodman (p. 187)* 756

SQUIRE, WILLIAM. A Note on the Blasius Equation With Three-Point Boundary Conditions* ... 678

STANIŠIĆ, MILOMIR M. A Remark Concerning the Vibration of a Delta Wing in Supersonic Flight* ... 679
STANIŠIĆ, M. M., AND L. K. SHIRELY. On the Torsion of a Cylindrical Beam Having a Trapezoidal Cross Section* 462
STAVSKY, YEHUDA. On a Cross-Elasticity Phenomenon in Symmetrically Nonhomogeneous Plates* ... 607
STEVENS, JOHN ERWIN. Relaxation Characteristics of Pneumatic Tires ... 343
STOJANOVIĆ, DRAGUTIN. Similar Temperature Boundary Layers ... 571
STRAND, T. Design of Missile Bodies for Minimum Drag at Very High Speeds—Thickness Ratio, Lift, and Center of Pressure Given ... 568
STRAND, T., AND H. YOSHIHARA. On Jones' Criterion for Optimum Lifting Wings (Vol. 25, p. 600)
Comment, Robert T. Jones* ... 382
Author's Reply, H. Yoshihara* ... 383
STRIKE, W. T., AND JACK D. WHITFIELD. Forebody Drag Characteristics of an Ogive Cylinder* ... 383
STUART, J. T. The Viscous Flow Near a Stagnation Point When the External Flow Has Uniform Vorticity* 124
SULLIVAN, ROGER D. A Two-Cell Vortex Solution of the Navier-Stokes Equations* ... 767
SUTTON, GEORGE PAUL. Rocket Propulsion Systems for Interplanetary Flight ... 609
SUTTON, GEORGE W. A Comparison of Several Approximate Theories of Melting Ablation* ... 397
SUTTON, GEORGE W. On the Stable Shape of a Slender Ablating Graphite Body* ... 681

TALBOT, L. Free Molecular Flow Forces and Heat Transfer for an Infinite Circular Cylinder at Angle of Attack (Vol. 24, p. 458)*
Errata* ... 61
TALBOT, L., T. KOGA, AND P. M. SHERMAN. Hypersonic Viscous Flow Over Slender Cones ... 723
TAN, H. S. Nose Drag in Free-Molecular Flow and Its Minimization ... 360
TAYLOR, J. LOCKWOOD. Comment on: The Determination of the Shear Center for a Special Solid Symmetrical Airfoil, Alphonse J. Sistino (Vol. 25, p. 402)* ... 118
Author's Reply* ... 118
TAYLOR, J. LOCKWOOD. Comment on: A Note on Blast-Wave Theory, Harvey Einbinder (p. 191)* ... 832
TELLEP, D. M. The Effect of Vehicle Deceleration on a Melting Surface* ... 537
TEMPELMEYER, K. E. Further Note on Isentropic Compressible Flow of Air With Variable Specific Heats* ... 312
THEODORSEN, THEODORE. Optimum Path of an Airplane —Minimum Time to Climb ... 637
TING, LU. On the Integral of Moment of Pressure in Supersonic Flow* ... 758
TRAMPOSCH, HERBERT, AND GEORGE GERARD. Photothermoelastic Investigation of Transient Thermal Stresses in a Multiweb Wing Structure ... 783
TRILLING, LEON, AND IVAN JASZLICS. An Experimental Study of the Flow Field About Swept and Delta Wings With Sharp Leading Edges ... 487
TYLER, EDMUND F. The Oscillating Inboard Flap at Supersonic Speeds* ... 56

VAN CAMP, WILLIAM M., AND BARRY L. REEVES. Aerodynamic Heating of Simple Geometries in the Slip- and Intermediate-Flow Regimes* ... 838
VAN TUYL, A. The Replacement of Lifting Surfaces by Lifting Lines With Variable Position* ... 127
VAS, IRWIN E., AND SEYMOUR M. BOGDONOFF. Preliminary Investigations of Spiked Bodies at Hypersonic Speeds .. 65
VESTINE, E. H., CARL GAZLEY, JR., AND W. W. KELLOGG. Space Vehicle Environment ... 770
VETTER, HANS C. Note on the Calculation of Equilibrium Skin Temperatures* ... 757
VISICH, MARIAN, JR., AND PAUL A. LIBBY. The Law of the Wake in Compressible Turbulent Boundary Layers* 541
VON KÁRMÁN, THEODORE. Some Significant Developments in Aerodynamics Since 1946 (The First Daniel and Florence Guggenheim Memorial Lecture) ... 129

WAGNER, RICHARD D., JR. Some Aspects of the Modified Newtonian and Prandtl-Meyer-Expansion Method for Axisymmetric Blunt Bodies at Zero Angle of Attack* .. 851
WAN, KOON-SANG. On an Exact Solution of Incompressible, Inviscid, Hypersonic, Stagnation-Point Flow for a Sphere* ... 755
WARREN, WALTER R. Determination of Air Stagnation Properties in a High-Enthalpy Test Facility* ... 835
WECKER, MYRON S. On the Use of a Spark-Driven Shock Tube to Prepare Nonequilibrium Gas Samples* ... 848
WEIKEL, RAYMOND C., AND ALBERT S. KOBAYASHI. On the Local Elastic Stability of Honeycomb Face Plate Subjected to Uniaxial Compression* ... 672
WHALEN, ROBERT J. Boundary-Layer Interaction on a Yawed Infinite Wing in Hypersonic Flow* ... 839
WHERRY, JOHN E., AND CHARLES E. JACKSON. A Comparison of Theoretical and Experimental Loads on the B-47 Resulting From Discrete Vertical Gusts ... 33
WHITFIELD, JACK D., AND J. LEITH POTTER. The Role of Unit Reynolds Number in Boundary-Layer Transition* 186
WHITFIELD, JACK D., AND W. T. STRIKE. Forebody Drag Characteristics of an Ogive Cylinder* ... 383
WILLIAMS, JAMES C., III. The Compressible Laminar Boundary Layer With Arbitrary Pressure Gradient and Wall Temperature Distribution* ... 677
WILSON, J., AND E. L. RESLER, JR. A Mechanism of Resonance Tubes* ... 461
WILSON, MERLE R., CHARLES E. WITTLIFF, AND ABRAHAM HERTZBERG. The Tailored-Interface Hypersonic Shock Tunnel ... 219
WINKLER, EVA M., AND MOON H. CHA. Experimental Investigations of the Effect of Heat Transfer on Hypersonic Turbulent Boundary-Layer Skin Friction* ... 123
WITTLIFF, CHARLES E., MERLE R. WILSON, AND ABRAHAM HERTZBERG. The Tailored-Interface Hypersonic Shock Tunnel ... 219
WOOD, ALBERT D., AND JOSEPH H. CLARKE. An Approximate Solution for Transonic Flow in Cascades* ... 318
WOOLSTON, DONALD S., AND ROBERT E. ANDREWS. Comment on: Analytical Results of Certain Nonlinear Flutter Problems, S. F. Shen and C. C. Hsu (Vol. 25, p. 136)* ... 51
Author's Reply, S. F. Shen* ... 52
WORKMAN, JOSEPH B., AND SINCLAIRE M. SCALA. The Stagnation-Point Boundary Layer on a Rotating Hypersonic Body* ... 183

YANG, KWANG-TZU. Unsteady Laminar Compressible Boundary Layers on an Infinite Plate With Suction or Injection ... 653
YASUHARA, MICHIRU. Comment on: Transformation of the Compressible Turbulent Boundary Layer, A. Mager (Vol. 25, p. 305)* ... 528
YEH, HSUAN. An Actuator Disc Analysis of Inlet Distortion and Rotating Stall in Axial Flow Turbomachines ... 739
YOSHIHARA, H., AND T. STRAND. On Jones' Criterion for Optimum Lifting Wings (Vol. 25, p. 600)
Comment, Robert T. Jones* ... 382
Author's Reply, H. Yoshihara* ... 383

ZAID, MELVIN, AND FREDERICK L. RYDER. Landing-Gear Vibration Instability ... 303
ZAKKAY, VICTOR. An Investigation of the Pressure Distribution on Conical Bodies in Hypersonic Flows* ... 457
ZAKKAY, VICTOR, AND ANTONIO FERRI. Pressure Distributions for a Two-Dimensional Blunt-Nosed Body at Different Angles of Attack* ... 395
ZUK, W. Thermal Buckling of Clamped Cylindrical Shells (Vol. 24, p. 389)*
Comment, David J. Johns* ... 59

129

851

755

835

848

672

839

33

186

383

677

461

219

123

219

318

51
52

183

653

528

739

382
383

303

457

395

59